Vrije Universiteit Brussel

Faculty of Sciences and Bio-engineering Sciences

Department of Bio-engineering Sciences

Research Group: Chemical Engineering

Academic year: 2015-2016

Multicolumn adsorption for the vapor phase recovery of acetone-butanol-ethanol fermentation products

Masters' thesis submitted to obtain the degree Master of Science in Bio-engineering Sciences: Chemistry and Biochemical Process Technology: Chemical Biotechnology

Promotor:

Prof. Dr. Ir. Joeri Denayer

Benjamin Claessens

Vrije Universiteit Brussel

Faculty of Sciences and Bio-engineering Sciences

Department of Bio-engineering Sciences

Research Group: Chemical Engineering

Academic year: 2015-2016

Multicolumn adsorption for the vapor phase recovery of acetone-butanol-ethanol fermentation products

Masters' thesis submitted to obtain the degree Master of Science in Bio-engineering Sciences: Chemistry and Biochemical Process Technology: Chemical Biotechnology

Promotor:

Prof. Dr. ir. Joeri Denayer

Benjamin Claessens

Date

Prof. Dr. Ir. Joeri Denayer

Benjamin Claessens

Preface

This results presented in this Masters' thesis were obtained after a year of hard work at the CHIS department. I, for one, would have never survived this last year of my studies without the help and support of some very important people, who therefore deserve a word of thanks.

First of all, I would like to thank my promotor, prof. Dr. ir. Joeri Denayer for the opportunity he has given me to discover the world of nanoporous materials. Further, I would like to thank our fresh PhD Dr.ir. Stijn Van Der Perre for the day-to-day support he has given me during all of the lab and modelling work that was performed for this thesis. Without Stijn, honestly, this thesis would be a one-page report about leaking adsorption columns and broken GC ovens. Special thanks should also be given to our Matlab wizard ir. Peter De Schepper for the support he has given me for the mathematical model development. Further, I would like to thank Dr. ir. Julien Cousin Saint Remi, our biobutanol expert, for the interesting discussions and advice. I would also like to thank Thomas Virdis, our expert VTI mirror cleaner, since the last measurements are indeed the hardest.

A special thanks is in place for my fellow thesis students Tavi, Vincent and Christia, who made every day at the CHIS lab a new adventure. I should also thank Claude Lammens for lending me his golden pen. And last but not least, a word of thanks goes out to my family and girlfriend, for giving me the support I needed to finish my last year at the VUB.

Table of Contents

1. Introduction

The large increase in world population during the final half of the 20th and the beginning of the 21st century is having an increasing effect on the natural environment. Among the different factors negatively impacting the environment due to human activities, are emissions of carbon dioxide and other greenhouse gasses. These gasses have a serious impact on the global climate, causing global warming and a worldwide change of climate. Fighting global warming and climate change was highlighted as one of the 17 goals for sustainable development by the United Nations (United Nations, 2016).

Biofuels could play a part in solving these environmental issues. Being produced using renewable resources, their production and use could theoretically be carbon dioxide neutral. Also, no fossil fuels are used as basis for the production process of biofuels. The European Union aims to have all European transport fuel consisting for 10 % of biofuels by 2020 (European Commission, 2016). Further, many of the molecules produced as biofuel could also be used as platform chemicals, leading to a greener chemical industry based on renewable resources (Olmedo *et al.*, 2014). Amongst the different biofuel candidates, bioethanol and biodiesel are already used and produced on large scale. Biobutanol, however, also shows very promising properties as biofuel and platform chemical (Dürre *et al.*, 2007).

1-Butanol is traditionally produced via petrochemical routes. It can, however, also be produced starting from a renewable feedstock via the acetone-butanol-ethanol (ABE) fermentation process. The traditional fermentation process via clostridial bacteria suffers from product inhibition (Tashiro *et al.*, 2010), leading to a significant decrease in substrate conversion and productivity. Therefore, research performed on this fermentation process is focused on two different themes. First of all, selection of butanol producing microorganisms showing resistance to higher solvent concentration in the fermentation broth is an important challenge (Branduardi *et al.*, 2014). Secondly, significant research efforts are directed towards integrated butanol recovery taking place during the fermentation process, relieving product inhibition and increasing productivity.

Traditional butanol recovery methods involve distillation (Vane *et al.*, 2008), which is an energy demanding process. Alternative processes which are highlighted as promising and energy efficient are pervaporation and adsorption (Qureshi *et al.*, 2005). By combining, for instance, fermentation with gas stripping and a vapor phase adsorption step, efficient butanol recovery can be achieved and product inhibition can be relieved (Abdehagh *et al.*, 2016a). For such a recovery process to be efficient, selective adsorbent materials need to be identified and an efficient process setup needs to be developed.

In this Master's thesis, four different adsorbent materials have been investigated on their applicability in vapor phase butanol recovery. Three of these adsorbents were zeolites: an all silica Linde Type A (LTA) zeolite, an all silica chabazite (CHA) zeolite and SAPO-34. The fourth adsorbent used for this thesis was a metal-organic framework (MOF) of the zeolitic imidazolate framework (ZIF) family: ZIF-8. Breakthrough experiments were performed, focusing on the development of a multicolumn adsorption process for high-purity biobutanol recovery. Further, these breakthrough results were used for the development of a mathematical model describing multicolumn adsorption processes.

2. Study of Literature

In this section, the current literature relevant to this thesis' topic will be reviewed. First of all, a brief history of the acetone-butanol-ethanol (ABE) fermentation will be given and the use of butanol as biofuel will be discussed. In a following section, the different aspects concerning the production of biobutanol via fermentative process will be discussed. The different (integrated) unit operations to recover the produced solvents during ABE fermentation will be reviewed in a third section. Finally, literature concerning the use of adsorptive processes in ABE solvent recovery will be covered. This with an emphasis on the different materials identified as showing a high adsorption capacity or a high selectivity for butanol. In a final section, simulated moving bed chromatography will be discussed, as an example of the use of multi column configurations in biofuel production.

2.1 Introduction

2.1.1 History

Acetone – butanol – ethanol fermentation has a long standing history as industrial fermentation process. Louis Pasteur already discovered butanol producing micro-organisms during the 19th century (Ranjan *et al.*, 2012). However, at the start of the 20th century, the synthetic rubber industry was the real driving force behind the development of the ABE fermentation process. A shortage of natural rubber drove the development of synthetic rubbers based on isoprene and butadiene, since these are important monomers used in the production of rubber and can be produced from butanol (Jones *et al.*, 1986). In his search for butanol producing microorganisms, Fernbach was the first to use an isolated culture for butanol production (Jones *et al.*, 1986; Ranjan *et al.*, 2012). It was Chaim Weizmann, however, who was the first to discover *Clostridium acetobutylicum* as a butanol producing micro-organism (Jones *et al.*, 1986).

The two world wars played a crucial role in further development of the ABE fermentation process. Acetone was used as colloidal solvent for nitrocellulose in the production of chordite (Jones *et al.*, 1986). Chordite was used as smokeless powder by the British Army during World War I. Depletion of maize, which was used as a substrate for the traditional Weizmann fermentation, even led to the brief use of horse chestnuts as substrate (Jones *et al.*, 1986). Weizmann was honored after the war by the British government and lobbied for a Jewish home in Palestine. He eventually became the first President of Israel.

After the first World War, butanol was used as a solvent in the production of quick-drying car lacquer (Jones *et al.*, 1986; Ranjan *et al.*, 2012). Molasses was then used as most important fermentation substrate (Jones *et al.*, 1986). The second World War led again to an increase in demand for acetone in the manufacturing of munitions. However, severe competition with a fast-growing petrochemical industry and an increase in molasses price led to a decline of acetone and butanol production via fermentation in the years following the second World War (Jones *et al.*, 1986). In recent years, the interest in research on ABE fermentation increased again, due to the interest in production of important chemicals based on renewable resources (Dürre *et al.*, 2007; Ranjan *et al.*, 2012; Tashiro *et al.*, 2013).

2.1.2 Butanol as biofuel and basic chemical

The increasing interest in ABE fermentation during recent years is due to the fact that butanol shows promising properties as biofuel and can be used to produce several other important basic chemicals (Dürre *et al.*, 2007; Ranjan *et al.*, 2012; Tashiro *et al.*, 2013). The most widespread biofuels are nowadays bio-ethanol as a replacement for gasoline and biodiesel as an alternative for diesel (Dürre *et al.*, 2007). Biodiesel can be produced via transesterification of fats and fatty acid compounds coming from animal fats and plant oils (Dürre *et al.*, 2007). Recently there is an increased interest in algal based oils as a feedstock for biodiesel production, since no arable land is used for production of these algae. This diminishes competition of the biofuel sector with the food sector for production of food and feed crops (Alaswad *et al.*, 2015). Bioethanol is usually produced using yeast, starting from various sugar substrates (Dürre *et al.*, 2007).

Butanol however, also shows some interesting properties as biofuel as an alternative for gasoline, since it has some distinct advantages over ethanol. For instance, it can be blended in all possible proportions with standard gasoline, whilst ethanol can only make up 85% of the total amount of fuel. In addition, butanol does not require any modifications to standard combustion engines. It can be used as such in a blend or as a sole fuel. The lower vapor pressure of butanol compared to ethanol also makes it a safer compound to handle. Butanol is also less hygroscopic, leading to less groundwater contamination in case of a spill and this also makes it possible to blend it with gasoline directly after refining. Ethanol has to be added shortly before use. Also, the energy content of butanol is higher than that of ethanol, leading to an increased mileage with butanol as compared to ethanol. Finally, butanol can be used to produce dibutyl ether, which can also be used as an alternative for diesel (Dürre *et al.*, 2007). Table 1 gives a comparison of biobutanol with bioethanol and gasoline as fuel.

Table 2.1: Comparison of gasoline to biofuel alternatives, adapted from Dürre *et al.* (2007).

Fuel	Caloric value (MJ/l)	Research octane number (RON)
Gasoline	32.5	91-99
Ethanol	21.2	129
Butanol	29.2	96

Butanol is also used as a precursor for various important bulk chemicals such as acrylate and methacrylate esters, glycol esters, butyl acetate, butyl amines and amino resins. These molecules are used in the production of various chemicals, ranging from antibiotics to all sorts of polymer products (Dürre *et al.*, 2007; Branduardi *et al.*, 2014)

2.2 Fermentation process for ABE production

2.2.1 Biochemistry and butanol producing micro-organisms

Most of the known butanol producing micro-organisms are part of the genus *Clostridium* (Jones *et al.*, 1986; Dürre *et al.*, 2007; Ranjan *et al.*, 2012; Kumar *et al.*, 2011; Branduardi *et al.*, 2014; Alaswad *et al.*, 2015). *Clostridium acetobutylicum* was the first microorganism that was employed to produce butanol on an industrial scale (Jones *et al.*, 1986). Other important butanol producing species of the genus Clostridium include *C. bejierinckii*, *C. saccharoperbutylacetonicum* and *C. saccharobutylicum* (Dürre *et al.*, 2007; Kumar *et al.*, 2011; Ranjan *et al.*, 2012). These microorganisms all grow anaerobically (Kumar *et al.*, 2011). However, not all butanol producing microorganisms are Clostridia, for instance *Buyribacterieum methylotrhophicum* and *Hyperthermus butylicis* have been reported to

produce butanol (Dürre *et al.*, 2007; Kumar *et al.*, 2011). This last organism is even not a bacterium but a member of the Archaea (Dürre *et al.*, 2007; Kumar *et al.*, 2011). Most clostridia are not able to use cellulose or hemicellulose as substrate, however recently some cellulolytic and hemicellulolytic clostridia have been identified (Tashiro *et al.*, 2010).

The biochemical pathways involved in ABE fermentation in *Clostridium sp.* are depicted in figure 2.1. Production of acetone, ethanol and butanol by clostridia consists of two phases. Fermentation starts with an acedogenic phase, in which a large amount of acetic and butyric acid is produced and the microorganism grows fast. Due to the production of acetic and butyric acid derived from butyryl- and acetyl-Coa, the pH of the fermentation broth drops. Crucial during this phase is the ferredoxin protein, which plays an important role as electron carrier. During the formation of acetyl-CoA, this protein is reduced and CO_2 is produced. To regenerate the ferredoxin, H_2 gas is formed by donating electrons to hydrogen ions. This leads to the large amount of CO_2 and H_2 produced during ABE fermentation (Tashiro *et al.*, 2010; Tashiro *et al.*, 2013).

After the acidogenic phase, the culture reaches a stationary phase which is called solventogenisis. The acetate and butyrate produced during acidogenesis are again transferred into the cell cytoplasm and converted to acetyl-CoA and butyryl-CoA. As a result, the pH of the fermentation broth again increases. The protein ferredoxin doesn't play its role of electron carrier during this phase of the fermentation. The cofactor nicotinamide adenine dinucleotide (NAD) is used instead. This cofactor needs to be regenerated and this happens via transfer of electrons to acetyl-CoA and butyryl – CoA, eventually leading to the production of acetone, ethanol and butanol (Tashiro *et al.*, 2010; Tashiro *et al.*, 2013). At the end of the fermentation, acetone, butanol and ethanol are present in the fermentation broth in relative amounts of 3:6:1 respectively when *C. acetobutylicum* is used as microorganism (Branduardi *et al.*, 2014).

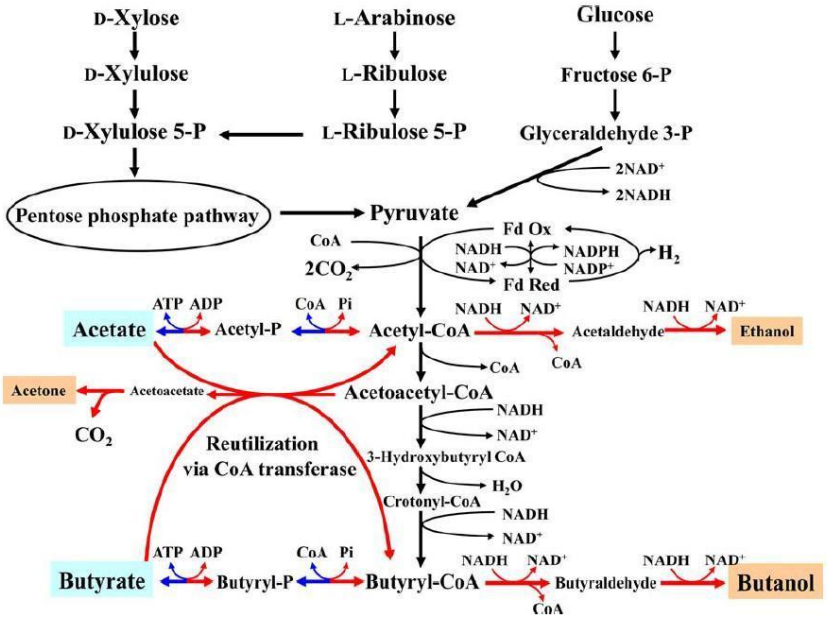

Figure 2.1: Metabolic pathway towards the production of acetone, butanol and ethanol in clostridia. The blue arrows depict the reactions during acedogenisis, whilst the red arrows depict the reactions during solventogenisis. The ferredoxin protein is used as electron carrier during acedogenisis and NAD and NADP during solventogenisis. From: Yukihiro *et al.* (2013). ABE product formation is shown starting from glucose, xylose and arabinose since these are the most common carbon substrates for ABE fermentation (Ranjan *et al.*, 2012).

One of the major problems associated with ABE fermentation is the low final solvent concentrations. *Clostridium acetobutylicum*, for instance, suffers from product inhibition by *n*-butanol and fermentation stops at a *n*-butanol concentration of 20 g/l (Tashiro *et al.*, 2010; Branduardi *et al.*, 2014). Although a lot of research has been performed to improve industrial clostridia strains to reduce this inhibition by the fermentation end products, another interesting solution might be the expression of the ABE pathway in a non-clostridial host. This has been done for several well-known industrial microorganisms, using genetic engineering and in silico metabolic analysis (Branduardi *et al.*, 2014). Table 2 compares the *n*-butanol production for these organisms with *C. acetobutylicum*, but none of the reported modified organisms can produce the same amount of butanol. The 30 g/l concentration of butanol for *Escherichia coli*, was reached due to gas stripping of the fermentation broth during fermentation, in fact the sensitivity of *E. coli* to product inhibition is comparable to that of *C. acetobutylicum* (Branduardi *et al.*, 2014).

It's also noteworthy to mention that algal hosts could possibly be used to produce butanol via photosynthesis. This is done by merging photosynthetic pathways in cyanobacteria or algae and fermentative pathways leading to butanol. Metabolic engineering in this fashion has already been successfully performed for ethanol and isobutanol fermentation (Yu-Sin *et al.*, 2012) and could possibly be extended towards n-butanol fermentation.

2.2.2 Substrate

The price of the raw material used in biobutanol fermentation has an important influence on the final cost of the production process (Qureshi *et al.*, 2000a; Qureshi *et al.*, 2001a). Selection of a cheap and renewable substrate is thus crucial for the economic feasibility of the ABE fermentation process.

Traditional substrates for ABE fermentation include cereal grains and sugar cane (Kumar *et al.*, 2011). These raw materials are however also used in food and feed industry and thus the intensification of the use of these materials in biofuel production processes could lead to an increase in food prices (Kumar *et al.*, 2011). Biofuels produced from these kinds of feedstocks are called first generation biofuels (Kumar *et al.*, 2011).

Because of this tension between fuel production and food production, recently more and more effort is being put in the use of alternative substrates originating from non-edible biomass for biofuel production, also called second generation biofuels (Kumar *et al.*, 2011). Some of the most common used substrates will be discussed in following paragraph.

2.2.2.1 Sucrose and starch

As mention before, sucrose and starch were traditionally the most popular carbon substrates for the ABE fermentation process (Kumar *et al.*, 2011; Jang *et al.* 2012; Ranjan *et al.*, 2012). As *Clostridium sp*. show strong amylase activity, they can use starch based substrates in an efficient way without the need for prior hydrolysis (Qureshi *et al.*, 2001a).

Sugar cane molasses were used in South Africa during the 1980s for biobutanol production. Other sugar based substrates that have been evaluated include soy molasses (Qureshi *et al.*, 2001b), Jerusalem artichoke tubers Marchal *et al.*, 2012) and cheesy whey (Kumar *et al.*, 2011; Yu sin *et al.*, 2012). Starch based substrates that were reported include starch based packing peanuts (Ezeji *et al.*, 2003), gelatinized sago starch (Madihah *et al.*, 2001), liquefied corn starch (Ezeji *et al.*, 2007) and cassava starch and chips (Thang *et al.*, 2010).

Table 2.2: Comparison of different heterologous expression hosts for the ABE fermentation pathway. From: Branduardi (2014).

	Clostridium acetobutylicum	***Esscherichia coli***	***Lactobacillus brevis***	***Pseudomonas putida***	***Bacillus subtilis***	***Synechoccus elongates***	***Saccharomyces cerevisiae***
Cellular type	Prokaryote	Prokaryote	Prokaryote	Prokaryote	Prokaryote	Prokaryote	Eukaryote
Oxygen tolerance	Obligate anaerobe	Facultative anaerobe	Facultative anaerobe	Facultative anaerobe	Obligate anaerobe	Facultative anaerobe	Facultative anaerobe
Substrate range	Large	Good	Good	Large	Good	Organic carbon independent	Small
Genetic tractability	Low	High	Good	High	Good	Good	High
Butanol tolerance %w/v (growth)	1.5	1.5	2 – 3	0.75	1.25	Not determined	2
Butanol tolerance %w/v (viability)	2	2	3-6	6	5	Not determined	Not determined
n-butanol production (mg/l)	19×10^3	30×10^3	300	122	24	29.9	2.5

As mentioned earlier, less and less effort is being put in development of processes based on these kinds of feedstock, since this causes a tension between fuel and food production (Kumar *et al.*, 2011; Jang *et al.*, 2012). Instead, other, alternative raw materials are being investigated.

2.2.2.2 Lignocellulosic raw materials

A possible solution for the food versus fuel dilemma could be the efficient use of lignocellulosic biomass. Cellulose, hemicellulose and pectin are the most important polysaccharide constituents of agricultural waste residues (Yu-Sin *et al.*, 2012). However, obtaining fermentable sugars starting from these raw materials can be very difficult. Different chemical, physical or biological pre-treatment steps are often necessary (Yu-Sin *et al.*, 2012). Also different fermentation inhibitory components are formed during these pre-treatment steps (Ranjan *et al.*, 2012; Jang *et al.* 2012). Acid treated hydrolysates, for instance, contain salts, furfurals, *p*-coumaric acid and phenolic compounds that could inhibit butanol fermentation (Ranjan *et al.*, 2012, Yu sin *et al.*, 2012). This leads to the necessity of other pre-treatment steps after hydrolysis such as adsorption on active carbon (Maddox *et al.*, 1983). It's important to mention that microorganisms of the Clostridium genus are able to ferment a great variety of hexose and pentose sugars (Tracy *et al.*, 2012) and thus are able to grow on cellulose and hemicelluloses hydrolysates.

A large variety of agricultural and other organic waste streams have been tested for use in butanol production. Agricultural residues such as wheat straw appear to be the most interesting (Yu-Sin *et al.*, 2012). Other possible substrates include saccharides from domestic organic waste, dried distiller's grains and soluble, rice bran, cassava bagasse, barley straw hydrolysates, corn stover hydrolysates and switchgrass hydrolysates (Yu-Sin *et al.*, 2012). An excellent summary of efficiency and productivity of butanol fermentation on these substrates is given in the review of Yu-Sin *et al.* (2012).

Integration of fermentation and polysaccharide hydrolysis could greatly improve the efficiency of butanol production starting from lignocellulosic raw materials. This is called consolidated bioprocessing (Yu-Sin *et al.*, 2012). *C. acetobutylicum* is for instance able to produce a large cellulose hydrolyzing enzyme complex called the cellulosome (Yu-Sin *et al.*, 2012). Further, the use of co-cultures has been investigated, where a butanol producing micro-organism is combined with a cellulose hydrolyzing organism (Ranjan, 2012). The combination of different *Clostridium sp.* as well as the combination of *Clostridium sp.* and cellulolytic fungi have been investigated (Ranjan *et al.*, 2012).

2.2.2.2 Glycerol

Glycerol is already an important substrate for 1,3-propanediol synthesis via fermentation by for instance *Klebsiela sp.*(Nakamura *et al.*, 2003). Since glycerol is an important by-product from biodiesel synthesis starting from triacylglycerides, using it as a substrate for further fermentation might increase economic efficiency of the biodiesel production process while providing a cheap substrate for butanol fermentation. *C. pasteurianum* has been reported as being able to produce butanol starting from glycerol (Biebl *et al.*, 2001). Optimal fermentation led to a final butanol concentration of 17g/l (Biebl *et al.*, 2001), which is close to the 20 g/l of *C. acetobutylicum* when fermenting on glucose (Tashiro *et al.*, 2010; Branduardi *et al.*, 2014). Also *C. acetobutylicum* has been reported as being able to grow on a mixture of glycerol and glucose (Andrade *et al.*, 2003). It should be mentioned that biodiesel can be used as an extractant for *in situ* butanol removal during fermentation, making integration of the biodiesel and butanol production process feasible (Adhami *et al.*, 2009).

2.2.2.3 Algae

Another solution to the food versus fuel debate could be the use of algae as a substrate for biofuel production. Since no land area has to be occupied to produce algal biomass, there's no competition for cultivable land between food and fuel crops. Also algal biomass can be produced using seawater or wastewater, so no fresh water has to be consumed during biomass production (Yu-Sin *et al.*, 2012). Butanol fermentation starting from *Dunaliella, nannochloropsis, Arthrospira platensis* biomass has been reported (Yu-Sin *et al.*, 2012). As mentioned before, algae or cyanobacteria can be metabolic engineered to produce butanol via photosynthesis (Yu-Sin *et al.*, 2012).

2.2.2.4 Syngas

Synthesis gas or syngas, a mixture of CO and H_2 gas, is currently being produced by catalytic reforming of natural gas (Yu-Sin *et al.*, 2012). Alternatively, it can also be produced starting from renewable biomass. Some clostridia are able to produce butanol starting from syngas (Yu-Sin *et al.*, 2012). This could lead to the use of certain difficult to hydrolyze biological substances (such as lignin) as substrate in butanol fermentation. Since using this substrate would lead to a gas and liquid phase in the bioreactor, good mass transfer between these two would be crucial for a successful fermentation (Yu-Sin *et al.*, 2012).

2.2.3 Fermentation technology

Several studies have focused on the different process parameters influencing butanol production in ABE fermentation. The key challenge arising during ABE fermentation is increasing butanol productivity whilst avoiding product inhibition. Important in this context is *in situ* butanol removal during fermentation. Techniques for in situ removal of butanol however, will be covered in a subsequent section. In this paragraph, the influence of other fermentation parameters will be discussed for the classical fermentation modes: batch, fed-batch and continuous culture.

2.2.3.1 Batch

Batch cultivation is the simplest fermentation mode and has been used to investigate the effect of different process parameters on solvent production by clostridia. Some of the studied parameters include pH, ratio of carbon to nitrogen substrate (C/N), hydrogen or carbon monoxide concentration in the headspace and the addition of extra electron carriers (Yukihiro *et al.*, 2013). Typical initial substrate concentrations for batch fermentation are (depending on the microorganism) between 60 and 80 g/l (Ranjan, 2012). A typical batch fermentation takes about 48 to 72 h (Ranjan, 2012).

The influence of pH on acidogenesis and solventogenisis appears to be organism dependent. *C. acetobutylicum* and *C. bejierinckii*, for instance produce high amounts of solvents at low pH and high amounts of acids at a higher pH (Monot *et al.*, 1984; Holt *et al.*, 1984). For the *C. acetobutylicum* ATCC 824 strain, 20 g/l of total organic acids were produced at a pH of 6, while 17 g/l of ABE was produced at a pH of 4.5 (Holt et al, 1984; Tashiro *et al.*, 2013). This effect is logical, since during non-pH controlled fermentation, the pH drops during acedogenisis and rises again during solventogenisis as already mentioned in paragraph 2.2.1. Other species however, such as *C. saccharoperbutylacetonicum* and *C. saccharobutylicum* can produce high amounts of ABE solvents without pH control (Yukihiro *et al.*, 2013).

The C/N ratio in the used substrate also has an important effect on the ABE fermentation process. A low C/N ratio stimulates acid production in *C. acetobutylicum* ATCC 824 for instance, whilst a high C/N ratio stimulates solvent production (Roos et al., 1985).

CO_2 and H_2 gas in the headspace of the fermenter also have significant influence on the batch fermentation profile. Since these two gasses are reported as being inhibitors of the hydrogenase that

produces hydrogen gas, an increase in partial pressure of CO and H_2 leads to an increase in butanol production (Yukihiro *et al.*, 2013). Some electron carriers such as methylene blue and methyl viologen exhibit the same behavior by increasing the reducing power supply of butanol producing clostridia (Yukihiro *et al.*, 2013).

Although the simplest method of fermentation, batch fermentation processes suffer from some important disadvantages. Product inhibition and substrate inhibition cause an important decrease in butanol productivity and yield (Ranjan *et al.*, 2012; Jang *et al.*, 2012; Tashiro *et al.*, 2013). When for instance a lignocellulose based substrate is used, carbon catabolite repression (CCR) can hinder efficient fermentation (Yukihiro *et al.*, 2013). Carbon catabolite repression occurs when a mixture of different sugars is used as fermentation substrate and one of these sugars is consumed preferably by the microorganism. CCR of xylose has been observed for instance in *C. acetobutylicum* ATCC 824 when more than 15 g/l of glucose was present in the fermentation broth (Fond et al., 1986).

2.2.3.2 Fed batch

During a fed-batch fermentation process, fermentation is started as a normal batch fermentation. After a certain amount of time however, extra substrate is fed to the reactor. Substrate inhibition can be efficiently avoided by using this technique. Fed-batch also allows for the use of high – viscosity substrates and helps avoiding carbon catabolite repression by allowing the control of the concentration of the different sugars in the reactor. Using fed-batch fermentation, the produced butanol is also automatically diluted with fresh medium, decreasing the inhibitory effect of the formed products. Fed-batch feed strategies allow for an extra amount of co-substrates (organic acids) to be added during the fermentation that can be further processed to butanol by the microorganism (Yukihiro *et al.*, 2013).

2.2.3.3 Continuous culture

By using a continuous fermentation method, the butanol concentration in the fermentation broth can be controlled to effectively overcome the problem of product inhibition. An important drawback, however, is the low concentration of butanol in the fermentation broth exiting the reactor. In a typical fermentation using a continuous stirred tank reactor (CSTR or chemostat) a steady state concentration is reached for all of the fermentation broth constituents including the cell concentration of the culture. Steady state typically occurs after a time equal to three times the dilution rate (feed flow rate divided by volume of the reactor) (Jang *et al.*, 2012; Tashiro *et al.* 2013).

Important parameters during continuous production are, as already mentioned, pH and CO_2 concentration (Yukihiro *et al.*, 2013). The dilution rate also has an important effect on solventogenisis and acidogenesis. High dilution rates lead to an increase in acid production, whilst low dilution rates induce solvent production (Yukihiro *et al.*, 2013). Murschelchner *et al.* (2000) therefore successfully used two CSTRs in series to mimic the batch fermentation profile. A first CSTR was operated at high dilution rates to mimic acidogenesis and the second one at low dilution rates to mimic solventogenisis.

During steady state in a CSTR, the growth rate of the microorganism equals the dilution rate of the reactor. The growth rate of the microorganism is however limited, leading to washing out of the microorganism at high dilution rates in free cell fermentation. The dilution rate for ABE fermentation is therefore limited to about 0.3 / h (Yukihiro *et al.*, 2013). Essentially two strategies can be utilized to prevent this phenomenon. The cell concentration in the reactor can be increased by immobilization or cells can be recycled by using microfiltration membranes for instance (Kumar *et al.*, 2011; Tashiro *et al.*, 2013). The use of a higher cell density leads to higher productivity for a smaller volume of reactor and also to higher possible dilution rates (Kumar *et al.*, 2011; Tashiro *et al.*, 2013).

Immobilization of cells on a solid substrate can occur by physical adsorption or via biofilm formation (Yu-Sin *et al.*, 2012). Different materials can be utilized for immobilization including coke, calcium alginate and brick (Yukihiro *et al.*, 2013). Qureshi *et al.* (2000b) were able to increase the dilution rate to 2.0 /h using clay brick as immobilization support using *C. bejierinckii*. By working at this dilution rate a productivity of 15.8 g l^{-1} h^{-1} was achieved. Some important issues that can arise using immobilized cells include limited substrate mass transfer, activity loss of the immobilized cells and accumulation of gas bubbles in the immobilization matrix (Ranjan, 2012). The use of fluidized beds instead of fixed beds has also been reported (Ranjan, 2012).

A second strategy consists in the use of microfiltration modules to concentrate the fermentation broth and recycle the concentrated cells to the reactor (Tashiro *et al.*, 2005; Kumar *et al.*, 2011; Jang *et al.*, 2012; Ranjan *et al.*, 2012). Tashiro *et al.* (2005) were able to improve the productivity of a continuous C. saccharoperbutylacetonicum N1-4 culture from 1.85 g l^{-1} h^{-1} to 7.55 g l^{-1} h^{-1} by using a combination of cell recycling via membrane filtration and cell bleeding by refreshing a part of the fermentation broth with cell-free substrate. This strategy allows an optimal internal control of the cell concentration in the bioreactor (Tashiro *et al.*, 2005).

2.3 Solvent recovery techniques

As explained in the previous sections, the solvent concentration after fermentation is typically low, with a maximum of 20 g/l for conventional strains during batch fermentation (Ranjan, 2012). Also, when *n*-butanol is the envisaged end product it has to be separated from the other fermentation products. Efficient downstream processing methods are thus necessary to concentrate and separate the formed solvents during ABE fermentation (Vane *et al.*, 2008; Abdehagh *et al.*, 2014; Huang *et al.*, 2014; Xue *et al.*, 2014; Kujawska *et al.*, 2015). These methods are often already applied during the fermentation process to relieve product inhibition (Vane *et al.*, 2008; Abdehagh *et al.*, 2014; Huang *et al.*, 2014; Xue *et al.*, 2014; Kujawska *et al.*, 2015). In the following section, some common solvent recovery techniques will be discussed. The use of adsorptive process in butanol recovery will be discussed in a following section.

2.3.1 Distillation

Distillation is the conventional process used in industry for ABE solvent recuperation (Vane *et al.*, 2008; Abdehagh *et al.*, 2014; Huang *et al.*, 2014; Xue *et al.*, 2014; Kujawska *et al.*, 2015). Often distillation is followed by a drying of the product streams using specific adsorbents (Vane *et al.*, 2008; Huang *et al.*, 2014). Just as is the case with ethanol distillation, a water – butanol azeotrope is formed during the distillation of a water – butanol mixture (Vane *et al.*, 2008; Huang *et al.*, 2014). The butanol azeotrope is formed at 55.5 wt% butanol at 93 °C (Huang *et al.*, 2014). Since this azeotrope lies close to the water boiling point at atmospheric pressure (100 °C), a lot of energy is necessary to separate the butanol water mixture during the downstream processing of the ABE fermentation broth (Vane *et al.*, 2008; Abdehagh *et al.*, 2014; Huang *et al.*, 2014; Xue *et al.*, 2014; Kujawska *et al.*, 2015). In fact, separation of butanol from the fermentation broth by distillation consumes more energy than can be produced via the produced butanol (Huang *et al.*, 2014).

Important to mention is the immiscibility of butanol and water at room temperature. Butanol has a lower solubility limit in water at 20 °C of 7.7 wt% and an upper solubility limit of 79.9% wt (Huang *et al.*, 2014). This means that the azeotrope formed by butanol in water is heterogeneous, as illustrated in figure 2.2 (Vane *et al.*, 2008; Huang *et al.*, 2014). This effect has important implication on the ABE downstream processing, since a watery butanol solution with a butanol concentration between 7.7 wt% and 79.9 wt% automatically separates in two immiscible phases. Thus, when such a mixture is formed after a separation step, an organic phase with a relative high butanol concentration can be

processed separately from the watery phase (Vane *et al.*, 2008; Abdehagh *et al.*, 2014; Huang *et al.*, 2014; Xue *et al.*, 2014; Kujawska *et al.*, 2015). The watery phase can for instance be recycled (Vane *et al.*, 2008; Abdehagh *et al.*, 2014; Huang *et al.*, 2014; Xue *et al.*, 2014; Kujawska *et al.*, 2015).

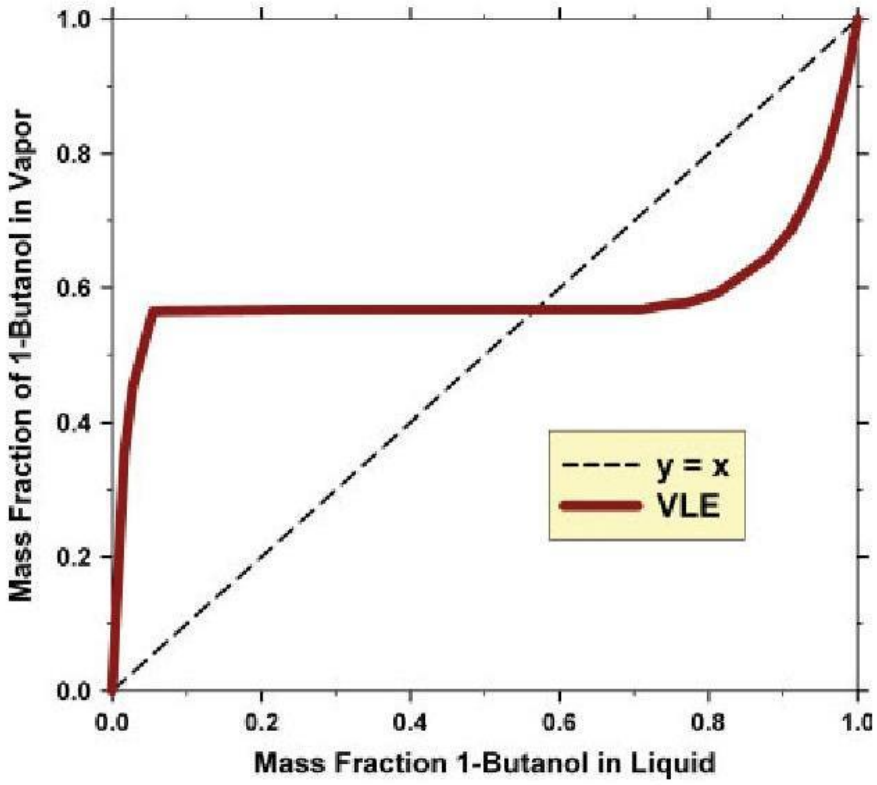

Figure 2.2: Vapor liquid equilibrium (VLE) of water *n*-butanol mixture at 20 °C and atmospheric pressure. The heterogeneous azeotrope is clearly visible. From: Vane *et al.* (2008).

A typical distillation downstream processing uses a series of four columns (Kujawska *et al.*, 2015). In a first step, the ABE fermentation broth is heated to 100 °C, leading to vapors containing 70 wt% water and 30 wt% ABE (Kujawska *et al.*, 2015). After this initial evaporation step, the vapors are separated in a first distillation column at 0.7 atm where 99.5 wt% of acetone is removed as vapor (Kujawska *et al.*, 2015). The bottom fraction is transported to an ethanol distillation column, operating at 0.3 atm (Kujawska *et al.*, 2015). During this step, a fraction of 95 wt% of ethanol is separated (Kujawska *et al.*, 2015). The bottom products of this step are then leaded to a system of two distillation columns and a decanter to separate the *n*-butanol (Vane *et al.*, 2008; Kujawska *et al.*, 2015). The watery phase of the heterogeneous azeotrope is distilled in the aqueous column and the butanol-rich phase is distilled in a butanol column (Vane *et al.*, 2008). The vapor phase of both columns is condensed and separated in a butanol and water rich phase in the decanter (Vane *et al.*, 2008). These two phases are recycled to their respective distillation columns (Vane *et al.*, 2008). In the butanol column, a concentration of more than 99 wt% butanol is separated (Vane *et al.*, 2008; Kujawska *et al.*, 2015). This two column process is illustrated in Figure 2.3.

2.3.2 Gas stripping

Since distillation is an energy and capital intensive process, a lot of research is focused on alternative separation processes. One of these possible alternatives is gas stripping.

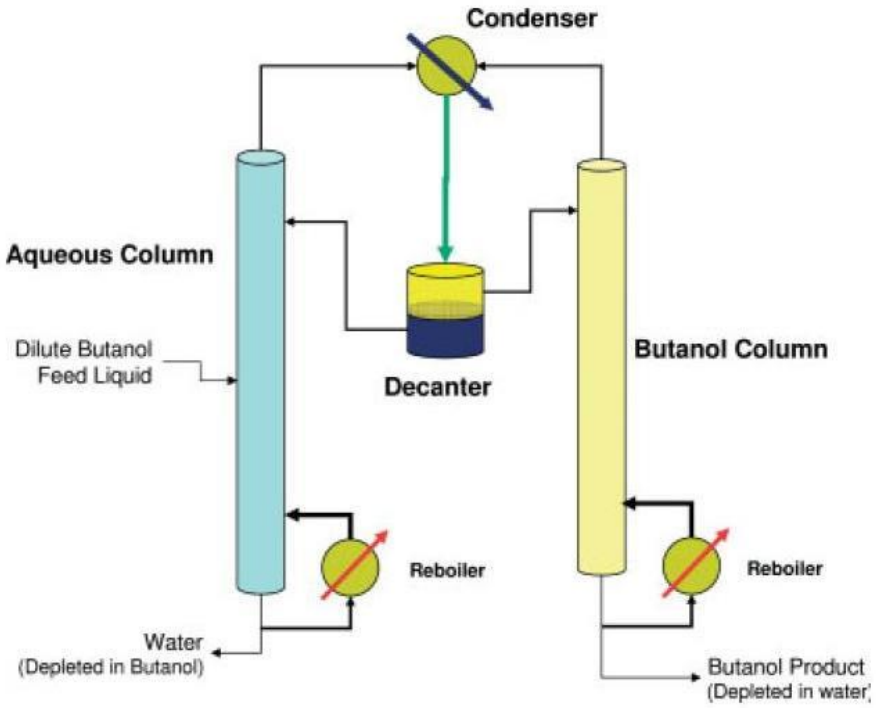

Figure 2.3: Final distillation step in ABE downstream processing. From: Vane *et al.* (2008).

Gas stripping is a simple approach to in situ butanol removal during fermentation. An inert gas, usually the gasses formed during fermentation (CO_2, H_2), is used as carrier gas to remove the ABE solvents from the fermentation broth (Vane *et al.*, 2008; Abdehagh *et al.*, 2014; Huang *et al.*, 2014; Xue *et al.*, 2014; Kujawska *et al.*, 2015). The separation is based on a one stage equilibrium between the inert gas phase and the liquid fermentation broth (Huang *et al.*, 2014). Solvents are then recovered from the gas phase via, for instance, a condenser (Huang *et al.*, 2014). This method can easily be integrated into the fermentation process but can also be applied separately (Vane *et al.*, 2008; Abdehagh *et al.*, 2014; Huang *et al.*, 2014; Xue *et al.*, 2014; Kujawska *et al.*, 2015). Figure 2.4 shows a simplified diagram for a fed batch fermentation system with integrated gas stripping. Important parameters influencing the gas stripping process are the gas flow rate, the amount and type of antifoam added and the presence of other fermentation components (Abdehagh *et al.*, 2014).

Qureshi *et al.* (2008) showed that gas stripping is not only beneficial for the ABE fermentation via product removal, but that it can also be used successfully as agitation system during simultaneous saccharification and fermentation of wheat straw. The observed productivity without gas stripping was 0.27 g^{-1} l^{-1}. The use of in situ gas stripping led to an increase of productivity to 0.31 g^{-1} l^{-1}.

The import advantages of gas stripping include the simplicity of the technology and use of the fermentation off-gas (Huang *et al.*, 2014). Also since no chemicals (except for antifoaming agents) or membrane have to be used, the risk for cell death due to added toxic components is minimal (Huang *et al.*, 2014). Important challenges associated with gas stripping are the energy requirements associated with the condensation step and also the low selectivity (Abdehagh *et al.*, 2014). Gas

stripping could be combined with an adsorption step to efficiently remove the ABE solvents from the stripping gas. Such a process can combine the high selectivity of adsorbents with the efficient relieve of product inhibition via gas stripping. Recently, Abdehagh *et al.* (2016) investigated the applicability of this combination, which will be further discussed in paragraph 2.4.2.

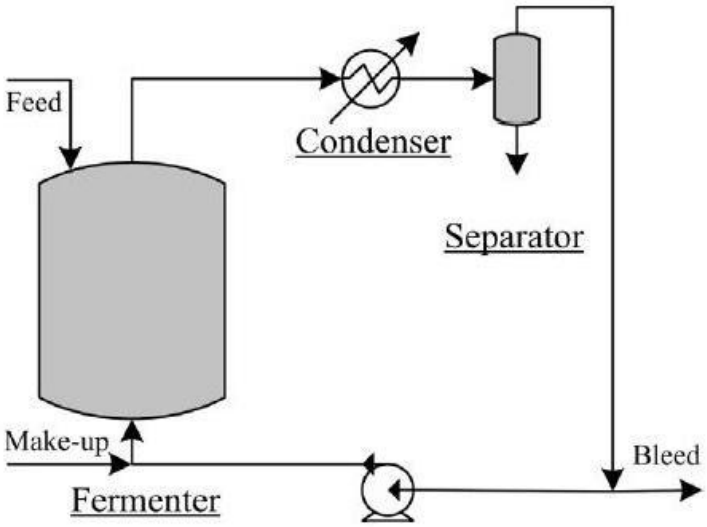

Figure 2.4: Gas stripping integrated into a fed batch fermentation system. From: Huang *et al.* (2014).

2.3.3 Vacuum flash evaporation

A second method for ABE solvent recovery makes use of an external heat exchanger and a vacuum chamber to evaporate the solvents produced during the fermentation. The liquid stream that isn't evaporated is recycled to the fermenter and the vapor phase is condensed. The volatile ABE solvents are condensed in this step, whilst the fermentation off – gasses are removed via a vacuum system. The condensed solvents are fed to a separator to separate the butanol and water rich fractions (Huang *et al.*, 2014; Kujawska *et al.*, 2015). Figure 2.5 depicts this technique for a fed batch fermentation.

Advantages of flash fermentation are that no additional equipment such as a membrane, sparger or agitator is necessary (Huang *et al.*, 2014). Also, the butanol concentration in the product vapor stream is significantly increased (Huang *et al.*, 2014). The major disadvantage is the necessity of a vacuum system (Huang *et al.*, 2014). The application of this technique has been reviewed by *Huang et al.* and *Kujawska et al.* (2014, 2015).

2.3.4 Liquid – liquid extraction

Solvent extraction, or liquid – liquid extraction, is a conventional separation process applied in a great variety of (bio)chemical production processes. Separation is based on a difference of solubility of the targeted solute in the fermentation broth and the extraction liquid. Since butanol is slightly hydrophobic, it can be extracted using hydrophobic extractants (Vane *et al.*, 2008; Abdehagh *et al.*, 2014; Huang *et al.*, 2014; Xue *et al.*, 2014; Kujawska *et al.*, 2015). Liquid – liquid extraction can be used in situ during the fermentation or after the fermentation (Vane *et al.*, 2008; Abdehagh *et al.*, 2014; Huang *et al.*, 2014; Xue *et al.*, 2014; Kujawska *et al.*, 2015).

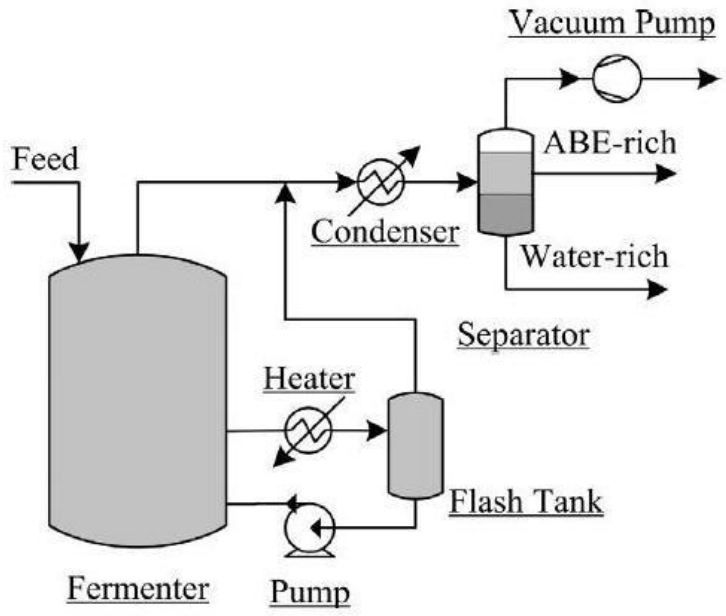

Figure 2.5: Flash fermentation applied to a fed – batch fermentation system. From: Huang *et al.* (2014)

Integration of solvent extraction and the fermentation process is called extractive fermentation (Vane *et al.*, 2008; Abdehagh *et al.*, 2014; Huang *et al.*, 2014; Xue *et al.*, 2014; Kujawska *et al.*, 2015). A process scheme for extractive fermentation is depicted in Figure 2.6. The organic, extractant phase is continuously removed from the fermentation broth and recuperated via distillation. The evaporated ABE solvent is further purified via, for example, distillation. If a non-volatile extractant is used, the distillation column can be replaced by a simple one stage evaporator (Huang *et al.*, 2014).

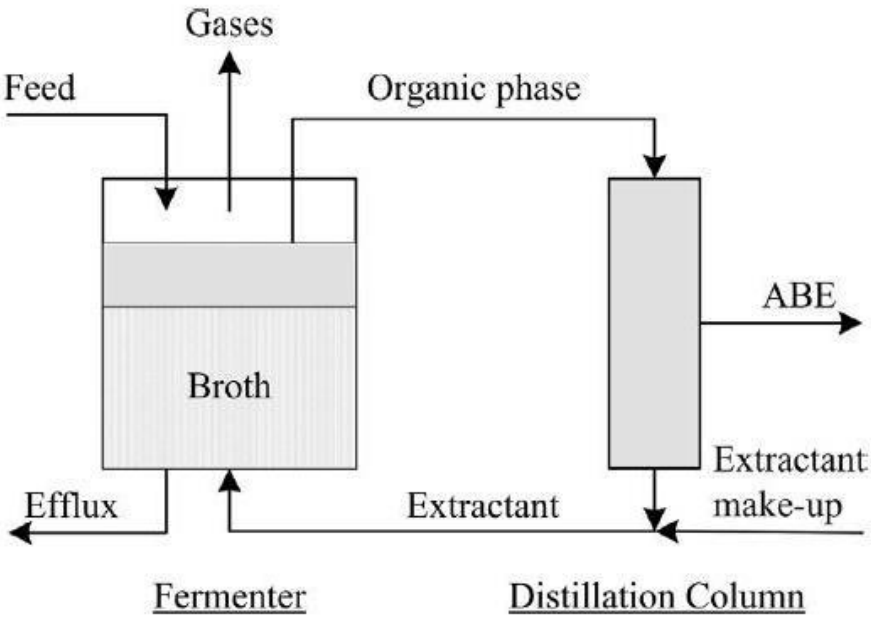

Figure 2.6: Process scheme of extractive fermentation. From: Huang *et al.* (2014).

Crucial for extractive fermentation is the use of a suitable extractant. The solvents used should be nontoxic for the microorganism, since fermentation broth and extractant are continuously in contact with each other. The extractant should have a high distribution and selectivity coefficient. Preferably, the density of the solvent and water are significantly different for easy phase separation. A low viscosity is important to minimize energy consumption during extraction. A large interfacial tension is necessary to aid the emulsion coalescence and phase separation. The volatility is preferably very high or very low to ease the separation of the ABE solvents from the extractant. And of course the used solvents have to be cost efficient (Vane *et al.*, 2008; Huang *et al.*, 2014).

The standard extractant used in butanol recovery is oleyl alcohol (Abdehagh *et al.*, 2014; Kujawska *et al.*, 2015; Xue *et al.*, 2014). However, a lot of research effort is going to the selection of new solvents with interesting properties. Among those, ionic liquids are highlighted as being very promising, due to their low vapor pressure and thus easy recovery. Also polarity and selectivity of these ionic liquids can be easily tuned. However, compatibility of these extractants with the fermenting microorganisms has yet to be confirmed (Abdehagh *et al.*, 2014; Huang *et al.*, 2014; Xue *et al.*, 2014; Kujawska *et al.*, 2015).

Further, biodiesel has been successfully used as biocompatible extractant in ABE fermentation (Adhami *et al.*, 2009). Using biodiesel as an extractant, no extra separation of butanol and extractant is necessary, since this mixture can directly be used as fuel (Adhami *et al.*, 2009; Abdehagh *et al.*, 2014).

2.3.5 Membrane processes

A lot of research is focused on the use of membrane technology in butanol recovery. This due to the high selectivity and energetic efficiency associated with membrane processes (Abdehagh *et al.*, 2014; Huang *et al.*, 2014; Xue *et al.*, 2014; Kujawska *et al.*, 2015). The most common used membrane process used in ABE solvent recovery will be briefly discussed.

2.2.5.1 Perstraction

Perstraction is a liquid-liquid extraction technique where the extraction solvent and the fermentation broth are separated by a membrane (Abdehagh *et al.*, 2014; Huang *et al.*, 2014; Xue *et al.*, 2014; Kujawska *et al.*, 2015). Removal of butanol from the fermentation broth is ensured via the use of a selective membrane and a selective extractant (Abdehagh *et al.*, 2014; Kujawska *et al.*, 2015). Problems associated with normal solvent extraction, such as solvent toxicity and bad emulsion formation, are avoided due to the separation of extraction solvent and fermentation broth (Abdehagh *et al.*, 2014; Huang *et al.*, 2014; Xue *et al.*, 2014; Kujawska *et al.*, 2015). Important disadvantages are the problems associated with clogging and fouling of the membranes and the high costs (Abdehagh *et al.*, 2014). Also, butanol flux through the membrane tends to be lower than when pervaporation is used (Abdehagh *et al.*, 2014).

2.3.5.2 Pervaporation

Pervaporation is a membrane based separation technique where the mixture components are selectively evaporated through a membrane (Abdehagh *et al.*, 2014; Huang *et al.*, 2014; Xue *et al.*, 2014; Kujawska *et al.*, 2015). The driving force for evaporation through the membrane can be a temperature difference, a sweeping gas or a vacuum at the permeate side of the membrane (Kujawska *et al.*, 2015). The permeated gas can then be recovered via, for example, condensation (Abdehagh *et al.*, 2014). Figure 2.7 depicts a process scheme for butanol recovery via vacuum pervaporation.

Membranes used in pervaporation are hydrophobic, due to the hydrophobic character of butanol (Huang *et al.*, 2014). Different types of membranes can be used: polymeric, inorganic, composite and supported liquid membranes (Huang *et al.*, 2014). The most important parameters influencing the

performance of the membrane are its selectivity and permeate flux (Abdehagh *et al.*, 2014). To improve membrane flux, research is focused around developing asymmetric membranes and decreasing membrane thickness (Abdehagh *et al.*, 2014). A decrease in membrane thickness, however also leads to a loss in selectivity (Abdehagh *et al.*, 2014; Huang *et al.*, 2014). Membranes used in pervaporation typically have a thickness between 10-200 µm (Abdehagh *et al.*, 2014).

Many hydrophobic polymeric membranes have been investigated, including polyether block amide (PEBA), polyvinylidene fluoride, polytetrafluoroethylene, polypropylene and polydimethylsiloxane (PDMS) (Huang *et al.*, 2014). Most single-polymer membranes suffer from low selectivity or low membrane fluxes (Huang *et al.*, 2014). To overcome these disadvantages, heterogeneous membranes consisting of a combination of different polymers have been tested (Huang *et al.*, 2014). However, these kind of membranes are usually thicker and thus suffer from low permeate flux (Huang *et al.*, 2014). Other disadvantages associated with the use of polymeric membranes include their lack of mechanical strength and their fast wearing in use (Huang *et al.*, 2014).

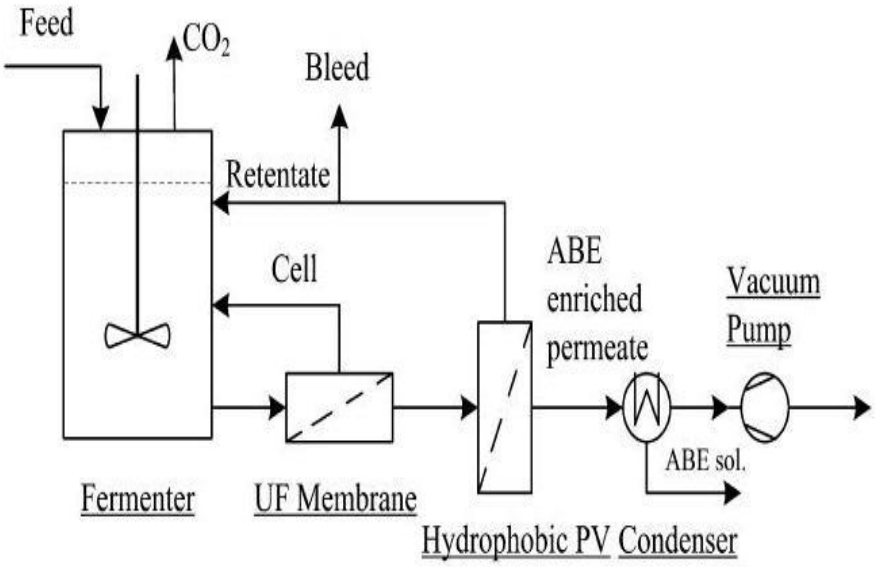

Figure 2.7: Process scheme for in situ vacuum pervaporation during a fed batch fermentation. Note that an ultrafiltration step is used before the vacuum pervaporation step to prevent fouling of the pervaporation membrane. From: Huang *et al.* (2014).

To overcome these disadvantages, inorganic filler materials are added to these polymeric membranes (Huang *et al.*, 2014). Usually, inorganic fillers with a high affinity for butanol are used such as silicalite zeolites (Huang *et al.*, 2014). For example, Tan *et al.* (2013) produced a composite membrane consisting of PEBA and the hydrophobic zeolite ZSM-5. Incorporation of the zeolite increased both membrane flux and selectivity (Tan *et al.*, 2013).

Another type of membrane used in pervaporation are supported liquid membranes (SLM) (Abdehagh *et al.*, 2014; Huang *et al.*, 2014; Xue *et al.*, 2014; Kujawska *et al.*, 2015). In a supported liquid membrane, a hydrophobic organic solvent is immobilized in a microporous support (Huang *et al.*, 2014). Different methods for immobilization exist, including covalent binding of ionic liquids, the use of ion exchange membranes, gelation of ionic liquids, inclusion of the solvent in the polymer matrix

and inclusion by silicone coating (Huang *et al.*, 2014). Conventional extractants, such as oleyl alcohol, are used as well as new types of solvents such as ionic liquids (Huang *et al.*, 2014).

The major issues associated with membrane pervaporation are membrane fouling, long-term membrane stability and the costs associated with membrane production (Huang *et al.*, 2014). Besides these disadvantages, different authors highlight this technique as very promising for butanol recovery from fermentation broths (Vane *et al.*, 2008; Abdehagh *et al.*, 2014; Huang *et al.*, 2014; Xue *et al.*, 2014; Kujawska *et al.*, 2015).

2.3.5.3 Reverse osmosis

Reverse osmosis is a membrane based technology typically used for water desalination. However, it can also be used to concentrate a watery butanol solution (Huang *et al.*, 2014; Abdehagh *et al.*, 2014). In the first step, a nanofiltration module is used to separate an aqueous butanol solution from the fermentation broth using a butanol permeable membrane. In a second step, the butanol permeate is concentrated under high pressure, using reverse osmosis. Finally, the concentrated butanol solution phase separates and is further purified via distillation (Huang *et al.*, 2014; Abdehagh *et al.*, 2014). However, due to the high pressures needed in the reverse osmosis process, it would probably be less economic than pervaporation (Huang *et al.*, 2014). It is however a mature technology that's already industrially applied for water desalination and thus easy applicable on short term (Huang *et al.*, 2014).

2.4 Adsorption: materials

Besides the separation techniques discussed in the previous paragraph, butanol purification via adsorption can also be used in an integrated butanol separation process. In a typical batch adsorption setup, a liquid or gas mixture is fed to a column packed with a fixed bed of a porous material. The different mixture components interact with the surface of this porous material and are in this way be adsorbed on the surface of the material. After a certain amount of time, all of the packed bed is saturated with one or a few of the mixture components, causing breakthrough of these components at the end of the column. When the column is completely saturated, it can be regenerated for further use. Selective adsorption of one or more of the mixture components thus leads to separation of the mixture (Ruthven *et al.*, 1984).

Qureshi *et al.* (2005) compared the energy needed for adsorption with other common separation processes. Starting from mass and energy balances, the amount of energy necessary for butanol separation via adsorption was estimated to be 1.948 kcal/kg. The energy needed for steam stripping distillation was calculated to be 5.789 kcal/kg. For separation via gas stripping or pervaporation 5.220 kcal/kg and 3.295 kcal/kg butanol are respectively required, making adsorption an energetically interesting separation technique.

In this paragraph, different types of adsorbents used in the separation of solvents from the ABE fermentation broths will be discussed. Mainly liquid phase ABE adsorption will be discussed, since few research has been performed on vapor phase separations. In the next paragraph a brief overview of different adsorption column regeneration methods will be given with an emphasis on simulated moving bed adsorption. Simulated moving bed chromatography will be discussed since this unit operation uses a combination of different adsorption columns in one setup. The use of different columns with different adsorbents might be interesting for efficient separation of the ABE solvents (Cousin Saint Remi *et al.*, 2012). However, very few research on the use of different adsorption columns in one configuration is published, making simulated moving bed chromatography the closest related subject to discuss.

2.4.1 Zeolites

Zeolites are crystalline, microporous adsorbents with SiO_4 and AlO_4 tetrahedra as basic building blocks, creating an open crystal lattice with pores of the same dimension as the adsorbing molecules (Ruthven, 1984). These silica and alumina polyhedra form so called secondary building units, forming the basis of the zeolite crystal structure. Since the porosity of these materials is embedded in their crystal structure, a very small pore size distribution and thus high selectivity can be attained (Ruthven, 1984). Since the positive alumina ion only has a charge of +3, the incorporation of alumina tetrahedra leads to the introduction of a negative charge in the zeolite framework. This negative charge is compensated by the incorporation of positive ions, such as Na^+ (Ruthven, 1984). The ratio of Si/Al that is incorporated in the zeolite structure thus also determines the polarity of the material and its affinity for different adsorbents. This is the reason why in ABE separations, zeolites with a high Si/Al ratio are used **(**Qureshi *et al.*, 2004; Oudshoorn *et al.*, 2009; Cousin Saint Remi *et al*, 2012.; Abdehagh *et al.*, 2013; Faisal *et al.*, 2013; Farzaneh *et al.*, 2015**)**. A higher amount of silica in the zeolite crystals leads to a less polar crystal structure and thus a higher affinity for butanol, which is the least polar molecule of acetone, butanol and ethanol.

The reference materials used in aqueous butanol separations and used to benchmark other adsorbents are zeolites of the ZSM-5 type with a high silica to alumina ratio (Qureshi *et al.*, 2004; Oudshoorn *et al.*, 2009; Cousin Saint Remi *et al*, 2012.; Abdehagh *et al.*, 2013; Faisal *et al.*, 2013; Farzaneh *et al.*, 2015). These zeolites are also called MFI zeolites or, when the crystal lattice exists of only Si, silicalite (Farzaneh *et al.*, 2015). Figure 2.8 depicts the pore structure of the ZSM-5 zeolite, with the different pores connected via channels. These channels typically have a diameter of about 6 Å (Ruthven, 1984).

Oudshoorn *et al.* (2009) compared three types of zeolites: a ZSM-5 type, a Y type and Beta type zeolite. Different types of model mixtures were used, from pure single component to real fermentation broth samples. Multicomponent isotherms were also fitted using multicomponent Langmuir and ideal adsorbed solution theory (IAS). Although the ZSM-5 zeolite shows the lowest butanol adsorption capacity in gas and liquid phase adsorption, it has the lowest water adsorption capacity, making it more selective. The ZSM-5 zeolite was shown to have a higher affinity for butanol, followed by acetone and ethanol. When using fermentation broth, competitive adsorption between butyric acid and butanol is observed.

ZSM-5 and a H-SDUSY type zeolite were compared by Saravan *et al.* (2009) in the form of extrudates for butanol recovery from ABE fermentation broth. ZSM-5 is identified as being more efficient for butanol recovery and was studied in detail performing breakthrough experiments and modelling these breakthrough curves. Different sizes of extrudates were compared, with the extrudates of a size between 0.71 and 1.0 mm being the most interesting, by giving the best trade-off between pressure drop and kinetic adsorption limitations. Modelling of the experimental breakthrough curves using a linear driving force (LDF) model, a basic packed bed mass balance and Langmuir isotherms shows mass transfer in the solid phase limiting adsorption kinetics.

Faisal *et al.* (2013) studied a ZSM-5 zeolite with high silica to alumina ratio for butanol separations from ABE model solutions. Pure component isotherms as well as isotherms on model solutions are measured. Also, the adsorption capacity of acetic and butyric acid is determined. The ZSM-5 zeolite shows a high adsorption capacity for butanol compared to acetone and ethanol. Butyric acid, a precursor of butanol, also adsorb on the zeolite at low pH. However, when the pH is elevated to 6, the adsorption capacity of butyric acid drops significantly, indicating the importance of pH on adsorption selectivity.

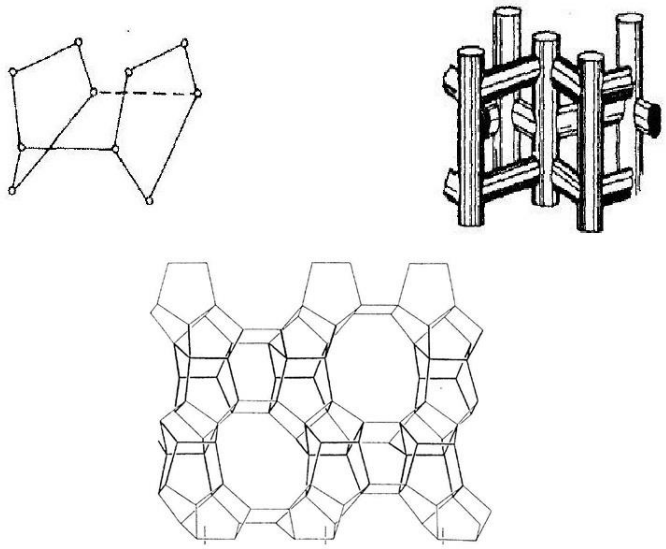

Figure 2.8: Upper-left**:** Secondary building unit of ZSM-5 zeolite. The lines represent the diameter of an oxygen atom, whilst the dots represent a Si or Al atom. From: Ruthven (1984). Upper right: Channel structure within the ZSM-5 crystals. From: Ruthven (1984). Under: Pore structure of the ZSM-5 zeolite with the secondary building units depicted in black. From: Ruthven (1984).

Silicalite, the pure silica analogue of ZSM-5, was studied by Farzaneh *et al.* (2015). Vapor phase adsorption of a water-butanol mixture using attenuated total reflectance fourier transformed infrared spectroscopy was studied. A silicalite film was used with application in adsorption as well as pervaporation in mind. When performing single component adsorption, a butanol adsorption capacity of 133 mg/g at 35°C is measured. The selectivity for water-butanol separation is measured to be 107 at 35°C.

Silicalite and ZSM-5 were also screened by Abdehagh *et al.* (2013) for selective butanol adsorption in liquid phase. In this study, another type of zeolite was also tested (NaY) and also carbon nanotubes and two types of active carbon. On these adsorbents, kinetic and equilibrium experiments were performed. Of the three tested zeolites, silicalite shows the fastest adsorption kinetics, with a first-order time constant of 32.5 min, the time necessary to reach 63.5% of the maximum adsorption capacity in batch adsorption. Interestingly, it is observed that at low concentration the adsorption capacity for butanol on ZSM -5 is lower than on silicalite, but at a higher concentration silicalite has a lower adsorption capacity than ZSM-5.

In a recent study, Faisal *et al.* (2016) compared the use of a structured adsorbent (a silicalite film coated on a steel monolith) with standard beads used in liquid phase breakthrough experiments. Results show slightly worse performance for this adsorbent during the adsorption phase, however butanol purity was higher during desorption due to less capillary water being retained in the column.

Further, Dejaco *et al.* (2016) performed a modelling study using Monte Carlo analysis to uncover the mechanisms of butanol adsorption in a binary water mixture on silicalite and an all-silica FER zeolite. Silicalite shows the highest adsorption capacity at low butanol concentration, making it the most interesting material for ABE solvent separations. A clear difference in affinity for different adsorption sites is observed at different amounts of loading for both zeolites, explaining the difficulties sometimes observed in thermally desorbing the ZSM-5 zeolite.

2.4.2 Activated carbon

Activated carbon (AC) is a microporous material made by activation of thermally decomposed carboneous material (Ruthven, 1984). As mentioned before, Abdehagh *et al.* (2013) screened different types of zeolites, activated carbon and carbon nanotubes for use in ABE solvent recuperation. Kinetic experiments showed that the activated carbons F-400 andF-600 show much faster butanol adsorption kinetics from a watery solution compared to the ZSM-5, NaY and silicalite zeolite adsorbents. Since activated carbon F-400 shows the largest adsorption capacity, this material was subsequently used by Abdehagh *et al.* (2013) for further research. Equilibrium experiments show selectivity of the adsorbent towards butanol and butyric acid compared to other fermentation broth components such as xylose, glucose, butyric acid, acetic acid, ethanol and acetone. Also the adsorption isotherms of binary mixtures of butanol and these components show no significant decrease in adsorption capacity for butanol compared to the single component isotherm (Abdehagh *et al.*, 2013).

In a subsequent study, Abdehagh *et al.* (2015) used AC F-400 in and adsorption breakthrough setup to test the influence of different desorption parameters on butanol recovery from butanol – water and ABE model solutions. Desorption was performed using CO_2 as purge gas and subsequent condensation of the desorbed butanol. Using a butanol concentration of 15 g/l and optimal desorption conditions, a butanol recovery of 82% can be attained. After performing different adsorption-desorption cycles, the adsorption capacity and recover stays relatively constant, indicating no significant decrease in quality of the material during use. Adsorption using an ABE model solution confirms the high affinity of the adsorbent for butanol and butyric acid. To support future modelling of adsorption on AC F-400, Abdehagh *et al.* (2016b) also fitted different multicomponent isotherms on their experimental data.

Recently, AC F-400 was used as an adsorbent for the recovery of butanol in combination with gas stripping (Abdehagh *et al.*, 2016a). In this study, CO_2 was used as carrier gas and the adsorption capacity was shown to be higher in gas phase than in liquid phase for binary butanol-water mixtures. When using ABE model solutions containing acetic and butyric acid, these acids are not found in the stripping gas, which is important, since these components are further transformed into ethanol and butanol by the fermenting microorganisms (Yukihiro *et al.*, 2013). Using gas stripping, gas phase breakthrough experiments on this adsorbent show that acetone and ethanol are completely displaced by butanol (Abdehagh *et al.*, 2016a).

Another type of AC, CR2050C-75, was investigated by Cao *et al.* for vapor phase butanol adsorption (2015a, 2015b). This active carbon shows a high surface area and a high micropore volume, much higher than that of ZSM-5 (Cao *et al.*, 2015a). By using hydrothermal treatment with H_2O_2, the native active carbon was modified, increasing surface area and micropore volume, but decreasing butanol adsorption capacity (Cao *et al.*, 2015a). Increasing the AC adsorption capacity via surface oxidation was again attempted in a subsequent study using a HNO_3 solution (Cao *et al.*, 2015b). However, the same trend is visible as for H_2O_2 modification: the surface area of the adsorbent increases, but the capacity for butanol decreases.

2.4.3 Polymers

Different polymeric resins have also been tested on their butanol adsorption capacity. For instance, Yang *et al.* (1994) used polyvinylpiridine (PVP) as adsorbent in an integrated batch fermentation process. Equilibrium as well as kinetic experiments were performed. The ABE solvents, acetic and butyric acid are observed to adsorb on the resin, but not glucose and other medium sugars. However, the resin shows to have a higher affinity for butyric acid then butanol. When the PVP is added to the fermentation broth at the start of the batch fermentation, a decrease in lag phase and the formation of biofilm around the adsorbent particles is observed. This effect led to an increase in cell growth rate

upon the addition of PVP. Product inhibition by acids and solvents is also relieved by removal of these components from the fermentation broth during the fermentation. Also, the total productivity increases by 130% and final product concentration by 54%, when *in situ* adsorption is applied.

Nielsen *et al.* (1988) screened different polymeric resins for butanol adsorption: Amberlite XAD-7 and XAD-4, Bonopore and nitrated Bonopore. When measuring single and multiple component isotherms, XAD-4 and Bonopore are identified as having the highest adsorption capacity. XAD-4 however, is shown not to be biocompatible with the clostridial strains used in ABE fermentation. Butyric acid and acetic acid are competitively adsorbed as well, an increase in pH however leads to a severe decrease in adsorption of these acids. Bonopore was then subsequently tested in integrated batch fermentation, leading to an increase in productivity.

Lin *et al.* (2012a, b) also screened three different types of polymeric adsorbents for selective butanol adsorption. The three tested adsorbents were H-511, KA-I (both polystyrene diethybenzene) and XD-41 (a cross-linked polyamide). The hydrophobic H-511 and KA-I resins show the highest adsorption capacities for butanol. Further research was performed on the KA-I resin, since this resin had a higher adsorption capacity in the low butanol concentration range (Lin *et al.*, 2012b). Single component isotherms of the most important fermentation broth components were also measured, confirming the high affinity of the resin for butanol and also indicating a high butyric acid adsorption capacity. Acetone and acetic acid also have a relative large adsorption capacity. Breakthrough experiments with ABE model mixtures of different ABE concentrations confirm the selectivity of the resin towards butanol, with acetone and ethanol adsorbing, but being displaced by butanol. To simulate real fermentation conditions, samples of the fermentation broth at different stages of a batch fermentation were also tested, confirming previous results. Different solvents were subsequently tested for butanol recovery, with methanol being the cheapest and most interesting one, leading to a recovery of 95%. Also, during different adsorption and desorption cycles, the performance of the adsorbent stays the same (Lin *et al.*, 2012b).

The kinetics and adsorption isotherms of the ABE solvents on KA-I were further studied by Lin *et al.* (2012a). Interestingly, the adsorption capacity of the resin increases with temperature. This can be explained by the influence of solubility on adsorption. The solubility of butanol in water decreases with higher temperature, leading to an increase in adsorption capacity. Since a higher temperature also positively influences adsorption kinetics, adsorption at higher temperature might be interesting in industrial application. In a subsequent study, Lin *et al.* (2013) investigated the influence of operational parameters on the breakthrough behavior of butanol in a fixed bed KA-I adsorption column. Increasing the initial butanol concentration and column length and decreasing the total flow rate led to an increased adsorption capacity on the resin.

Liu *et al.* (2014) combined the use of a biofilm reactor, a fixed bed KA-I column and methyl viologen to optimize an ABE fed-batch fermentation. In a first step, however a planktonic batch fermentation was performed with addition of the adsorbent to the reactor. The timing of adsorbent addition turns out to be crucial, as addition during the acidogenic phase leads to a decrease in butanol production due to adsorption of butyric acid. Subsequently, using the fed-batch biofilm reactor with fixed bed KA-I adsorption, a total solvent concentration of 59.8 g/l is achieved. This is almost three times the amount achieved during batch fermentation. When also taking acetone inhibition into account, and replacing the KA-I column by a fully desorbed column before full butanol breakthrough, the solvent yield can be increased even further. Finally, addition of methyl viologen increases the ABE productivity even further, by changing the redox balance of the used clostridial strain (Yukihiro *et al.*, 2013). Liu *et al.* clearly showed that not only the use of an improved production strain is important, but also that a good process design and setup can greatly increase the performance of the ABE fermentation process.

Wu *et al.* (2015) further modelled the breakthrough behavior of different ABE mixtures on the KA-I (single component, binary, ternary) using a simple mass balance over a packed bed combined with a linear driving force (LDF) model and multicomponent Langmuir isotherms. By fitting experimental data, more or less the same values for this LDF parameter are found for different types of mixtures, indicating independent kinetic behavior of adsorption of the different mixture components. Further, in binary butanol-ethanol mixtures, a higher adsorption capacity for butanol is observed than in single component breakthrough experiments, indicating enhanced adsorption of butanol on the KA-I resin by ethanol.

2.4.4 Metal-organic frameworks

Metal-organic frameworks (MOF) are another type of microporous adsorbents consisting of organic ligands linked by transition metals (Van der Perre *et al.*, 2015). The zeolitic imidazolate frameworks (ZIF) are a special class of MOFs adapting zeolitic structures. The basic building blocks of ZIFs are tetrahedral transition metals, such as Zn and Co, that are linked by imidazolate ligands. The angle between the linkers and metal ions resembles the Si-O angle found in zeolitic materials (Park *et al.*, 2006).

Cousin Saint Remi *et al.* (2011,2012) studied the use of ZIF-8 as an adsorbent for butanol purification and proposed a butanol purification mechanism using the ZIF-8 MOF and the SAPO-34 zeolite. In a first study, adsorption isotherms in vapor and liquid phase were measured on ZIF-8, showing an S-shaped isotherm for butanol (Cousin Saint Remi *et al.*, 2011). Intriguingly, the adsorption capacity for butanol in isobutanol (a non-adsorbing solvent) was lower than in water, clearly indicating the importance of solvent effects on adsorption. Breakthrough experiments confirm the capability of ZIF-8 for butanol separation from ABE mixtures (Cousin Saint Remi *et al.*, 2011).

In a subsequent study, comparing ZIF-8 to silicalite and an active carbon adsorbent, ZIF-8 is again shown to have the greatest adsorption capacity for butanol (Cousin Saint Remi *et al.*, 2012). The effect of other fermentation broth components was also considered in this study, but no decrease in adsorbent capacity is observed. A non-optimized desorption procedure is also proposed, using a stepwise increase of temperature and an inert nitrogen gas flow. Subsequently, use of the zeolite SAPO-34 is proposed to further purify the desorbed butanol stream. SAPO-34 selectively adsorbs alcohols and water up to ethanol. Alcohols with an alkyl chain larger than three methyl groups are not or poorly adsorbed on this zeolite (Daems *et al.*, 2007; Remy *et al.*, 2011). SAPO-34 can thus be used to remove ethanol from the butanol-ethanol mixture resulting from ZIF-8 desorption, as confirmed by Cousin Saint Remi *et al.* (2012). Further, Fan *et al.* (2012) used ZIF -8 to create a mixed PDMS membrane for selective biobutanol pervaporation.

Zhang *et al.* also identified ZIF-8 as being an interesting adsorbent for butanol separation (2013a). In another study by Zhang *et al.* (2013b), ZIF-8, ZIF-71 and ZIF-90 were evaluated for use in butanol recovery. Using ideal adsorbed solution theory (IAST), vapor phase selectivities were calculated starting from single component isotherms. Both ZIF-8 and ZIF-71 show a very low affinity for water. ZIF-90 however, has a significant affinity for water at higher vapor pressures, making it not useful for vapor phase butanol recovery. ZIF-8 and ZIF-71, however, show high butanol-water selectivity, making them interesting candidates for butanol recovery (Zhang *et al.*, 2013b). Further, Li et al (2014) used ZIF-71 to prepare a mixed PDMS membrane for *sec*-butanol separation via pervaporation.

Another MOF that can possibly be applied in biobutanol purification is ZIF-68. Vapor phase isotherms indicate a higher adsorption capacity for butanol as compared to ethanol at low vapor pressures. Further, liquid phase adsorption isotherms on a mixture of ethanol, butanol and water also indicate a higher capacity for butanol (200 mg/g) than for ethanol (40 mg/g). However, water stability of ZIF-68

is observed to be lower than ZIF-8, which can be a possible issue regarding butanol recovery (Van der Perre *et al.*, 2014).

Most of the adsorbents discussed in paragraph 2.4 are listed in table 2.3 with their respective butanol adsorption capacities from different mixtures.

2.5 Adsorption: column regeneration methods

The research performed during this Master's thesis was focused around the use of a combination of different adsorption columns towards the effective separation of the different ABE solvents. Therefore, a small review on the different methods to regenerate adsorption columns is given. First, cyclic batch processes are briefly discussed. Subsequently an overview of the use of simulate moving bed systems is given, with a focus on biofuel separations.

2.5.1 Batch regeneration of adsorption columns

The simplest adsorptive processes are employed in a batch fashion. A continuous feed of a certain mixture is fed to an adsorption column. After a certain amount of time, the adsorptive material is completely saturated and breakthrough of the mixture components is observed. At this point, continuous feed to the column is stopped and the saturated column is regenerated. The compound of interest can be the adsorbed species or can be the first component to break through. Since a column in desorption phase can't be used during adsorption, different columns have to be used in parallel in a continuous production system. Figure 2.9 compares this cyclic batch operation with a theoretical continuous operation (see also simulated moving bed chromatography). Four basic types of column desorption methods exist: thermal swing, pressure swing, pure gas stripping and displacement desorption (Ruthven *et al.*, 1984).

During thermal swing desorption, the adsorption column is purged using a hot gas or liquid and thus effectively desorbing the adsorbed compounds by shifting the thermodynamic equilibrium. Pressure swing desorption is used only for gaseous components and is performed by lowering the pressure in the adsorption column and purging with an inert gas stream. This process is performed isothermally. Just as for other two techniques mentioned, purge gas stripping is performed by just flushing the column with an inert gas stream. However, temperature or pressure is not changed during desorption. This technique can only be used for weakly adsorbed components. Finally, using displacement desorption, a component with a high affinity for the adsorption column is used to displace the adsorbed compounds. This method is used in displacement chromatography (Ruthven *et al.*, 1984).

Table 2.3: Adsorbents used in biobutanol separation with mentioned adsorption capacities. Adapted from Abdehagh *et al.* (2014). R.T. indicating room temperature

Adsorbent	Butanol adsorption capacity (mg/g)	Butanol or ABE concentration	Type of mixture	Temperature (°C)	Reference
ZSM-5 zeolite	120	batch – fitted qmax	Butanol	R.T.	Faisal *et al.* 2013
	110	20 g/l	ABE	R.T.	Faisal *et al.* 2013
	120	pure	Butanol (vapor)	25	Oudshoorn *et al.* 2009
	139	10 g/l	Butanol – water	R.T.	Abdehagh *et al.* 2013
Silicalite	133	batch – fitted qmax	Butanol (vapor)	35	Farzaneh *et al.* 2015

Adsorbent	Butanol adsorption capacity (mg/g)	Butanol or ABE concentration	Type of mixture	Temperature (°C)	Reference
Silicalite	103	10 g/l	Butanol	R.T.	Abdehagh *et al.* 2013
	-	2 wt%	Butanol – water (vapor)	35	Farzaneh *et al.* 2015
	56	0.2wt% butanol	ABE	30	Faisal *et al.* 2016
Beta zeolite	340	pure	Butanol (vapor)	25	Oudshoorn *et al.* 2009
	120	pure	Butanol	25	Oudshoorn *et al.* 2009
Y zeolite	370	pure	Butanol (vapor)	25	Oudshoorn *et al.* 2009
	160	pure	Butanol	25	Oudshoorn *et al.* 2009
	107	10 g/l	Butanol – water	R.T.	Abdehagh *et al.* 2013
AC F-400	258	10 g/l	Butanol – water	R.T.	Abdehagh *et al.* 2013
	220	0.1 mg/l	ABE fermentation broth (vapor)	37	Abdehagh *et al.* 2016
ACF-600	149	10 g/l	Butanol – water	R.T.	Abdehagh *et al.* 2013
AC CR2050C-75	259.6	Pure	Butanol (vapor)	24	Cao *et al.* 2015a
XAD -4	69	2 wt%	Butanol – water	R.T.	Nielsen *et al.* 1988
XAD-7	83	2 wt%	Butanol – water	R.T.	Nielsen *et al.* 1988
Bonopore	74	2 wt%	Butanol – water	R.T.	Nielsen *et al.* 1988
Nitrated Bonopore	55	2 wt%	Butanol – water	R.T.	Nielsen *et al.* 1988
XD-41	127	fitted q max	Butanol – water	25	Lin et al (2012b)
KA-I	167	fitted q max	Butanol – water	25	Lin et al (2012b)
	99	20 g/l	ABE	25	Lin et al (2012b)
ZIF-8	300	3.5 wt%	ABE	R.T.	Cousin Saint Remi *et al.* 2012
ZIF-68	200	-	Ethanol-butanol-water	R.T.	Van der Perre *et al.* (2014)
H-511	206	fitted q max	Butanol – water	25	Lin et al (2012b)

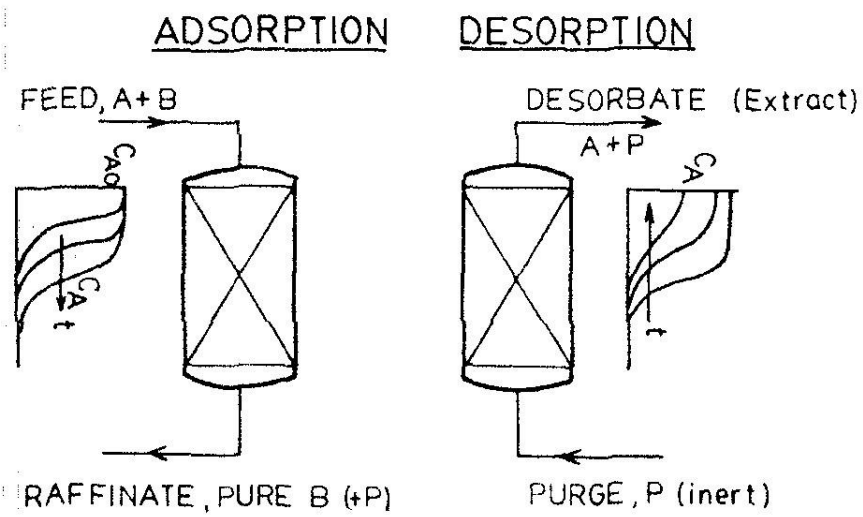

Figure 2.9: Cyclic batch operation of adsorption columns with an adsorption and desorption step. From: Ruthven *et al.* (1984).

2.5.2 Simulated moving bed chromatography

As mentioned in the previous paragraph, traditional breakthrough operational setups are operated in a cyclic batch fashion. Similarly, in preparative chromatography, a comparable system of batch elution is used (Seidel-Morgenstern *et al.*, 2008). In theory, a counter current adsorption system could be developed for continuous operation (Ruthven *et al.*, 1984; Seidel-Morgenstern *et al.*, 2008; Gomez & Rodrigues, 2012). This operational setup, also called true moving bed chromatography will first be explained. Since this setup can't be realized in practice, a technique called simulated moving bed (SMB) chromatography is used and will be discussed subsequently.

2.5.2.1 True moving bed chromatography

As mentioned before, chromatography in a continuous fashion would be possible by moving the adsorbent bed in a counter current fashion to the mobile phase. Such a theoretical system for the separation of a binary mixture is depicted in Figure 2.10. The binary mixture is fed to the center of the moving bed. One of the components (B) has a high affinity for the adsorbent, whilst the other component (A) has a lower affinity. The velocity of the moving fixed bed and the used eluent are chosen in such fashion that the most retained component B moves together with the fixed bed towards the exit for the extract. Component A is less strongly adsorbed and thus moves in the direction of the exit for the raffinate. Both the used adsorbent and the eluent are recycled in a counter current fashion (Seidel-Morgenstern *et al.*, 2008; Gomes & Rodrigues, 2011).

By operating the column in this way, four distinct zones are formed in the adsorption column, as shown in Figure 2.10. Separation of the two components A and B takes place in zone II and III, with component B moving in the direction of the extract outlet and component A moving in the direction of the raffinate outlet. Zone I is used for adsorbent regeneration, any residual adsorbed components are desorbed in this zone by fresh and recycled eluent. Recycling of the desorbent happens in zone IV, where any components still present in the used solvent are adsorbed on regenerated adsorbent. The concentration profiles in the different column zones are shown in Figure 2.10 (Seidel-Morgenstern *et al.*, 2008; Gomes & Rodrigues, 2011).

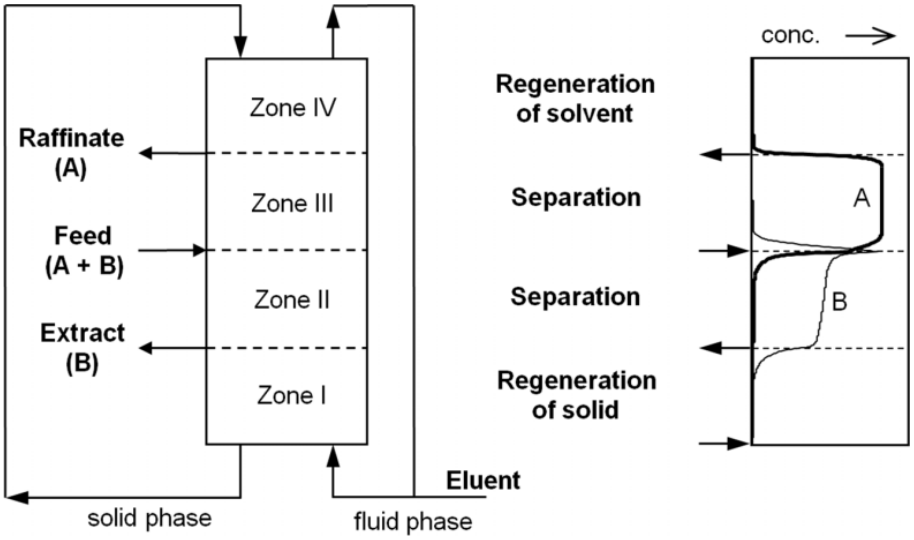

Figure 2.10: Left: a theoretical total moving bed setup with four different functional zones. Right: internal concentration profile for this kind of separation. From: Seidel-Morgenstern *et al.* (2008).

2.5.2.2 Simulated moving bed chromatography

Continuous recycling of the solid adsorbent is not possible in practice due to the fragility of the solid phase, making it difficult to transport (Seidel-Morgenstern *et al.*, 2008; Gomes & Rodrigues, 2011). To overcome this problem, some sort of discretization of the different zones shown in figure 2.10 is performed. Instead of using one single column with moving adsorbent, different columns in series are used, with the different outlets and inlets located at the beginning or ends of the different columns. Also, instead of switching the positions of the columns, the positions of inlets and outlets are switched after a certain amount of time, giving the same result as a counter current movement of the columns. An example for a SMB system with six columns is shown in figure 2.11. The positons of the inlet and outlet feed, extract, raffinate and eluent flows are shown after each switch of position (Seidel-Morgenstern *et al.*, 2008; Gomes & Rodrigues, 2011).

Using the simplest operational mode, all of the inlet and outlet flow rates are constant and their positions are switched after a constant amount of time. However different modifications have been made to these operational conditions to improve separation efficiency. For instance, the internal flow rates can be varied during operation (PowerFeed process). Another possible operational parameter that can be tuned is the inlet concentration (ModiCon process), which is especially interesting for components showing non-linear adsorption behavior. A final possibility of operational tuning is the use of asynchronous shifts of inlet and outlet ports, leading to variability in the length of the different zones of the SMB (Seidel-Morgenstern *et al.*, 2008; Gomes & Rodrigues, 2011). Many other modifications of the SMB chromatography process exist, including the use of solvent gradients for separations as well as the use of SMB for the separation of ternary mixtures. These processes are reviewed in more detail by Seidel-Morgenstern *et al.* (2008) and Gomez & Rodrigues (2012).

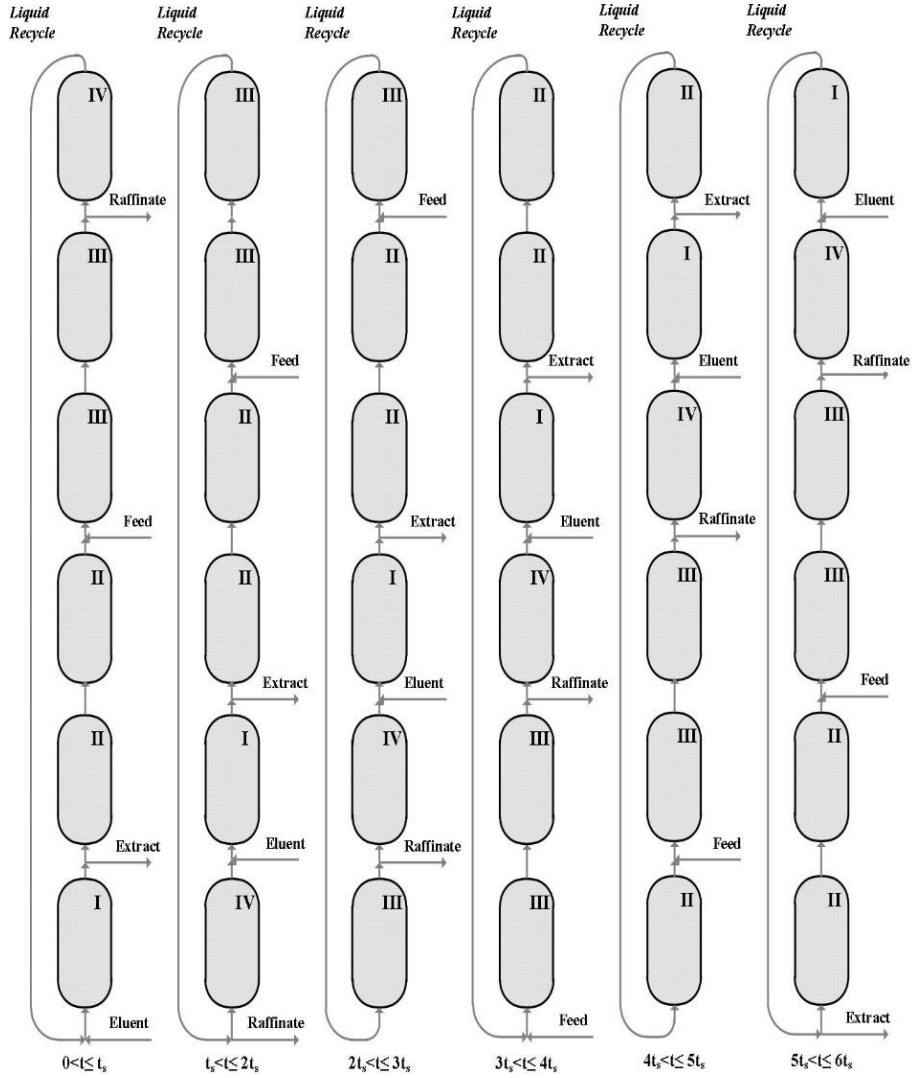

Figure 2.11: Six column SMB chromatography system with different input and output positions during operation shown. From: Gomez & Rodrigues (2012).

2.5.2.3 Use of SMB chromatography in biofuel production

Use of simulated moving bed technology in biofuel production is twofold. First of all, it can be applied as separation technology in the production of fermentable sugars starting from hydrolyzed biomass (Caes *et al.*, 2013; Kim *et al.*, 2015a). A second possible application is the use of simulated moving bed reactors for the production of green chemicals, combining reaction and separation in one integrated process (Geier *et al.*, 2010a; Geier *et al.*, 2010b; Silva *et al.*, 2010). This integration is achieved by either using the same material as catalyst and adsorbent or by combining two different materials in one pellet (Silva *et al.*, 2010).

Kim *et al.* (2015a) optimized a SMB chromatography setup for the separation of a ternary mixture containing galactose, 5-hydroxy-methylfurfural (HMF), levulinic acid. Galactose, 5-HMF and levulinic acid are important products formed during the hydrolysis of agarose produced starting from algal biomass (Kim *et al.*, 2015a). The galactose produced by the hydrolysis of agarose can be used as substrate for bio-ethanol production, however 5-HMF and levulinic acid are important inhibitors of the fermentation process (Kim *et al.*, 2015a). 5-HMF and levulinic acid are also interesting biomass-based platform molecules and could thus also be potentially economically valuable (Olmedo *et al.*, 2014).

Instead of opting for a single SMB setup to separate the complete mixture, Kim *et al.* (2012) proposed a system of two separate SMB chromatography units: one for the separation of galactose from the mixture and one for the separation of 5-HMF and levulinic acid. Interestingly, an open loop SMB setup was used, with a cut-off between zone I and II, as shown in figure 2.12. A Dowex-50WX8 resin was used as solid phase adsorbent. Single component breakthrough experiments were performed first, to generate the model parameters necessary for numerical process optimization. The performance of this modelled system was then verified experimentally, confirming the modelled results and showing the possible economic viability of this setup (Kim *et al.*, 2012).

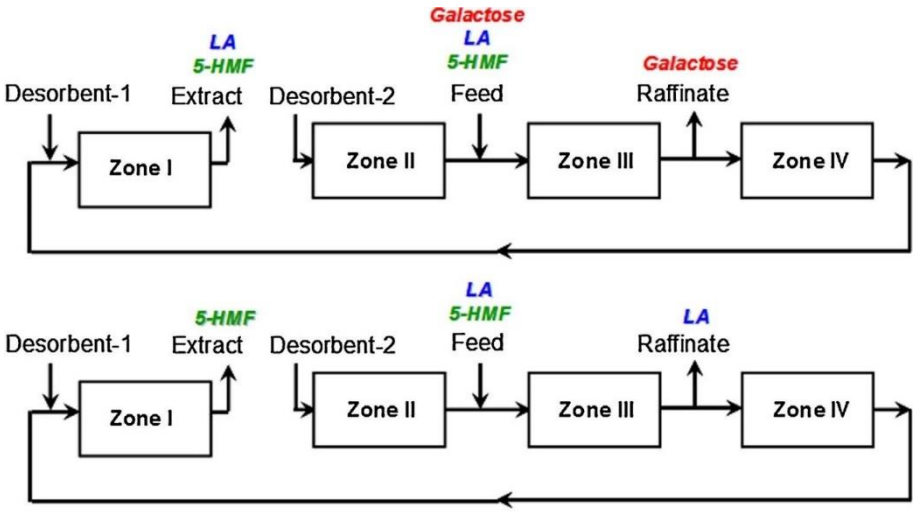

Figure 2.12: Open – loop SMB chromatography setup used by Kim *et al.* (2015a). Upper part: SMB for separation of galactose and the levulinic acid (LA) 5-HMF mixture. Lower part: SMB for separation of LA and 5-HMF. Desorbent 1 and 2 are water. From: Kim *et al.* (2015a).

Caes et al. (2013) applied SMB chromatography in a process to recover fermentable sugars from corn stover hydrolysates. The recovery process consists of two steps. The first step being an acidic hydrolisation using the ionic liquid 1-butyl-3-methylimidazolium chloride ([BMIM]Cl) to simultaneously extract the formed sugars. In a second step, SMB chromatography was used to separate the ionic liquid and the hydrolyzed sugars. The viability of this method was confirmed by using the formed sugars as substrate in a fermentation with *E. coli*.

A variation on SMB chromatography, using the combination of a catalyst and adsorbent, called a SMB reactor can also be used in biofuel production processes. Geier *et al.* (2010a, 2010b) for instance applied for two patents concerning the use of a SMB reactor in the production process of biodiesel.

Silva *et al.* (2010) developed an even more integrated process, combining a SMB reactor with pervaporation for the production of the green solvent ethyl lactate and the biofuel candidate 1,1-diethoxyethane (diethylacetal). The simulated moving bed membrane reactor (PermSMBR) has the same configuration as a standard SMB chromatography or reactor configuration, however each column contains a set of membranes. The catalyst or adsorbent layer is then packed on the inside or outside of the membranes, depending on the selective side of the membrane. Using pervaporation, this leads to an extra gaseous outlet stream on every column. Depending on the application, these streams can also be switched off on certain columns. Figure 2.13 shows a simplified diagram of the PermSMBR configuration.

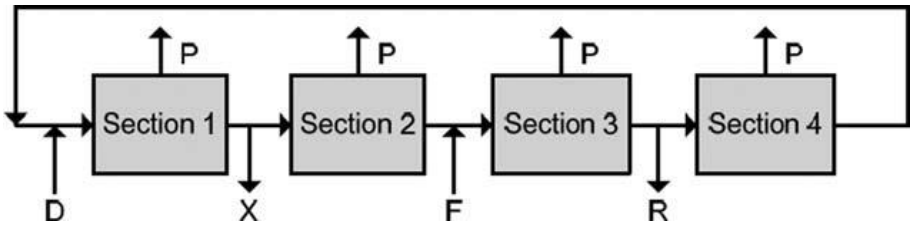

Figure 2.13: Schematic representation of the PermSMBR configuration. D, X, F an R are the desorbent, extractant, feed and raffinate streams also found in standard SMB reactor or chromatography setups. P is the permeate stream from the membranes in every column. From: Silva *et al.* (2010)

A modification of the configuration represented in Figure 2.13 was used by Silva *et al.* (2010) for the synthesis of ethyl lactate. When performing numerical simulations to compare a standard SMB reactor with a four zone PermSMBR, Silva *et al.* (2010) found a clear improvement in productivity using the PermSMBR process. However, a three zone PermSMBR shows worse performance, unless a greater vacuum can be applied to increase pervaporation performance. When comparing PermSMBR to reactive distillation, productivity during reactive distillation is also much higher, due to the higher temperatures used in this process. However, ethanol consumption is much lower using the PermSMBR process. Also, when comparing a standard SMB reactor with PermSMBR for diethylacetal, Silva *et al.* (2010) found a higher productivity and lower ethanol consumption for the PermSMBR process.

3. Goal

As was discussed in detail in the previous chapter, the butanol production process via ABE fermentation suffers from product inhibition. To relieve this product inhibition, gas stripping is an interesting *in situ* recovery technique, but suffers from low selectivity (Abdehagh *et al.*, 2014). Further simulations using AspenPlus 4.11 showed an enrichment of ABE solvents in the fermenter head space (Gelin, 2015). Most of the scientific literature on adsorptive separations is focused around isotherm or breakthrough measurements. The use of multiple adsorption columns in one configuration has been little reported.

The research performed for this Masters' thesis is thus focused around the development of a multicolumn adsorption process for high-purity butanol recovery from a vapor phase humidified ABE mixture. It is investigated to which extent the combination of microporous solids with different properties (hydrophobicity, pore structure) allows to increase the recovery and purity of the butanol product. Additionally, since CO_2 is an important by-product produced during ABE fermentation (Tashiro *et al.*, 2010; Tashiro *et al.*, 2013), the use of CO_2 as carrier gas during adsorption and desorption of the different used adsorption materials is evaluated.

First of all, four different materials are screened on their affinity for the different ABE components by measuring the vapor phase adsorption isotherms. The influence of CO_2 as carrier gas during these adsorption equilibrium experiments is evaluated. Single-column breakthrough experiments are subsequently performed to analyze the selectivity of these materials in dynamic conditions.

Subsequently, different adsorption columns containing these selective materials are combined in two-column configurations. These combinations were experimentally evaluated on their performance for high-purity butanol recovery. Some of the column combinations could not be tested in the provided experimental setup. Therefore, a third goal was to develop a mathematical model describing the breakthrough behavior of combinations of these different adsorption columns. The model was first validated with multicomponent breakthrough data and then developed in such a way that a qualitative comparison of different configurations was possible.

The work presented in this Masters' thesis is part of the research program of the CHIS department, focused around the use of adsorptive materials in the purification of biochemicals.

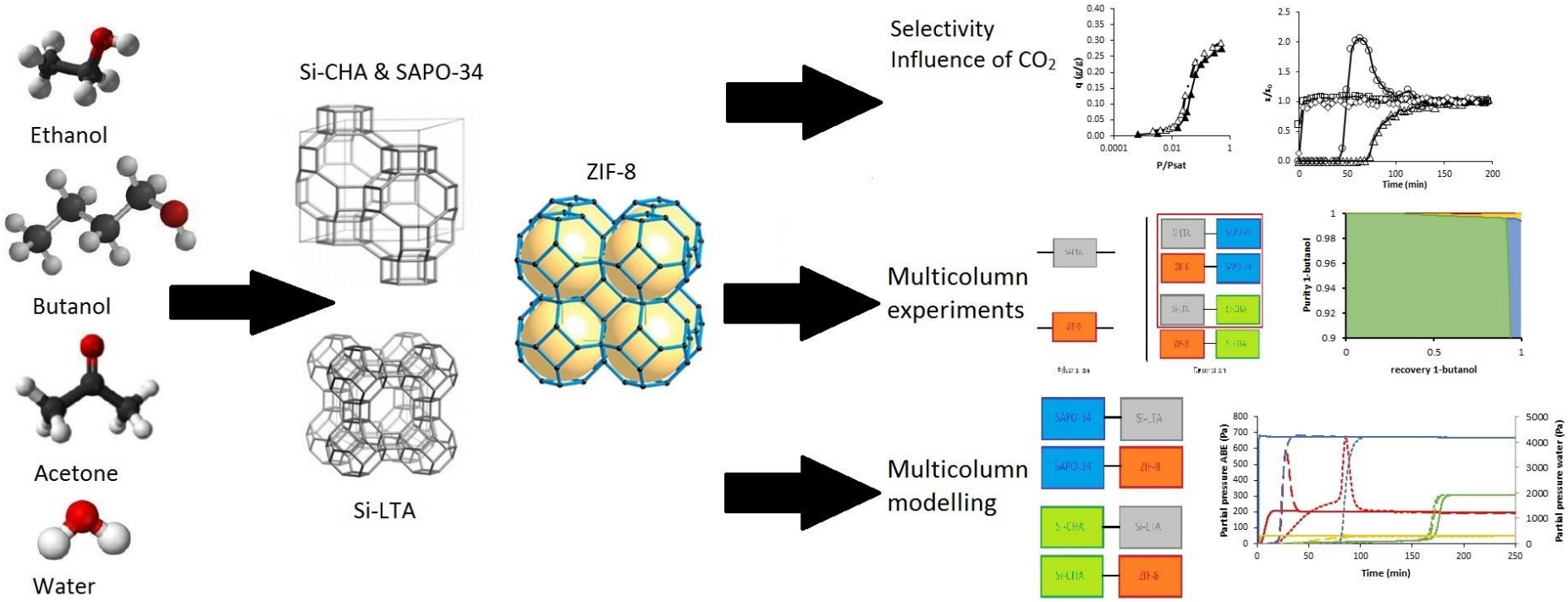

Figure 3.1: Schematic representation of the work presented in this Masters' thesis.

4. Materials & Methods

In the first two sections of this chapter, the different materials (adsorbents and adsorbates) used for the experimental work will be described. The following sections will discuss the experimental breakthrough and modelling methods.

4.1 Adsorbents

Four different adsorbents have been used during this thesis for experimental and modelling study. Three of these adsorbents were zeolites: an all-silica Linde Type A zeolite (Si-LTA), also called ITQ-29 (Technological Institute, Polytechnical University of Valencia, Valencia, Spain), an all-silica chabazite (Si-CHA, Department of chemical and biomolecular engineering, University of Melbourne, Melbourne, Victoria, Australia) and SAPO-34 (ACS Materials, Medford, Massachusetts, USA) which also has the basic chabazite structure. The fourth adsorbent used was a MOF of the ZIF type: ZIF-8 (Sigma-Aldrich, Diegem, Belgium). The basic properties of these adsorbents will be described in the following paragraph.

Both Si-CHA and SAPO-34 are zeolites of the chabazite type. Chabazite zeolites have a three dimensional pore structure with ellipsoidal cages, connected via eight membered ring pores. These eight membered ring pores typically have a size of 3.8 Å x 3.8 Å. Each of these ellipsoidal cages is connected to six neighboring cavities, with a cage size of 6.7 Å x 10 Å. The shape and size of these cages and windows has an in important influence on adsorption and pore diffusion mechanisms (Daems *et al.*, 2007; Denayer *et al.*, 2008; Krishna & Van Baten, 2011).

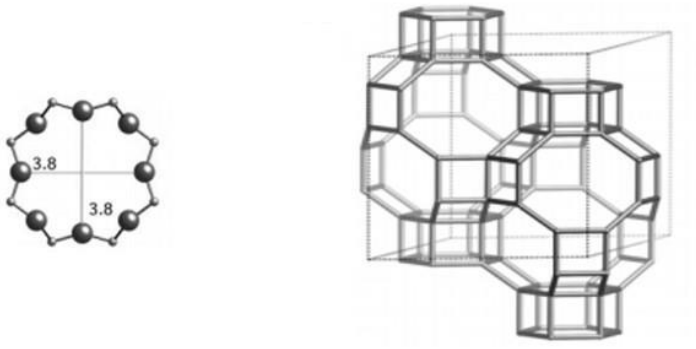

Figure 4.1: Eight membered ring window of a CHA zeolite with dimension of 3.8 x 3.8 Å and cage structure of a CHA type zeolite.

The crystal unit cell of LTA type zeolites consists of two types of cages: an α-cage with a diameter of around 11 Å and a sodalite cage with a diameter of 6.6 Å. This last cage is not accessible for adsorbates. In standard LTA type zeolites, the extra framework cations have an influence on the window size of the cages. The larger the cation, the smaller the window, with Na^+, K^+ and Ca^{2+} leading to 3 Å, 3.8 Å and 5 Å window sizes respectively. However, the all-silica LTA used in this thesis doesn't possess these extra framework cations, leading to the window dimensions of 4.1 Å x 4.1 Å (Gelin, 2015). Figure 4.1 and figure 4.2 show the cages and window openings of a CHA and an LTA zeolite.

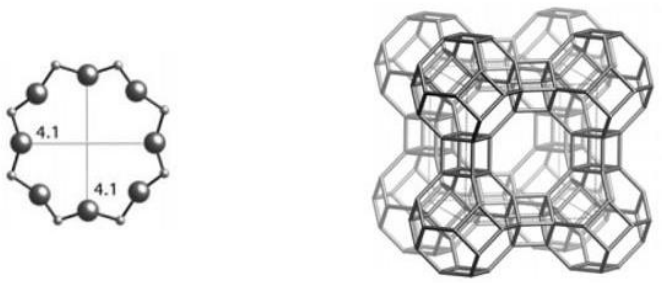

Figure 4.2: Eight membered ring window of a LTA zeolite, with dimension of 4.1 Å x 4.1 Å and cage structure of a LTA zeolite. From: Olson *et al.* (2007).

ZIFs are adsorbents of the MOF family, who crystallize in a structure similar to those of zeolites (Park *et al.*, 2006). ZIF-8 has sodalite cages as fundamental building blocks, generating a structure with cages with a diameter of 12.5 Å (Huang *et al.*, 2006). These cages are connected via hexagonal windows with a size of 3.3 Å (Huang *et al.*, 2006). ZIF-8 is a highly hydrophobic MOF (Küsgens *et al.*, 2008), showing promising results for ABE separations (Cousin Saint-Remi *et al.*, 2011;2012). Moreover, ZIF-8 is a very stable MOF, making industrial application viable (Park *et al.*, 2006). Figure 4.3 shows the cage structure of ZIF-8. The properties of the used adsorbents are summarized in table 4.1.

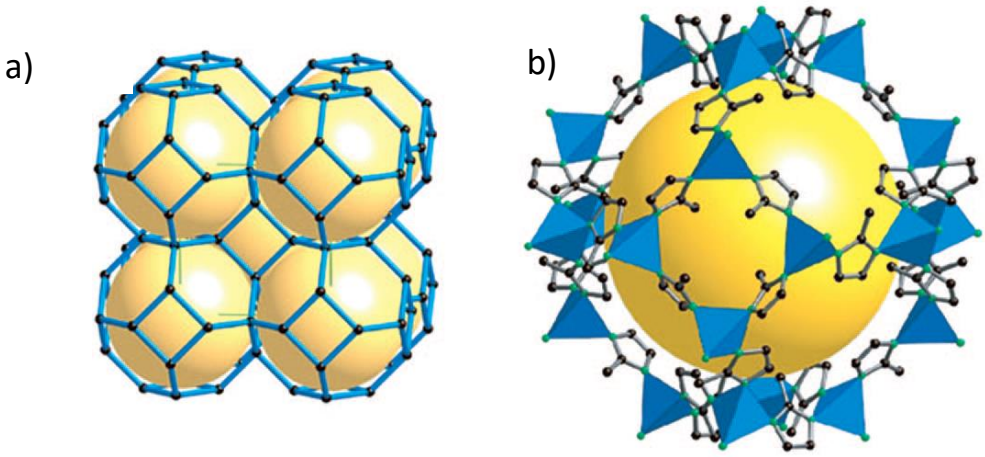

Figure 4.3: a) Cage structure of ZIF-8 as stick diagram. b) Largest cage of ZIF-8 with imidazolate tetrahedra colored blue. From: Park *et al.* (2006).

Table 4.1: Properties of the adsorbents. Adapted from Gelin (2015). SAPO-34 data was obtained from Remy *et al.* (2011) and ZIF-8 data from Küsgens *et al.* (2008).

	Si-CHA	**SAPO-34**	**Si-LTA**	**ZIF-8**
Unit cell formula	$Si_{36}O_{72}$	$Si_{4.02}Al_{18.32}P_{14.58}O_{72}$	$[Si_{24}O_{48}]_8$	$Zn_{12}(MeIm)_{24}$
Pore volume (cm^3/g)	0.27	0.30	0.29	0.64
BET surface area (m^2/g)	718	590	794	1255
Cage dimension	6.7 Å x 10 Å	6.7 Å x 10 Å	11.4 Å x 11.4 Å	12.5 Å
Window dimension	3.8 Å x 3.8 Å	3.8 Å x 3.8 Å	4.1 Å x 4.1 Å	3.3 Å x 3.3 Å

4.2 Adsorbates and carrier gasses

An overview of the other chemicals used for this thesis is given in table 4.2. Deionized water was obtained using a Millipore Simplicity water purifying system (Merck Millipore, Darmstadt, Germany) with a SIMPACKOD2-filter. Table 4.2 summarizes the used adsorbates and carrier gasses.

Table 4.2: Used adsorbates and carrier gasses

Adsorbate	**Purity (%)**	**Supplier**
Acetone	99.5	Fisher Chemical
Ethanol	99.7	VWR Chemicals
1-Butanol	99.5	Sigma-Aldrich
Carrier Gas		
He	99.996	Air liquide
CO_2	99.995	Air liquide

4.3 Measuring of adsorption isotherms

4.3.1 VTI measurements

Vapor phase adsorption isotherms using CO_2 and N_2 were measured for the different aqueous ABE mixture components using a gravimetrical method (VTI, TA-instruments, New Castle, Pennsylvania, USA). The principle of this setup is depicted in figure 4.4. Two types of evaporators are present in the instrument: one for organic components and one for measurements of water isotherms. The chosen carrier gas can be bubbled through the evaporators. This leads to a certain amount of adsorbate in the carrier gas, depending on the temperature of the evaporator. The carrier gas can then be diluted with a second gas stream, or can be directly sent to the oven containing a small pan with adsorbent sample. For water vapor isotherms, a dew point hygrometer is present (Dew Prime I, Edgetech Instruments, Hudson, Massachusetts). The oven temperature controls the temperature at which adsorption takes place and this temperature is controlled using a water bath. Measurement of the sample mass allows the determination of the amount of adsorbate adsorbed.

Vapor partial pressures were calculated from measurement of the evaporator temperature using the empirical Wagner equation (4.1 and 4.2). Coefficients for the calculations were obtained from Poling *et al.* (2001). The amount of mass adsorbed measured by the VTI and the calculated vapor pressure can then be combined to determine the adsorption isotherm. The used Wagner coefficients were valid over the experimental temperature range (Polin *et al.*, 2001).

$$\ln(Pv) = \ln(Pc) + \left(\frac{Tc}{T}\right) * (a * \tau + b * \tau^{1.5} + c * \tau^{2.5} + d * \tau^{5}) \quad (4.1)$$

$$\tau = (1 - \frac{Tc}{T}) \quad (4.2)$$

With:

Pv = vapor pressure (bar)
Pc = Wagner coefficient (bar)
Tc = Wagner coefficient (K)
a = Wagner coefficient
b = Wagner coefficient

c = Wagner coefficient
d = Wagner coefficient

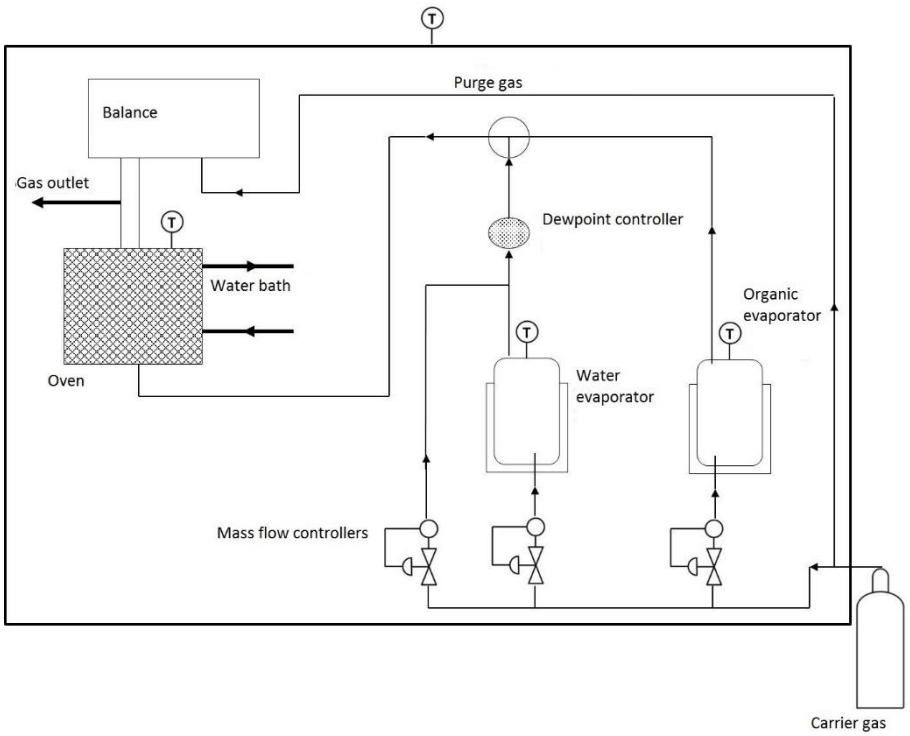

Figure 4.4: Principle of the VTI gravimetric analysis setup. Adapted from: Gelin (2015).

Before start of the measurements, the different adsorbent samples needed to be activated. Activation of the adsorbents was achieved by heating the samples at a 1 °C/min, followed by holding them at constant temperature for a certain amount of time. Final activation times and temperatures for the different adsorbents are shown in table 4.3. The activation procedure was terminated before the end of this final time if no more desorbing mass was measured. Isotherms were only measured on the Si-LTA, ZIF-8 and SAPO-34 samples in powder form.

Table 4.3: Final activation time and temperature for the different adsorbents. Adsorbents were activated using a 1 °C/min temperature gradient.

Adsorbent	Final activation time (min)	Final activation temperature (°C)
Si-LTA	360	350
SAPO-34	360	300
ZIF-8	120	140

4.3.2 IGA measurements

To obtain better isotherm data in the lower pressure region for the adsorption of ethanol on Si-LTA, measurements were performed using an IGA-002 system (Hiden Isochema Limited, Warrington,

England). This system works according to a similar principle as the VTI. A sample pan with sample is loaded into a sample oven and the adsorbed mass is measured, giving rise to the isotherm. On the IGA, however, a vacuum pump is installed, allowing for lower partial pressure to be reached during vapor phase adsorption. Further, no carrier gas is used, since the partial pressure is regulated by the vacuum system. Activation of the Si-LTA sample was achieved by heating the sample at 1 °C/min to a final temperature of 350 °C, which was held for 10 h. The overall layout of this measurement system is shown in figure 4.5. Isotherm measurements were executed under a constant temperature of 40 °C.

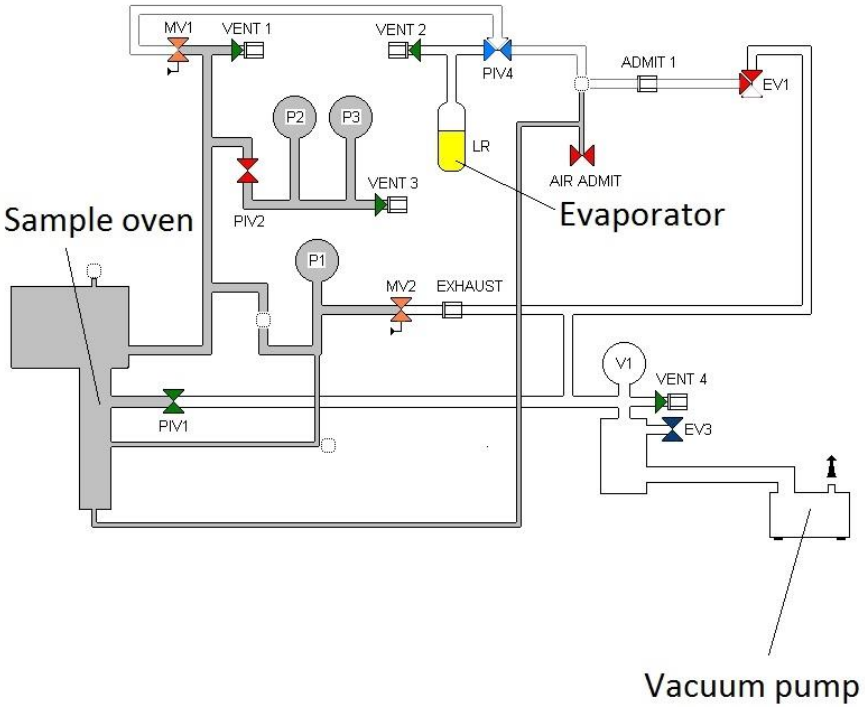

Figure 4.5: Principle of IGA-002 isotherm measurement system.

4.4 Breakthrough experiments

4.4.1 Column packing

Since the pure adsorbent samples were available as powder, pellets were firstly synthesized before packing of the columns for breakthrough measurements. All of the used adsorbent columns had an internal diameter of 2.1 mm and a length of 10 cm. The adsorbent powder was first pressed in a French press (Piqua, Ohio, USA) at a pressure of 5 to 7 kPa. The pressed cakes were then sieved using micrometer sieves. Subsequently, the sieved pellets were packed into an adsorption column. Extra quartz particles were added to the Si-CHA column, since not enough adsorbent material was present to fill the complete column (Gelin, 2015). Two different Si-LTA columns were used. Table 4.4 summarizes the properties of the packed columns.

4.4.2 Activation of adsorption columns

Just as for isotherm measurements, the adsorbents packed in the adsorption columns were activated prior to use in breakthrough experiments. Activation of the columns was achieved by placing them in

an oven under a constant helium flow of 10 ml/min. The columns were heated with a temperature gradient of 1 °C/min to a certain final temperature, this final temperature was then held constant during a certain amount of time, followed by controlled cooling of the column at 1°C/min to 40 °C. The ZIF-8 column and the repacked Si-LTA were activated for 120 min at a final temperature of 150 °C and 180 min at a final temperature of 200°C respectively. Temperature of the SAPO-34 was first held for 10 min at 40°C, followed by a temperature ramp of 0.5 °C/min and was subsequently held for 180 min at 80 °C.

Table 4.4: Properties of the used adsorption columns.

Column	Pellet size (µm)	Adsorbent mass (mg)
Si-LTA	250-500	108
Si-LTA	250-500	91
Si-CHA	250 <	49
ZIF-8	250-280	70
SAPO-34	250-450	230

4.4.3 Principle and setup

Breakthrough experiments were performed to compare the difference in separation performance using He and CO_2 as carrier gas and to investigate separation efficiency in a multicolumn adsorption-desorption process. During a breakthrough experiments, a mixture of different components is continuously transported by a liquid or gas phase over a packed column. This leads to a step in concentration at the entrance of the column at the beginning of the experiment. Due to their different affinity for the packed adsorbent material, different amounts of the different mixture components are adsorbed. This leads to a concentration front of the different components moving through the column at different velocities. Components with a low adsorption capacity move faster through the column, since the adsorbent is saturated faster by these compounds. When the adsorbent is completely saturated with a compound, presence of this component can be measured at the end of the column in the liquid or gas phase, leading to a so called breakthrough curve. In some cases, when the different adsorbates compete for the same adsorption sites in the adsorbent, roll-up of the breakthrough curve can be observed. Roll-up is a phenomenon caused by the “pushing out” of weaker adsorbed components by stronger adsorbed components who compete for the same adsorption sites, leading to an increase in concentration of these weakly retained components at the end of the column. The concentration observed at the column outlet in this way becomes larger than the concentration at the inlet.

A vapor phase breakthrough setup was used as schematically shown in figure 4.5. A chosen carrier gas (He or CO_2) could be sent to four separate mass flow controllers (Bronkhorst, Ruurlo, Netherlands). Gas flowing through the first two mass flow controllers could be sent to two separate evaporators, each with their own oil bath heating system (Julabo, Seelbach, Germany). By fixing the evaporator temperature, the vapor pressure of the component or mixture present in the evaporator could be regulated. The carrier gas flowing to the third mass flow controller could be used to dilute the gas streams coming from both evaporators. Gas flows from these first three mass flow controllers were mixed and directed towards a first switching valve. Carrier gas coming from the fourth mass flow controller was sent directly to this valve. By changing its position, either carrier gas with or without mixture could be sent over the adsorption column. If necessary, the carrier gas sent through the fourth mass flow controller could be connected to a different gas bottle than the carrier gas sent through the

first three mass flow controllers, thus enabling adsorption and desorption using a different carrier gas. After the adsorption column, a second switching valve made it possible to either direct the out coming flow of the column towards the gas chromatograph (HP-6890, Agilent Technologies, Santa Clara, California, USA) or towards a waste stream. By changing the position of the first and second valve, the mixture components could also be sent directly towards the GC, bypassing the adsorption column.

The GC was equipped with an automatic gas injection valve, injecting 1 ml of sample at chosen time intervals. Two detectors could be used: a flame ionization detector (FID), only able to detect organic components and a thermal conductivity detector (TCD), able to detect organic components and water. However, since the TCD detector suffers from background noise, each experiment was performed once with each detector. The GC was equipped with a Stabilwax® capillary column (Restek, Bellefonte, California) with a length of 15 m, an internal diameter of 250 µm an a 0.5 µm thick solid phase.

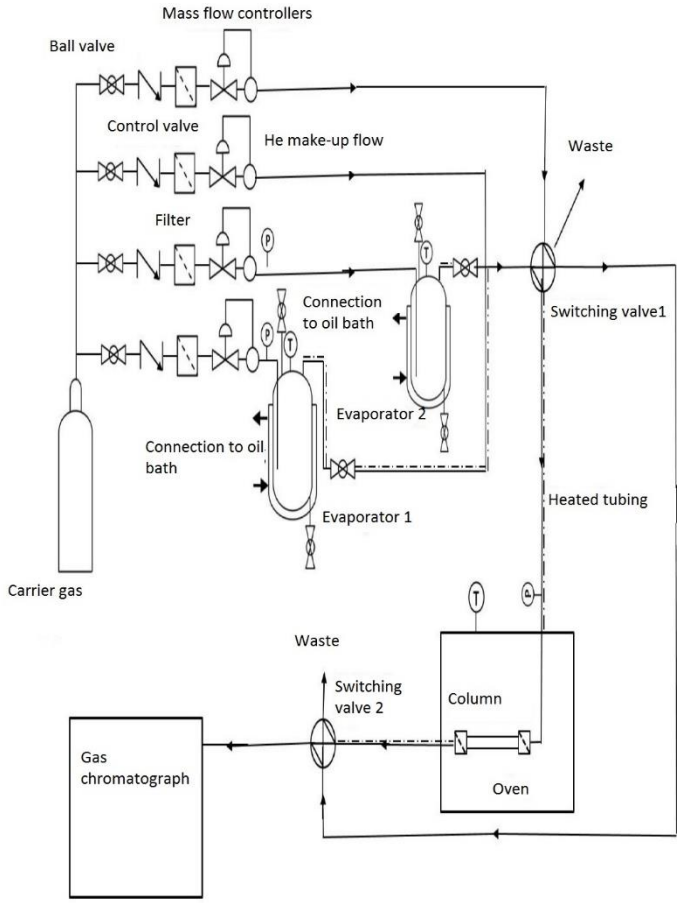

Figure 4.5: Vapor phase breakthrough setup. Adapted from Gelin (2015).

4.4.4 Calculation of the adsorption capacity

Starting from the overall mass balance over the adsorption column, the adsorption capacity can be calculated as follows:

$$q_i = \frac{V_{st,tot} \times P_{st}}{m_{ads} \times R \times T_{st}} \times \int_0^t (y_{i,inlet} - y_i(t))dt \quad (4.3)$$

With:

q_i = adsorption capacity of component i (mol/kg)
$V_{st,tot}$ = total volumetric flow rate at the inlet (m^3/s)
P_{st} = standard pressure (1.013×10^5 Pa)
m_{ads} = adsorbent mass in adsorption column (kg)
R = universal gas constant ($J\ mol^{-1}\ K^{-1}$)
T_{st} = standard temperature (273 K)
t = time (s)
$y_{i,inlet}$ = mole fraction of component i at the inlet of the column
y_i (t) = mole fraction of component i at time t at the outlet of the column

Since pressure varied between different experiments, flow rates were recalculated to standard temperature and pressure. Volumetric flow rates at standard pressure and temperature were calculated using the ideal gas law (equation 4.4).

$$V_{st} = \frac{P_{room} \times V \times T_{st}}{T_{room} \times P_{st}} \tag{4.4}$$

With:

V_{st} = volumetric flow rate at standard pressure and temperature (m^3/s)
P_{room} = pressure in setup room (Pa)
V = volumetric flow rate at non-standard conditions (m^3/s)
T_{st} = standard temperature (273K)
T_{room} = room temperature (297K)
P_{st} = standard pressure (1.013×10^5 Pa)

The total volumetric flow rate sent to the adsorption column was calculated as shown in equation 4.5.

$$V_{st,tot} = V_{st,carrier,evap,1} + V_{st,carrier,evap,2} + \sum_{i=1}^{n} V_{st,i} \tag{4.5}$$

With:

$V_{st,tot}$ = total standard volumetric flow rate at column entrance (m^3/s)
$V_{st,carrier,evap,1}$ = standard volumetric flow rate of carrier gas entering the first evaporator (m^3/s)
$V_{st,carrier,evap,1}$ = standard volumetric flow rate of carrier gas entering the second evaporator (m^3/s)
$V_{st,i}$ = standard volumetric flow rate of component i (m^3/s)
n = number of mixture components

The volumetric flow rate of carrier gas could be regulated by the mass flow controllers. These mass flow controllers had to be calibrated before use. The calibration curves for He and CO_2 were added in Appendix 1. The flow rate of each mixture component could be calculated from the vapor pressure as shown in equation 4.6.

$$V_{st,i} = \frac{P_{vap,i} \times V_{st,carrier,evap}}{P_{carrier}} \tag{4.6}$$

With:

$V_{st,i}$ = standard volumetric flow rate of component i (m^3/s)
$P_{vap,i}$ = vapor pressure of component i in evaporator 1 or 2 (Pa)

$V_{st,carrier,evap}$ = standard volumetric flow rate of carrier gas flowing to evaporator 1 of 2 (m^3/s)
$P_{carrier}$ = pressure of carrier gas flowing towards evaporator 1 or 2 (Pa)

Knowledge of the vapor pressure of each component and the carrier gas pressure thus allows for the calculation of the standard total flow rate using equations 4.5 and 4.6 and the adsorption capacity via equation 4.3. The vapor pressure of each mixture component could be calculated using the Wagner equation (equation 4.1 and equation 4.2) and Raoult's law (equation 4.7). Although the ratio of acetone butanol and ethanol in liquid ABE fermentation broth is reported to be 3:6:1 (Branduardi *et al.*, 2014), simulations using AspenPlus 4.11 showed the vapor phase ratios in the headspace of the fermenter to be 4:6:1 (Gelin, 2015) and these ratios were used in all breakthrough experiments.

$$P_{vap,i} = x_i \times P_{pure,vap,i} \tag{4.7}$$

With:

$P_{vap,i}$ = vapor pressure of component i in evaporator 1 or 2 (Pa)
x_i = mole fraction in liquid phase of component i in evaporator 1 or 2 (Pa)
$P_{pure,vap,i}$ = vapor pressure of pure component i at evaporator temperature (Pa)

The carrier gas pressure could be calculated from the total evaporator pressure, measured by a pressure sensor:

$$P_{carrier} = P_{tot,evap} - \sum_{i=1}^{n} P_{vap,i} \tag{4.8}$$

With:

$P_{carrier}$ = pressure of the carrier gas in evaporator 1 or 2 (Pa)
$P_{tot,evap}$ = total evaporator pressure (Pa)
$P_{vap,i}$ = vapor pressure of component i in evaporator 1 or 2 (Pa)

Knowledge of all these parameters allows for the calculation of the mole fraction at the inlet of the column:

$$y_{i,inlet} = \frac{P_{vap,i} \times (V_{st,carrier,evap} + V_{st,i})}{P_{tot} \times V_{st,tot}} \tag{4.9}$$

With:

$P_{vap,i}$ = vapor pressure of component i in evaporator 1 or 2 (Pa)
$V_{st,carrier,evap}$ = standard volumetric flow rate of carrier gas through evaporator 1 or 2 (m^3/s)
$V_{st,i}$ = standard volumetric flow rate of component i through evaporator 1 or 2 (m^3/s)
P_{tot} = pressure measured in evaporator 1 or 2 (Pa)
$V_{st,tot}$ = standard total volumetric flow rate (m^3/s)

The mole fraction at a time t could be calculated from the integration of the GC signal peaks as shown in equation 4.10.

$$y_i(t) = \frac{A(t)}{A_{bt}} \times y_{i,inlet} \tag{4.10}$$

With:

y_i (t) = mole fraction of component i at the outlet of the adsorption column at time t
A (t) = peak area of component i at column outlet at time t
A_{bt} = peak area of component i at column outlet after complete breakthrough

The dead time of the breakthrough setup was taken in to account when calculating the adsorption capacity and was measured to be 0.24 min (Gelin, 2015). The molar amount of component i present in the dead volume was subtracted from the total amount adsorbed. Knowing the adsorption capacity, a selectivity comparing two components can be calculated:

$$\alpha = (\frac{q_i}{P_i})/(\frac{q_j}{P_j}) \tag{4.11}$$

With:

q = adsorption capacity of component i or j (mol/g)
P = vapor phase partial pressure at the column inlet of component i or j (Pa)
α = selectivity

4.4.5 Calculation of butanol purity and recovery

To compare different desorption methods, single and multicolumn, the purity of a certain recovered amount of butanol was calculated. Using equation 4.10, the area of a GC peak during desorption could be related to the gas phase mole fraction of a component i. Integration of the desorption curve for a component i gives rise to equation 4.12 for the purity of a component i, recovered between a point in time t_s and t_f.

$$p_i = \frac{\int_{t_s}^{t_f} y_i dt}{\sum_{i=1}^{n} \int_{t_s}^{t_f} y_i dt} \tag{4.12}$$

With:

p_i = purity of recovered component i
t_s = time at the start of collection of component i (s)
t_f = time at the end of collection of component i (s)
y_i = gas phase mole fraction of component i
n = number of components in desorption mixture

Equation 4.12 is further clarified in figure 4.6, showing the desorption profile of a Si-LTA column under He. By integrating the curve for the butanol mole fraction between t_s and t_f and dividing this by the sum of the areas under the desorption curve for all of the mixture components, the purity of the fraction recovered between t_s and t_f can be calculated. This calculation thus gives the relative amount of butanol present in the collected fraction. Ideally, the purity of butanol would be 1, indicating the absence of other impurities.

Using the same method, the amount of butanol recovered between a point of time t_s and t_f can be calculated by dividing the area under the desorption curve between these two points by the total area under the butanol desorption curve (equation 4.13). This ratio gives the relative amount of butanol present in the fraction collected between t_s and t_f, compared to the total amount of butanol present in the adsorbent. Ideally, all of the butanol desorbed is recovered, leading to a recovery of 1.

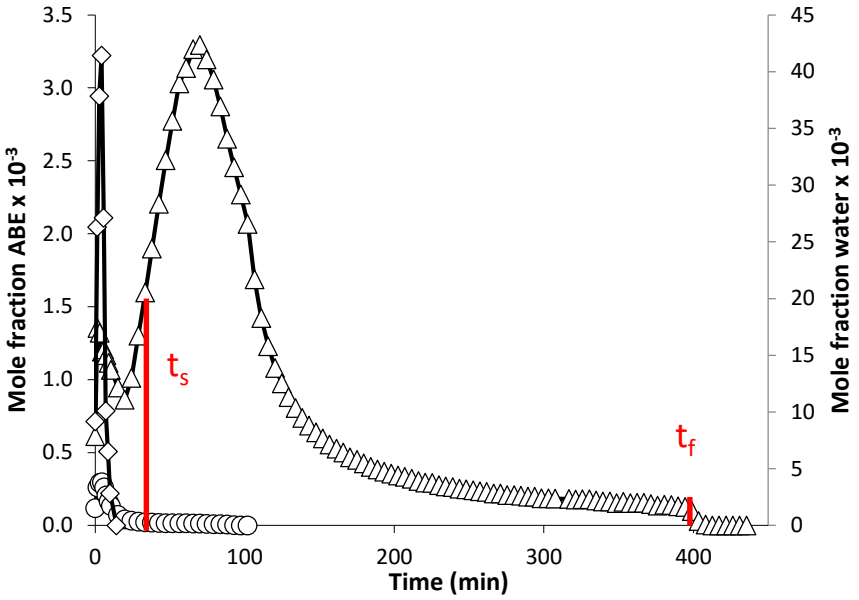

Figure 4.6: Desorption profile for Si-LTA with t_s and t_f shown. The ratio of the area under the desorption curve for butanol and the sum of the areas for all of the components gives the purity of the recovered butanol between t_s and t_f. Ethanol (O), water (◇) and butanol (△) concentrations are shown.

$$r_i = \frac{\int_{t_s}^{t_f} y_i dt}{\int_0^{+\infty} y_i dt} \tag{4.13}$$

With:

r_i = recovery of component i
t_s = time at the start of collection of component i (s)
t_f = time at the end of collection of component i (s)
y_i = mole fraction of component i

In the calculation of purity and recovery in this thesis, t_f was always taken to be the final measurement time. This means that calculation of purity and recovery was performed by integrating the desorption curve until the final measurement point. Purity and recovery were calculated in this way, because most of the impurities desorbed at an early stage during regeneration of the columns (figure 4.6). In practice, it could thus be interesting to start collection of the desorbed fractions at a later point of time, leading to a purer final end product, but a lower recovery of butanol. By starting collection later on during desorption, the purity thus increases, but recovery decreases. When calculating these two parameters for different starting points t_s, purity can be plotted as a function of recovery. In the most ideal case, both values are 1 for every point t_s chosen.

4.4.6 Single column breakthrough experiments

In a first step, adsorption and desorption breakthrough experiments were performed using only one adsorption column in the breakthrough setup. The goal of these experiments was to examine the capacity and selectivity of the different adsorbents in dynamic conditions in order to select the most ideal multicolumn butanol purification setup. Further, a comparison was made between adsorption and desorption using He and CO_2 as carrier gas.

In all of the experiments, a mixture of ABE was used, containing acetone, butanol and ethanol in a 4:6:1 ratio. Thus, a model mixture containing 1.8 g ethanol, 145.7 g butanol and 2.4 g acetone was placed in the first evaporator, which was held at a constant temperature of 30 °C, leading to a 4:6:1 vapor phase composition. Water was added to the second evaporator, which was held at 35 °C. This led to typical vapor phase pressures of 49 Pa for ethanol, 297 Pa for butanol, 191 Pa for acetone and 4222 Pa for water. Carrier gas flow rates through the ABE evaporate were always set at 3.5 ml/min and at 10 ml/min for the water evaporator, leading to a water content of 90% in the total feed mixture (Gelin, 2015).

Si-CHA and Si-LTA were already studied by Gelin (2015), however little attention was given to the desorption procedure used for these adsorbents. Different regeneration methods were evaluated for optimal butanol recovery, the optimal conditions further used in this Masters' thesis are presented in table 4.5. For every column, the carrier gas flow rate was set at 10 ml/min. The temperature gradient was each time set to 1 °C/min with a different final temperature and final time. Controlled cooling was not possible with the column oven used. Starting and final temperatures were always 40 °C. For ZIF-8 desorption using a temperature program and isothermal desorption at 40 °C was compared. For SAPO-34 a slower heating ratio was applied, to avoid steaming of the pores, leading to loss of selectivity. As explained in paragraph 4.4.3, the carrier gas used during adsorption and desorption could be different. An overview of the different adsorption and desorption experiments is given in table 4.6.

Table 4.5: Temperature program used during desorption of the different columns. On ZIF-8, desorption was also performed isothermally at 40°C.

Column	Start temperature (°C)	Start time (min)	Heating gradient (°C/min)	Final temperature (°C)	Final time (min)
ZIF-8	40	1	1	100	90
ZIF-8	40	0	0	40	600
Si-LTA	40	20	1	120	300
Si-CHA	40	20	1	120	300
SAPO-34	40	1	0.5	200	360

4.4.7 Multicolumn breakthrough experiments

To obtain a maximal recovery of high-purity butanol, different adsorption columns were combined in a two column setup. In a first step an adsorption breakthrough experiment was performed using a humid ABE model mixture, as descried in paragraph 4.4.6, until the first column was saturated. However, during desorption of the first column, a second column was added in series to further purify the desorbing butanol stream. After a certain amount of time, this second column was removed, to avoid desorption of the adsorbed impurities on the second column and contamination of the incoming butanol stream. In practice, a second column oven was added behind the first column oven in the breakthrough setup shown in figure 4.5 to be able to hold the second column at a constant temperature whilst the first column is desorbing under a temperature program. The principle of this adsorption and desorption procedure is explained in figure 4.7.

During these experiments He and CO_2 were evaluated as carrier gas with adsorption and desorption begin performed using the same gas as carrier. Table 4.7 summarises the different column combinations that have been experimentally tested and the amount of time the second column was placed behind the first during desorption of the first column. No experiments were performed

combining ZIF-8 and Si-CHA, since the Si-CHA column was not available anymore at the time of the experiments.

Table 4.6: Summary of adsorption and desorption experiments using different carrier gasses.

Column	Carrier gas during adsorption	Carrier gas during desorption	Desorption temperature
ZIF-8	He	He	Program
	He	He	Isothermally
	CO_2	CO_2	Program
	CO_2	CO_2	Isothermally
	He	CO_2	Isothermally
Si-LTA	He	He	Program
	CO_2	CO_2	Program
	He	CO_2	Program
SAPO-34	He	He	Program

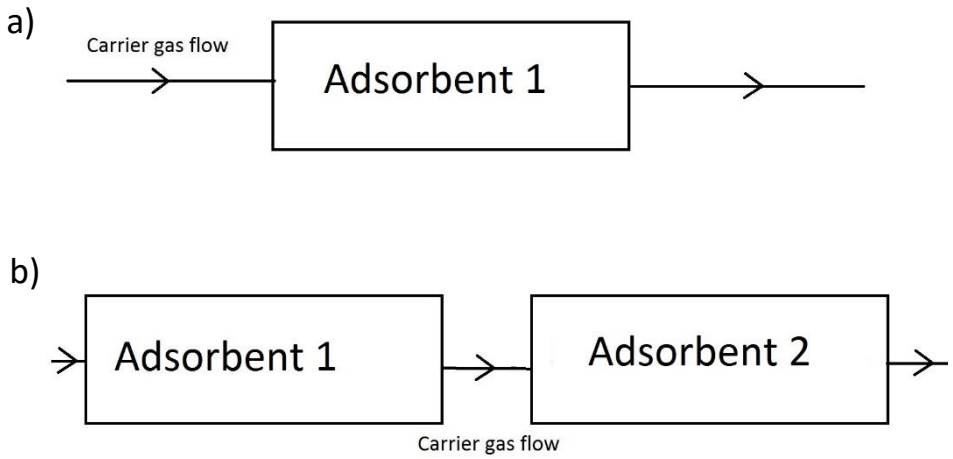

Figure 4.7: Schematic depiction of column configurations during adsorption and desorption. a) Column configuration during adsorption. Carrier gas leaving this column is sent to the GC for analysis. b) Configuration during desorption of the first column. Carrier gas leaving the second column is sent to the GC for analysis. After a certain amount of time, the second column is removed and the setup returns to the configuration shown in a).

For the first column, the same adsorption and desorption experimental conditions apply as described in paragraph 4.4.6. Desorption on ZIF-8 was always performed isothermally at 40 °C. The second column was always held at 40 °C in a separate oven. Except for the isothermal desorption experiments with ZIF-8, where both columns were placed in the same column oven. The flow rate during desorption was always set at 10 ml/min. The second column was regenerated in a separate column oven by heating it at 1 °C/min to 90 °C, holding this temperature for 60 min, followed by heating to 250°C. This final temperature was held for 360 min, followed by cooling to 40 °C.

Table 4.7: Column configurations tested during desorption of the first column.

First column	Second column (at 40 °C)	Carrier gas (10 ml/min)	Time of presence second column (min)
Si-LTA	Si-CHA	He	Whole desorption
Si-LTA	Si-CHA	He	50
Si-LTA	SAPO-34	He	50
Si-LTA	SAPO-34	CO_2	50
ZIF-8	SAPO-34	He	40
ZIF-8	SAPO-34	CO_2	40

4.5 Mathematical modelling

One of the goals of this Master's thesis was to develop a mathematical model to describe the combination of two columns in breakthrough processes, allowing the qualitative evaluation of different multicolumn configurations. Modelling of this multicolumn system could give further insight in the behavior of systems combining different adsorption columns and would allow to identify interesting configurations for maximal butanol recovery and purity. The methodology concerning the development of this model will be discussed in this section. In a first step, isotherm models were developed to describe the adsorption behavior of the different ABE components on the different materials. In a second step, multicomponent breakthrough simulations were graphically fitted to experimental data to obtain model parameters to describe column adsorption and desorption. Finally, a method was developed to combine these single column models in a multicolumn model.

4.5.1 Isotherm fitting

To develop a good model describing column breakthrough profiles, well-described adsorption isotherms are necessary. In ABE fermentation especially, simultaneous breakthrough of four different components needs to be described. Developing equations for multi-component adsorption is not simple, since not only the adsorbent-adsorbate interaction, but also the adsorbate-adsorbate interactions need to be taken into account. As a first approach, the single component isotherm data that was available of the different adsorbents was fitted using the single component Langmuir equation (4.14). This isotherm model is only valid for type I isotherms. Not all of the ABE components on all of the modelled adsorbents show this behavior. However, since the ABE components are present at low vapor pressure, this part of the isotherm could be fitted with a single component Langmuir model.

$$q = q_{sat} \times \frac{K \times P}{1 + K \times P} \tag{4.14}$$

With:

q = adsorbed amount (mol/kg)
q_{sat} = maximal adsorbed amount (mol/kg)
K = Langmuir constant (Pa^{-1})
P = pressure of adsorbate (Pa)

Important assumptions of the Langmuir model include: homogeneity of the adsorbent surface, localized adsorption (a fixed amount of well-defined adsorption sites) and equivalence of these individual sites (Duong, 1998). Since only single component isotherms were available, these single component Langmuir parameters were used to describe multi component adsorption via a multiple

component Langmuir model (equation 4.15). The assumptions made for the multi component Langmuir model are the same as for the single component model (Duong, 1998).

$$q_i = q_{sat,i} \times \frac{K_i \times P_i}{1 + \sum_{i=j}^{n} K_j \times P_j} \quad (4.15)$$

With:

q_i = adsorbed amount of component i (mol/kg)
$q_{sat,i}$ = adsorbed amount at saturation of component i (mol/kg)
K_i = Langmuir constant of component i (Pa^{-1})
P_j = vapor pressure of component j (Pa^{-1})
P_i = vapor pressure of component i (Pa^{-1})
n = amount of mixture components

For fitting of the isotherms Athena Visual Studio 4.2 was used. As an extra fitting restriction, all parameters were defined to be positive. Isotherm fitting was performed using the least square algorithm.

4.5.2 Single column adsorption and desorption

4.5.2.1 Model development and discretization

As a basic equation for the modelling of multicomponent breakthrough on both Si-LTA and Si-CHA a plug flow model with axial dispersion was used (equation 4.16). This equation can be derived from the mass balance over a finite part dx of a packed bed column (Ruthven, 1984). Axial dispersion coefficients were estimated to be equal to the molecular diffusion coefficient in air (Lug, 1968). Column porosity was defined as the ratio between the total empty volume in the column and the total column volume. The superficial velocity was calculated by dividing the chosen flow rate by the column cross section.

$$\frac{\partial P_i}{\partial t} = D_{ax,i} \times \frac{\partial^2 P_i}{\partial x^2} - \frac{v}{\varepsilon} \times \frac{\partial P_i}{\partial x} - \frac{1-\varepsilon}{\varepsilon} \times R \times T \times \rho_{ads} \times \frac{\partial q_i}{\partial t} \quad (4.16)$$

With:

P_i = the vapor phase partial pressure of mixture component i (Pa)
$D_{ax,i}$ = axial dispersion coefficient (m^2/s)
t = time (s)
x = column position (m)
v = superficial velocity of gas phase (m/s)
ε = column porosity
R = universal gas constant ($J\ K^{-1}\ mol^{-1}$)
T = column temperature (K)
ρ_{ads} =adsorbent density (kg/m^3)
q_i = adsorbed amount of component i (kg/mol)

Adsorption kinetics were described using a linear driving force model (equation 4.17). The equilibrium adsorption capacity could be calculated from the fitted isotherm models.

$$\frac{\delta q_i}{\delta t} = h_i \times (q_{eq,i} - q_i) \quad (4.17)$$

With:

q_i = adsorbed amount of component i (mol/kg)
h_i = linear driving force constant (s^{-1})
$q_{eq,i}$ = equilibrium adsorption capacity of component i (mol/kg)

For numerical simulation, these models were spatially discretized by dividing the column in a finite amount of points (equation 4.18). In this way, a system of N differential equations is formed, only being time-dependent. This because the adsorption kinetics, shown on the right side of equation 4.18 can be related to the partial pressure at point j of the column using equation 4.16 and the multicomponent isotherm (equation 4.15). For the first order derivative, a backward discretization method was applied, calculating the pressure at position j starting from the pressure on the previous point in the column. The second order derivative was calculated using a central discretization method.

$$\frac{\partial P_i(j)}{\partial t} = D_{ax,i} \times \frac{P_i(j+1) - 2 \times P_i(j) - P_i(j-1)}{(\Delta x)^2} - \frac{v}{\varepsilon} \times \frac{P_i(j) - P_i(j-1)}{\Delta x} - \frac{1-\varepsilon}{\varepsilon} \times R \times T \times \rho_{ads} \times \frac{\partial q_i(j)}{\partial t} \quad (4.18)$$

With:

P_i (j) = the vapor phase partial pressure of mixture component i on position j (Pa)
Δx = spatial difference between two differentiation points (m)
q_i(j) = adsorbed amount of component i on column position j (kg/mol

4.5.2.2 Column parameters, initial values and boundary conditions

The system of differential equations given by equation 4.17 was subsequently solved using the Matlab® ode15s solver. Since equation 4.16 is a partial differential equation of the second order in the spatial variable and of the first order in time variable, two boundary conditions and one initial value needs to be chosen. Depending on whether an adsorption or desorption process was simulated, different initial values and boundary conditions were used.

The boundary condition at the inlet of the column was implemented as a Neumann boundary (equation 4.19). At the end of the column, a constant boundary condition was used: the partial pressure at the outlet of the column was taken equal to the partial pressure on the last discretization point inside the column.

$$D_{ax,i} \times \left.\frac{\partial P_i}{\partial x}\right|_{x=0} = v \times (P_i - P_{\infty,i}) \quad (4.19)$$

With:

P_i = partial pressure of component i at the start of the column (Pa)
v = superficial gas phase velocity (m^2/s)
$D_{ax,i}$ = axial dispersion coefficient of component i (m^2/s)
$P_{\infty,i}$ = gas phase partial pressure of component i fed to the column (Pa)
x = column position (m)

For the single column simulations, partial pressures at the inlet were taken equal to the values used in the breakthrough experiments. This allowed fitting of the kinetic parameters and the column porosity to the experimental data. For the different columns, the boundary conditions at the column inlet are shown in table 4.8.

Table 4.8: Boundary conditions at column intel during adsorption.

Boundary condition	Si-LTA (Pa)	Si-CHA (Pa)	SAPO-34 (Pa)	ZIF-8 (Pa)
$P_{\infty,acetone}$	193	192	189	194
$P_{\infty,butanol}$	308	298	296	308
$P_{\infty,ethanol}$	50.0	49.8	49.0	50.2
$P_{\infty,water}$	4209	4110	4229	4209

Further, initial values had to be assigned to every discretization point. For an adsorption simulation, all partial pressures and all adsorbed amounts inside the column were set equal to zero at the start of the calculations. When subsequently a desorption simulation was run, the partial pressures and adsorbed amounts present at every discretization point at the end of the adsorption step were taken as initial values.

To obtain realistic simulation results, the porosity and linear driving force parameter were graphically fitted to experimental breakthrough data. Modelling desorption was used using the same equations, but a different flow rate to compare with experimental data. Column lengths were chosen to be 10 cm for good comparison with experimental data, except for those of the Si-CHA. The length of this column was corrected for the quartz beads present and the equivalent length was calculated to be 3.65 cm. For multicolumn breakthrough experiments, however, a length of 10 cm was used to allow comparison with the SAPO-34 column. The internal diameter was chosen the same as those of the experimental columns. Flow rates of during adsorption were chosen to be 15.9 ml/min and 11.9 ml/min during desorption. The column temperature was always 40 °C. Material densities were calculated from the zeolites' unit cell formula (Olson *et al.*, 2007), those of SAPO-34 were obtained from Cousin Saint Remi *et al.* (2015). For ZIF-8 data obtained from the supplier was used. Table 4.9 summarizes the used crystal densities. An example of the Matlab® code used for numerical simulation of adsorption and desorption on the Si-CHA column is presented in Appendix 2.

Table 4.9: Model parameters for the Si-LTA and Si-CHA column.

Material	Density (x10^3 kg/m^3)
Si-LTA	1.29
Si-CHA	1.45
SAPO-34	1.51
ZIF-8	0.35

4.5.3 Combination of different adsorption columns

As a final step, simulations were performed to compare the behavior of the combination of two columns during adsorption of a vapor phase ABE mixture. The same equations described in paragraph 4.5.1 and 4.5.2 were used, with the same column parameters and the fitted kinetic parameters and column porosities. In this configuration, the vapor phase mixture was send to a first adsorption column, directly followed by a second column (see paragraph 5.3.1). This generates difficulties at the inlet boundary of the second adsorption column: instead of a constant value, the dynamic breakthrough profile of the first column becomes the boundary condition. To cope with this time dependency, a

simple if test was implemented in each iteration of the ode15s solver (Appendix 3). In a first step, a complete adsorption breakthrough of the first column was simulated. The return of such a calculation is a time vector, containing all different calculated points in time, and the corresponding partial pressures and adsorbed amounts. For adsorption on the second column, each iteration the time t used by the ode15s solver was compared to the time values returned from the adsorption breakthrough calculations of the first breakthrough. An index i was used to track the position in this time vector and the corresponding partial pressures and adsorbed amounts of the different mixture components. As long as the solver time t was lower than the time in the results time vector at position t'_{i+1} the partial pressure value corresponding to t'_i was used as boundary condition. When, after several iterations, the solver time value t exceeded the value t'_{i+1}, the value of the index was increased with 1. In this way, the output of the first column was implemented as an inlet boundary condition for the second column in a step-wise way.

For calculation of the purity of a component i on the different adsorbent columns, the calculated adsorbed amounts were used (equation 4.20). The amount of a component i adsorbed between two discretization points in the column was estimated using the average calculated adsorbed value. By adding all these values over the total column length, the total adsorbed amount of a component i could be calculated. Using the molecular weights of the different adsorbed components, a purity in weight percent was calculated, corresponding to 100% recovery of the adsorbed ethanol or butanol.

$$n_i = \sum_{j=1}^{N_x} n_{i,j} = \sum_{j=1}^{N_x} \frac{q_{j+1} + q_j}{2} \times \rho \times \Omega \times \Delta x \times (1 - \epsilon) \tag{4.20}$$

With:

N_i = adsorbed amount of component i (mole)
$N_{i,j}$ = adsorbed amount of component i at position j of the column (mole)
N_x = number of column discretization points – 1
q_j = adsorbed amount at column position j
ρ = adsorbent density (kg/m^3)
Ω = column cross section (m^2)
Δx = distance between two column discretization points (m)
ε = column porosity

5. Results & Discussion

In this chapter, the different experimental and modelling results will be discussed. First of all, the measured adsorption isotherms on the different materials, comparing CO_2 and N_2 as carrier gas, and their selectivity will be discussed. Secondly, the results of the different single column breakthrough experiments will be presented, also comparing He and CO_2 as carrier gas. In a third part, results of the multicolumn breakthrough experiments will be shown. A fourth section will cover the results concerning isotherm model development. In the following section, the obtained isotherm parameters will be used to describe single column breakthrough profiles. The developed column models will subsequently be used to simulate the combination of different adsorption columns. In the last section a comparison is made between the different simulated and experimentally tested multicolumn configurations.

5.1 Isotherms & selectivity

In this section, the measured isotherms using CO_2 as carrier gas will be compared to isotherm measurements using N_2. Since the Si-CHA sample was not available at the time of the isotherm measurements, no CO_2 isotherm measurements could be presented for this material. However, the Si-CHA material was characterized in detail by Gelin (2015), so its selectivity will be discussed.

5.1.1 Si-LTA

Figure 5.1 shows the experimentally determined vapor phase adsorption isotherms on Si-LTA. Clearly, the Si-LTA adsorbent shows a low affinity for water, demonstrating its hydrophobic nature. The isotherm has a type III shape, with an increase in the slope of the isotherm at high vapor pressures. This shape is typical for hydrophobic adsorbents. Due to adsorption of water on the adsorbent at low vapor pressures, the adsorbent surface becomes more polar. In this way, its affinity for water increases with increasing amount of water adsorbed. The butanol isotherm showed a typical type I Langmuir behavior, with a higher adsorption capacity. Further, Si-LTA shows a high adsorption capacity for ethanol and almost no affinity for acetone (figure 5.1, Gelin, 2015). The low uptake of acetone for the Si-LTA material can be attributed to the higher polarity of acetone and the small pore size of Si-LTA (4.1 Å x 4.1 Å), which is smaller than the kinetic diameter of acetone (4.7 Å) (Gelin, 2015). This makes Si-LTA an interesting adsorbent for the removal of ethanol and butanol from ABE vapor phase. The ethanol isotherm on Si-LTA also clearly shows an S-shape, as for butanol on ZIF-8 (Cousin Saint Rem *et al.*, 2011). In general, isotherm shape has an important influence on the breakthrough curve shape during adsorption and desorption, as will be discussed further.

Comparing CO_2 to N_2 as carrier gas, a lower adsorption capacity was observed at high vapor pressures for water, ethanol and butanol. A first possible explanation for this observation lies in the fact that CO_2 competitively adsorbs on the Si-LTA material. Since the gravimetric method used, measures the mass of the adsorbed components, it cannot discriminate between adsorption of CO_2 and adsorption of ABE components. Adsorption of CO_2 on Si-LTA was observe by Palomino *et al*. (2010) and confirmed by gas phase isotherm measurement of CO_2 on Si-LTA (Appendix 4). Due to this competitive adsorption effect, the adsorption capacity for the ABE components decreases at higher vapor pressures. A second possible explanation lies in the mass of the completely desorbed sample used by the gravimetric instrument to calculate the adsorption isotherm. After termination of the activation procedure, the sample mass is chosen to be the reference mass of completely desorbed material. However, when fast CO_2 adsorption occurs, the gravimetric device is not able to correctly determine this initial mass.

Indeed, at the start of the adsorption experiment, fast CO_2 uptake could be noticed, making this explanation plausible. However, this uptake was not sufficient to completely explain the difference between the isotherms using CO_2 and N_2.

For the ethanol isotherm, the adsorption capacity at low vapor pressure was higher for adsorption under CO_2 than for N_2. This isotherm shift to the left has important implications for separation efficiency, since the ethanol adsorption capacity at lower vapor pressure becomes higher. In this way, the selectivity of the material at low vapor pressures decreases. This change of the isotherm could be caused by CO_2 adsorption changing hydrophobicity of the material.

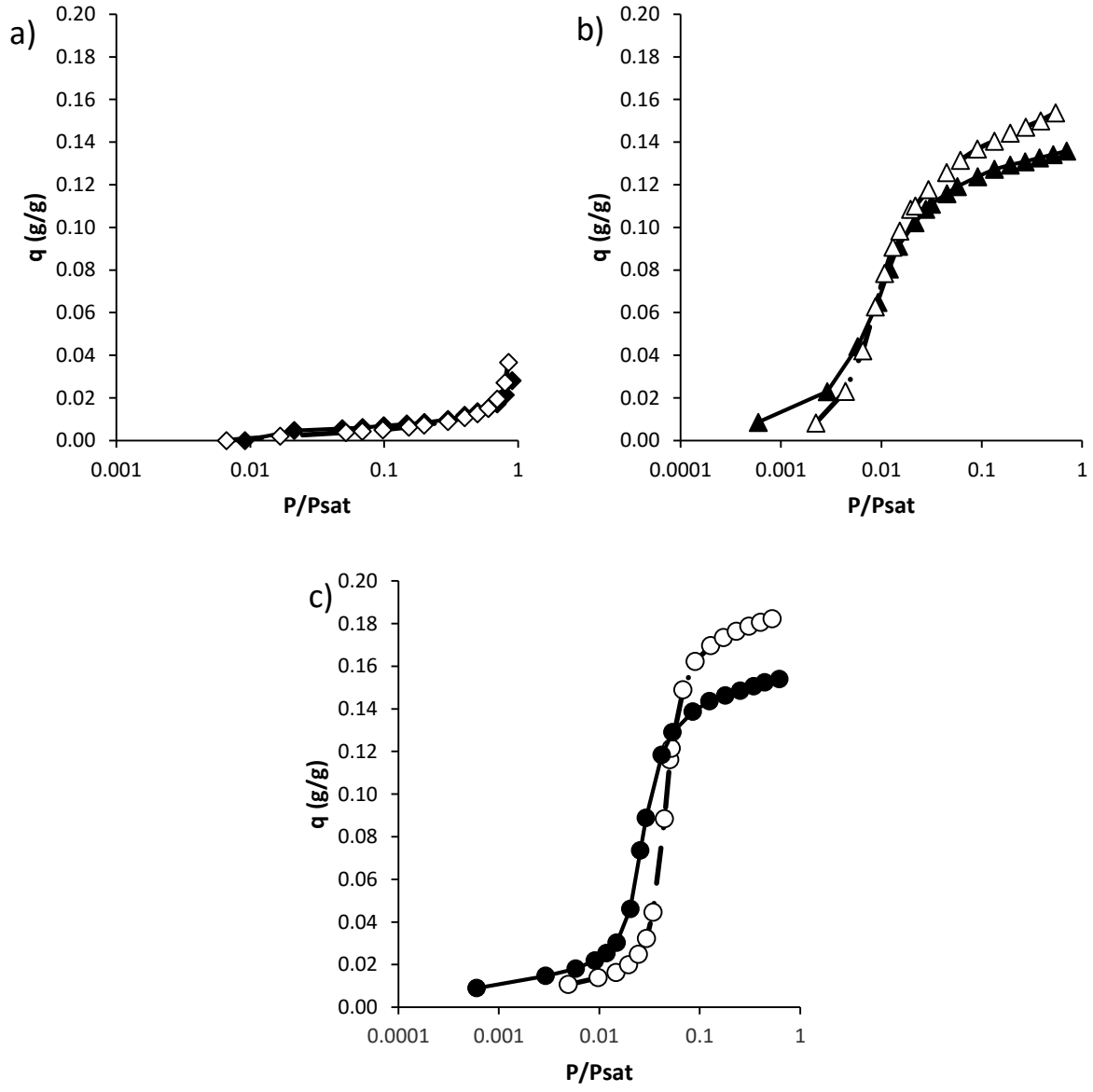

Figure 5.1: Comparison of the adsorption isotherms under CO_2 and N_2 on Si-LTA at 40 °C. a) Water isotherm under N_2 (◇) and CO_2 (◆). b) butanol isotherm under N_2 (△) and CO_2 (▲). c) ethanol isotherm under N_2 (○) and CO_2 (●). Adsorption isotherms under N_2 were obtained from Gelin (2015).

5.1.2 ZIF-8

The different vapor phase adsorption isotherms on ZIF-8 are depicted in figure 5.2. Being a hydrophobic material, ZIF-8 showed little to no affinity for water, as is visible in the water adsorption isotherm. Clearly, the affinity of ZIF-8 for butanol was higher than for acetone and ethanol under N_2. Although the ZIF-8 framework is relatively rigid, the imidazolate linkers are able to tilt under higher pressure (Moggach *et al.*,2009), leading to larger pore sizes and pore volumes. This flexibility might also play a role in the adsorption of butanol, since the kinetic diameter of butanol is larger than the size of the ZIF-8 windows (Cousin Saint Remi *et al.*, 2011). Indeed, Jimenez *et al.* (2011, 2012) confirmed that flexibility of imidazolate linkers plays a role in gas phase adsorption for smaller and larger (ethane, propane, butane) gas molecules. However, using molecular simulations and experimental isotherm data, Anai *et al.* (2012) concluded that not only flexibility of the ZIF-8 structure, but also size and polarizability plays an important role in the gas phase adsorption mechanism of larger molecules on ZIF-8.

The ethanol, butanol and acetone isotherms on ZIF-8 were clearly S-shaped as also observed by Cousin Saint Remi *et al.* (2011) and Zhang *et al.* (2013b, 2013c). Zhang *et al.* (2013c) proposed a mechanism for alcohol adsorption based on molecular simulations, explaining the isotherm S-shape. At first the alcohol molecules coordinate with the imidazolate linkers of ZIF-8, leading to localized adsorption corresponding to the slow increase of adsorption capacity at low vapor pressures (figure 5.2). At higher vapor pressure, the ZIF cages start filling rapidly due to adsorbate-adsorbate interactions. Especially for alcohols, this clustering effect takes places by strong hydrogen bonding (Krishna & Van Baten, 2010). Finally, saturation of the MOF is reached, corresponding to the final plateau observed in the isotherm (figure 5.2). Especially for butanol, the isotherm S-shape has important implications for behavior in breakthrough experiments. The effects of these peculiar isotherm shapes on breakthrough profiles will be discussed later on.

Comparing the adsorption isotherms with CO_2, N_2, or He as carrier gas, some interesting effects were observed. For butanol, the adsorption capacity was again measured to be lower using CO_2 compared to nitrogen. The butanol isotherm showed a clear shift to the right, indicating competitive adsorption of CO_2. The ethanol isotherm also shows this shift, but the effect is smaller compared to butanol. As for the water isotherm on Si-LTA, the water isotherm on ZIF-8 shifts to the left, indicating an increase in water uptake at low vapor pressures. The acetone isotherm also shows a shift to the right using CO_2 as carrier gas. The affinity of ZIF-8 for CO_2 was confirmed by Danaci *et al.* (2015), who studied its properties for CO_2/CH_4 separations.

Vapor phase isotherm data of ZIF-8 thus confirmed its affinity for vapor phase acetone, butanol and ethanol. Moreover, liquid phase breakthrough experiments confirmed its selectivity for butanol over the other two ABE components (Cousin Saint Remi *et al.*, 2011, 2012), making this an interesting alternative for Si-LTA in vapor phase breakthrough.

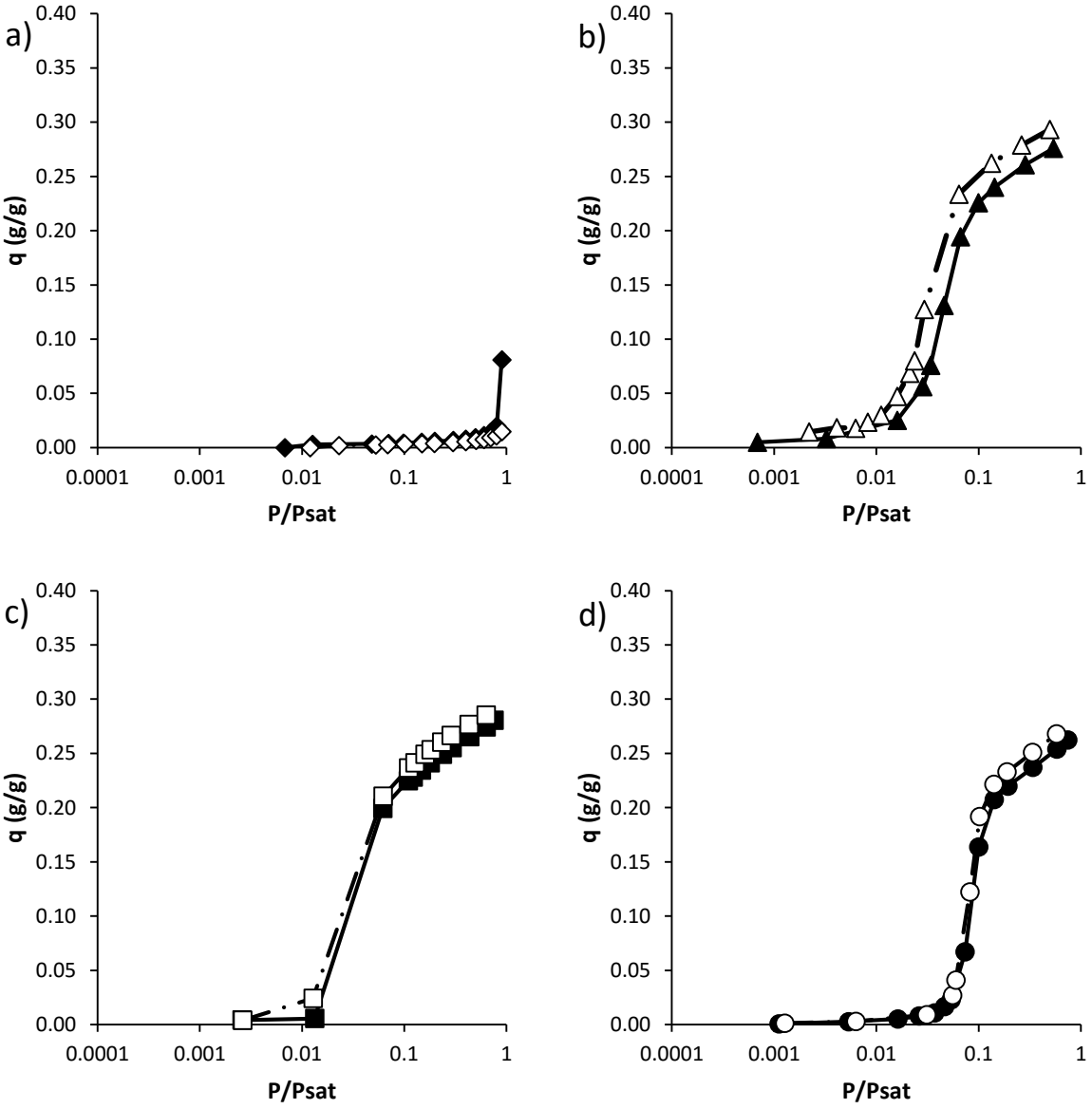

Figure 5.2: Comparison of the adsorption isotherms under CO_2 and N_2 on ZIF-8 at 40 °C and 50 °C. a) Water isotherm under N_2 (◇) and CO_2 (◆) at 40 °C. b) Butanol isotherm under He (△) and CO_2 (▲) at 50 °C. c) Acetone isotherm under N_2 (❑) and CO_2 (■). d) Ethanol isotherm under N_2 (○) and CO_2 (●). Butanol isotherm data was obtained from Cousin Saint Remi *et al.* (2011).

5.1.3 SAPO-34 & Si-CHA

The isotherms measured under CO_2 and N_2 for SAPO-34 are depicted in figure 5.3. Clearly, a large adsorption capacity for ethanol and water was observed, whereas the butanol isotherm never reached complete equilibrium. These results are consistent with those of Daems *et al.* (2007) and Remy *et al.* (2011), who showed the SAPO-34 zeolite to selectively adsorb 1-alcohols up to ethanol. 1-alcohols with a size larger then 1-propanol do not fit in the small chabazite cages of SAPO-34 in there stretched out conformation and are thus unable to efficiently adsorb on this material (Daems *et al.*, 2007). This is further clarified in figure 5.4, visualizing the adsorption of ethanol and butanol on a chabazite zeolite. Ethanol is able to adsorb perpendicular to the cage axis, making efficient stacking in the pores possible, butanol however is too large to adsorb in this way and is thus packed less efficiently in the zeolite cages

(Daems *et al.*, 2007). However, molecular simulations of Krishna & Van Baten (2011) showed chabazite zeolites to selectively adsorb alcohols up to 1-hexanol. The difference between theoretical and simulation results can be explained by the small window size of SAPO-34, which does not allow for efficient diffusion of these longer alcohols into the zeolite cages (Cousin Saint Remi *et al.*, 2013).). Our own isotherm measurements showed that the adsorption equilibrium for butanol was not even reached after 9 hours. The selectivity of SAPO-34 for alcohols smaller than 1-propanol thus does not only lies in a more efficient adsorption mechanism, but also in faster diffusion kinetics. SAPO-34 is thus an interesting material for water and ethanol removal from vapor phase ABE mixtures (Cousin Saint Remi *et al.*, 2012 The all-silica chabazite used in this thesis, shows the same basic selective behavior for ethanol, although its affinity for water is considerably lower than that of the polar SAPO-34 (Gelin, 2015). The ABE isotherms measured on Si-CHA by Gelin (2015) are available in Appendix 4.

Comparison of the isotherms using CO_2 as carrier gas shows large differences with N_2 for ethanol adsorption and water adsorption. This difference can be explained by the affinity of CO_2 for the SAPO-34 zeolite. For instance, Kim *et al.* (2015b), showed that the weak acid sites of H-SAPO-34 play an important role in the adsorption mechanism of CO_2. They showed the CO_2 adsorption capacity in ranges close to atmospheric pressure to be higher (3.0 mmol/g) than zeolites with other topologies, such as ZSM-5 (1.3 mmol/g) and zeolite Y (2.7 mmol/g). Due to CO_2 adsorption, the water and ethanol isotherm shifts to the left, decreasing selectivity for ethanol at lower vapor pressures. The effect of CO_2 uptake at the start of the gravimetric analysis was taken into account for the isotherm calculations on SAPO-34. For ZIF-8 and Si-LTA, this uptake was too low to completely explain the changes in isotherm behavior.

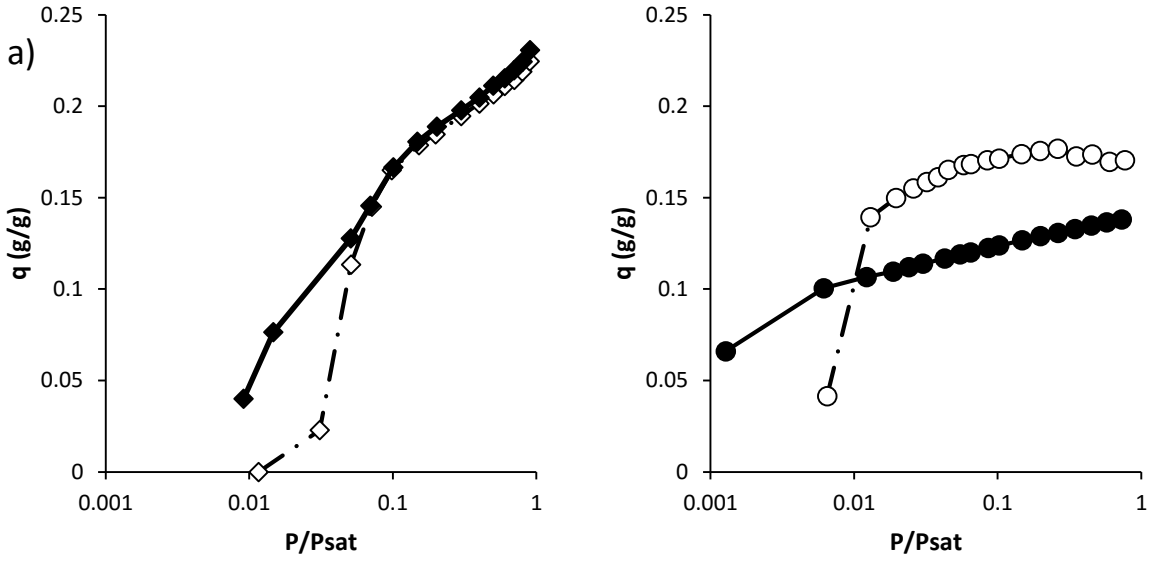

Figure 5.3 a) Water isotherm on SAPO-34 at 40 °C with CO_2 (◆) and He (◇) as carrier gas. b) Isotherm data of ethanol on SAPO-34 at 40 °C with CO_2 (●) and He (O) as carrier gas.

The higher adsorption capacity of SAPO-34 compared to Si-CHA for water has important implications for their combination with other adsorption columns, as will be discussed further. The adsorption capacities measured in this thesis for SAPO-34 lie in the same range as those of Henninger *et al.* (2010). Water adsorption on the hydrophobic Si-CHA zeolite can be explained by the formation of hydrophilic

silanol groups in the zeolite framework, causing an increase in polarity and facilitating further water adsorption (Trzpit *et al.*, 2008).

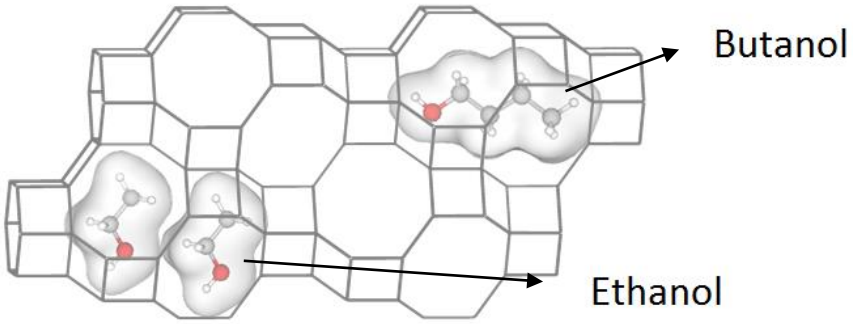

Figure 5.4: Comparison of ethanol and butanol adsorption on a chabazite type zeolite. Ethanol is able to adsorb perpendicular to the cage axis, whereas butanol hardly fits in one zeolite cage. Adapted from: (Daems *et al.*, 2007).

Due to the small window size (3.8 Å), acetone (kinetic diameter 4.7Å) adsorption capacity on Si-CHA and SAPO-34 is small (Cosseron *et al.*, 2013; Gelin, 2015). Interestingly, the adsorption capacity of acetone of Si-CHA material increases with temperature (starting from 75 °C), due to opening of the chabazite windows (Cosseron *et al.*, 2013). No acetone isotherms were measured on the SAPO-34 material, but breakthrough data of this component confirmed the same low adsorption capacity for acetone as for Si-CHA.

5.2 Single column breakthrough experiments

Isotherm measurements thus showed that each of the four presented materials have their own selectivity for the different ABE mixture components. The hydrophobic zeolite Si-LTA and the hydrophobic MOF ZIF-8 showed promising butanol adsorption properties. The Si-LTA material, however, had a high saturation capacity for ethanol, whilst ZIF-8 showed to have some adsorption capacity for both ethanol and acetone. On the other hand, the hydrophobic zeolite Si-CHA shows a high capacity for ethanol and a smaller affinity for water and is thus a possible candidate for ethanol removal from the ABE mixture (Gelin, 2015). The hydrophilic SAPO-34 zeolite shows a similar affinity for ethanol, but has a higher water adsorption capacity than Si-CHA. To fully understand the behavior of these materials in dynamic conditions and to identify the relative importance of possible co-adsorption of different ABE mixture components, breakthrough experiments were performed on columns containing these materials, using a vapor phase model ABE mixture. Also, a comparison is made between the use of He and CO_2 as carrier gas, since large amounts of CO_2 are produced during clostridial ABE fermentation.

5.2.1 Si-LTA column

5.2.1.1 Adsorption

Breakthrough experiments using an ABE model mixture were performed as described in the Materials & Methods section. A typical breakthrough profile is depicted in figure 5.5. As expected from the isotherm data, acetone and water showed almost immediate breakthrough. The Si-LTA column clearly showed affinity for ethanol and butanol. However, competitive adsorption between butanol and

ethanol occurred, leading to roll-up of the ethanol breakthrough curve. The selectivity of Si-LTA was thus clearly bigger for ethanol than for butanol, most of the adsorbed ethanol was pushed out by the adsorbing butanol molecules (table 5.1, figure 5.7). However, as was shown by Gelin (2015), this effect is especially important for low ethanol vapor pressures. The ethanol vapor pressure at the inlet of the column was calculated to be around 50 Pa, whilst the butanol vapor pressure was around 300 Pa, leading to a larger driving force for butanol adsorption, as can be observed from the adsorption isotherms (figure 5.1). The measured adsorption capacity in breakthrough was shown in figure 5.7, highlighting the high butanol adsorption capacity and showing that traces of ethanol and acetone are adsorbed as well. The major contaminant co-adsorbing is water, however. Especially for the components with a high concentration, oscillatory behavior of the concentrations was observed after breakthrough. However, these oscillations were a property of the measurement system, as was verified by performing a breakthrough experiment with an empty column (Appendix 5).

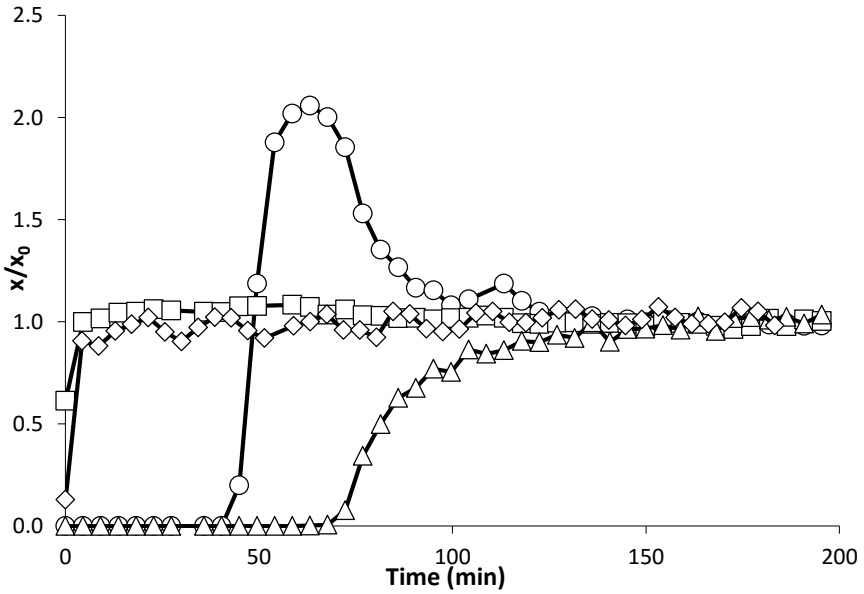

Figure 5.5: Breakthrough profile using He as carrier gas for the Si LTA column at 40 °C. The mole fractions at the column outlet, normalized by their values at breakthrough, are plotted as a function of time for acetone (❑), butanol (△), ethanol (○) and water (◇). Roll-up could clearly be observed on the ethanol breakthrough profile. Vapor phase partial pressures at the column inlet were 49 Pa for ethanol, 295 Pa for butanol, 190 Pa for acetone and 4230 Pa for water.

Comparing He and CO_2 as carrier gas, a faster breakthrough time and thus lower adsorption capacity and selectivity was observed for ethanol and butanol (table 5.1, figure 5.6, figure 5.7). This can be explained by the CO_2 adsorption capacity of the Si-LTA material (Appendix 4; Palomino *et al.*, 2010)) and confirms the results of the isotherm measurements (figure 5.1). The lower butanol adsorption capacity was also reflected in a lower selectivity for butanol (table 5.1). Especially for water, the adsorption capacity stayed the same using CO_2, whilst that of butanol decreased (figure 5.7). This also confirms the effect of CO_2 on the hydrophobicity of the Si-LTA material (paragraph 5.1.1). Interestingly, an effect on butanol adsorption kinetics could also be observed, with a more spread out butanol adsorption profile for adsorption under CO_2 (figure 5.6). Adsorption under CO_2 thus shows slightly worse performance than using He as carrier gas. This kinetic effect can be explained by the preferential adsorption of CO_2 in the window opening. Molecular simulations have shown that this adsorption

hindered the gas phase diffusion of methane and nitrogen gas into the pores of LTA and CHA zeolites (Krishna & Van Baten, 2008). This effect could also play a role in the vapor phase adsorption of alcohols using CO_2 as carrier gas, hindering the diffusion of these components into the zeolite structure.

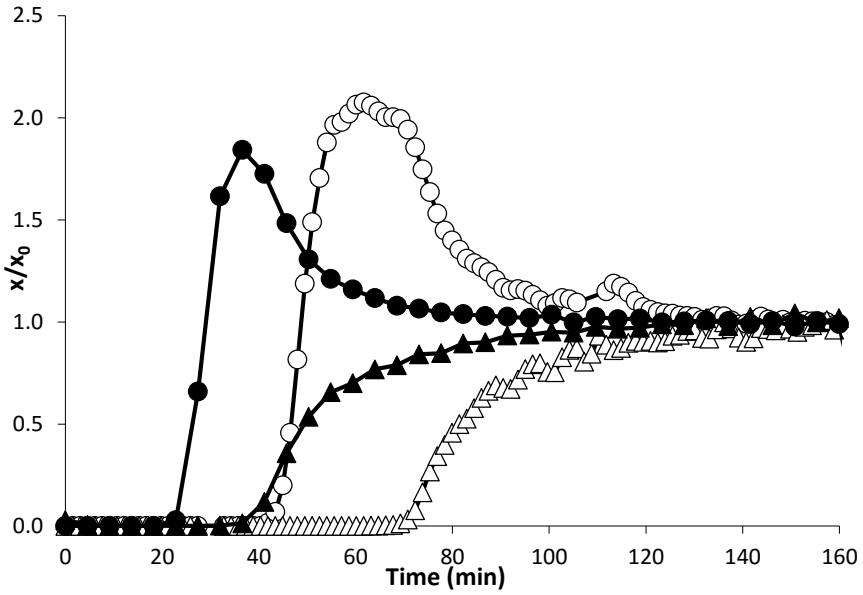

Figure 5.6: Comparison between ethanol and butanol breakthrough profiles under He and CO_2 at 40 °C. A clear shift in breakthrough time was observed for ethanol and butanol using He (○, △) and CO_2 (●, ▲). Mole fractions at the end of the column, normalized by their breakthrough value, were plotted as a function of time. Vapor phase partial pressures at the column inlet were 49 Pa for ethanol, 295 Pa for butanol, 190 Pa for acetone and 4230 Pa for water.

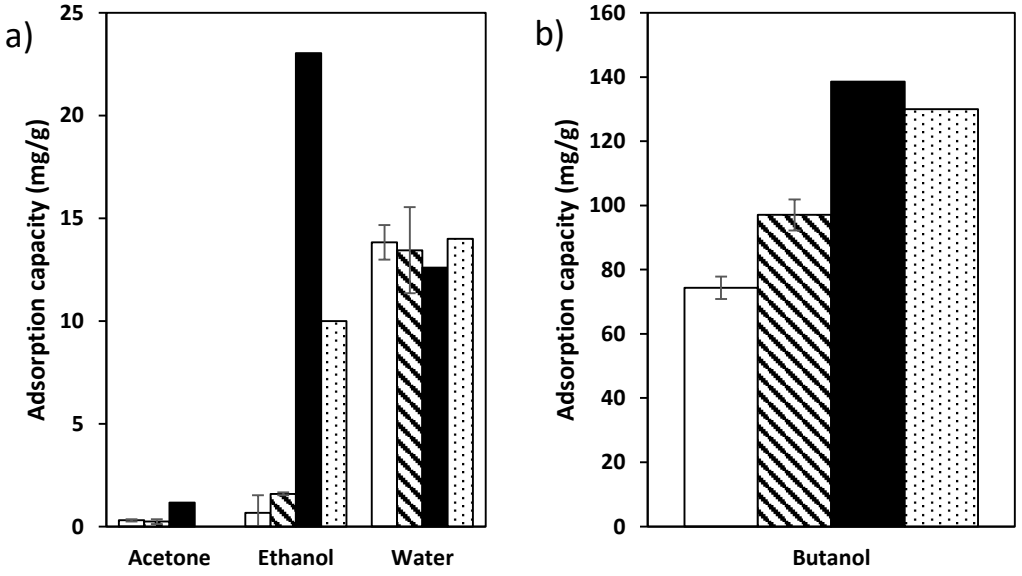

Figure 5.7: Comparison of the adsorption capacities of the different vapor phase ABE components using CO_2 (blank bars) and He (shaded bars) as carrier gas for breakthrough experiments at 40 °C on the Si-LTA column.

Single component isotherm capacity values under N_2 (black bars) and CO_2 (dotted bars) are also shown. Error on breakthrough adsorption capacity calculations was estimated using the standard deviation on the calculated values (shown on graph). a) Adsorption capacities of acetone, ethanol and water. b) Adsorption capacity of butanol.

Table 5.1: Comparison of the selectivity of the Si-LTA column in dynamic conditions using He and CO_2 as carrier gas.

Selectivity	Adsorption using He	Adsorption using CO_2
Butanol/ethanol	17	6
Butanol/acetone	192	103
Butanol/water	58	17

5.2.1.2 Desorption

The desorption profile using He as carrier gas is depicted in figure 5.8. As could be expected from the calculated adsorption capacities and the breakthrough profiles (table 5.1, figure 5.5), a significant amount of water and ethanol was desorbed during the initial stage of the desorption procedure. Further, only a trace amount of acetone was observed during the whole desorption measurement. The butanol desorption profile shows long tailing, which is typical behavior for components with a type I Langmuir isotherm (Helfferich *et al.*, 1993). The influence of isotherm shape on breakthrough profiles during adsorption and desorption will be further discussed in paragraph 5.2, but the long tailing during desorption is clearly not beneficial for efficient butanol recovery. This because this tailing effect leads to small butanol concentrations desorbing from the column for a long time, leading to an increase in recovery cost, since the Si-LTA column needs to be heated during the whole duration of the desorption procedure. Further, a larger amount of carrier gas is consumed due to this longer desorption time.

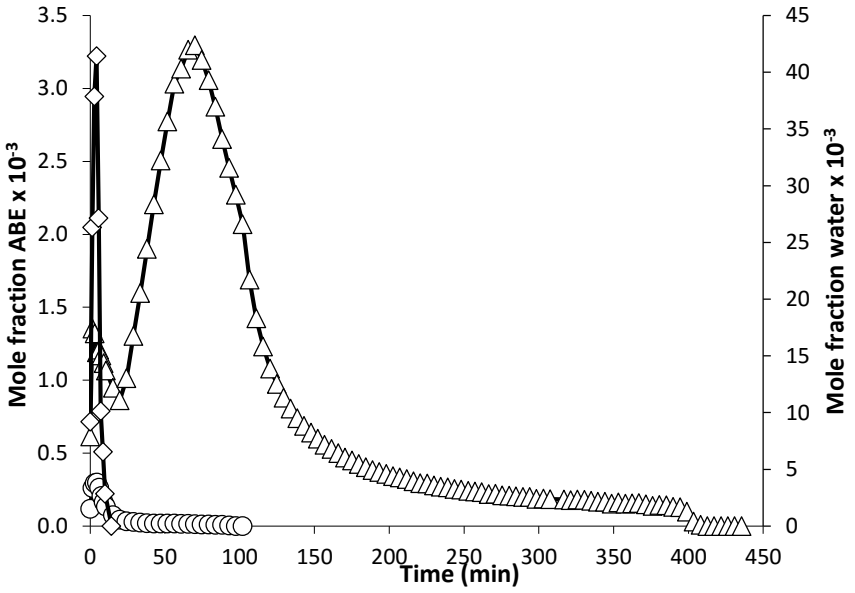

Figure 5.8: Desorption profile of the Si LTA column using He as carrier gas. The mole fraction at the outlet of the column of ethanol (○) and butanol (△) are shown on the left axis, whereas water mole fractions are presented on the right axis (◇). Acetone mole fractions are not shown, since only a trace amount of acetone was observed during desorption.

The desorption profile using CO_2 as carrier gas during adsorption and desorption of the Si-LTA column was added in Appendix 5. Essentially the same desorption profile was observed as for desorption using He as carrier gas, indicating the viability of the use of CO_2 as desorption carrier gas. The absolute butanol concentration was of course lower than for desorption using He, since the butanol and ethanol adsorption capacities were also lower using CO_2 as carrier gas (figure 5.7).

Interestingly, when using CO_2 as a desorbing agent, an increase in butanol concentration during the early stages of desorption was observed compared to experiments were He was used as carrier gas in both adsorption and desorption (figure 5.8). This increase in butanol concentration could be attributed to the adsorption of CO_2, pushing out the adsorbed butanol, since adsorption was performed using He as carrier gas. However, the same larger initial butanol concentration was observed after adsorption using CO_2 as carrier gas(Appendix 5, figure A5.2), hinting on a fundamental effect of CO_2 on the desorption behavior of butanol. Due to the increase in butanol concentration at the start of the desorption process, a corresponding decrease in butanol concentration is observed later on. This increase in butanol concentration in the early stages of desorption could lead to extra loss of butanol during recovery, because of the fact that most impurities desorb in the same time frame. Thus, if only the butanol fraction desorbing after the impurities is recovered, a higher amount of butanol is lost.

Further, temperature elevation during desorption is clearly necessary for efficient desorption of the Si-LTA column. A simultaneous plot of the temperature profile and the butanol desorption profile clearly shows a drop in butanol concentration at the column outlet corresponding to the end of the desorption temperature program (figure 5.9).

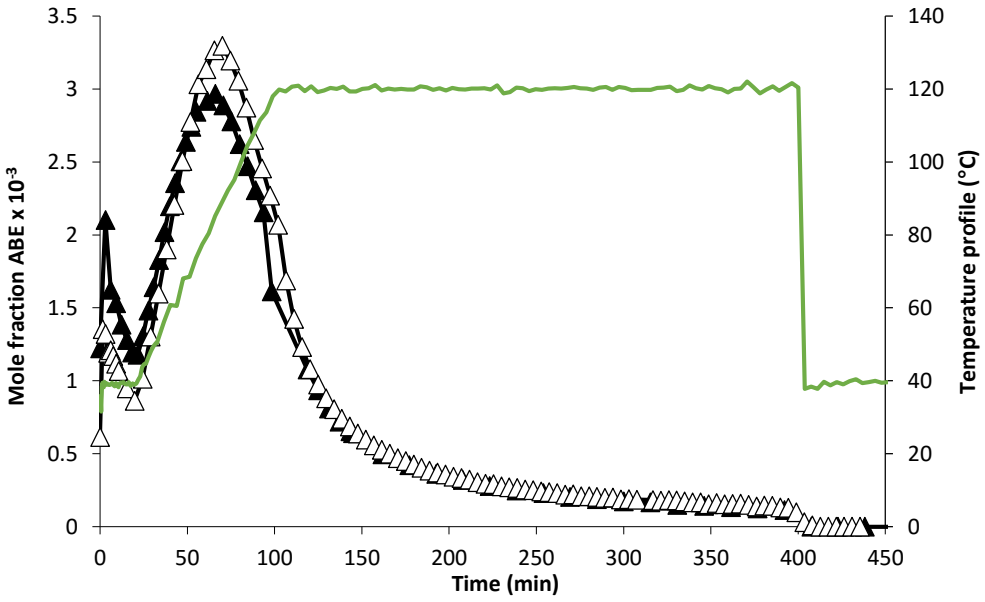

Figure 5.9: Comparison of the butanol desorption profile using He (△) and CO_2 (▲) during desorption. In both cases, adsorption of the column was performed using He as carrier gas. The temperature profile was included on the graph (green line).

5.2.2 ZIF-8 column

5.2.2.1 Adsorption

The breakthrough profile of a vapor phase ABE model mixture during adsorption on the ZIF-8 column is shown in figure 5.10. As could be predicted from the adsorption isotherms, ZIF-8 clearly showed the highest affinity for butanol of all four mixture components. The hydrophobicity of ZIF-8 caused almost immediate breakthrough of water, whereas a small amount of acetone and ethanol were adsorbed as well. These results lie in line with the results of Cousin Saint Remi *et al.* (2013), who performed liquid phase breakthrough experiments on ZIF-8.

Intriguingly, the butanol breakthrough profile did not show the standard S-shape as for the breakthrough profiles on Si-LTA. The reason for this lies in the in the butanol isotherm shape on ZIF-8, which does not show the standard type I shape, but itself has an S-shape (figure 5.2; Cousin Saint Remi *et al.*, 2011, Zhang *et al.*, 2013b). In fact, the velocity at which the concentration profile of a certain adsorbate i (also called chromatographic wave) propagates through a packed adsorbent column is dependent of the slope of the isotherm. This dependency is given by equation 5.1 (Ruthven, 1984; Helfferich & Carr, 1993), which is valid under ideal circumstances, meaning: equilibrium between stationary and mobile phase, ideal plug flow, no axial dispersion, axial uniform volumetric flow rate and isobaric and isothermal behavior:

$$v_{c_i} = \frac{v}{1 + (\frac{\rho}{\varepsilon})(\frac{dq}{dc}\Big|_{c_i})} \tag{5.1}$$

With:

v_{ci} = velocity at witch a concentration c_i of solute i propagates through the column (m/s)
v = bulk gas phase velocity (m/s)
ρ = sorbent bulk density (kg/m^3)
ε = porosity
q = adsorption capacity (kg/kg)
c = concentration of component i (kg/m^3)
$\frac{dq}{dc}\Big|_{c_i}$ = slope of the isotherm at concentration c_i (m^3 / kg)

Consequently, even under ideal conditions, the shape of a concentration step applied at an adsorbent column inlet can change when moving through the adsorbent column. In the simple case of a linear isotherm, the isotherm slope is a constant for all solute concentrations in the mobile phase. According to equation 5.1, the velocity at which a concentration c_i propagates in the breakthrough profile is thus the same for all concentrations. The broadening of the concentration profile is in this case only caused by kinetic effects: axial dispersion, deviations from plug flow and mass transfer limitations. In this case, wave broadness increases with the square root of distance or time (Helfferich & Carr, 1993).

However, when isotherms are not linear, the situation becomes more complex. For instance, consider a type I isotherm during adsorption, such as the butanol isotherm on Si-LTA (figure 5.1). During an adsorption process, the wave travelling through the adsorption column consist of a step with an increase in concentration, meaning that the lowest mixture concentrations move first through the column, followed by higher concentrations. Looking at the relation between isotherm slope and concentration velocity (equation 5.1), it's clear that for steeper isotherm slopes, the concentration velocity is lower. Since for a Langmuir isotherm, the isotherm slope is bigger at lower adsorbate concentrations, the low concentrations of the breakthrough wave move at a lower velocity than the

high concentrations. However, this would mean that the higher concentrations of an adsorbate would break through first, followed by the lower concentrations. Such a breakthrough would be physically impossible.

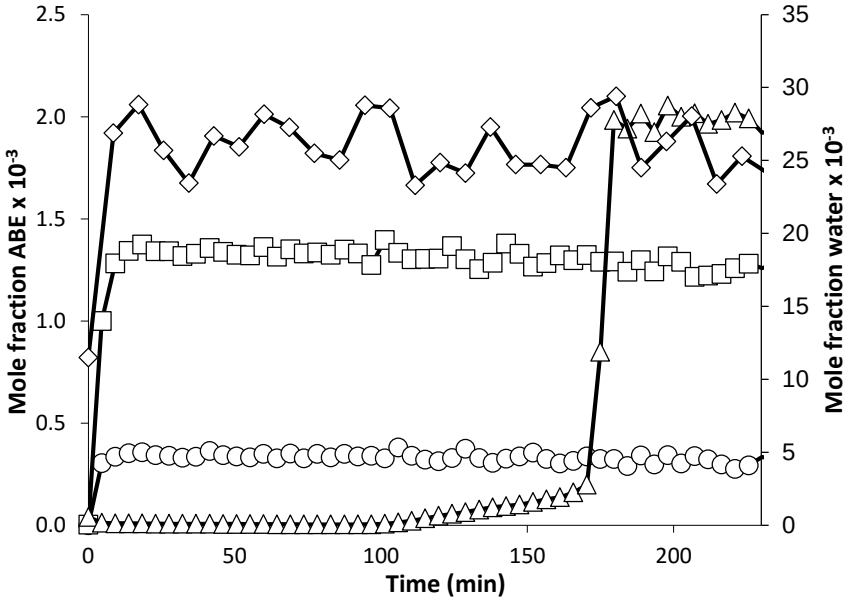

Figure 5.10: Breakthrough profile of the ZIF-8 column at 40 °C using He as carrier gas. The mole fractions at the column outlet are plotted as a function of time for acetone (❑), butanol (△), ethanol (○) and water (◇). For butanol, a slow increase in concentration was observed, followed by sharp breakthrough, as could be expected from the S-shaped isotherm. Vapor phase partial pressures at the column inlet were 50 Pa for ethanol, 305 Pa for butanol, 196 Pa for acetone and 4185Pa for water.

In ideal conditions, this velocity difference gives rise to a shock wave: a perfect concentration step that travels at a velocity given by equation 5.2 (Helfferich & Carr, 1993). The velocity at which the shock wave propagates is thus not dependent of the isotherm slope, but of the slope of the chord connecting the two extreme concentrations of the concentration step. For butanol on Si-LTA during adsorption, these two concentrations correspond to zero partial pressure and the partial pressure at the column inlet, as is shown in figure 5.11. In reality, the concentration profile is not a perfect step, but has an S-shape due to broadening of the profile due to axial dispersion, deviation from plug flow or mass transfer limitations (figure 5.11). Such a wave is called a self-sharpening wave. In the case of butanol on Si-LTA, mass transfer limitations in diffusion of butanol into the zeolite pores, further leads to an asymmetric breakthrough curve (figure 5.5; Helfferich & Carr, 1993).

$$v_{shock} = \frac{v}{1 + (\frac{\rho}{\varepsilon})\frac{\Delta q}{\Delta c}} \tag{5.2}$$

With:

v_{shock} = propagation velocity of shock (m/s)
q = difference in adsorption capacity corresponding to the difference in adsorbate concentration (kg/kg)
Δc = difference in adsorbate concentration over shock (kg/m^3)

During isothermal desorption of a component with a type I isotherm, a reverse phenomenon takes place. The concentration step at the column inlet is now inversed: initially, the column is completely saturated with adsorbate and is flushed with a carrier gas containing no adsorbing molecules.

Therefore, the concentration wave broadens whilst traveling through the column (figure 5.11). This because higher adsorbate concentrations have a higher propagation velocity than the lower concentrations in the wave (equation 5.1, figure 5.11). This effect is clearly visible for desorption of butanol on the Si-LTA column, after a certain amount of time, when the temperature reached its highest value, a very broad desorption profile was observed (figure 5.8, figure 5.9). The broadness of such a wave increases linearly with time or distance travelled (Helfferich & Carr, 1993).

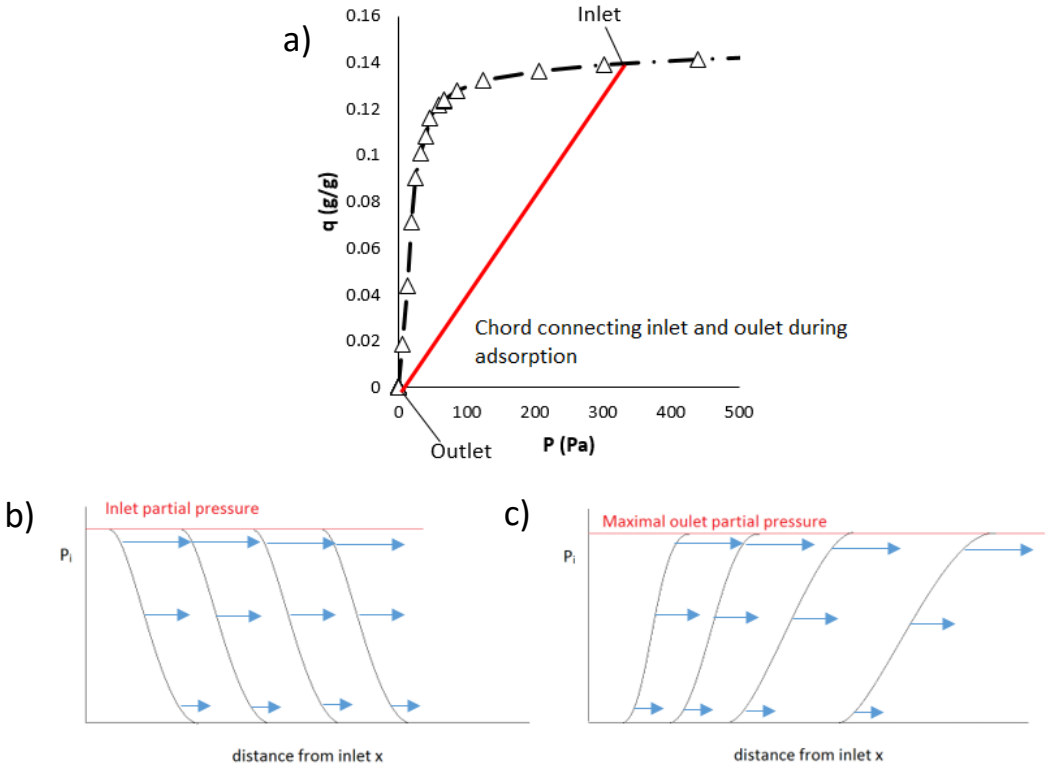

Figure 5.11: Theoretical breakthrough profiles predicted from a type I isotherm. a) Butanol isotherm on Si-LTA at 40 °C, with chord connecting inlet and outlet partial pressure. The slope of this chord is related to the propagation velocity of the shock wave via equation 5.2. b) theoretical butanol shock wave propagating through the Si-LTA column during adsorption. Arrows depict the velocity of the different concentrations in the wave as described by equation 5.1. c) Broadening wave during butanol desorption of the Si-LTA column propagating through the column. Arrows depict the velocity of the different concentrations in the wave as described by equation 5.1.

Such a broadening wave is also observed during adsorption of components showing type III isotherm behavior and is also called non-sharpening (Helfferich & Carr, 1993). Type III isotherms have the opposite shape of a type I isotherm and show an increase in isotherm slope with increasing concentration (Ruthven, 1984). Thus their behavior during adsorption and desorption is exactly opposite of that of a type I isotherm: a broad, non-sharpening wave is observed during adsorption and a self-sharpening wave during desorption. An isotherm showing type I behavior is therefore called a favorable isotherm, whereas an isotherm showing type III behavior is called an unfavorable isotherm (Ruthven, 1984). For clarity, the shape classification of isotherms is shown in Appendix 10.

Isotherms containing an inflection point, such as the S-shaped isotherms of ZIF-8, thus show a behavior that is a combination of a type III and a type I isotherm. Golden (1969) described a simple rule to

understand the breakthrough behavior of components with these types of complex isotherms. One could take a small piece of string and put it on the isotherm point corresponding to the initial conditions of the adsorption column. This corresponds to a bulk concentration of zero and an adsorption capacity of zero in the case of an adsorption breakthrough experiment as performed in this thesis. Then, the other side of the piece of string is moved counter clockwise to the point corresponding to equilibrium with the inlet conditions. All the points were the isotherm touches the piece of string, correspond to concentrations at which a dispersive, non-sharpening wave is observed. The points at which the isotherm does not touch the string, correspond to self-sharpening behavior. Applying this rule to a simple type I isotherm also holds true, with the piece of string corresponding to the chord drawn in figure 5.11.

Applying this rule to the butanol breakthrough profile observed on ZIF-8 (figure 5.10), explains the butanol breakthrough behavior. As is clarified in figure 5.12, the butanol breakthrough profile consists of two zones: a first zone where clearly a very broad breakthrough profile was observed and a second zone with a sharp breakthrough profile. Applying Goldens' string rule to the ZIF-8 isotherm also shown in figure 5.12, these two zones correspond to the two zones where the piece of string touches and does not touch the isotherm. The partial pressure of the transition between the two zones on the isotherm corresponds well with the point where the second zone starts in the breakthrough profile. A slight difference could be caused by kinetic effects, who should also be taken into account (Helfferich & Carr, 1993). A similar breakthrough profile could be expected for ethanol on ZIF-8 or ethanol on Si-LTA, since these isotherms also have an S-shape (figure 5.1 and figure 5.2, respectively). The vapor phase partial pressure of ethanol (50 Pa) at the inlet, however, was too low to create an effect on the breakthrough profile. In this partial pressure range, the ethanol isotherms are more or less linear.

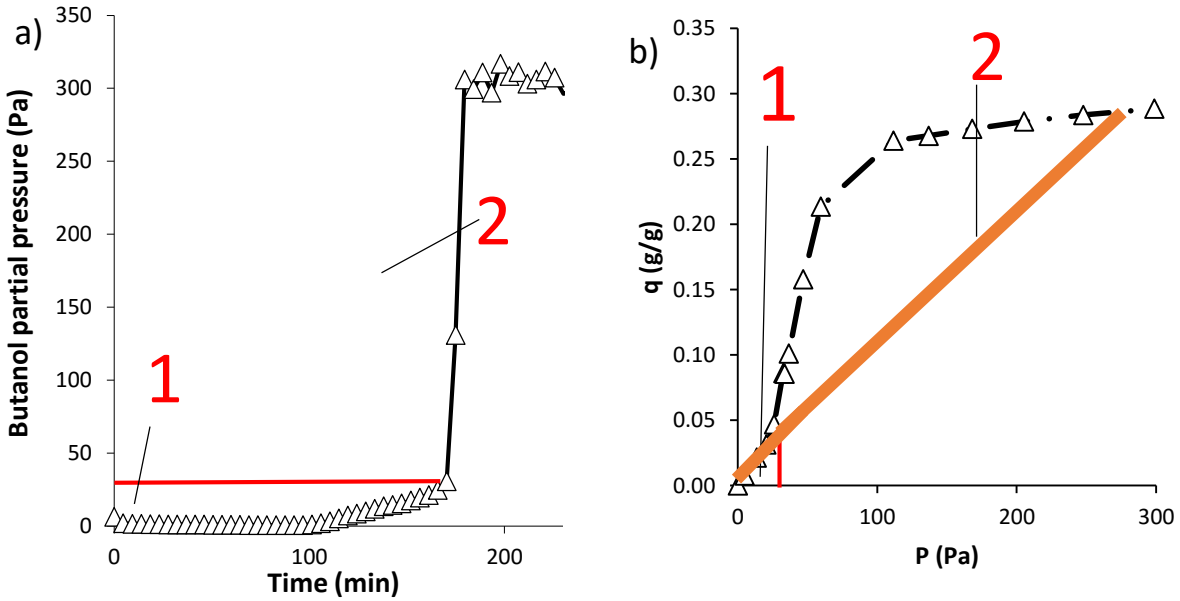

Figure 5.12: Application of Goldens' string rule to the ZIF-8 single component isotherm. a) Breakthrough profile of butanol on ZIF-8 with non-sharpening zone (1) and self-sharpening zone (2). These two zones correspond to two distinct zones in the ZIF-8 isotherm as shown in figure b). The partial pressures at which the transition between the two zones is observed was also marked. These partial pressures seem to match very well, although competitive adsorption and kinetic effects are not taken into account.

Comparing the adsorption capacity under dynamic conditions for Si-LTA and ZIF-8, ZIF-8 had a butanol adsorption capacity more than twice of that of Si-LTA (figure 5.13). Comparing the amount of adsorbed contaminants between the two materials, it's clear that ZIF-8 column adsorbed less water, but had a higher adsorption capacity for acetone.

When comparing CO_2 and He as carrier gas on the ZIF-8 material, some interesting phenomena were observed. First of all, the adsorption capacity for butanol was lower when CO_2 was used as carrier gas than when He was the carrier gas (figure 5.7 and figure 5.13). This could be expected, knowing that ZIF-8 shows some affinity for CO_2 (Danaci *et al.*, 2015). Secondly, for the ethanol, and especially the acetone breakthrough profiles, a large amount of tailing was observed (figure 5.12, Appendix 5). This tailing effect could be caused by a change in isotherm shape. However, for ethanol, the isotherm using CO_2 as carrier gas still has the same S-shape (figure 5.2). A second possible explanation could lie in a kinetic effect: the adsorbed CO_2 has to leave the pores of the MOF whilst simultaneously the adsorbing ethanol and acetone should enter those same pores, leading to slower diffusion of the ABE mixture components into the adsorbent.

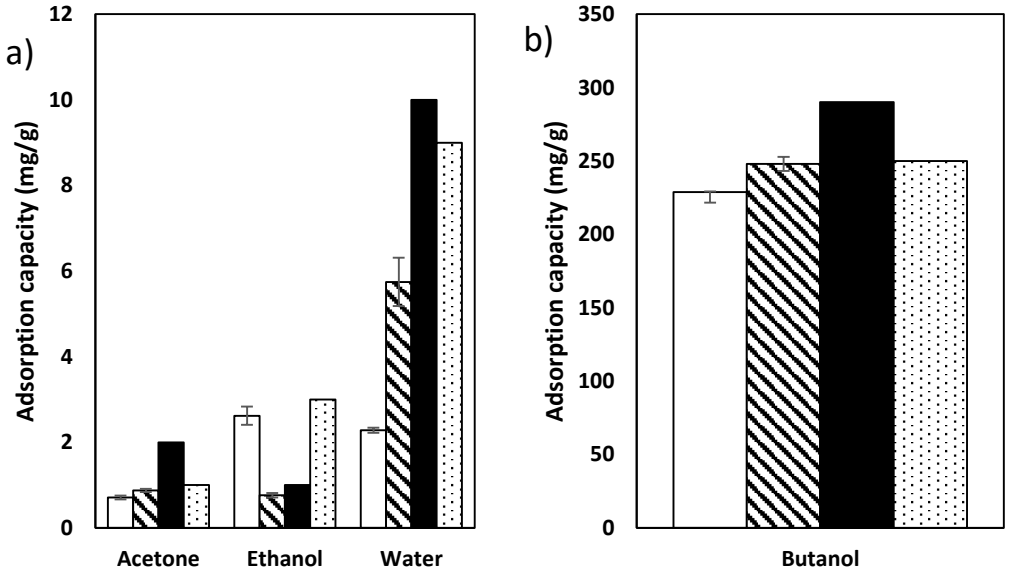

Figure 5.13: Comparison of the adsorption capacities of the different vapor phase ABE components using CO_2 (blank bars) and He (shaded bars) as carrier gas for breakthrough experiments at 40 °C on the Si-LTA column. Single component isotherm capacity values under N_2 (black bars) and CO_2 (dotted bars) are also shown. Error on breakthrough adsorption capacity calculations was estimated using the standard deviation (shown on graph). a) Adsorption capacities of acetone, ethanol and water. b) Adsorption capacity of butanol.

For butanol, the slow increasing concentration front observed during adsorption was even larger under CO_2 (figure 5.14) and a clear shift in retention time was also observed. However, this retention time shift did not lead to a larger adsorption capacity (figure 5.7, figure 5.13), due to the fact that the pressure drop over the ZIF-8 column increased, leading to a decrease in mole fraction of the different components and a corresponding decrease in adsorption capacity (equation 4.3). Thirdly, the ethanol adsorption capacity on ZIF-8 using CO_2 as carrier gas is lower than using He as carrier gas. The cause for this lies in the ethanol and butanol isotherm shift (paragraph 5.1.2). Whilst the butanol isotherm shifts to the right, the ethanol isotherms showed a slight shift to the left (figure 5.2). This was also reflected in the selectivity of the column for butanol (table 5.2). The butanol selectivity compared to ethanol is higher with He then with CO_2. The combination of the two shifts in the isotherms led to an

increase in ethanol adsorption under CO_2 in breakthrough adsorption. Selectivity for butanol compared to water and acetone increased using CO_2 as carrier gas during adsorption, since the decrease in adsorption capacity of butanol was proportionally lower than that of water and acetone (figure 5.13, table 5.2). A complete adsorption profile using CO_2 as carrier gas was added as appendix (Appendix 5).

Table 5.2: Comparison of the selectivity of the ZIF-8 column for butanol in dynamic conditions using He and CO_2 as carrier gas.

Selectivity	Adsorption using He	Adsorption using CO_2
Butanol/ethanol	39	8
Butanol/acetone	5	168
Butanol/water	220	346

Thus as an overall conclusion, the adsorption breakthrough experiments on the ZIF-8 column confirmed its selectivity for butanol, though some minor amounts of acetone, butanol and ethanol were adsorbed as well. The ZIF-8 capacity for butanol was higher than that of the Si-LTA column. Due to the S-shaped isotherm of butanol, fronting of this breakthrough profile was observed, leading to worse separation performance during adsorption. Comparison of He and CO_2 as carrier gas showed the adsorption capacity of butanol to be lower using CO_2 as a carrier gas.

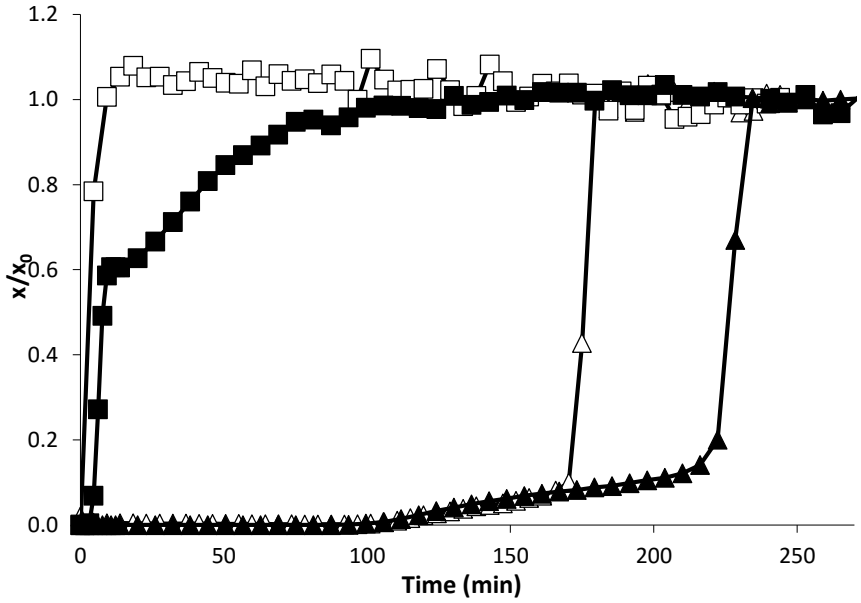

Figure 5.14: Comparison of adsorption breakthrough profiles on ZIF-8 for acetone and butanol using He (□, △) and CO_2 (■, ▲) as carrier gas. Mole fractions normalized to their breakthrough values are plotted as a function of time. Tailing of the acetone breakthrough profile could be clearly observed, as well as increased fronting of the butanol breakthrough profile. Vapor phase partial pressures at the column inlet were 49 Pa for ethanol, 295 Pa for butanol, 190 Pa for acetone and 4230 Pa for water.

5.2.2.2 Desorption

For the desorption of the ZIF-8 column, different conditions were tested and compared. First of all, desorption using a temperature gradient was compared with isothermal desorption. Secondly, the influence of the carrier gas on desorption was examined, comparing He and CO_2.

Results of the desorption experiment using a temperature gradient of 1 °C/min from 40 °C to 100 °C, followed by isothermal desorption at 100 °C for 90 min are shown in figure 5.15. As could be expected from the adsorption breakthrough data, a certain amount of acetone, ethanol and water desorbed from the ZIF-8 column. Interestingly, a sudden sharp decrease in butanol concentration at the column outlet was observed. Again, this can be explained by the S-shaped butanol isotherm, as will be discussed further. Further, all of the adsorbed butanol desorbed before the regeneration temperature of 100 °C was reached, making the desorption more energy efficient, compared to Si-LTA (figure 5.14).

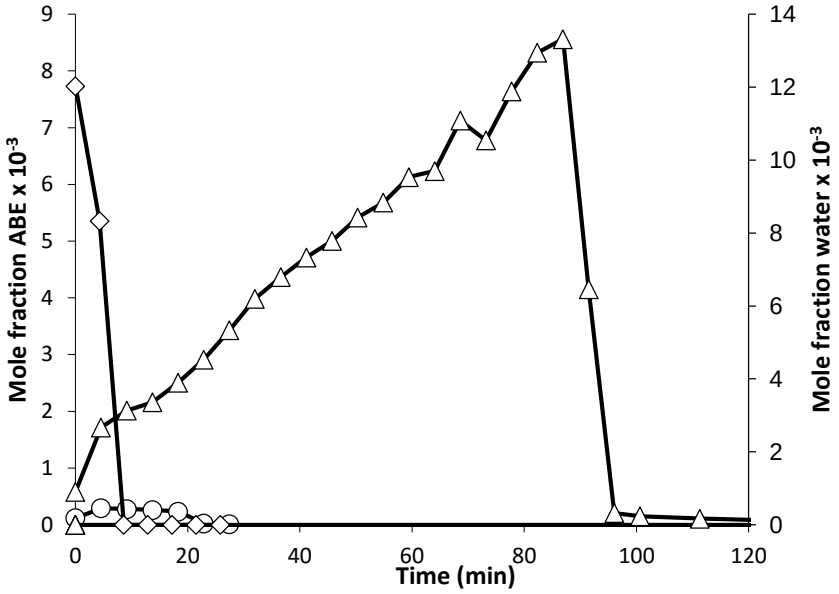

Figure 5.15: Desorption breakthrough profile for the ZIF-8 column using a temperature gradient and He as carrier gas. Acetone (❑), butanol (△), ethanol (○) and water (◇) mole fractions were plotted as a function of time.

Indeed, due to the high reversibility of the adsorption equilibrium, even isothermal desorption at 40 °C was feasible within an acceptable time-frame for the ZIF-8 column (figure 5.16). This contrary to the Si-LTA column, where higher temperatures were absolute necessary for efficient desorption (figure 5.9). Off course, desorption at lower temperatures, leads to lower concentrations at the column outlet. These results are confirmed by Cousin Saint Remi *et al.* (2012), who performed breakthrough experiments in liquid phase and showed a temperature of 90 °C to be sufficient for complete butanol desorption. A trade-off thus needs to be made between higher temperature desorption, which leads to faster desorption times and higher concentrations, and desorption at lower temperatures, which is more energy efficient. For this reason, desorption experiments on ZIF-8 during the multicolumn experiments were performed isothermally. A full isothermal desorption profile was added in appendix (appendix 5).

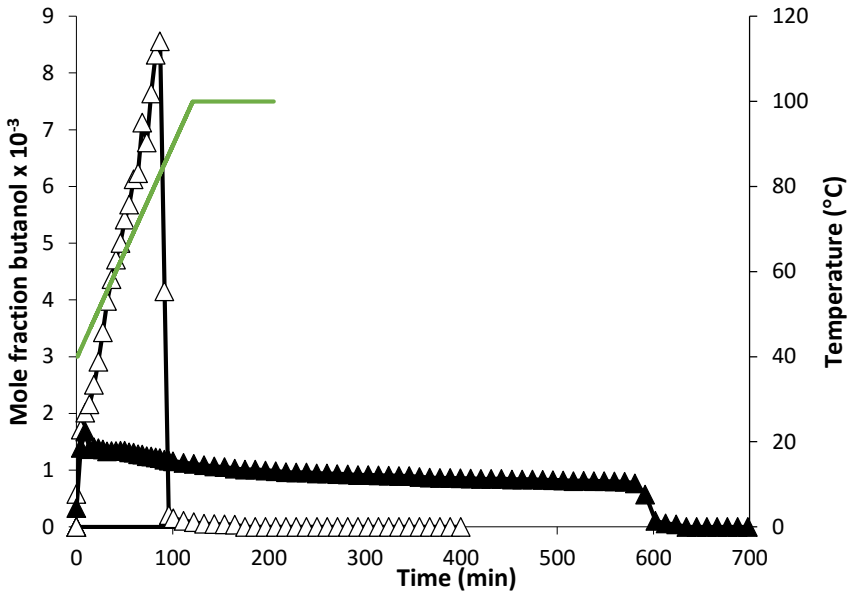

Figure 5.16: Comparison between the butanol desorption profile using a temperature gradient (△) and isothermal desorption (▲). At 80 °C, most of the adsorbed butanol was completely desorbed. The temperature profile used during gradient desorption is shown in green.

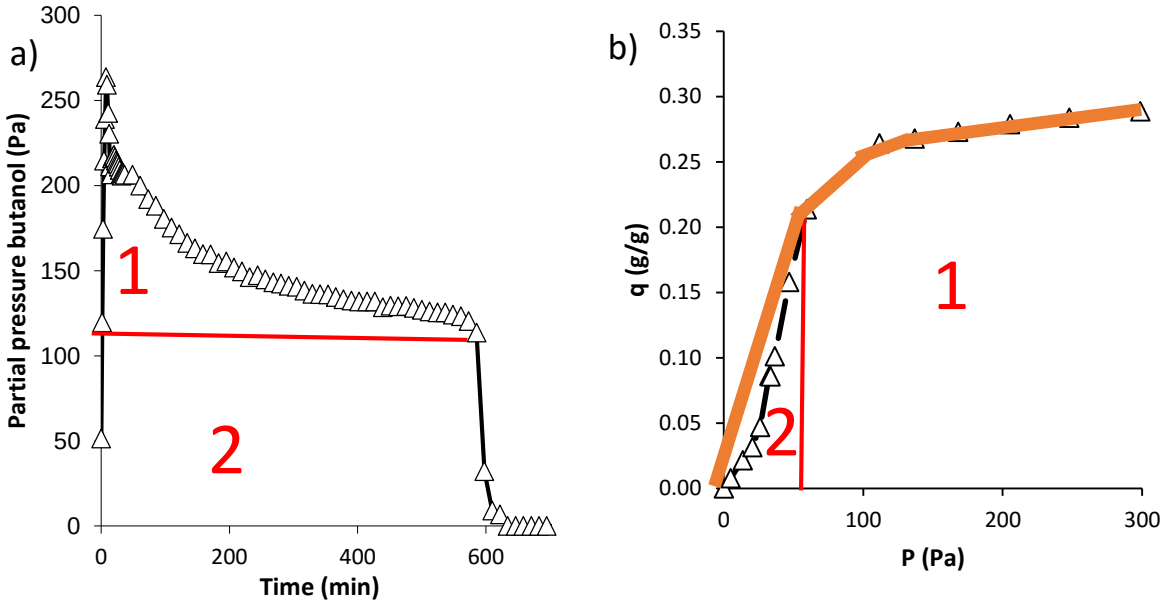

Figure 5.17: Application of Goldens' string rule during isothermal butanol desorption on ZIF-8. a) Butanol desorption profile at 40 °C. b) Butanol isotherm at 40 °C using N_2. Two distinct zones are visible in the isotherm and in the breakthrough profile, leading to self-sharpening and non-sharpening behavior.

To investigate the effect of CO_2 during desorption, an adsorption experiment was performed using He as carrier gas, followed by desorption under CO_2. Figure 5.18 compares the butanol desorption curve using He as carrier gas and using CO_2 as carrier gas during desorption. The adsorption of CO_2 on ZIF-8 caused a push-out of the adsorbed components, especially butanol. This reduced the time necessary for the desorption experiment drastically. The use of a different carrier gas for adsorption and desorption thus might seem interesting, however, different conclusions can be drawn looking at

butanol purity and recovery calculations. For the isothermal desorption under He, if one would like to recover 100% pure butanol, 92% of the adsorbed butanol can be recovered. However, for desorption under CO_2, only 90% of the adsorbed butanol can be recovered at 100% purity. The cause of this effect lies in the fact that not only butanol is pushed out at higher concentrations, but also the other contaminants. This increased the total amount of butanol contaminated in the early stages of the desorption experiments. The desorption profile using CO_2 as carrier gas during adsorption and desorption showed the same general shape as the He desorption profile, making CO_2 thus a viable carrier gas for butanol recovery. This isothermal desorption profile was added in appendix (Appendix 5).

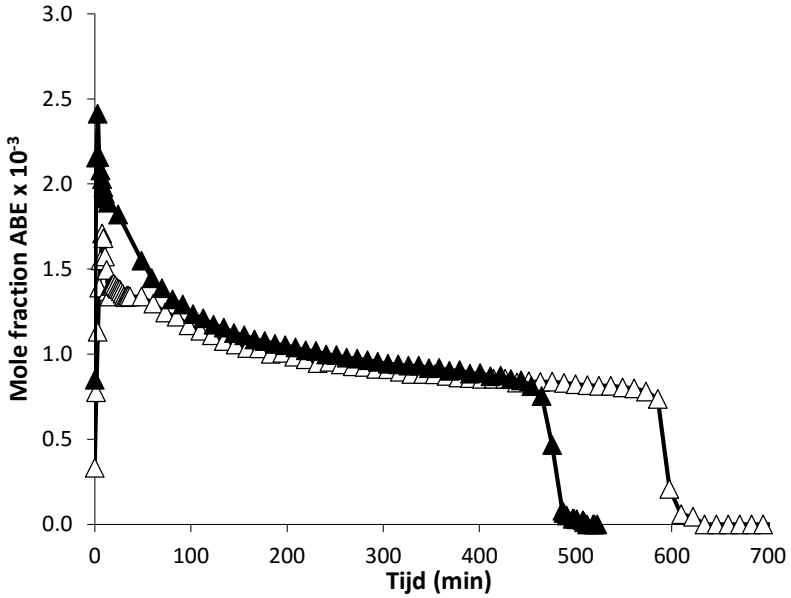

Figure 5.18: Comparison of butanol desorption on ZIF-8 at 40 °C using He (△) and CO_2 (▲) as carrier gas. The column was first completely saturated under He.

5.2.3 SAPO-34 & Si-CHA columns

5.2.3.1 Adsorption

So far, the multicomponent breakthrough behavior of ZIF-8 and Si-LTA have been discussed. Both of these hydrophobic materials show a high selectivity for butanol. However, as could be assumed from the isotherm measurements (figure 5.3), the hydrophilic SAPO-34 material should show a higher affinity for ethanol and water. For this material, breakthrough experiments using a model vapor phase ABE mixture were performed, also evaluating He and CO_2 as carrier gas. The breakthrough profile under He, presented in figure 5.19, confirmed the selectivity of the SAPO-34 material for ethanol and water.

As was discussed earlier, the Si-CHA shows the same selectivity for ethanol, though it adsorbs less water than the polar SAPO-34 zeolite. Figure 5.20 compares the adsorption capacities of SAPO-34 and Si-CHA under dynamic conditions. Clearly, the SAPO-34 column had a lower ethanol adsorption capacity, due to the higher amount of water adsorbed compared to Si-CHA. The butanol capacity of Si-CHA was measured by Gelin (2015) to be higher than that of SAPO-34, which can be explained by the hydrophobicity of Si-CHA. Although the window size of chabazite zeolites is too small for fast butanol adsorption (Remy *et al.*, 2011), a certain affinity of Si-CHA for butanol is predicted via molecular simulations (Krishna & Van Baten, 2011). Because of this small amount of butanol adsorption on Si-CHA, the ethanol/butanol selectivity is lower on this material (table 5.3).

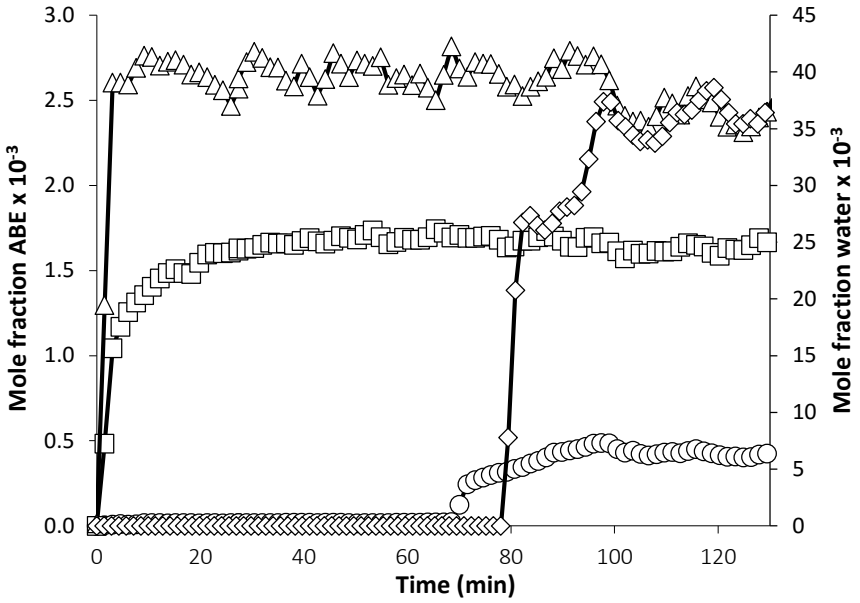

Figure 5.19: Adsorption breakthrough profile of SAPO-34 at 40 °C using He as carrier gas. Acetone and butanol showed almost no affinity for the SAPO-34 column, whilst ethanol and water were adsorbed in larger amounts. Mole fractions of acetone (❑), butanol (△), ethanol (○) and water (◇) at the column outlet were plotted as function of time. Vapor phase partial pressures at the column inlet were 49 Pa for ethanol, 295 Pa for butanol, 196 Pa for acetone and 4185Pa for water.

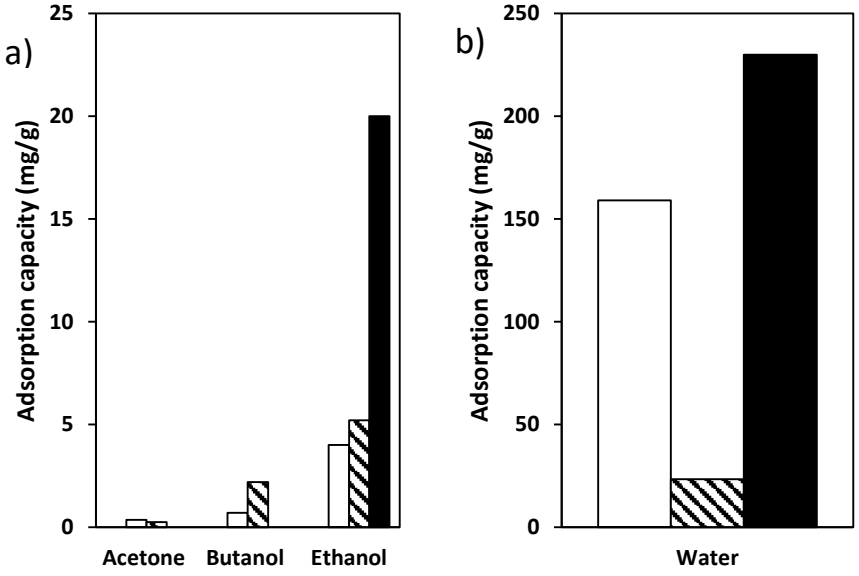

Figure 5.20: Comparison between the dynamic adsorption capacities of SAPO-34 (blank bars) and Si-CHA (shaded bars; Gelin, 2015) using a model ABE mixture and an adsorption temperature of 40 °C. Since no water breakthrough profile was available, the data of an ethanol-butanol-water vapor mixture with the same partial pressures was used. The N_2 isotherm adsorption capacity on SAPO-34 was added as a comparison (black bars).

Remarkably, during adsorption using CO_2 as carrier gas, the SAPO-34 sample showed catalytic activity. On the GC chromatograms, a second peak, with a retention time close to that of ethanol was observed. Catalytic activity of the SAPO-34 sample could be expected, since this zeolite is commonly used in the

methanol-to-olefin (MTO) process (Lefevre *et al.*, 2013; Galadima & Muraza, 2015). SAPO-34 was also investigated as possible catalyst for bio-ethanol conversion to ethylene (Chen *et al.*, 2010). Thus conversion of ethanol to other products could be expected during the performed experiments. Indeed, the signal intensities measured for ethanol at breakthrough were much lower than measured for a blanc measurement. However, catalytic activity at 40 °C is quite remarkable, since these conversion processes usually take place at much higher temperatures. Temperatures for bio-ethanol conversion, for instance, lie in the range of 200 °C-400 °C (Chen *et al.*, 2010). A possible explanation for the catalytic activity of SAPO-34 using CO_2 as carrier could lie in the simultaneous presence of CO_2 and H_2O in feed mixture, leading to a change in acidity of the environment in the zeolite pores. The acidic sites of the SAPO-34 zeolite that play an important role in the ethanol conversion mechanism to ethylene and propylene, for instance (Chen *et al.*, 2010). However, this catalytic activity could also be caused by acetone, since SAPO-34 is also reported as catalyst for the acetone-to-olefin process (Hirota *et al.*, 2012). An experimental chromatogram showing the extra peak was added in appendix (Appendix 6).

Table 5.3: Comparison of the selectivity of the SAPO-34 and Si-CHA column (Gelin, 2015) in vapor phase ABE breakthrough at 40 °C using He as carrier gas.

Selectivity	SAPO-34	Si-CHA
Ethanol/butanol	55	10
Ethanol/water	0.8	3.0

5.2.3.2 Desorption

Following the adsorption experiments, measurements of desorption breakthrough profiles occurred. Desorption on the SAPO-34 zeolite was performed using the temperature program described in the materials & methods section. As could be expected from the known catalytic activity of the SAPO-34 zeolite, during the temperature increase, an extra component was observed on the GC chromatograms. However, this component had a different retention time than the one observed during adsorption using CO_2 as carrier gas. Because this catalytic activity poses difficulties for the correct calculation of the component mole fractions, the signal intensities normalized to their breakthrough values were plotted as function of time (figure 5.21).

SAPO-34 thus shows promising properties for the removal of ethanol from vapor phase ABE mixtures. A possible showstopper might be the catalytic activity observed using CO_2 and during the desorption of the material at higher temperature. Si-CHA was already described in detail by Gelin (2015) and shows the same selectivity for ethanol, but has a lower adsorption capacity for water.

5.3 Multicolumn breakthrough experiments

5.3.1 Introduction

Characterization of the four adsorbents used in this thesis via isotherm measurements and breakthrough experiments clarified their selectivity for the different ABE mixtures. The hydrophobic zeolite Si-LTA shows a high butanol adsorption capacity, with minor amounts of ethanol and water also adsorbing on the zeolite framework (figure 5.7). This makes the Si-LTA material an interesting candidate for the removal of butanol from the ABE vapor phase mixture. A second candidate for butanol removal was also identified, being the hydrophobic MOF ZIF-8 (figure 5.13). Important contaminants co-adsorbing on this material were acetone, ethanol and water. Two chabazite-structured zeolites were also evaluated. The polar SAPO-34 material was shown to selectively remove

ethanol and water from the vapor phase ABE mixture (figure 5.19). The Si-CHA material studied by Gelin (2015) showed the same selectivity for water and ethanol. However, due to the hydrophobicity of this material, it showed a higher ethanol adsorption capacity (figure 5.20).

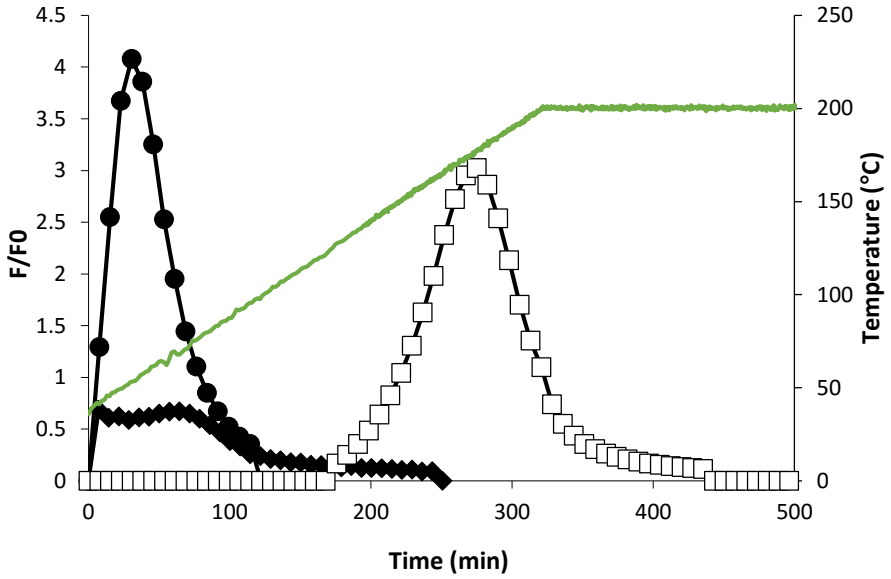

Figure 5.21: Signal intensities normalized to their breakthrough value plotted as a function of time. CO_2 was used as carrier gas and the values for ethanol (●), water (◆) and the second catalytic component (❑) are shown. The temperature profile used during desorption is represented by the green line.

The goal of this Master's thesis was to identify a combination of adsorption columns leading to a purified butanol stream. Different combinations of these columns can be imagined, they can even be combined during adsorption and desorption, giving rise to a large amount of operational and configurational possibilities. Bearing in mind the selectivity of each column, these combinations could result in a higher or purer butanol yield, compared to a single-column setup. Since the SAPO-34/Si-CHA and the ZIF-8/Si-LTA materials showed affinity for ethanol and butanol respectively, they could replace each other in a multicolumn butanol purification configuration. Therefore, different column combinations were evaluated in an experimental and theoretical way for ethanol and butanol recovery, with a strong focus on butanol purification.

A first simple system that can be imagined would be the combination of a SAPO-34 or Si-CHA column with a ZIF-8 or Si LTA column in series, sending the feed ABE vapor phase mixture first through one of both columns and the exit stream, subsequently through a second column. These different configurational possibilities are shown in figure 5.22. However, looking in more detail to the properties of each adsorption column, some of these possibilities could be expected to be more efficient than others. For instance, both ZIF-8 and Si-LTA were shown to adsorb some ethanol in breakthrough experiments (figure 5.7 and figure 5.13). Thus, placing the SAPO-34 or Si-CHA column before the Si-LTA or ZIF-8 column would be more logical than placing them the other way around. In this way, ideally only a mixture of water, acetone and butanol is fed to the second ZIF-8 or Si-LTA column. When these columns are subsequently desorbed, no contamination of the purified butanol with ethanol occurs. However, some extra problems might arise using such a configuration.

First of all, the SAPO-34 shows a high water adsorption capacity. As a consequence, its adsorption capacity for ethanol becomes lower. This means a large amount of SAPO-34 material would be necessary to feed a complete ethanol-free ABE model mixture to the following column. The Si-CHA material thus would be a better a candidate to use as a first column. Since this material was not available at the moment of the experiments, this configuration was evaluated using modelling methods.

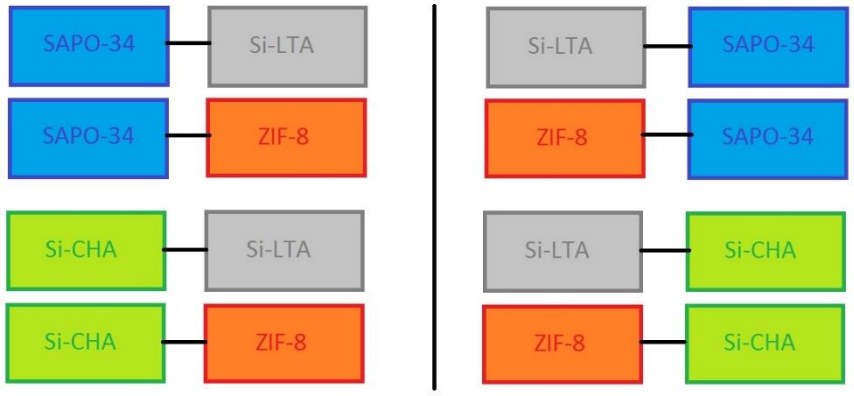

Figure 5.22: Different possible column combinations for direct purification of the ABE vapor stream, meaning a full vapor phase mixture was fed to the first column and subsequently through the second column. The combinations on the right side of the figure were not tested, since these would not lead to a higher final butanol purity. The combinations on the left side of the figure were verified using modelling methods.

As mentioned before, a large amount of SAPO-34 or Si-CHA material will be necessary to completely remove ethanol from the incoming ABE vapor stream to maximize the amount of pure butanol adsorbed on the following ZIF-8 or Si-LTA column. An alternative method could consist of the complete saturation of the ZIF-8 or Si-LTA column using the full ABE vapor phase mixture. During the following desorption step, a second SAPO-34 or Si-CHA column could be placed behind this first column. In this way, the small amount of ethanol and/or water desorbing from these materials could be removed by SAPO-34 and Si-CHA. Combinations of the Si-LTA and ZIF-8 column with SAPO-34 column were evaluated experimentally using this configuration. The combination of Si-LTA and Si-CHA was also tested, though no experiments were performed with the ZIF-8 and Si-CHA, since the Si-CHA material was not available at the time of the experiments. These different combinations are shown in figure 5.23. For the combination of ZIF-8/Si-LTA and SAPO-34, a comparison was made between CO_2 and He as carrier gas.

5.3.2 Si-LTA desorption

Desorption of the Si-LTA column was performed in combination with the Si-CHA and the SAPO-34 column. For desorption in combination with the SAPO-34 column, a comparison in performance was made between desorption using CO_2 and He as carrier gas. Since ethanol and water desorb during the early stages of the Si-LTA desorption process, the Si-CHA and SAPO-34 column were only placed behind the Si-LTA column for 50 min. Using them during the complete desorption of the Si-LTA column could lead to desorption of the adsorbed ethanol and water on the Si-CHA and SAPO-34 column before complete butanol desorption of the Si-LTA column. In this way, the separation performance of the Si-LTA is ruined (figure 5.24b). The residence time of the Si-CHA and SAPO-34 column were chosen for

maximal high-purity butanol recovery (figure 5.24c, d). Desorption profiles for the different tested column combinations are shown in Appendix 7.

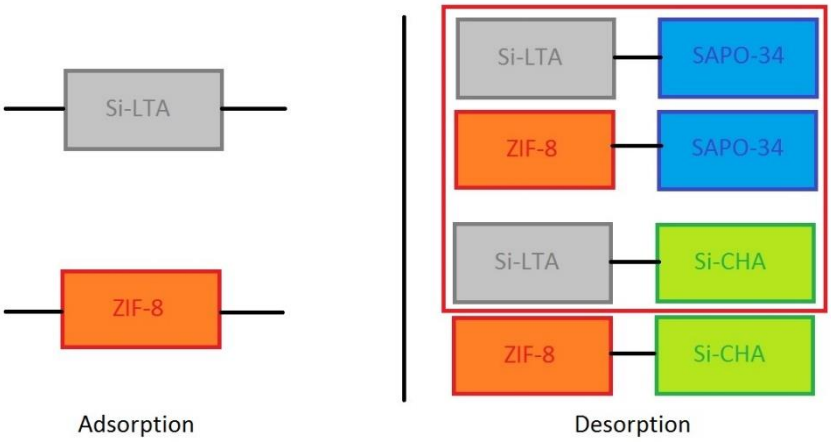

Figure 5.23: Lay-out of the two-column configurations evaluated in this thesis. In a first step, the Si-LTA or ZIF-8 column was completely saturated with an aqueous ABE mixture in vapor phase. During the desorption of this first Si-LTA or ZIF-8 column, a second column was added to adsorb the ethanol and water desorbing from the first column. The combinations encapsulated by the red square were experimentally verified.

A comparison between the purity and recovery plots shows the great benefit of the addition of an extra column to further purify the butanol stream. For the combination of Si-LTA and Si-CHA already a smaller amount of ethanol and water is present in the desorbing butanol, leading to a higher purity at higher recovery. However, the results for the combination of Si-LTA and SAPO-34 showed the greatest improvement. No measureable amount of water was present in the purified butanol product stream and only a small amount of ethanol could be detected (figure 5.24).

The combination of SAPO-34 and Si-LTA column led to a final butanol purity of 99.9 wt% whilst recovering all of the desorbing butanol. These values are high compared to butanol purity values found in the literature. Faisal *et al.* (2016) for instance performed adsorption in liquid phase on a silicalite adsorbent, but desorbed using nitrogen gas. The product stream resulting from desorption was subsequently send to a condenser, with the maximal butanol purity reported to be 88.5 wt%. Liquid phase desorption results of Cousin Saint Remi *et al.* (2011) on ZIF-8 show a maximum butanol concentration of 20 wt%. Abdehagh *et al.* (2015) used a similar approach as Faisal *et al.* (2016) on their AC F-400, first performing adsorption of an ABE model mixture in liquid phase, followed by desorption using CO_2 as carrier gas. In their study, a final concentration of 15 wt% was reported. This approach was also used by Saravanan *et al.* (2010) on ZSM-5. Inert argon was used as purging gas, yielding a maximal butanol concentration of 84.3 wt%. Similarly, Lin *et al.* (2012b) observed a final butanol concentration of 14 wt% using methanol as desorbent after liquid phase adsorption of an ABE model mixture. In this context, it should be mentioned that a butanol purity of 76 wt% could be achieved on the Si-LTA column without combining it with a second adsorption column and recovering all of the desorbing butanol.

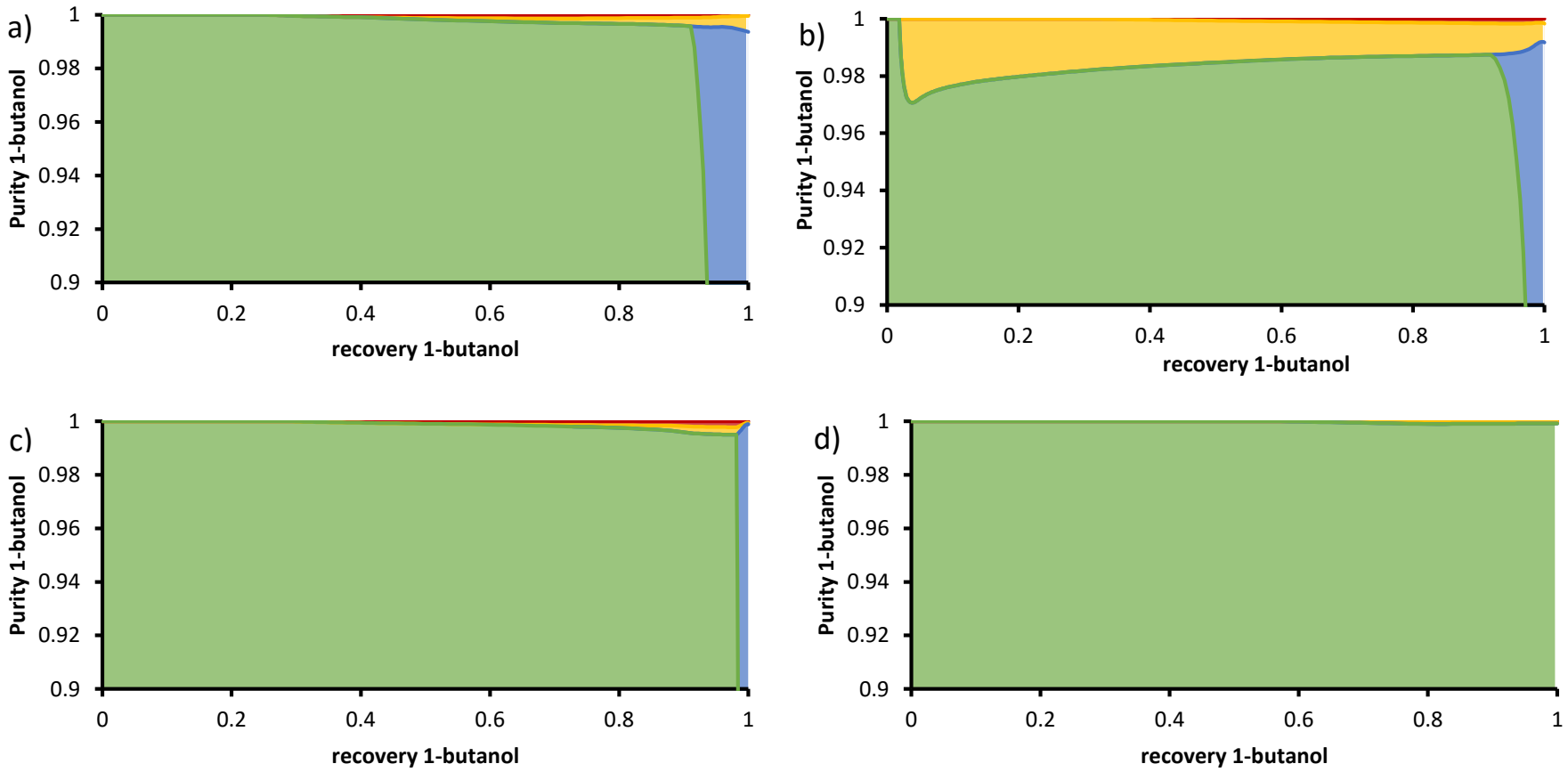

Figure 5.24: Comparison of purity versus recovery plots for desorption of the Si-LTA in combination with the Si-CHA and SAPO-34 column. The green curve represents the plot of the purity of 1-butanol versus the recovery. The colored areas representing acetone (red), butanol (green), water (blue) and ethanol (yellow) visualize the amount of impurities present for a certain amount of butanol recovered. Purity is expressed on a mole % base. a) Results for desorption of the Si-LTA column without the use of a second column. b) Results for desorption of the Si-LTA column in combination with the Si-CHA column. The Si-CHA column was placed behind the Si-LTA column for the whole of the desorption procedure. c) Results for desorption of the Si-LTA column in combination with the Si-CHA column for 50 min. d) Results of the desorption of the Si-LTA column in combination with the SAPO-34 column for 50 min.

The same experiments were repeated using CO_2 as carrier gas during adsorption and desorption (figure 5.25). A comparison was made between desorption of the Si-LTA column with and without the SAPO-34 column. The SAPO-34 column was again placed behind the Si-LTA column for 50 min. Similar results were obtained as for desorption using He as carrier gas, confirming the viability of the use of CO_2 as carrier gas for vapor phase butanol recovery. For 100 % butanol recovery, a butanol purity of 99.9 wt% was obtained, compared to the 68 wt% without the second column. Interestingly, the catalytic products observed during SAPO-34 breakthrough using CO_2 were not observed during this experiment. Probably, the absence of catalytic activity was caused by the low concentration of ethanol desorbing from the Si-LTA column and entering the SAPO-34 column.

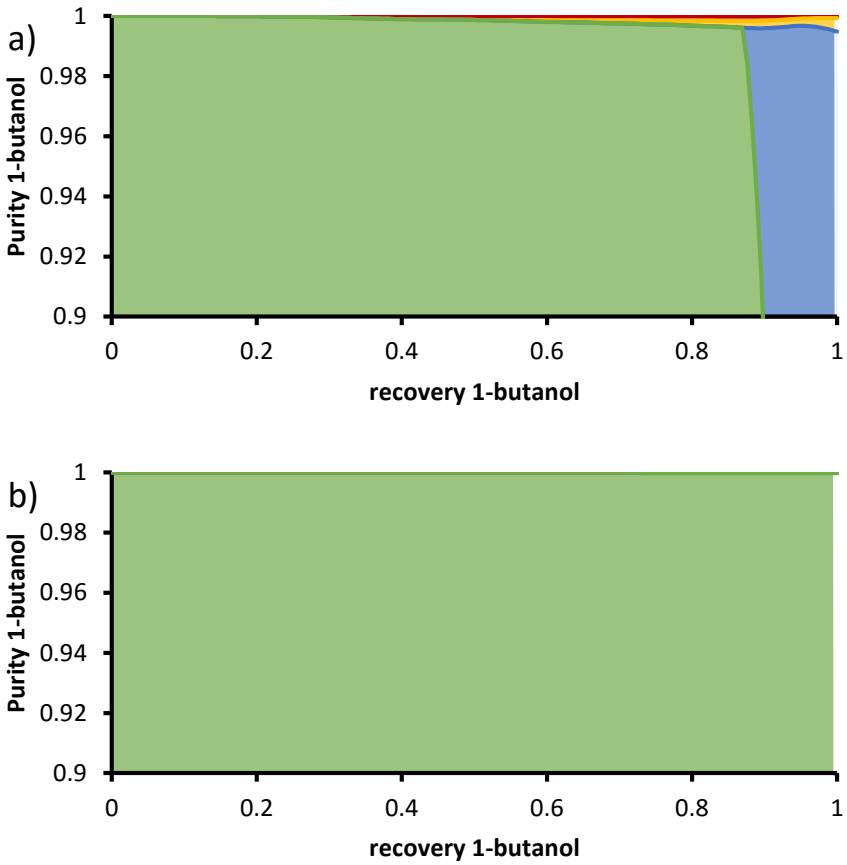

Figure 5.25: Plot of butanol purity as a function of butanol recovery. The colored areas represent the amount of ABE components present in the desorbing mixture: acetone (red), butanol (green), ethanol (yellow) and water (blue). Purity is expressed on a mole % base. a) Desorption results for the Si-LTA column without SAPO-34. The lower figure shows the desorption results of the combination Si-LTA and SAPO-34. Saturation of the column and desorption was performed using CO_2 as carrier gas.

5.3.3 ZIF-8 desorption

For the desorption of the ZIF-8 column, only the desorption with and without SAPO-34 was performed experimentally (figure 5.26). A comparison was made between separation performance using He and CO_2 as carrier gas. All the desorption experiments were performed isothermally. For desorption with ZIF-8, the SAPO-34 column was used during the first 40 min of the desorption experiment.

The results for the use of He as carrier gas during adsorption and desorption are presented in figure 5.26 (a and b). The relevant desorption profiles were added in appendix (Appendix 7). Similar results

were obtained as for the combination of the Si-LTA and SAPO-34 column. The small amounts of water and ethanol desorbing from the ZIF-8 column were completely adsorbed by the SAPO-34 column, leading to an increase in final butanol concentration from 76 wt% to 99.5 wt% at 100 % butanol recovery. The reason for the higher amount of impurities when desorbing with the ZIF-8 column lies in the larger amount acetone adsorbing on this material and thus contaminating the desorbing butanol stream. Again these concentration values are much higher than the maximum values presented in literature for liquid and vapor phase desorption (Cousin Saint Remi *et al.*, 2011; Lin *et al.*, 2012b; Abdehagh *et al.*, 2015; Faisal *et al.*, 2016). Unfortunately, catalytic activity of SAPO-34 was observed during the experiments with ZIF-8. However, the amounts of catalytic product observed were very low. For purity and recovery calculations, the peak areas were compared with those of ethanol to approximate the real mole fraction. The catalytic activity observed during the desorption of ZIF-8 with SAPO-34 was not observed in the combination of Si-LTA and SAPO-34. The reason for this could lie in the higher amount of acetone adsorbed on ZIF-8, leading to catalytic conversion of acetone (figure 5.13; Hirota *et al.*, 2012).

The experiments using He as carrier gas were repeated using CO_2. The results show the same trend as for He as carrier gas (figure 5.26 c and d). Desorption without SAPO-34 led to a butanol concentration of 93 wt%, whilst the combination with of ZIF-8 and the SAPO-34 column led to 99.5 wt% of butanol. These results are similar to those obtained using He as carrier gas. Again, the same catalytic product was visible on the GC chromatogram. For calculation of recovery and purity and mole fraction calculation, the equivalent peak area of ethanol was used as approximation. It should also be mentioned that desorption using CO_2 as carrier gas shows a better purity recovery-profile compared to adsorption and desorption using He as carrier gas. This is due to the lower adsorption capacity of acetone and water on ZIF-8 during adsorption with CO_2 (figure 5.13). This effect is also visible in the butanol selectivity values (table 5.2).

5.3.4 First comparison

After discussion of the results of the two-column breakthrough experiments, some interesting conclusions can be drawn. First of all, for the Si-LTA column, desorption was shown to be the most efficient using the Si-LTA column in combination with the SAPO-34 column. This because the most important impurities present on this material were water and ethanol. The hydrophilic zeolite SAPO-34 efficiently removed these components from the desorbing butanol stream (figure 5.24, figure 5.22). Further, the same high purities were obtained using CO_2 as carrier gas (figure 5.22). This is an important result, since large amounts of CO_2 are produced during ABE fermentation. Use of this gas in the downstream processing should thus greatly increase the overall efficiency of the production process.

Further, for the combination of ZIF-8 and the SAPO-34 column, the same high final butanol purities were obtained (figure 5.26). Final butanol purity was slightly lower than obtained with Si-LTA, because of the higher amount of acetone adsorbed by the ZIF-8 material (figure 5.13). Catalytic activity of SAPO-34 could also be observed during these experiments. The choice between Si-LTA and ZIF-8 as butanol adsorbing material would thus be a trade-off between the slightly higher butanol purity when using Si-LTA or the higher energetic efficiency of desorption on the ZIF-8 column. In the following part of this chapter, the different model development steps and most important modelling results will be discussed.

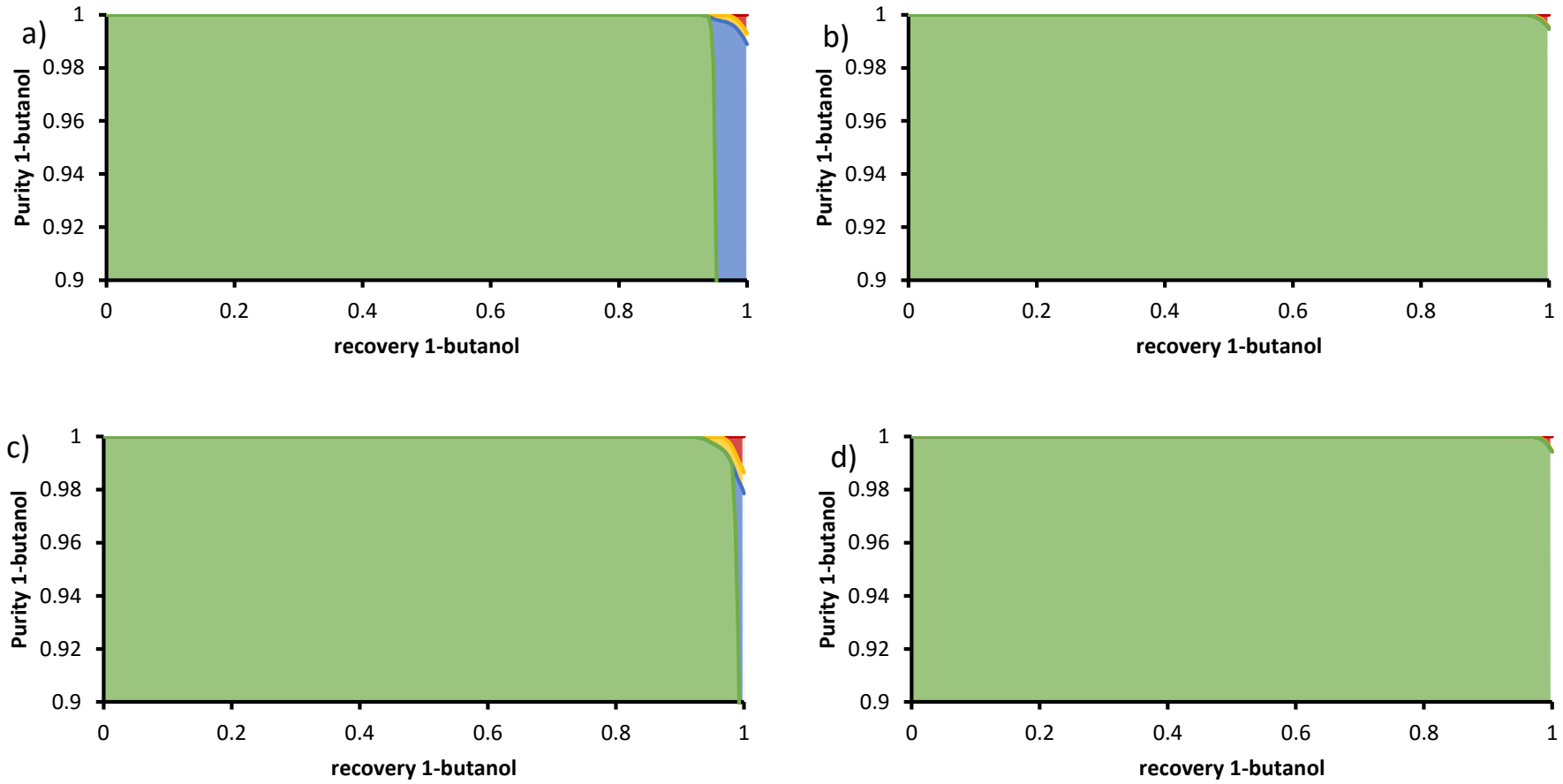

Figure 5.26: Comparison between desorption of ZIF-8 with (b and d) and without (a and c) the SAPO-34 column. Desorption was performed using He as carrier gas (a and b) and CO_2 as carrier gas at a temperature of 40 °C. The green curve represents the purity of butanol as a function of recovery. The areas represent the amounts of ABE components: acetone (red), butanol (green), the catalytic product (yellow) and water (blue)..

5.4 Isotherm model development

The basis for the development of a mathematical model describing breakthrough behavior lies in a sufficiently accurate description of the adsorption isotherms. As was explained in the Materials & Methods sections, a multicomponent Langmuir model was used for the description of the adsorption of the different ABE mixture components (equation 4.15). The multicomponent Langmuir parameters were estimated by fitting of the single component Langmuir model to the experimental data (equation 4.14). As can be observed from the isotherm measurements presented in paragraph 5.1, not all of the single component isotherms show perfect type I behavior. In all of the cases however, the relevant part of the adsorption isotherm could be described by a Langmuir model. For instance, the ethanol isotherm on Si-LTA showed a distinct S-shape (figure 5.1). However, since ethanol was only present at very low vapor pressures in the ABE mixture (50 Pa), the first part of the isotherm could be described with a single component Langmuir model. The single component Langmuir parameters, their 95 % confidence interval and the adjusted R^2 values of the isotherm fit are presented in table 5.4. A graphical comparison between the fitted models and the experimental data is shown in Appendix 8.

Table 5.4: Summary of the single component Langmuir parameters determined from fitting of the single component isotherms. The 95% confidence intervals were shown for each modelled parameter. In the case that not the complete isotherm was fitted, the fitted pressure range was added. All isotherms were measured at 40 °C.

Column	Component	q_{sat} (mmol/g)	K x10^{-3} (Pa^{-1})	Adjusted R^2	Pressure range (Pa)
Si-LTA	Acetone	1.2 ± 0.1	0.21 ± 0.04	0.99	-
	Butanol	2.04 ± 0.09	50 ± 10	0.95	-
	Ethanol	0.5 ± 0.1	14 ± 7	0.93	0 - 500
	Water	1.0 ± 0.2	0.5 ± 0.3	0.97	0 - 5000
ZIF-8	Acetone	5.4 ± 0.4	0.4 ± 0.2	0.97	-
	Ethanol	0.4 ± 0.3	2 ± 3	0.98	0 - 500
	Water	0.4 ± 0.1	0.8 ± 0.6	0.91	0 - 5000
Si - CHA	Acetone	0.27 ± 0.03	60 ± 30	0.90	-
	Butanol	4 ± 1	0.2 ± 0.1	0.99	-
	Ethanol	3.5 ± 0.3	0. 6 ± 0. 4	0.99	-
	Water	31 ± 44	0.02 ± 0.04	0.99	-
SAPO-34	Ethanol	4.1 ± 0.4	7 ± 4	0.92	-
	Water	13 ± 1	1.9 ± 0.9	0.91	-

As can be observed not all isotherm models fitted perfectly to the experimental data. In all of the cases, this was not a significant problem for multicomponent breakthrough modelling. As was shown experimentally, only a small amount of ethanol adsorbs on ZIF-8 in breakthrough (figure 5.13). The S-shaped isotherm was Langmuir fitted for the low vapor pressures present in the vapor phase ABE mixture. However, the adsorption capacity at these low vapor pressures is very low (figure 5.2), making accurate prediction of the capacity difficult. Further, the water isotherm on Si-CHA was linear (Gelin, 2015). Although the Langmuir isotherm model becomes linear for low vapor pressures, the use of this model for linear isotherms leads to overfitting of the data. This was however necessary for the development of the multicomponent Langmuir model.

Three isotherms were not described in table 5.4. Since acetone and butanol were shown to hardly adsorb on SAPO-34 (paragraph 5.2.3), the values of their saturation adsorption capacity and equilibrium constant were artificially set very low. As was highlighted previously (paragraph 5.1.2), the isotherm of butanol on ZIF-8 is S-shaped. Since this S-shape has severe consequences for the behavior of butanol during adsorption and desorption breakthrough (paragraph 5.2.2), a separate model needed to be developed to describe this isotherm. Further, this model needed to be compatible with a multicomponent Langmuir description of the other ABE mixture components.

To solve the problem associated with the isotherm shape of butanol on ZIF-8, experimental isotherm data was fitted using a combination of a Langmuir model and a logistic equation. In general, logistic models can be used to describe S-shaped curves, such as growth curves of microbial populations (Tsoularis & Wallace, 2002). However, to ensure compatibility with the multicomponent Langmuir model, this logistic equation was combined with a single component Langmuir equation. The equilibrium constant of this Langmuir part was then used for the multicomponent Langmuir description. Different combinations of Langmuir and logistic equations were considered, however equation 5.3 was finally used for fitting the ZIF-8 isotherms. The single component Langmuir isotherm can clearly be recognized. However, the Langmuir adsorption capacity at saturation now becomes a function of pressure described by the logistic equation. Fitted model parameters obtained are presented in table 5.5 and a comparison of fitted and experimental isotherm results are shown in figure 5.27.

$$q = \frac{q_{sat}}{1 + \exp\left(-r \times (P - P_{crit})\right)} \times \frac{K \times P}{1 + K \times P} \tag{5.3}$$

With:

q = butanol adsorption capacity at pressure P (mmol/g)
q_{sat} = saturation adsorption capacity (mmol/g)
r = parameter influencing steepness of S-curve (Pa^{-1})
P_{crit} = critical pressure corresponding to the sudden increase in adsorption capacity (Pa)
P = butanol partial pressure
K = Langmuir equilibrium constant (Pa^{-1})

Table 5.5: Model parameters for butanol on ZIF-8 with their 95% confidence intervals. The adjusted R^2 value was 0.99.

Parameter	Value
q_{sat}	4.0 ± 0.2 mmol/g
K	0.016 ± 0.008 Pa^{-1}
r	0.020 ± 0.005 Pa^{-1}
P_{crit}	105 ± 20 Pa

5.5 Single column breakthrough models

The isotherm models developed in the previous paragraph were subsequently used to describe the behavior of the individual adsorption columns in breakthrough. A comparison was made between simulation and experimental results to gain an accurate description of the different adsorbent columns: column porosity and kinetic parameters (linear driving force parameter h, axial dispersion coefficient D_{ax}) were fitted to experimental data, if available.

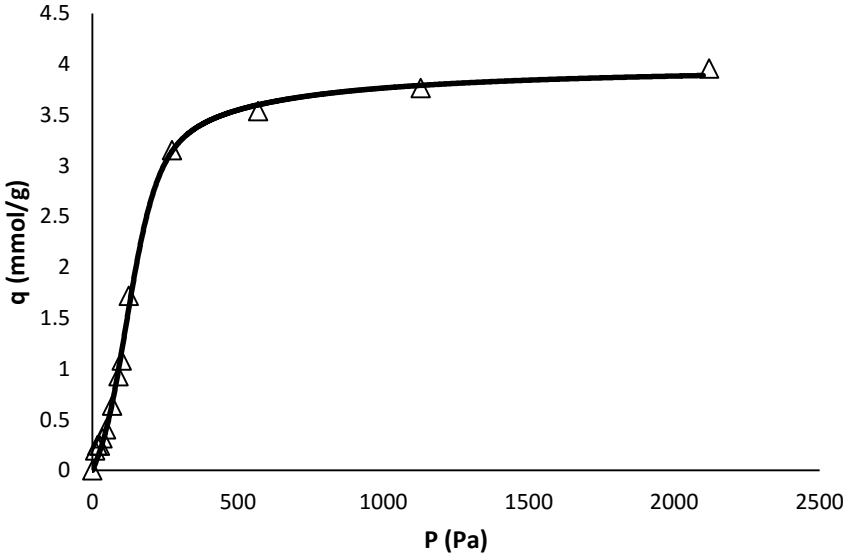

Figure 5.27: Comparison between experimental butanol isotherm values (△) and modelled results using equation 5.3 (solid line).

5.5.1 Si-LTA column

For adsorption of a vapor phase ABE mixture at 40 °C on the Si-LTA column, a comparison between experimental and modelling results is presented in figure 5.28. Decent agreement between modelled and experimental results was achieved. The roll-up of ethanol that was also experimentally observed (figure 5.5) could clearly be described correctly. Only the roll-up on the acetone breakthrough curve was not observed experimentally, though the breakthrough times are quite similar. For ethanol, the Langmuir parameters were further adjusted to obtain a decent breakthrough profile (q_{sat} = 0.8 mmol/g, K = 0.03 Pa^{-1}). Some difference could be expected, since single component data was used for the description of the multicomponent model, whilst the different mixture components could influence each other's adsorptive behavior (Abdehagh *et al.*, 2016b). The kinetic data shows a trend that could be reasonably expected, comparing ethanol and butanol, the mass transfer coefficient for butanol is much lower. This is a logical result, since butanol is the larger molecule, thus slower diffusion into the zeolite pores could be expected, leading to a larger mass transfer coefficient (table 5.6). Wu *et al.* showed that diffusion coefficients of water, methanol and ethanol in an LTA 4A zeolite were one order of magnitude smaller for each component respectively (2009). Although in this case, the mass transfer parameter for water is larger than for ethanol, it should be emphasized that many diffusion phenomena (such as macropore diffusion, micropore diffusion and film resistance) are lumped into one linear driving force parameter, making exact interpretation of this parameter difficult.

To describe desorption on the Si-LTA column, isotherm data at different temperatures would be necessary. The Langmuir equilibrium constants obtained from data fitting on those isotherms would allow for the calculation of the adsorption enthalpy and thus the description of a temperature dependent desorption process via the Van't Hoff equation (Ruthven, 1984). Unfortunately, only isotherm data at 40 °C was available. Therefore, desorption on the Si-LTA column was simulated isothermally. As was already mentioned in paragraph 5.2.1.2, a temperature increase is absolutely necessary for desorption on a reasonable time-scale. This is confirmed by simulation data, showing a

theoretical isothermal desorption process to take several days (figure 5.29). The cause of this phenomenon lies in the type I isotherm shape of butanol, as explained in paragraph 5.2.2.

Table 5.6: Kinetic parameters h and D_{ax} obtained from fitting model data to experimental data for ABE vapor phase breakthrough on Si LTA at 40°C. The obtained column porosity ε was 0.45.

Component	h (1/s)	D_{ax} ($x10^{-5}$ m^2/s)
Acetone	0.005	1.09
Butanol	0.003	8.40
Ethanol	0.5	1.10
Water	0.18	2.40

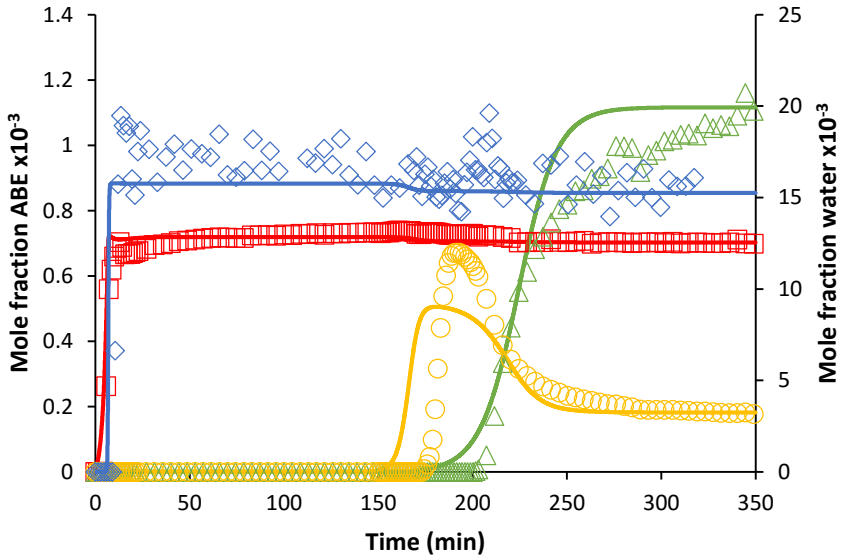

Figure 5.28: Comparison between modelled and experimental results for single column breakthrough at 40 °C on the Si-LTA column. Acetone (red), butanol (green), ethanol (yellow) and water (blue) mole fractions were plotted as a function of time. The solid lines represent the modelled data, whilst the individual points represent the experimental data.

5.5.2 ZIF-8 column

The same procedure was used for the ZIF-8 column as for the Si-LTA column. Breakthrough simulations for a vapor phase ABE mixture at 40°C showed decent fitting of the experimental results (figure 5.30). Although an empirical equation was used to describe the S-shaped isotherm of ZIF-8 (equation 5.3), the expected broad adsorption profile followed by a steep increase was clearly observed. However, the length of this broad adsorption peak was clearly overestimated. As was explained in paragraph 5.2.2, the shape of the adsorption breakthrough profile is a function of the slope of the isotherm (equation 5.1). Therefore, the derivate of the fitted isotherm equation has its influence on the adsorption breakthrough profile shape, with different models inevitably giving rise to different breakthrough shapes. This effect is also visible when simulating a desorption breakthrough on this material. The long, dispersive wave at high concentrations is simulated to be much broader than in

reality (figure 5.30). This makes the developed model applicable for adsorption simulations, however applicability in desorption simulations is more difficult, due to the big difference between predicted and real breakthrough curves.

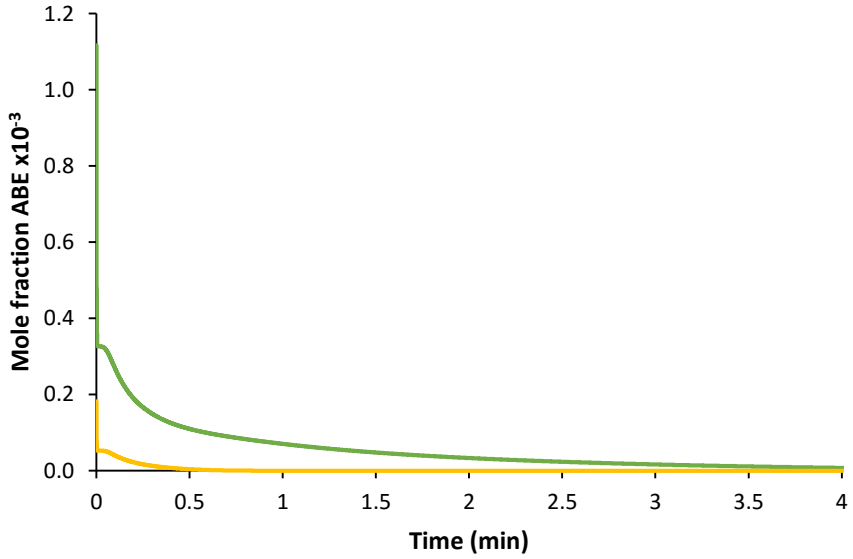

Figure 5.29: Simulated isothermal desorption on the Si-LTA at 40 °C. Butanol (green), ethanol (yellow) desorption profiles were plotted as a function of time. Full desorption of the Si-LTA column would take several days at 40 °C.

Fitted linear driving force mass transfer parameters for the different vapor phase mixture components are presented in table 5.7. The values of the linear showed a reverse order of what would reasonably be expected: the mass transfer parameter of butanol is the highest followed by ethanol and then by water. These results also contradict those of Zhang *et al.* (2013a), who showed the crystal diffusivities of water to be the greatest, followed by that of ethanol and butanol respectively. However, as mentioned before, the linear driving force parameter is a lumped parameter, combining many mass transfer phenomena. Further, for water, ethanol, acetone and the first part of the butanol profile, the broadness of the concentration profile is greatly influenced by the isotherm shape, since these are dispersive waves (Helfferich & Carr, 1993). As will be explained in paragraph 5.6.2, the fact that multicomponent breakthrough data was used for parameter fitting also had his effect on the modelling results. This makes correct parameter estimation difficult. The same arguments are valid for the high axial dispersion coefficient of acetone.

Table 5.7: Kinetic parameters obtained from fitting model data to experimental data for ABE vapor phase breakthrough on ZIF-8 at 40°C. The obtained column porosity ε was 0.28.

Component	**h (1/s)**	**D_{ax} (x10^{-5} m^2/s)**
Acetone	0.1	109
Butanol	1.0	8.40
Ethanol	0.5	1.10
Water	0.18	2.40

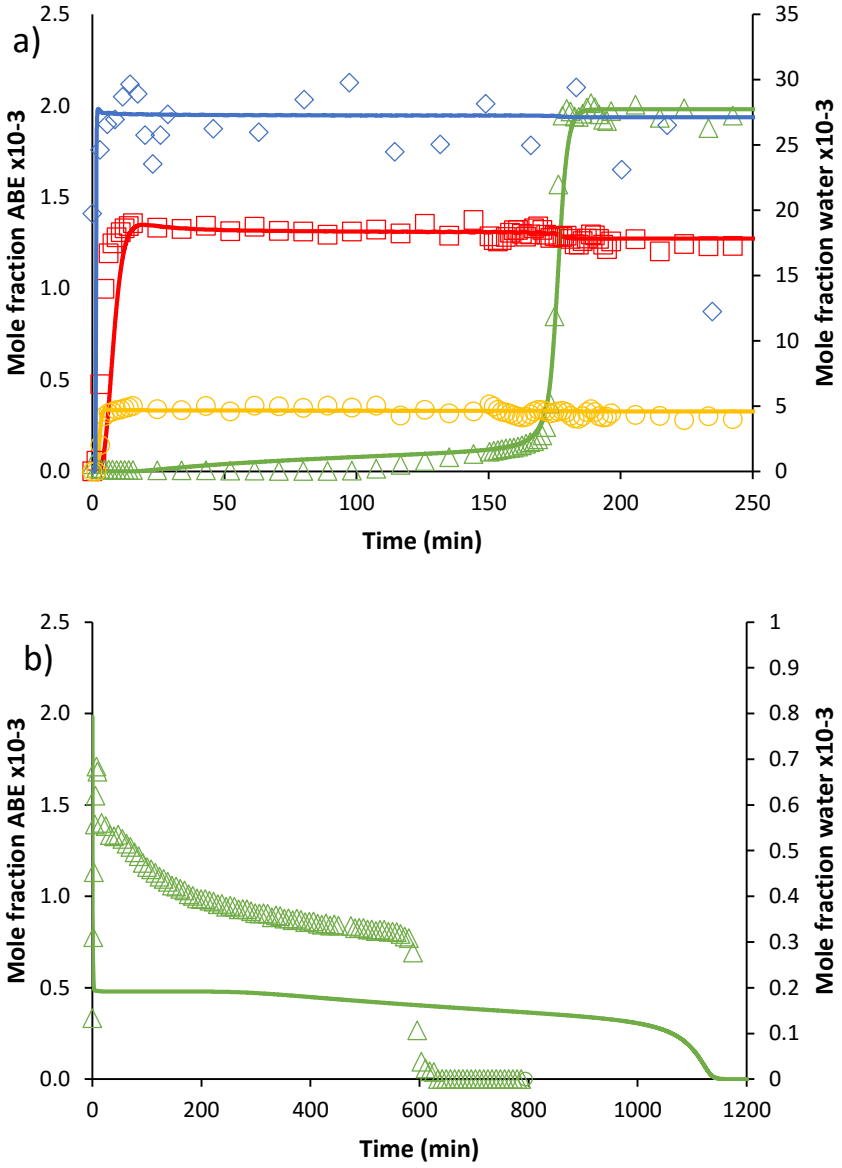

Figure 5.30: a) Comparison between experimental (individual data points) and simulated (lines) adsorption breakthrough curves on ZIF-8 of an ABE vapor phase mixture at 40 °C. Acetone (red), butanol (green), ethanol (yellow) and water (blue) outlet mole fraction are shown as a function of time. b) Comparison between simulated (lines) and experimental (individual data points) isothermal desorption profile of butanol after saturation with a vapor phase ABE mixture on ZIF-8 at 40 °C using He as carrier gas.

5.5.3 SAPO-34

For the SAPO-34 material, only ethanol and water isotherms were available using N_2 as carrier gas. Since breakthrough experiments showed little to no affinity of this material for acetone and butanol (paragraph 5.2.3), the adsorption parameters for these adsorbates were set artificially low as well as the value of their mass transfer parameters. This supposition is reasonable, since experimental results of Daems *et al.* (2007), Remy *et al.* (2011), Cousin Saint Remi *et al.* (2013) and Cosseron *et al.* (2013) confirmed slow butanol and acetone uptake kinetics for chabazite zeolites. A summary of the used kinetic parameters and the column porosity is given in table 5.7. Good fitting of the experimental data was possible (figure 5.31). The low value of the mass transfer parameters found for this column compared to the Si-LTA column make sense, since the Si-LTA pores are larger than those of SAPO-34 (table 4.1). For ethanol, the linear driving force parameter is lower than that measured by Cousin Saint

Remi *et al*. (2013). However, this parameter shows the same order of magnitude for butanol (Cousin Saint Remi *et al*., 2013). Comparison between these values and the study of Cousin Saint Remi should be done with care, however. The parameters determined in this Masters' thesis were obtained by fitting with breakthrough data using a multicomponent mixture. In the study of Cousin Saint Remi *et al.* (2013), liquid phase batch uptake measurements were performed with pure components, making exact comparison difficult. The water linear driving force parameter was the highest, which could be expected since Remy *et al.* (2011) showed methanol to have the fastest uptake kinetics in vapor phase compared to longer linear alcohols. Since water is an even smaller molecule, fast kinetics could be expected.

Table 5.7: Kinetic parameters obtained from fitting model data to experimental data for ABE vapor phase breakthrough on SAPO-34 at 40°C. The obtained column porosity ε was 0.67. For butanol and acetone, the adjusted thermodynamic parameters were also shown.

Component	h ($x10^{-3}$ s^{-1})	D_{ax} ($x10^{-5}$ m2/s)	q_{sat} (mmol/g)	K (Pa^{-1})
Acetone	0.9	1.09	0.68	5.9×10^{-4}
Butanol	0.005	8.40	0.1×10^{-4}	1.0×10^{-5}
Ethanol	0.2	1.10	-	-
Water	5	2.40	-	-

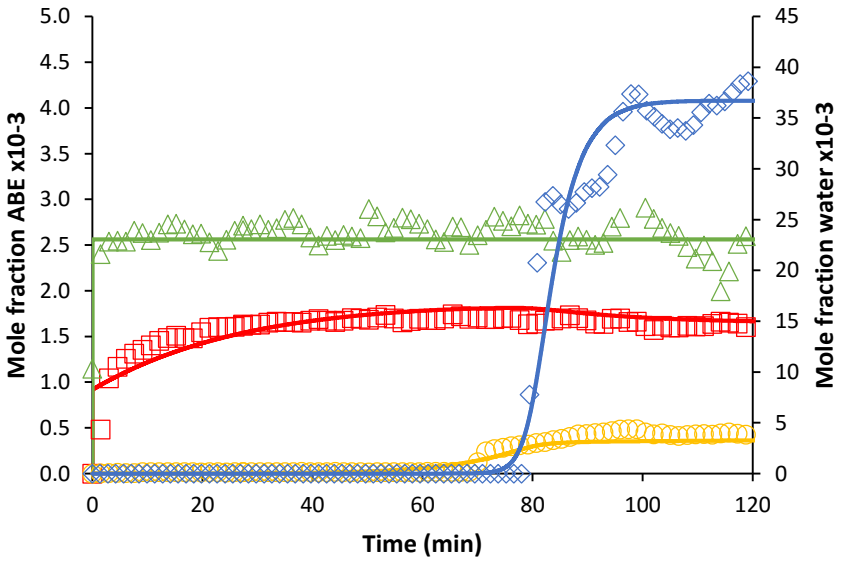

Figure 5.31: Comparison between experimental and modelling results on SAPO-34 at 40 °C (under He). The individual data points represent experimental data, whilst the modelling results are presented as solid lines. Mole fractions of acetone (red), butanol (green), ethanol (yellow) and water (blue) were plotted as a function of time.

5.5.4 Si-CHA

For the column modelling of Si-CHA only breakthrough data of an ABE vapor mixture without the measured water profile was available. Therefore, the linear driving force parameter of water was set artificially high. This is a reasonable supposition, since Remy *et al*. observed fast uptake kinetics in vapor phase for methanol on SAPO-34 (2011). Since water is an even smaller molecule than methanol, fast water uptake kinetics can be assumed on the similar chabazite structure of Si-CHA. Using the fitted parameters, a decent description of results could be obtained (figure 5.32). Again, as was the case for

the mass transfer parameter on SAPO-34, values are much lower for Si-CHA compared to Si-LTA. The butanol mass transfer parameter showed the same order of magnitude as for SAPO-34 (table 5.7). These results are also consistent with the experimental results Daems *et al.* (2007), Remy *et al.* (2011) and Cousin Saint Remi *et al.* (2013), showing very slow diffusion of butanol in chabazite zeolites. As for SAPO-34, the linear driving force parameter for acetone was set artificially low (table 5.7). The butanol and acetone thermodynamic adsorption parameters were also lowered artificially, as for SAPO-34.

Table 5.8: Kinetic parameters obtained from fitting model data to experimental data for ABE vapor phase breakthrough on Si-CHA at 40°C. The obtained column porosity ε was 0.60. The adjusted thermodynamic parameters for acetone and butanol are also shown.

Component	h (1/s)	D_{ax} ($x10^5$ m^2/s)	q_{sat} (mmol/g)	K (Pa^{-1})
Acetone	$5x10^{-9}$	1.09	0.26	$5.6\ x10^{-2}$
Butanol	$3.0\ x\ 10^{-6}$	8.40	3.8	$2.4\ x10^{-3}$
Ethanol	$4\ x\ 10^{-3}$	2.51	-	-
Water	15	4.35	-	-

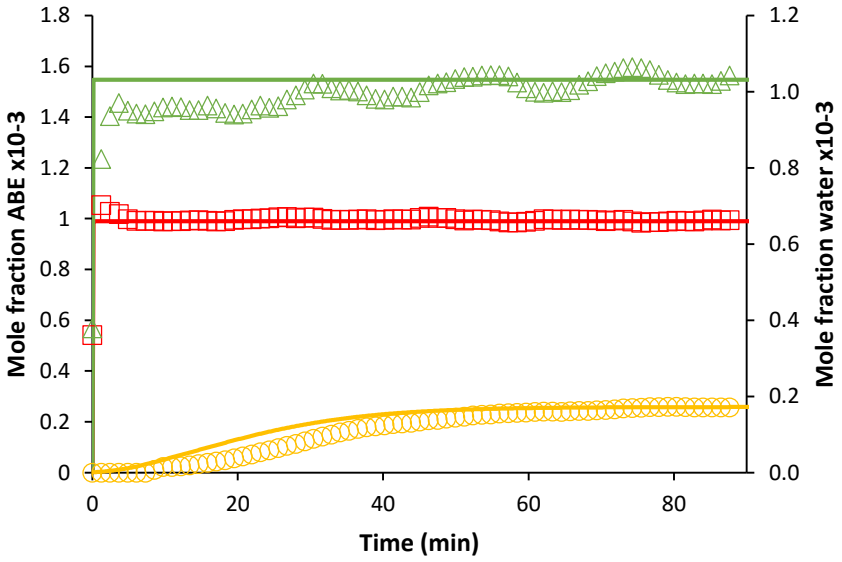

Figure 5.32: Comparison of experimental and modelled breakthrough data of a vapor phase ABE mixture on Si-CHA at 40 °C, using He as carrier gas. The breakthrough curves for acetone (red), ethanol (yellow) and butanol (green) are shown, with solid lines representing modelled data and the individual data points representing the experimental measurements.

5.6 Multi column breakthrough modelling

The column parameters described in section 5.5 were subsequently used to verify the performance of the combination of these different adsorbents. By combining two adsorption columns in series, the boundary conditions at the second column inlet become dynamic. The method to cope with these dynamic boundary conditions was described in the Materials & Methods section.

As was already explained in section 5.3, only column combinations using a desorbing Si-LTA/ZIF-8 column with an adsorbing SAPO-34/Si-CHA column were experimentally verified. As was further explained in this section, the combination of a desorbing Si-LTA/ZIF-8 column with an adsorbing SAPO-

34/Si-CHA column leads to a very pure butanol product stream. However, the ethanol present in the vapor phase mixture in this way is lost. Since ethanol could be a valuable side product (as biofuel or platform molecule), its recovery might lead to a higher economic efficiency of the ABE fermentation process. Further, such a column configuration would also lead to a higher butanol purity, since no ethanol would be adsorbed on the second column. Therefore, simulations were performed to evaluate these column configurations (figure 5.29). A comparison in butanol purity between a single column breakthrough simulation and the multi column simulations was made. Also the obtained ethanol purity on SAPO-34 and Si-CHA was compared.

5.6.1 Si-LTA column

A first comparison of breakthrough simulations for the combination of SAPO-34/Si-CHA and Si-LTA showed some interesting results (figure 5.33). A clear shift in breakthrough time was observed for all of the ABE components, except for butanol on the combination with SAPO-34, even when the extra dead time caused by the first column in the configuration was taken in to account. These shifts were in the line of expectations. Both the Si-CHA and the SAPO-34 column adsorbed about the same amount of ethanol. However, a large difference in water adsorption behavior could be observed for both components. The more polar zeolite SAPO-34 clearly adsorbed a much higher amount of water than the Si-CHA column.

For acetone a large roll-up could be observed. This roll-up was only slightly visible on the single column breakthrough profile and was caused by the separation of the different component fronts on the first adsorption column (figure 5.28). In fact, this roll-up probably is a subtle consequence of the model definition, rather than a phenomenon that could would be physically realistic. According to equation 4.17, the acetone uptake rate is a function of the adsorbed amount on the column material and the adsorption capacity at equilibrium. This equilibrium capacity is defined by the multicomponent Langmuir model (equation 4.15). When a normal adsorption breakthrough simulation is started, the whole vapor phase mixture starts flowing through the column from the very beginning of the simulation. In this way, the driving force for acetone adsorption on the Si-LTA column will be low, since the equilibrium adsorption capacity will be low. Therefore, a linear driving force parameter describing the acetone breakthrough time correctly tends overcompensate this low adsorption capacity, by having a higher value than it should have in reality. However, in the situation shown in figure 5.33, a pure acetone and butanol front will reach the Si-LTA at the start of the adsorption process, since the ethanol and water will initially adsorb on the first column. Therefore, the equilibrium adsorption capacity will be higher for acetone, leading to faster mass transfer and thus an overestimation of the amount of acetone adsorbed. When the water front subsequently reaches the Si-LTA column, the equilibrium adsorption capacity of acetone suddenly drops due to the presence of water at a high vapor pressure. This leads to the roll-up of acetone observed in figure 5.33. Therefore, the adsorbed amount of acetone after complete breakthrough might be predicted correctly, even with the roll-up observed. A more correct estimation of the acetone linear driving force parameter might result from fitting kinetic parameters to single component breakthrough curves and measurement of multicomponent isotherms.

To compare the purity of the obtained butanol using this process, the calculated adsorbed amounts on the Si-LTA column were used, as explained in the Materials & Methods section. As can be observed in figure 5.33, butanol breakthrough took place between 200 and 250 min. However, one would like to stop the adsorption process before complete butanol breakthrough takes place, since the butanol eluting after the start of the breakthrough process is lost. Therefore, the calculated adsorption capacities at 200 min were used for purity calculations, reflecting incomplete breakthrough of butanol. For the SAPO-34 and Si-CHA column, the same point in time was used for calculation of the ethanol

purity. Purity was expressed on a weight percent basis. It should be mentioned that these purities correspond to 100% recovery of ethanol and butanol. As shown in section 5.3, higher purities can be reached by discarding a part of the desorbing ethanol or butanol (leading to lower recovery).

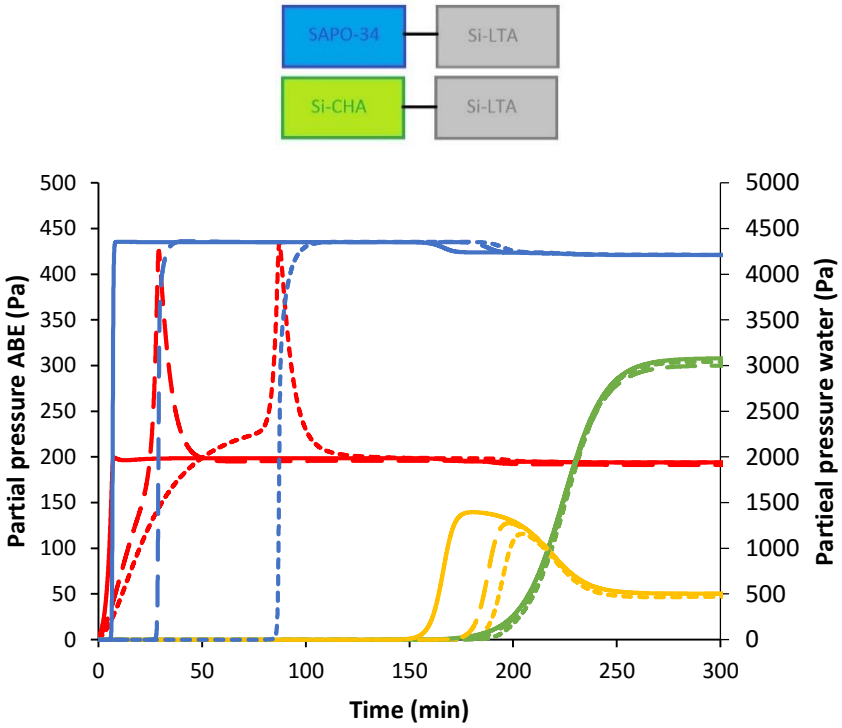

Figure 5.33: Comparison between adsorption breakthrough profiles using only the Si-LTA column (uninterrupted line) and the combination of this column with the SAPO-34 (short dotted line) column and Si-CHA (long dotted line) column. The partial pressures at the Si-LTA column outlet are shown for acetone (red), butanol (green), ethanol (yellow) and water (blue). Dead time caused by the extra column before the Si-LTA inlet was taken into account in comparison of the profiles. The tested column combinations are shown above the graph. Butanol breakthrough profiles showed almost perfect overlap.

At first instance, the addition of a second ethanol removing column during adsorption does not lead to an increase in butanol purity (figure 5.34). On the contrary, for Si-CHA, a decrease in butanol purity is observed. This is caused by the fact that, although a significant amount of ethanol is adsorbed on the first column, the ethanol concentration profile actually overtakes the butanol concentration profile in the Si-LTA column. Therefore, the SAPO-34 or Si-CHA column should either be larger (containing a larger amount of adsorbent), or the saturated first column needs to be continuously replaced in a cyclic fashion. This overtaking of the butanol concentration profile by the ethanol concentration profile is further illustrated in figure 5.35. The ethanol adsorbed on the SAPO-34 or Si-CHA column showed low purity. The reason for this lies in the large amount of water simultaneously adsorbing on these columns. Recovering the adsorbed ethanol from the SAPO-34 or Si-CHA column would thus imply the need of an extra separation step, removing the excess water. Although clearly, ethanol purity on the Si-CHA column is higher, since a lower amount of water is adsorbed on this column.

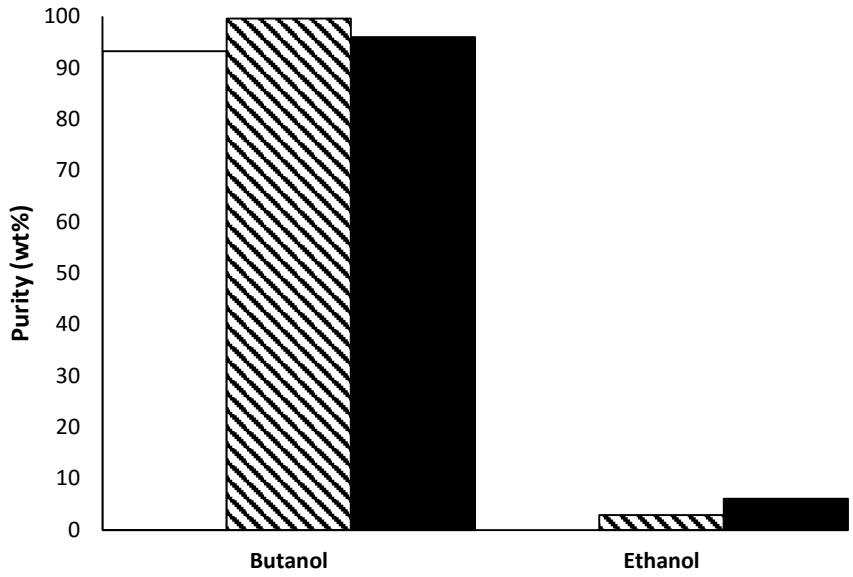

Figure 5.34: Comparison between butanol purity adsorbed on the Si-LTA column without second column (blank bars), with the SAPO-34 column (shaded bars) and Si-CHA (black bars). The purity of the adsorbed ethanol on the second column is also shown for SAPO-34 (shaded bars) and Si-CHA (black bars).

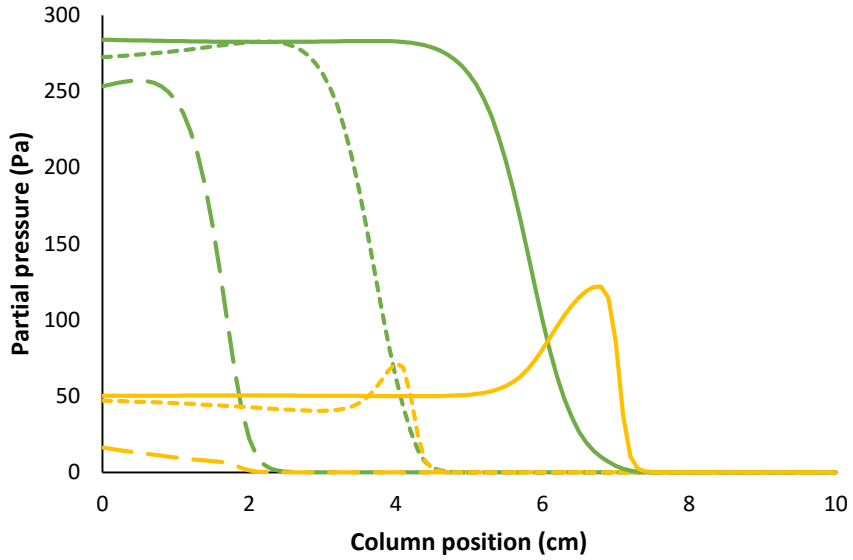

Figure 5.35: Overtaking of the butanol concentration profile by the ethanol concentration profile on the Si-LTA column in combination with the Si-CHA column. Ethanol (yellow) and butanol (green) partial pressures are shown on different points in time for different column positions. The different points in time shown are t = 50 min (long dotted lines), t = 100 min (short dotted lines) and t = 150 min (uninterrupted line).

To further verify the viability of this configuration, the column length of the first column (SAPO-34 or Si-CHA) was increased in such a way that the second column could be completely saturated with butanol, without co-adsorption of ethanol. Simulations were thus performed using a column length of 40 cm for both the SAPO-34 and Si-CHA column. These values, however, were not optimized, but purely taken to study the effect of a longer column length on butanol purity. A comparison of the

resulting butanol purity is presented in figure 5.31, these values were again calculated using the adsorbed amounts on the Si-LTA column at the start of butanol breakthrough. In this case, the butanol purity did increase slightly for adsorption with Si-CHA, although the largest increase was observed for the combination with the SAPO-34 column. This because of the higher adsorption capacity for water of the SAPO-34 column, leading to less water entering the Si-LTA column. Due to the low adsorption capacity of acetone on Si-LTA, a purity of 99 wt% could be reached in the combination with SAPO-34.

Breakthrough simulations using these different column lengths showed the adsorption capacity of Si-LTA for butanol to increase, due to the purer vapor stream entering the column (figure 5.36). Whilst a roll-up of the ethanol curve is observed on normal vapor phase breakthrough, this effect is inverted when the Si-CHA or SAPO-34 column of sufficient capacity is placed in front of the Si-LTA column. In this case, roll-up of the butanol curve is observed at high partial pressures. This roll-up is caused by two effects. For the combination of Si-LTA and Si-CHA, only the adsorption of ethanol is responsible for the small observed roll-up. In the combination of Si-LTA with the SAPO-34 column, the adsorption of water might play an extra effect on the observed butanol push-out. Here probably a mechanism similar to the roll-up of acetone plays a role, since the adsorption capacity of water on the Si-LTA column is low, though the high water vapor pressure can influence the equilibrium butanol adsorption capacity.

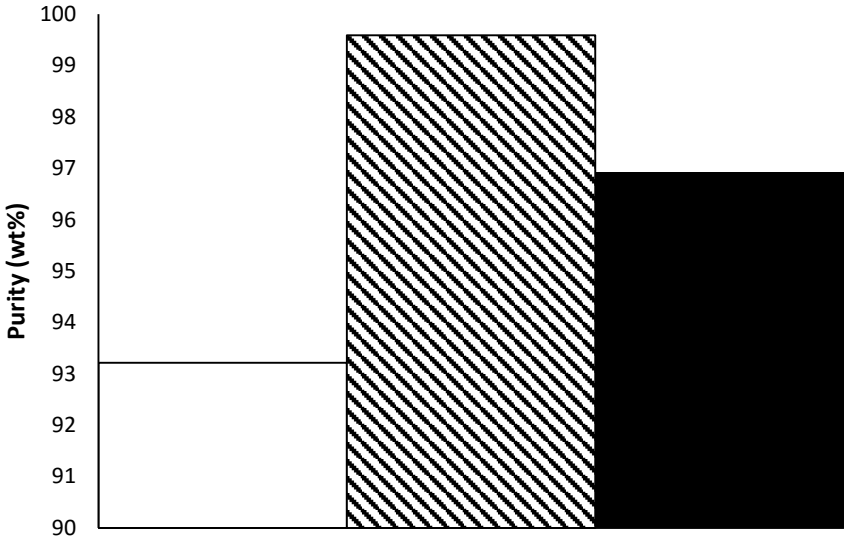

Figure 5.36: Comparison between butanol purity on Si-LTA using a column length of 40 cm for SAPO-34 and 40 cm for Si-CHA. Adsorption without second column (blank bars) is compared with the combination with SAPO-34 (shaded bars) and Si-CHA (black bars).

For the Si-LTA column, a combination with Si-CHA or SAPO-34 is thus a viable option during adsorption. Especially the combination with SAPO-34 leads to a high-purity butanol yield. However, looking at ethanol purity, the ethanol adsorbed on these two materials is very water-diluted. This could thus make the use of an extra ethanol separation step necessary after desorption of this first column. Further, comparing the amounts of SAPO-34 and Si-CHA used here to those in the experimental section, significant larger columns were necessary for high-purity butanol recovery. It's thus clear that

a process using the Si-LTA column and recovering high-purity butanol and ethanol would be possible, but more expensive. Also worth mentioning is the fact that before the start of ethanol breakthrough, pure acetone is eluting from the Si-LTA column, making high-purity acetone recovery possible using this process.

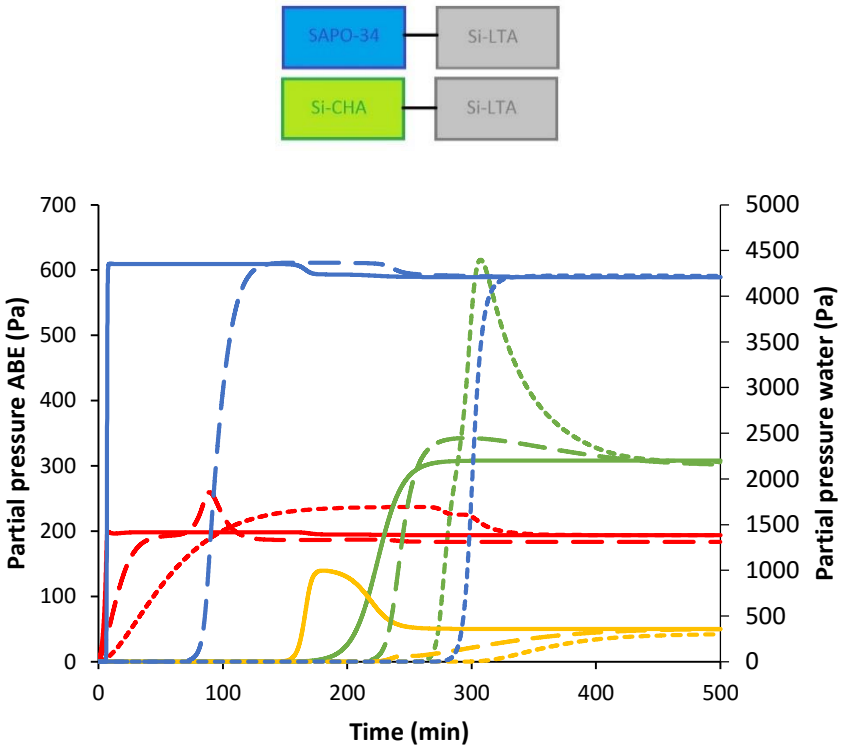

Figure 5.37: Breakthrough profile at the end of the Si-LTA column without (uninterrupted line) and in combination with Si-CHA (long dotted line) and SAPO-34 (short dotted line). Acetone (red), butanol (green), ethanol (yellow) and water (blue) partial pressures are shown as a function of time. Column lengths of Si-CHA and SAPO-34 were 40 cm.

5.6.2 ZIF-8 column

The same procedure used for modelling the different column combinations with Si-LTA was followed for modelling on the ZIF-8 column. In a first instance, a comparison was made between the combination of a 10 cm Si-CHA/SAPO-34 column before the ZIF-8 column during adsorption of a humid vapor phase ABE mixture (figure 5.22). Subsequently, the column length was adjusted for higher butanol purity.

A comparison between the use of Si-CHA and SAPO-34 with native ZIF-8 adsorption is given in figure 5.34. At first glance, the butanol adsorption capacity of ZIF-8 lowers when combining it with the Si-CHA or SAPO-34 column. However, while the steep breakthrough part of the butanol profile shifts to left, a shift to right is observed for the dispersive part of the butanol breakthrough profile. A close-up of this profile was added in appendix for further clarity (Appendix 9). Further, the start of the dispersive part of the breakthrough profile seemed to correspond to the breakthrough time of water. Snapshots taken from the moving butanol and water front through the ZIF-8 column showed a remarkable phenomenon taking place: roll-up of the butanol curve by adsorption of water (figure 5.39). It is this

roll-up, similar to that of acetone observed on Si-LTA (figure 5.33), that could be responsible for the observed shift in breakthrough time. However, these results should be interpreted with care, since single component isotherms were used to describe the multicomponent breakthrough behavior of the ABE components, thus possibly overestimating the water effect on adsorption, similar to the effect of water on the acetone breakthrough curve on Si-LTA (figure 5.33, figure 5.37). Also, a shift in ethanol breakthrough time could be noticed, however, as was the case with Si-LTA (figure 5.33), the adsorption capacity of the 10 cm SAPO-34 or Si-CHA column was not large enough to completely purify the feed mixture of the ZIF-8 column of ethanol. The shift of the butanol profile was taken into account when the butanol purity was calculated. The purity of the adsorbed butanol was always calculated at the time corresponding to the steep breakthrough of butanol: 160 min for native butanol adsorption and 150 min for adsorption using the SAPO-34 and Si-CHA material.

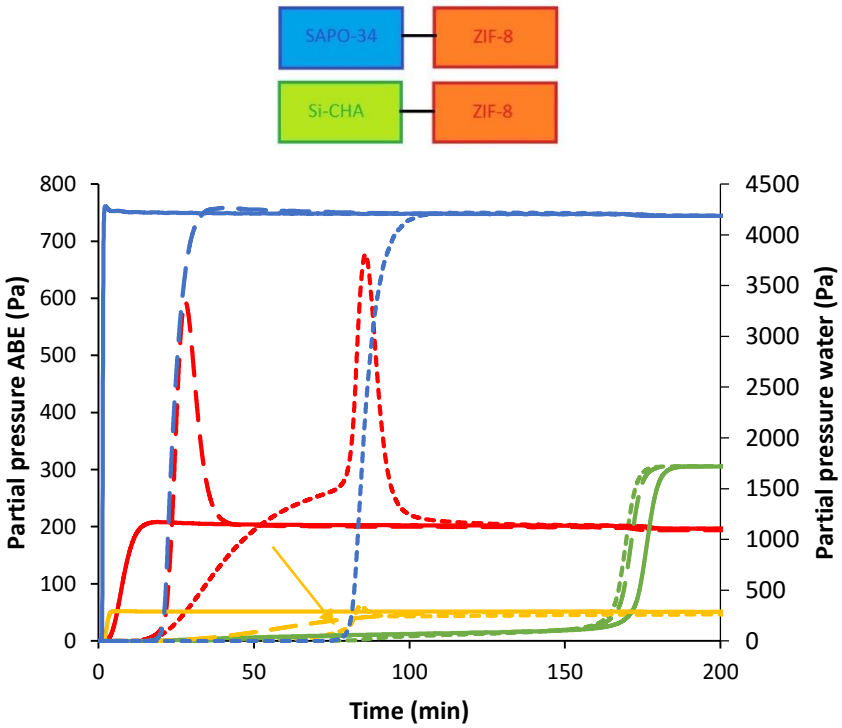

Figure 5.38: Breakthrough profile at the end of the ZIF-8 column without (uninterrupted line) and in combination with Si-CHA (long dotted line) and SAPO-34 (short dotted line). Acetone (red), butanol (green), ethanol (yellow) and water (blue) partial pressures are shown as a function of time. A close-up of the shift in the butanol breakthrough profile was added in appendix (Appendix 9). Butanol breakthrough profiles of the combinations of ZIF-8 with Si-CHA and SAPO-34 showed almost perfect overlap. The ethanol breakthrough profile on SAPO-34 is marked with an arrow and clearer visualized in Appendix 9.

A comparison of butanol purity for the different simulated combinations showed the same result as for Si-LTA. Due to the insufficient adsorption of ethanol on the first column in the system, no extra gain in butanol purity is achieved (figure 5.40). Compared to Si-LTA, native butanol purity on the ZIF-8 column was simulated to be very high, probably overestimating the achieved butanol purity in reality (figure 5.28). The same low purity of the ethanol adsorbed on Si-CHA and SAPO-34 was observed, due to the high amount of water adsorbed on these materials (paragraph 5.6.1). As for Si-LTA, the Si-CHA and SAPO-34 column lengths were increased, to increase their ethanol adsorption capacity for higher butanol purity.

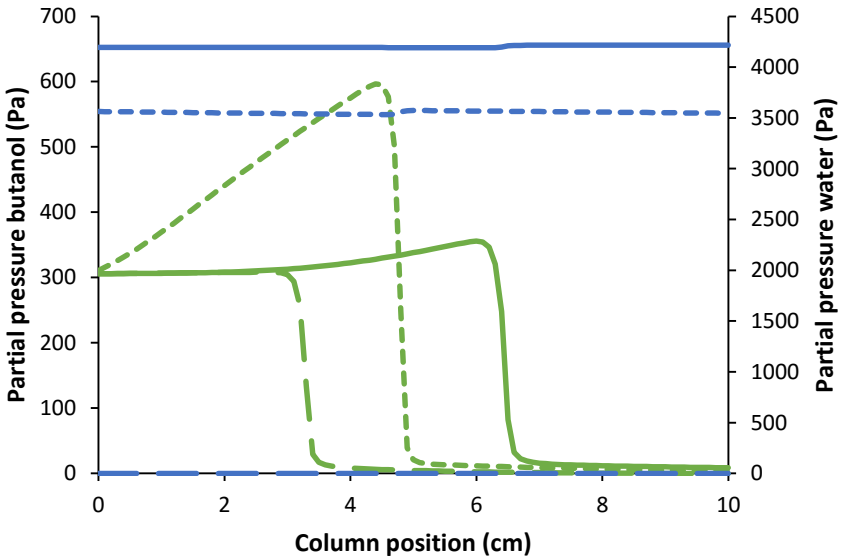

Figure 5.39: Roll-up of the butanol adsorption curve due to simultaneous water adsorption. Butanol (green) and water (blue) partial pressures over the length of the column were plotted at a simulation time of 70 min (long dotted lines), 90 min (short dotted lines) and 110 min (uninterrupted lines).

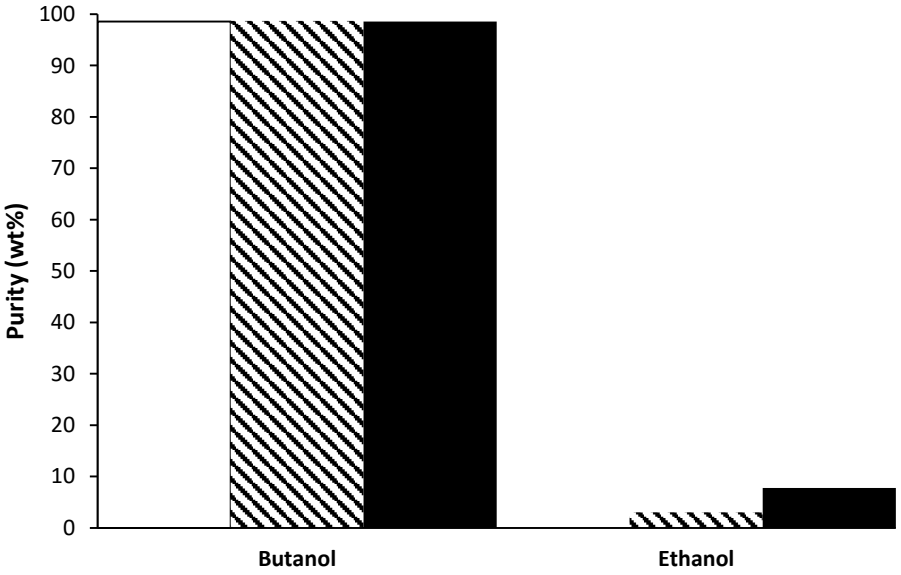

Figure 5.40: Comparison of butanol purity adsorbed on ZIF-8 and ethanol adsorbed on SAPO-34 and Si-CHA. For butanol, native ZIF-8 adsorption (blank bars) is compared with the combination with SAPO-34 (shaded bars) and Si-CHA (black bars). For ethanol the purity of the adsorbed component is compared for SAPO-34 (shaded bars) and Si-CHA (black bars).

For both combinations, a 40 cm column of Si-CHA or SAPO-34 was placed before the ZIF-8 column during adsorption, leading to complete ethanol adsorption before butanol breakthrough on the ZIF-8 column (figure 5.41). The greatest increase in butanol adsorption capacity could be observed with the

use of the SAPO-34 column in combination with ZIF-8. However, this increase in butanol adsorption capacity could not be attributed to ethanol removal. On the contrary, it is the water removal that was observed to be the most important factor influencing the higher adsorption capacity of butanol. Indeed, a roll-up of the butanol breakthrough curve is observed at larger breakthrough times, corresponding to water breakthrough. A similar effect was also visible on the Si-LTA column (figure 5.33). This further confirms the theory that the shift in the butanol breakthrough profile observed in figure 5.38 is caused by the water vapor entering the ZIF-8 column. As was discussed before, this roll-up might be overestimated by the model. It should also be emphasized that during the period before the start of butanol breakthrough, pure acetone is eluting from the ZIF-8 column. In this way, the three ABE vapor phase products could be separated using the SAPO-34 column in combination with ZIF-8.

As a consequence of this effect of water on the breakthrough behavior, the butanol purity was observed to be the highest for the combination of ZIF-8 and SAPO-34, as was the case for the Si-LTA column (figure 5.36 and figure 5.38). This was also experimentally observed, with acetone and water being the more important impurities for adsorption on ZIF-8 than ethanol (paragraph 5.2.2 and paragraph 5.3.3). A butanol purity of 99% could be reached using the combination SAPO-34 and ZIF-8.

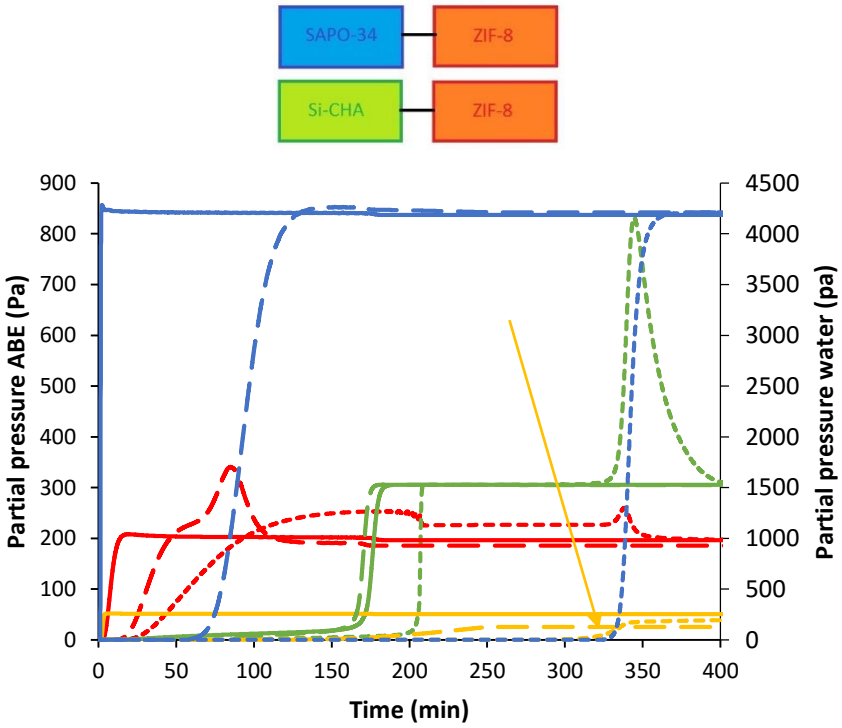

Figure 5.41: Breakthrough profile at the end of the ZIF-8 column without (uninterrupted line) and in combination with a Si-CHA (long dotted line) and a SAPO-34 (short dotted line) of 40 cm. Acetone (red), butanol (green), ethanol (yellow) and water (blue) partial pressures are shown as a function of time. The ethanol breakthrough in the combination of ZIF-8 with SAPO-34 is marked with a yellow arrow.

The combination of Si-CHA and SAPO-34 with ZIF-8 during vapor phase ABE adsorption, could thus lead to high purity butanol recovery (figure 5.42). However, the gain in butanol purity would be less in this case than for the Si-LTA column. This due to acetone and water being the more important impurities co-adsorbing on the ZIF-8 column (paragraph 5.2.2). The combination of both Si-CHA and ZIF-8 could lead to high purity ethanol and butanol recovery, although the large amounts of water adsorbing on the Si-CHA column should be further removed.

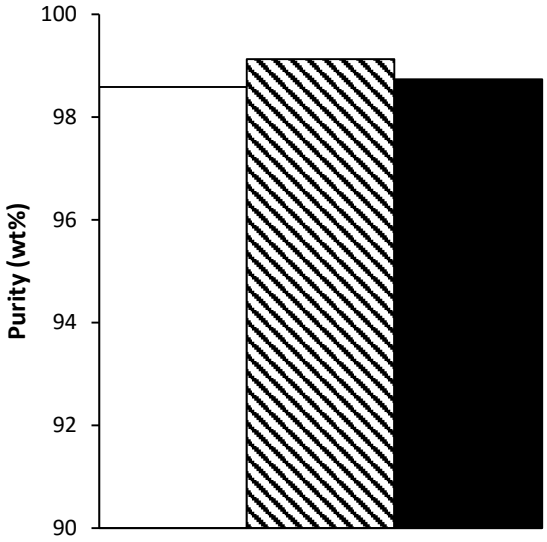

Figure 5.42: Comparison of butanol purity for the different tested column combinations during adsorption. Results are shown for native ZIF-8 adsorption (blank bars), adsorption with SAPO-34 (shaded bars) and adsorption with Si-CHA (black bars).

5.7 Final comparison

In the work presented in this Masters' thesis, different combinations of columns containing different types of selective adsorbents were evaluated on their performance for high purity butanol recovery from a vapor phase ABE mixture. Via the performance of adsorption and desorption breakthrough experiments, the performance of the combination of a butanol selective Si-LTA or ZIF-8 packed column and an ethanol selective SAPO-34 or Si-CHA packed column was evaluated. In this configuration, the Si-LTA or ZIF-8 packed column was first completely saturated with a vapor phase ABE mixture. During the subsequent desorption, a Si-CHA or SAPO-34 column was placed behind the column to purify the desorbing butanol stream (figure 5.22). For this configuration, a comparison was made between the use of He and CO_2 as carrier gas. A summary of the separation performance of the different tested configurations is presented in figure 5.43a.

Using He as carrier gas, butanol purity on ZIF-8 and Si-LTA was quite comparable (figure 5.43b and c). For desorption of the Si-LTA column, the addition of the Si-CHA column led to an improvement in butanol purity and recovery. However, a high amount of water was still present in the desorbing mixture, leading to lower purity at high recovery compared to desorption without extra column (paragraph 5.3.2). The best results were obtained by using the SAPO-34 column, leading to the highest purity and recovery. Although catalytic activity of this column could hinder efficient ethanol removal. Comparing CO_2 to He as carrier gas, butanol purity and recovery were higher for the ZIF-8 column, but lower for the Si-LTA column. For ZIF-8, the reason for this lied in the lower amount of water and acetone adsorbed under CO_2 (paragraph 5.2.2.1). The lower purity and recovery for the Si-LTA column using CO_2 as carrier were caused by the higher butanol concentrations observed at the start of the desorption experiment (paragraph 5.2.1.2).

Figure 5.44 summarizes the simulation results. Different column configurations were tested using a SAPO-34 or Si-CHA column to purify the feed stream to a butanol adsorbing ZIF-8 or Si-LTA column (figure 5.44a). Two column sizes of SAPO-34 or Si-CHA were evaluated: 10 cm and 40 cm, since the

capacity of the 10 cm column was observed to be too low for high purity butanol recovery (figure 5.43b and c). The SAPO-34 column seemed the most promising, not only because of its ethanol adsorption capacity, but also because of its high water adsorption capacity. Further, a pure acetone stream could be obtained using this column combination. Using the SAPO-34 column in combination with the ZIF-8 or Si-LTA column, all of the three ABE vapor phase components could be separated. However, the ethanol fraction was observed to be very diluted, making an extra concentration step necessary for this fraction.

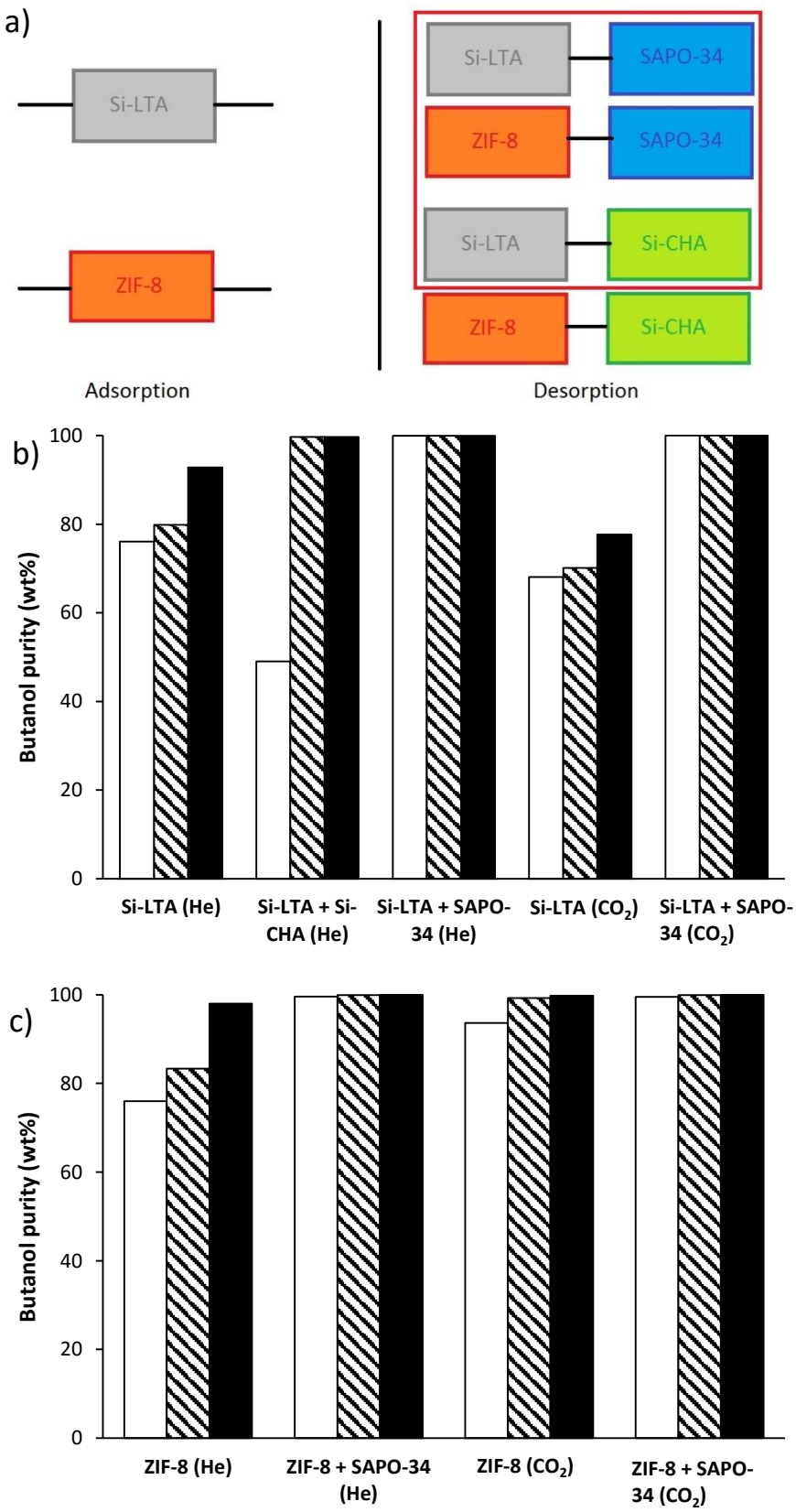

Figure 5.43: a) Different column configurations tested experimentally (red square). b) and c) Comparison of the performance of the different column configurations used experimentally Si-LTA (b) and ZIF-8 column (c). Butanol purity is shown for different recovery percentages: 100% (blank bars), 98% (shaded bars) and 95% (black bars). Desorption of ZIF-8 was always performed isothermal at 40 °C.

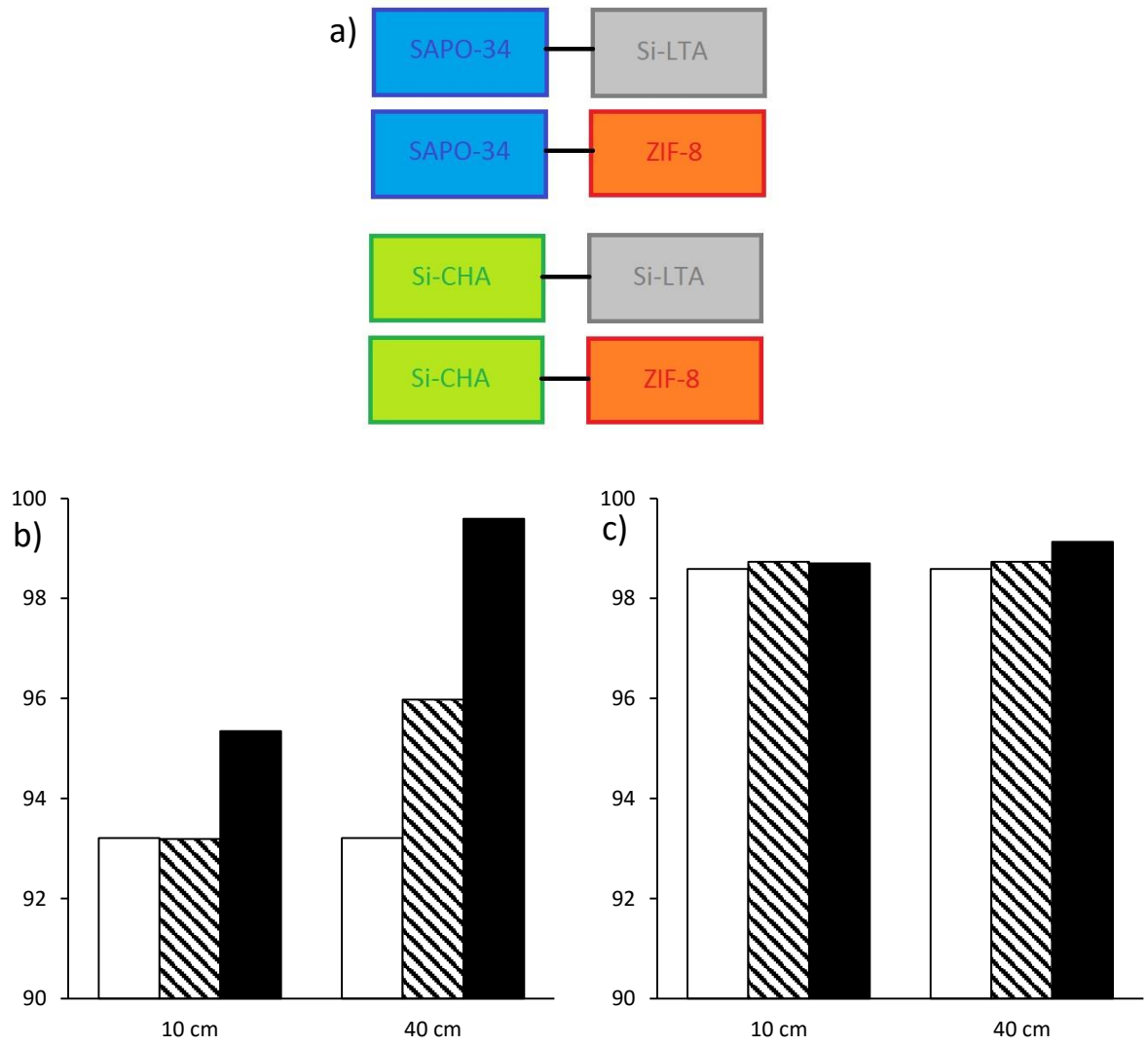

Figure 5.44: a) Column configurations tested using mathematical modelling. b) Column configurations tested for Si-LTA during adsorption: adsorption without second column (blank bars), with Si-CHA (shaded bars) and SAPO-34 (black bars). c) Column configurations tested with ZIF-8 during adsorption: adsorption without second column (blank bars), with Si-CHA (shaded bars) and SAPO-34 (black bars). Results are shown for different column lengths of the SAPO-34 and Si-CHA column (10cm or 40cm).

6. Conclusion

The research performed for this Masters' was focused around the development of a multicolumn adsorption process for high-purity butanol recovery. First of all, four different materials were tested on their adsorption capacity and selectivity for the different vapor phase ABE mixture components: a hydrophobic MOF (ZIF-8), two hydrophobic zeolites (Si-LTA and Si-CHA) and a hydrophilic zeolite (SAPO-34). Since CO_2 is an important by-product produced during ABE fermentation, the influence of CO_2 on the adsorption properties of the different materials was investigated. Subsequently, packed adsorption columns of these different materials were combined for optimal high-purity butanol recovery. Not all of the different material combinations could be tested experimentally. Therefore, a mathematical model was developed, describing these different column combinations. This model allowed qualitative comparison of different possible combinations for optimal high-purity butanol recovery.

Isotherm measurements on Si-LTA confirmed the high adsorption capacity of this material for butanol. Due to competitive adsorption of CO_2, the adsorption capacities at high vapor pressures decreased for the different ABE mixture components. Further, the isotherm using CO_2 as carrier gas showed a shift towards lower vapor pressures for ethanol and water, thus decreasing the selectivity of this material for butanol at low vapor pressures. Single column adsorption and desorption breakthrough measurements using He as carrier gas further confirmed the selectivity and capacity (97 mg/g) of this zeolite for butanol and showed the viability of the use of CO_2 as carrier gas during adsorption and/or desorption. However, the use of CO_2 as carrier gas had some effect on adsorption kinetics, leading to broader breakthrough profiles of butanol during adsorption of a packed Si-LTA column. Also, adsorption capacities and selectivity for butanol were lower using CO_2 as carrier gas. Desorption of this column using CO_2 as carrier gas also showed a slight loss in performance.

The hydrophobic MOF ZIF-8 showed a similar high adsorption capacity for butanol. As for adsorption on Si-LTA, the adsorption capacities observed during isotherm measurement at high vapor pressure were lower using CO_2 as carrier gas. The ethanol isotherm showed a shift towards low vapor pressures using CO_2 as carrier gas, lowering butanol selectivity. Breakthrough measurements with a vapor phase ABE mixture using He as carrier gas confirmed this materials' capacity (247 mg/g) and selectivity for butanol. Due to the S-shape of the butanol isotherm, the observed breakthrough profiles of butanol during adsorption and desorption had a peculiar shape. The butanol breakthrough profile during adsorption was observed to be much broader than for Si-LTA, worsening separation performance during adsorption. However, during desorption, a sharp decrease in concentration was observed in the breakthrough profile, positively influencing desorption characteristics. Due to the reversibility of butanol adsorption on ZIF-8, isothermal desorption at the same temperature as adsorption was possible, positively influencing the energy requirements for a butanol adsorption process using a ZIF-8 column. As for Si-LTA, butanol adsorption capacities were lower using CO_2 as carrier gas in adsorption breakthrough experiments. Selectivity for butanol compared to ethanol also decreased, but selectivity of butanol compared to acetone and water increased using CO_2 as carrier gas. Also leading to higher purity of butanol during desorption

Both the hydrophilic SAPO-34 zeolite and the hydrophobic Si-CHA zeolite showed inverse selectivity compared to ZIF-8 and Si-LTA. Due to the small chabazite cage size, ethanol and water were adsorbed by these materials, whilst butanol was excluded in dynamic adsorption experiments. Vapor phase breakthrough experiments of an ABE mixture showed the adsorption capacity (4 mg/g) and selectivity

of the SAPO-34 zeolite for ethanol to be lower than that of the Si-CHA material (5.2 mg/g). However, the water adsorption capacity of SAPO-34 (159mg/g) was significantly higher than that of Si-CHA (23.4 mg/g). Unfortunately, catalytic activity of SAPO-34 was observed using CO_2 as carrier gas for vapor phase ABE adsorption. Similarly, catalytic products were formed during high-temperature desorption of a saturated SAPO-34 column. However, both SAPO-34 and Si-CHA showed potential for ethanol removal from the vapor phase ABE mixture.

With the knowledge obtained from the isotherm and single column breakthrough measurements, a proposition of different multicolumn configurations was made for optimal butanol recovery. A column packed with ZIF-8 or Si-LTA pellets could be used for butanol removal, whilst a column paced with Si-CHA or SAPO-34 pellets could be used for ethanol and/or water removal. Not all of the proposed configurations could be tested experimentally, therefore a mathematical model was developed to perform multicolumn breakthrough simulations. This model allowed for qualitative comparison of the different simulated configurations.

Experimentally, a butanol adsorbing column (ZIF-8 or Si-LTA) was first completely saturated with a vapor phase ABE mixture. During the desorption of this first column, a second column (SAPO-34 or Si-CHA) was placed behind it to adsorb the desorbing ethanol and water from the first column. Using this configuration, it was shown that the second column should be removed after a certain amount of time. Otherwise, the adsorbed ethanol and water on the Si-CHA column starts to desorb, thus lowering butanol purity at the end of the Si-LTA desorption. Therefore, the duration of the coupling to the second column was optimized for the combination of Si-LTA and Si-CHA or SAPO-34. A comparison of the performance of SAPO-34 and Si-CHA in this configuration showed that the highest butanol purity could be obtained using SAPO-34 as second column. An increase in butanol purity at 100% recovery could be obtained from 76 wt% to 99.9 wt% using SAPO-34 as second column. A similar improvement in butanol purity could be obtained using CO_2 as carrier gas, indicating the viability of the use of CO_2 in such a column configuration. For the column combinations tested with ZIF-8, the same conclusion could be drawn: a high increase in butanol purity was obtained using SAPO-34 as second column. In this way, an increase in butanol purity at 100% recovery of 76 wt% to 99.5 wt% could be obtained. Unfortunately, catalytic activity of the SAPO-34 column was observed in the combination with ZIF-8. Probably this is caused by the higher amount of acetone adsorbing on ZIF-8. The same performance could be obtained using CO_2 as carrier gas, showing the viability of the use of this gas as carrier for adsorptive vapor phase butanol recovery.

The mathematical model used to compare other multicolumn configurations was developed using single component isotherm data and multicomponent breakthrough data. For all four of the studied columns, good fitting of experimental breakthrough data could be obtained. Using the developed adsorption column parameters, different column combinations were simulated. The multicolumn configurations simulated consisted of a first column for ethanol and water removal (Si-CHA or SAPO-34) and a second column in series for butanol adsorption (Si-LTA or ZIF-8). A vapor phase ABE mixture was fed to the first column and the stream coming out of the first column was subsequently sent to the second column. Again, for both Si-LTA and ZIF-8 as second column, the best results were obtained using SAPO-34 as first column. In this way, butanol purity could be increased from 93 wt% to 99 wt% for the Si-LTA column and from 98 wt% to 99 wt% for the ZIF-8 column. Such a configuration allows for the recovery of ethanol, butanol and acetone from the vapor phase ABE mixture, although a larger amount of Si-CHA or SAPO-34 material would be necessary for high-purity butanol recovery. Further, the ethanol adsorbed on the Si-CHA or SAPO-34 column is highly diluted in water, making an extra ethanol concentration step necessary.

Therefore, the chosen combination of adsorption columns for butanol recovery form the vapor present in the headspace of an ABE fermenter, or from the gas stream used in gas stripping, will depend of process economics. Using the simple, two column configuration validated experimentally, a butanol vapor stream of very high purity can be obtained. Such a separation process could be relatively cheap, since only a small amount of SAPO-34 or Si-CHA material would be necessary to purify the butanol stream. However, in this way a large amount of possibly valuable ethanol and acetone is lost. The column combination which was verified model-wise allows for the recuperation of all three ABE solvents. However, the investment cost will be higher, since a larger amount of adsorbent is necessary and the adsorbed ethanol product on SAPO-34 or Si-CHA is quite diluted, making an extra ethanol concentration step necessary.

Reflecting on the choice of adsorption material, ZIF-8 showed the most promising results as butanol adsorbent due to its efficient desorption which can be performed at low temperatures and its high capacity. For the removal of ethanol and water, SAPO-34 would be the material of choice, giving the best results in all of the tested column configurations. However, catalytic activity could be a problem using this material. Although the adsorption capacities and selectivities for butanol on ZIF-8 and Si-LTA were usually slightly lower using CO_2 as carrier gas instead of He, the use of CO_2 as carrier gas for vapor phase ABE solvent recovery might be viable. Especially on ZIF-8, where the purity of adsorbed butanol increased, using CO_2 as carrier gas during adsorption.

The research performed for this Masters' thesis thus showed that high-purity butanol recuperation from a vapor phase ABE mixture is possible, using the right combination of selective adsorbents in the right configuration.

Summary

The large increase in world population during the last half of the 20th and during the 21st century is having an increased impact on the natural environment. One of the important effects of human activity on the planet's ecosystem is global warming due to the use of fossil fuels for energy production. Further, most of the organic chemicals and polymers used today are produced starting from petroleum, which is a non-renewable resource. One of the possible solutions to this energy problem is the use of renewable resources as a base for fuel production. Further, these biofuels can often also be used as a platform molecule or monomer for the synthesis of more complex organic molecules and polymers thus decreasing the dependency of chemical industry from non-renewable resources.

One of the possible biofuel and platform molecule candidates is 1-butanol. This molecule is conventionally produced via a petroleum-based chemical route, but can also be produced via fermentation using bacteria of the genus *Clostridium*. This so-called acetone-butanol-ethanol (ABE) fermentation process yields acetone, 1-butanol and ethanol starting from different types of renewable resources. However, this fermentation process leads to a low final butanol concentration (lower than 20 g/l) due to inhibition of clostridial growth by the produced solvents. Therefore, most of the research on ABE fermentation is either focused on improvement of solvent resistance of the used production strains or on development of *in situ* butanol recovering methods to allow simultaneous solvent recovery and relief of product inhibition. The conventional process for ABE solvent recovery is distillation, however this is a very energy intensive process. Different authors indicate adsorption to be the most energy efficient recovery method.

One of the possible *in situ* recovery methods is gas stripping. However, this separation method suffers from a lack of butanol selectivity. Further, a large amount of more concentrated solvent vapor is present in the head space of the fermenter. Therefore, selective recovery of the formed ABE solvents from the vapor phase via adsorption might increase the efficiency of the ABE fermentation process. While liquid phase adsorption of butanol from ABE model solutions and ABE fermentation broth is well-described in the literature, few research has been performed on vapor phase ABE solvent recovery.

Most of the literature on adsorptive separation technologies is focused around isotherm and breakthrough experiments. However, the goal of the research performed in this Masters' thesis was to develop a setup consisting of different adsorption columns with different selectivities for optimal butanol recovery from a vapor phase ABE mixture. During the ABE fermentation process, a high amount of CO_2 is produced. Therefore, the effect of CO_2 on vapor phase adsorption was investigated in detail.

In a first step, four different adsorbents were evaluated on their adsorption capacity and selectivity for the different vapor phase ABE components: the hydrophobic zeolite Si-LTA, the hydrophobic metal organic framework (MOF) ZIF-8, the hydrophobic zeolite Si-CHA and a hydrophilic zeolite SAPO-34.

The hydrophobic Si-LTA zeolite showed a high capacity for butanol, as was verified via isotherm measurements. This due to the size of its windows (4.1 Å x 4.1 Å), which are big enough for the butanol molecules (kinetic diameter: 4.0 Å) to allow them to enter the zeolite pores. Since ethanol is an even smaller molecule, it adsorbs as well. Acetone, however is excluded from the zeolite pores and due to the hydrophobicity of the material, water adsorption capacities are low. Isotherm measurements using CO_2 as carrier gas showed competitive adsorption effects. Due to the CO_2 adsorbing on the zeolite, the

butanol adsorption capacity decreases. Further, the ethanol isotherm showed a shift to low vapor pressures, thus decreasing the selectivity of the material for butanol.

Similar to the hydrophobic Si-LTA material, the hydrophobic MOF ZIF-8 showed a high butanol adsorption capacity. Acetone and ethanol were also able to adsorb on this material. The effects of CO_2 on the adsorption properties were similar as for the Si-LTA zeolite: the ABE components showed a lower adsorption capacity at high vapor pressures and the ethanol isotherm showed a shift towards lower vapor pressures.

The Si-CHA and SAPO-34 zeolite are isostructural materials: both contain cages that exclude alcohols larger than propanol. However, the Si-CHA material is hydrophobic due to its very low Al content and thus showed a higher adsorption capacity for ethanol, whilst SAPO-34 showed a larger capacity for water. Neither of the materials adsorbed acetone or butanol on a reasonable timescale. Isotherm measurements showed the adsorption capacity of SAPO-34 for water and ethanol to be lower using CO_2 as carrier gas.

The selectivity and capacity of these different materials were further investigated performing vapor phase breakthrough experiments with a model ABE mixture at 40 °C. A comparison was made between He and CO_2 as carrier gas. For the Si-LTA column, results of the isotherm measurements were confirmed: butanol was adsorbed in high amounts (97 mg/g), whilst ethanol, acetone and water were largely excluded. Using CO_2 as carrier gas, the adsorption capacity and selectivity for butanol decreased. A kinetic effect on the breakthrough profile was also visible: broadening of the butanol profile could be observed, leading to worse separation characteristics. Desorption experiments also showed slightly worse performance using CO_2 as carrier gas.

The column packed with ZIF-8 showed similar behavior to the Si-LTA column. Butanol was adsorbed with a high capacity (247 mg/g). Acetone, ethanol and water were only adsorbed in minor amounts. Due to the S-shaped butanol isotherm on ZIF-8, a peculiar breakthrough profile was observed during adsorption and desorption. The S-shaped isotherm led to fronting of the butanol breakthrough profile during adsorption, whilst a sudden sharp decrease in butanol concentration was observed in the desorption profile. The reversibility of the adsorption equilibrium on ZIF-8 made the use of much milder temperature conditions possible during the desorption of this column compared to Si-LTA, greatly increasing energetic efficiency of the process. As for Si-LTA, butanol adsorption capacity and was lower using CO_2 as carrier gas. The selectivity for butanol compared to ethanol also decreased, however the selectivity for butanol compared to acetone and water increased. This also led to a higher purity of butanol adsorbed on this column.

Vapor phase ABE breakthrough experiments on SAPO-34 using He as carrier gas confirmed the high water (159mg/g) and ethanol (4 mg/g) adsorption capacity of this material. The Si-CHA material has a much lower adsorption capacity for water (23.4 mg/g) and a higher ethanol adsorption capacity (5.2 mg/g). Unfortunately, the SAPO-34 material showed catalytic activity during breakthrough using CO_2 as carrier gas and during desorption using an increase in temperature.

Based on the adsorptive properties of the different materials, different configurations combining columns packed with these different materials were proposed. Not all of these configurations could be verified experimentally. Therefore, a mathematical model was developed to describe the dynamic behavior of these different combinations of adsorption columns.

The experimentally verified configurations consisted of a butanol adsorbing column (ZIF-8 or Si-LTA) that was first completely saturated using a vapor phase ABE mixture. When desorption of the first column was started, a second column (Si-CHA or SAPO-34) was placed behind it to adsorb the

impurities desorbing from the first column. The second column could only be held behind the first column for a certain amount of time, else the adsorbed impurities would start to desorb, leading to loss of separation performance. This configuration was evaluated using He and CO_2 as carrier gas.

For desorption of the Si-LTA column, a comparison was made between performance of the Si-CHA and SAPO-34 as second column. The highest separation performance was obtained with the SAPO-34 column as second column, increasing butanol purity at 100% recovery from 76 wt% to 99.9 wt% using He as carrier gas. A similar separation performance was observed using CO_2 as carrier gas. Similarly, the combination of ZIF-8 and SAPO-34 was observed to be very effective, butanol purity at 100% recovery could be increased from 76 wt% to 99.5 wt%. Unfortunately, catalytic activity of the SAPO-34 column was observed, probably due to the higher amount of acetone adsorbing on the ZIF-8 column. For ZIF-8, the same separation performance could be obtained using CO_2 as carrier gas.

The column configuration evaluated experimentally was a simple two-column system leading to high-purity butanol recovery. However, a large amount of acetone and ethanol produced during the ABE fermentation is lost using this process. Therefore, an alternative separation process was proposed, sending a vapor phase ABE mixture through a first column for water and/or ethanol removal. The gas flow coming out of this first column was subsequently sent to a second column for butanol adsorption.

These column combinations were verified using a mathematical model describing the behavior of the different columns. Model parameters were first developed using single component isotherms and multicomponent breakthrough data. In a subsequent step, the multicolumn adsorption simulations were performed. A first combination of the Si-CHA and SAPO-34 column as first column and Si-LTA as second column showed that a larger amount of Si-CHA or SAPO-34 was necessary to obtain butanol of high purity compared to the configuration evaluated experimentally. For both the ZIF-8 and Si-LTA column as second column, performance of Si-CHA and SAPO-34 was compared. Due to the high water adsorption capacity of SAPO-34, the use of this material as first column led to the highest butanol purity. For ZIF-8, an increase in butanol purity of 98 wt% to 99 wt% was realized, whilst the butanol purity on Si-LTA increased from 93 wt% to 99 wt%. Using this column combination, all of the ABE solvents could be separated: acetone, which does not adsorb on any of the materials in large quantities, ethanol and water adsorbing on SAPO-34 and butanol adsorbing on ZIF-8 or Si-LTA. However, investment costs using such a configuration will be inevitably higher since more SAPO-34 or Si-CHA material would be necessary, compared to the configuration tested experimentally. Further, the ethanol adsorbed on SAPO-34 or Si-CHA is very diluted, making the use of second separation step necessary for further ethanol concentration.

Therefore, the optimal configuration for vapor phase ABE separation will depend on process economics: the simple and cheaper configuration evaluated experimentally will yield a high-purity butanol stream. However, the possibly valuable ethanol and acetone fractions are lost. The column configurations evaluated via simulations could separate all of the ABE solvents, but at a higher cost. In both cases, simulations and experiments showed that high-purity butanol recovery is possible using a combination of different selective adsorbents.

Reflecting on the choice of adsorption material, ZIF-8 showed the most promising results as butanol adsorbent due to its efficient desorption which can be performed at low temperatures and its high capacity. For the removal of ethanol and water, SAPO-34 would be the material of choice, giving the best results in all of the tested column configurations. However, catalytic activity could be a problem using this material. Although the adsorption capacities and selectivities were slightly lower using CO_2 as carrier gas instead of He, the use of CO_2 as carrier gas for vapor phase ABE solvent recovery might

be viable. Especially for ZIF-8, due to the higher purity of the adsorbed butanol after adsorption using CO_2 as carrier gas.

The research performed for this Masters' thesis thus showed that high-purity butanol recuperation from a vapor phase ABE mixture is possible, using the right combination of selective adsorbents in the right configuration.

Samenvatting

De aanzienlijke toename van de wereldbevolking tijdens de tweede helft van de 20ste en tijdens de 21ste eeuw heeft ook een toegenomen impact op de natuur. Een van de belangrijke gevolgen van menselijke activiteit op onze planeet is de opwarming van de aarde, die is toe te schrijven aan het gebruik van fossiele brandstoffen voor energieproductie. Bovendien worden de meeste organische chemische stoffen en polymeren die we vandaag gebruiken, geproduceerd op basis van petroleum, een niet-hernieuwbare grondstof. Een van de mogelijke oplossingen voor dit energieprobleem is het gebruik van hernieuwbare grondstoffen voor brandstofproductie. Deze biobrandstoffen kunnen bovendien vaak dienen als platformmolecule of monomeer voor de synthese van complexere organische moleculen en polymeren, wat dan ook de chemische industrie minder afhankelijk maakt van niet-hernieuwbare grondstoffen.

Een van de mogelijke kandidaten als biobrandstof en platformmolecule is 1-butanol. Deze molecule wordt gewoonlijk geproduceerd via een petroleum-gebaseerd chemisch proces, maar het kan ook worden gemaakt via fermentatie, door gebruik te maken van bacteriën van het geslacht *Clostridium*. Dit zogenaamde aceton-butanol-ethanol (ABE) fermentatieproces produceert aceton, 1-butanol en ethanol, op basis van diverse soorten hernieuwbare grondstoffen. Dit fermentatieproces leidt echter tot een lage eindconcentratie aan butanol (minder dan 20g/l), wat te wijten is aan het feit dat de groei van *Clostridum sp.* wordt afgeremd door de solventen die worden geproduceerd. Het meeste onderzoek rond ABE-fermentatie is dan ook ofwel toegespitst op de verbetering van solventresistentie van de gebruikte productiestammen, ofwel op de ontwikkeling van *in situ* butanol scheidingsmethoden om solventwinning mogelijk te maken en tegelijk de productinhibitie te verminderen. Het conventionele proces waarmee ABE solventen worden gescheiden is distillatie, maar dat is een zeer energie-intensief proces. Meerdere auteurs geven aan dat adsorptie de meest energie-efficiënte winningsmethode is.

Een van de mogelijke in *situ* scheidingsmethoden is gas stripping. Maar met deze scheidingsmethode is de butanolselectiviteit te laag. Bovendien is er in de *head space* van de fermentor een grote hoeveelheid solventdamp aanwezig. De selectieve winning van de tijdens de dampfase gevormde ABE solventen via adsorptie zou dan ook de efficiëntie van het ABE-fermentatieproces kunnen verhogen. Daar waar er al heel wat literatuur bestaat over butanoladsorptie uit de vloeibare fase gebaseerd op ABE-modeloplossingen en op ABE-fermentatiemedia, is er nog niet veel onderzoek gedaan naar ABE-solventwinning uit de dampfase.

De meeste literatuur over scheidingstechnieken op basis van adsorptie concentreert zich op isothermexperimenten en doorbraakexperimenten. Het doel van het onderzoek dat in deze Masterthesis werd gevoerd, was echter om een opstelling te ontwikkelen die bestaat uit meerdere adsorptiekolommen met verschillende selectiviteit, om op een optimale manier butanol te recupereren uit een waterig ABE-dampmengsel. Tijdens het ABE-fermentatieproces wordt er een grote hoeveelheid CO_2 geproduceerd. Daarom werd het effect van CO_2 op de dampfase-adsorptie in detail onderzocht.

In eerste instantie werden er vier verschillende adsorbenten beoordeeld op hun adsorptiecapaciteit en selectiviteit voor de verschillende ABE-componenten tijdens de dampfase: de hydrofobe zeoliet Si-LTA, het hydrofobe metaal-organisch netwerk (*metal organic framework* of MOF) ZIF-8, de hydrofobe zeoliet Si-CHA een hydrofiele zeoliet SAPO-34.

De hydrofobe zeoliet Si-LTA bleek voor butanol een hoge capaciteit te hebben, wat werd nagegaan via de meting van adsorptie-isothermen. Dit is toe te schrijven aan de grootte van zijn porie-openingen (4.1 Å x 4.1 Å), die groot genoeg is om de butanolmoleculen (kinetische diameter: 4.0 Å) in staat te stellen in de zeolietporiën binnen te dringen. Ook ethanol adsorbeert, aangezien dit molecule nog kleiner is. Maar aceton wordt uit de zeolietporiën uitgesloten, en omwille van het hydrofobe karakter van het materiaal zijn ook de adsorptiecapaciteiten voor water, laag. Door meting van adsorptie-isothermen met CO_2 als draaggas werden er competitieve adsorptie-effecten vastgesteld. Doordat CO2 adsorbeert op de zeoliet, daalt de butanol-adsorptiecapaciteit. Bovendien verschoof de ethanol isotherm naar lagere dampdrukken, waardoor de selectiviteit van het materiaal voor butanol daalde.

Net als bij het hydrofobe Si-LTA-materiaal, vertoonde ook de hydrofobe MOF ZIF-8 een hoge adsorptiecapaciteit voor butanol. Ook aceton en ethanol konden op dit materiaal adsorberen. De effecten van CO_2 op de adsorptie-eigenschappen waren gelijkaardig aan die van de Si-LTA-zeoliet: de ABE-componenten bleken een lagere adsorptiecapaciteit te hebben bij hoge dampdrukwaarden en de ethanol isotherm vertoonde een verschuiving naar lagere dampdrukken.

De Si-CHA en de SAPO-34 zeolieten zijn isostructurele materialen: allebei hebben ze een porie-openingsgrootte die alcoholen groter dan propanol uitsluit. Het Si-CHA-materiaal is echter hydrofoob, door zijn laag gehalte aan Al, en vertoonde dan ook een hogere adsorptiecapaciteit voor ethanol, daar waar SAPO-34 een hogere adsorptiecapaciteit voor water vertoonde. Geen van beide materialen adsorbeerden binnen een redelijke tijdsschaal aceton of butanol. Isotherme metingen toonden aan dat de adsorptiecapaciteit van SAPO-34 voor water en ethanol lager waren dan wanneer CO_2 wordt gebruikt als draaggas.

De selectiviteit en capaciteit van deze verschillende materialen werd verder onderzocht aan de hand van doorbraakexperimenten in de dampfase op een mengeling volgens het ABE-model bij 40° C. Er werd een vergelijking gemaakt tussen He en CO_2 als draaggas. Voor de Si-LTA-kolom werden de resultaten van de metingen van adsorptie-isothermen bevestigd: butanol werd in grote hoeveelheden geadsorbeerd (97 mg/g), terwijl ethanol, aceton en water in aanzienlijke mate werden uitgesloten. Met CO2 als draaggas daalde de adsorptiecapaciteit en selectiviteit voor butanol. Ook was er een kinetisch effect op het doorbraakprofiel zichtbaar: er kon een verbreding van het butanolprofiel worden waargenomen, wat leidde tot minder goede scheidingskarakteristieken. Desorptie-experimenten toonden ook een wat slechtere performantie aan wanneer CO_2 als draaggas werd gebruikt.

De ZIF-8 kolom en de Si-LTA-kolom vertoonden gelijkaardig gedrag. Butanol werd met hoge capaciteit geadsorbeerd (247 mg/g). Aceton, ethanol en water werden slechts in kleine hoeveelheden geadsorbeerd. Door de S-vormige butanol isotherm op ZIF-8 werd een merkwaardig doorbraakprofiel waargenomen tijdens de adsorptie en de desorptie. De S-vormige isotherm bracht een *fronting* van het butanol-doorbraakprofiel tijdens de adsorptie teweeg, terwijl er een plotse en aanzienlijke daling van de butanolconcentratie werd waargenomen in het desorptieprofiel. De omkeerbaarheid van het adsorptie-evenwicht op ZIF-8 maakte het mogelijk om veel zachtere temperatuurvoorwaarden te gebruiken tijdens de desorptie van deze kolom vergeleken bij Si-LTA, wat de energie-efficiëntie van het proces aanzienlijk verhoogde. Net als voor Si-LTA was de adsorptiecapaciteit en de selectiviteit voor butanol vergeleken met ethanol lager wanneer CO_2 werd gebruikt als draaggas. De selectiviteit ten opzichte van aceton en water steeg echter. Hierdoor steeg ook de zuiverheid van het geadsorbeerde butanol op de ZIF-8 kolom.

Doorbraakexperimenten met een ABE-modeloplossing in de dampfase op SAPO-34, waarbij He werd gebruikt als draaggas, bevestigden de hoge adsorptiecapaciteit van dit materiaal voor water (159mg/g)

en voor ethanol (4 mg/g). Het Si-CHA-materiaal heeft een veel lager adsorptievermogen voor water (23.4 mg/g) en een hogere adsorptiecapaciteit voor ethanol (5.2 mg/g). Helaas vertoonde het SAPO-34 materiaal katalytische activiteit tijdens de doorbraak wanneer CO_2 als draaggas werd gebruikt, en tijdens de stijging in temperatuur bij desorptie.

Op basis van de gekende adsorptie-eigenschappen van de verschillende materialen, werden er verschillende configuraties voorgesteld die kolommen met deze verschillende materialen combineren. Niet al deze configuraties konden experimenteel worden getest. Vandaar dat er een mathematisch model werd ontwikkeld om het dynamisch gedrag van deze verschillende combinaties van adsorptiekolommen te beschrijven.

De experimenteel geteste configuraties bestonden uit een butanol adsorberende kolom (ZIF-8 of Si-LTA), dat eerst helemaal werd gesatureerd door gebruik te maken van een ABE-mengsel in de dampfase. Wanneer deze eerste kolom gedesorbeerd werd, werd een tweede kolom (Si-CHA of SAPO-34) erachter geplaatst om de onzuiverheden te adsorberen die desorbeerden uit de eerste kolom. De tweede kolom kon maar een bepaalde tijdspanne achter de eerste kolom worden gehouden omdat de geadsorbeerde onzuiverheden op de tweede kolom anders zouden beginnen te desorberen, wat zou leiden tot een verlies aan scheidingsperformantie. Deze configuratie werd geëvalueerd met He en CO_2 als draaggas.

Voor de desorptie van de Si-LTA-kolom werd er een vergelijking gemaakt tussen de performantie van Si-CHA en SAPO-34 als tweede kolom. De grootste scheidingsperformantie werd verkregen met de SAPO-34 kolom als tweede kolom, waardoor de butanolzuiverheid bij 100 % butanolrecuperatie werd verhoogd van 76 wt% tot 99.9 wt% met He als draaggas. Verder werd er geen katalytische activiteit van SAPO-34 waargenomen, noch met He, noch met CO_2. Een gelijkaardige scheidingsperformantie werd waargenomen bij wanneer CO_2 werd gebruikt als draaggas. Ook werd vastgesteld dat de combinatie van ZIF-8 en SAPO-34 bijzonder effectief was: butanolzuiverheid bij 100% recuperatie steeg van 76 wt% tot 99.5 wt%. Helaas werd er katalytische activiteit van de SAPO-34 kolom waargenomen, wellicht toe te schrijven aan de hogere hoeveelheid aceton die adsorbeerde op de ZIF-8 column. Voor ZIF-8 kolom kon ook dezelfde scheidingsperformantie worden verkregen met CO_2 als draaggas.

De experimenteel geëvalueerde configuratie was een eenvoudig systeem van twee kolommen dat leidde tot butanolrecuperatie met hoge zuiverheid. Wanneer dit proces wordt gebruikt gaat er echter een grote hoeveelheid aceton en ethanol verloren die wordt geproduceerd tijdens de ABE-fermentatie. Daarom werd een alternatief scheidingsproces voorgesteld, waarbij een ABE-mengsel in dampfase door een eerste kolom werd gestuurd om er water en/of ethanol uit te halen. Het gas dat uit deze eerste kolom kwam, werd vervolgens naar een tweede kolom gedreven voor de adsorptie van butanol.

Deze kolomcombinaties werden geëvalueerd met een mathematisch model dat het gedrag van de verschillende kolommen beschreef. Eerst werden de modelparameters ontwikkeld door gebruik te maken van gegevens die gebaseerd waren op isothermen van de enkelvoudige componenten. Kinetische parameters werden gefit op multicomponent doorbraakprofielen. In een volgende stap werden de adsorptiesimulaties van de combinaties van verschillende kolommen uitgevoerd. Een eerste combinatie van de Si-CHA en de SAPO-34 kolom als eerste kolom, en Si-LTA als tweede kolom toonde aan dat er een grotere hoeveelheid Si-CHA of SAPO-34 nodig was om butanol met hoge zuiverheidsgraad te verkrijgen, vergeleken bij de configuratie die experimenteel werd geëvalueerd. Voor zowel de ZIF-8 als de Si-LTA-kolom als tweede kolom, werd de performantie van Si-CHA en SAPO-34 vergeleken. Door de hoge wateradsorptiecapaciteit van SAPO-34 leidde het gebruik van dit materiaal als tweede kolom tot de hoogste butanolzuiverheid. Voor ZIF-8 werd er een toename in

butanolzuiverheid van 98 wt% tot 99 wt% gerealiseerd, terwijl de butanolzuiverheid op Si-LTA toenam van 93 wt% tot 99 wt%. Door gebruik te maken van deze kolomcombinatie konden alle ABE solventen worden gescheiden: aceton dat niet in grote hoeveelheden adsorbeert op geen enkel van de materialen, ethanol en water die adsorberen op SAPO-34, en butanol dat adsorbeert op ZIF-8 of Si-LTA. De investeringskosten bij het gebruik van een dergelijke configuratie zullen echter onvermijdelijk hoger zijn aangezien er meer SAPO-34 of Si-CHA-materiaal zou nodig zijn. Verder is het ethanol dat wordt geadsorbeerd op SAPO-34 of Si-CHA zeer verdund, waardoor het gebruik van een tweede scheidingsstap vereist is om de ehtanolconcentratie te verhogen.

De optimale configuratie voor ABE in de dampfase zal dan ook afhankelijk zijn van de economische aspecten van het proces: de eenvoudige en goedkopere configuratie die experimenteel werd geëvalueerd, zal zeer zuiver butanol produceren. Maar de mogelijks waardevolle ethanol- en acetonfracties gaan verloren. De kolomconfiguraties die via simulaties werden geëvalueerd, zouden alle ABE solventen kunnen scheiden, maar aan een hogere investeringskost. In beide gevallen toonden experimentele en gesimuleerde data aan dat butanolrecuperatie aan hoge zuiverheid mogelijk is, gebruik makend van een combinatie van selective adsorbenten.

Wat de keuze van het adsorptiemateriaal betreft, bleken de resultaten van ZIF-8 als butanoladsorbent de meest veelbelovende te zijn, dankzij de efficiënte desorptie die kan bereikt worden bij lage temperatuur, en dankzij de hoge capaciteit ervan. Voor de ethanol- en waterextractie zou de beste materiaalkeuze SAPO-34 zijn, waarmee de beste resultaten werden bereikt in alle geteste kolomconfiguraties. Katalytische activiteit zou bij het gebruik van dit materiaal echter een probleem kunnen zijn. Hoewel de adsorptiecapaciteiten en selectiviteit enigszins lager lagen wanneer CO_2 als draaggas werd gebruikt in plaats van He, zou het gebruik van CO_2 als draaggas voor solventwinning uit ABE in de dampfase een interessante optie kunnen zijn. Zeker voor ZIF-8, waar de zuiverheid van het geadsorbeerde butanol steeg bij het gebruik van CO_2 als draaggas.

Het onderzoek uitgevoerd in het kader van deze Masterthesis, toonde dus aan dat een hoge butanolzuiverheid kon bekomen worden uit een dampfase ABE-mengsel, door gebruik te maken van een combinatie van adsorptiekolommen met een verschillende selectiviteit.

References

Abdehagh, N., Tezel, F.H. & Thibault, J. (2013). Adsorbent screening for biobutanol separation by adsorption: Kinetics, isotherms and competitive effect of other compounds. *Adsorption*, **19**(6), pp.1263–1272.

Abdehagh, N., Tezel, F.H. & Thibault, J. (2014). Separation techniques in butanol production: Challenges and developments. *Biomass and Bioenergy*, **60**, pp.222–246.

Abdehagh, N., Gurnani, P., Tezel, F.H. & Thibault, J. (2015). Adsorptive separation and recovery of biobutanol from ABE model solutions. *Adsorption*, **21**(3), pp.185-194.

Abdehagh, N., Dai, B., Thibault, J. & Tezel, F.H. (2016a). Biobutanol Separation from ABE Model Solutions and Fermentation Broths Using a Combined Adsorption-Gas Stripping Process. *Journal of Chemical Technology & Biotechnology*, Available at: http://doi.wiley.com/10.1002/jctb.4977

Abdehagh, N., Tezel, F.H. & Thibault, J., (2016b). Multicomponent adsorption modeling: isotherms for ABE model solutions using activated carbon F-400. *Adsorption*, **22**(3), pp.357–370.

Adhami, L., Griggs, B., Himebrook, P. & Taconi, K. (2009). Liquid–Liquid Extraction of Butanol from Dilute Aqueous Solutions Using Soybean-Derived Biodiesel. *Journal of the American Oil Chemists' Society*, **86**(11), pp.1123-1128.

Alaswad, A., Dassisti, M., Prescott, T. and Olabi, A. (2015). Technologies and developments of third generation biofuel production. *Renewable and Sustainable Energy Reviews*, **51**, pp.1446-1460.

Andrade, J. & Vasconcelos, I. (2003). Continuous cultures of Clostridium acetobutylicum: culture stability and low-grade glycerol utilisation. *Biotechnology Letters*, **25**(2), pp.121-125.

Ania, C., García-Pérez, E., Haro, M., Gutiérrez-Sevillano, J., Valdés-Solís, T., Parra, J. & Calero, S. (2012). Understanding Gas-Induced Structural Deformation of ZIF-8. *J. Phys. Chem. Lett.*, **3**(9), pp.1159-1164.

Biebl, H. (2001). Fermentation of glycerol by *Clostridium pasteurianum* - batch and continuous culture studies. *Journal of Industrial Microbiology and Biotechnology*, **27**(1), pp.18-26.

Branduardi, P., de Ferra, F., Longo, V. & Porro, D. (2013). Microbial n -butanol production from Clostridia to non-Clostridial hosts. *Eng. Life Sci.*, **14**(1), pp.16-26.

Caes, B., Van Oosbree, T., Lu, F., Ralph, J., Maravelias, C. & Raines, R. (2013). Simulated Moving Bed Chromatography: Separation and Recovery of Sugars and Ionic Liquid from Biomass Hydrolysates. *ChemSusChem*, **6**(11), pp.2083-2089.

Cao, Y., Wang, K., Wang, X., Gu, Z., Gibbons, W. & Vu, H. (2015a). Butanol vapor adsorption behavior on active carbons and zeolite crystal. *Applied Surface Science*, **349**, pp.1-7.

Cao, Y., Wang, K., Wang, X., Gu, Z., Gibbons, W. & Vu, H. (2015b). Adsorption of butanol vapor on active carbons with nitric acid hydrothermal modification. *Bioresource Technology*, **196**, pp.525-532.

Chen, Y., Wu, Y., Tao, L., Dai, B., Yang, M., Chen, Z. & Zhu, X. (2010). Dehydration reaction of bio-ethanol to ethylene over modified SAPO catalysts. *Journal of Industrial and Engineering Chemistry*, **16**(5), pp.717-722.

Climent, M., Corma, A. & Iborra, S. (2014). Conversion of biomass platform molecules into fuel additives and liquid hydrocarbon fuels. *Green Chemistry*, **16**(2), pp.516-547.

Cousin Saint Remi, J., Rémy, T., Van Hunskerken, V., van de Perre, S., Duerinck, T., Maes, M., De Vos, D., Gobechiya, E., Kirschhock, C., Baron, G. & Denayer, J. (2011). Biobutanol Separation with the Metal-Organic Framework ZIF-8. *ChemSusChem*, **4**(8), pp.1074-1077.

Cousin Saint Remi, J., Baron, G. & Denayer, J. (2012). Adsorptive separations for the recovery and purification of biobutanol. *Adsorption*, **18**(5-6), pp.367-373.

Cousin Saint Remi, J., Baron, G. & Denayer, J. (2013). Nonuniform Chain-Length-Dependent Diffusion of Short 1-Alcohols in SAPO-34 in Liquid Phase. *J. Phys. Chem. C*, **117**(19), pp.9758-9765.

Cousin Saint Remi, J., Lauerer, A., Chmelik, C., Vandendael, I., Terryn, H., Baron, G., Denayer, J. & Kärger, J. (2015). The role of crystal diversity in understanding mass transfer in nanoporous materials. *Nature Materials*, **15**(4), pp.401-406.

Cosseron, A., Daou, T., Tzanis, L., Nouali, H., Deroche, I., Coasne, B. & Tchamber, V. (2013). Adsorption of volatile organic compounds in pure silica CHA, ∗BEA, MFI and STT-type zeolites. *Microporous and Mesoporous Materials*, **173**, pp.147-154.

Daems, I., Singh, R., Baron, G. & Denayer, J. (2007). Length exclusion in the adsorption of chain molecules on chabazite type zeolites. *Chemical Communications*, **13**, pp.1316-1318.

Danaci, D., Singh, R., Xiao, P. & Webley, P. (2015). Assessment of ZIF materials for CO2 capture from high pressure natural gas streams. *Chemical Engineering Journal*, **280**, pp.486-493.

DeJaco, R., Bai, P., Tsapatsis, M. & Siepmann, J. (2016). Adsorptive Separation of 1-Butanol from Aqueous Solutions Using MFI- and FER-Type Zeolite Frameworks: A Monte Carlo Study. *Langmuir*, **32**(8), pp.2093-2101.

Denayer, J.F.M., Devriese, L., Couck, S., Martens, J., Singh, R., Webley, P. & Baron, G. (2008). Cage & Window Effects in the Adsorption of n -Alkanes on Chabazite and SAPO-34. *J. Phys. Chem. C*, **112**(42), pp.16593-16599.

Dürre, P. (2007). Biobutanol: An attractive biofuel. *Biotechnol. J.*, **2**(12), pp.1525-1534.

Duong, D. (1998). *Adsorption analysis*. Imperial College Press., London, United Kingdom. 830pp.

European Commision (2016). *Biofuels*. https://ec.europa.eu/energy/en/topics/renewable-energy/biofuels. Accessed on May 3, 2016.

Ezeji, T., Groberg, M., Qureshi, N. & Blaschek, H. (2003). Continuous Production of Butanol from Starch-Based Packing Peanuts. *Applied Biochemistry and Biotechnology*, **106**(3), pp.375-382.

Ezeji, T., Qureshi, N. & Blaschek, H. (2007). Production of acetone butanol (AB) from liquefied corn starch, a commercial substrate, using Clostridium beijerinckii coupled with product recovery by gas stripping. *Journal of Industrial Microbiology & Biotechnology*, **34**(12), pp.771-777.

Faisal, A., Zarebska, A., Saremi, P., Korelskiy, D., Ohlin, L., Rova, U., Hedlund, J. & Grahn, M. (2013). MFI zeolite as adsorbent for selective recovery of hydrocarbons from ABE fermentation broths. *Adsorption*, **20**(2-3), pp.465-470.

Faisal, A., Zhou, M., Hedlund, J. & Grahn, M. (2016). Recovery of butanol from model ABE fermentation broths using MFI adsorbent: a comparison between traditional beads and a structured adsorbent in the form of a film. *Adsorption*, **22**(2), pp.205-214.

Fairen-Jimenez, D., Moggach, S., Wharmby, M., Wright, P., Parsons, S. & Düren, T. (2011). Opening the Gate: Framework Flexibility in ZIF-8 Explored by Experiments and Simulations. *J. Am. Chem. Soc.*, **133**(23), pp.8900-8902.

Fan, H., Shi, Q., Yan, H., Ji, S., Dong, J. & Zhang, G. (2014). Simultaneous Spray Self-Assembly of Highly Loaded ZIF-8-PDMS Nanohybrid Membranes Exhibiting Exceptionally High Biobutanol-Permselective Pervaporation. *Angewandte Chemie*, **126**(22), pp.5684-5688.

Farzaneh, A., Zhou, M., Potapova, E., Bacsik, Z., Ohlin, L., Holmgren, A., Hedlund, J. & Grahn, M. (2015). Adsorption of Water and Butanol in Silicalite-1 Film Studied with in Situ Attenuated Total Reflectance–Fourier Transform Infrared Spectroscopy. *Langmuir*, **31**(17), pp.4887-4894.

Fond, O., Engasser, J., Matta-El-Amouri, G. & Petitdemange, H. (1986). The acetone butanol fermentation on glucose and xylose. I. Regulation and kinetics in batch cultures. *Biotechnol. Bioeng.*, **28**(2), pp.160-166.

Galadima, A. & Muraza, O. (2015). Recent Developments on Silicoaluminates and Silicoaluminophosphates in the Methanol-to-Propylene Reaction: A Mini Review. *Industrial & Engineering Chemistry Research*, **54**(18), pp.4891-4905.

Geier, D., Hilaly, A. & Soper, J. (2010a). *Method of preparing fatty acid alkyl esters from waste or recycled fatty acid stock*. US Patent 7705170.

Geier, D., Hilaly, A. & Soper, J. (2010b). *Simultaneous synthesis and purification of a fatty acid monoester biodiesel fuel*. US Patent 7828978.

Gelin, P. (2015). *Dampfase scheiding van 1-butanol uit een waterig mengsel door middel van hydrofobe adsorbenten*. Vrije Universiteit Brussel, Brussel, België. pp.135.

Golden, F.M.(1969). *Theory of fixed beds performance for ion exchange accompanied by chemical reactions.* Berkeley: University of California, Berkeley, California, USA. 504pp.

Gomes, P.S. and Rodrigues, A. (2011). Simulated Moving Bed Chromatography: From Concept to Proof-of-Concept. *Chemical Engineering & Technology*, **35**(1), pp.17-34.

Helfferich, F. & Carr, P. (1993). Non-linear waves in chromatography. *Journal of Chromatography A*, **629**(2), pp.97-122.

Henninger, S., Schmidt, F. & Henning, H. (2010). Water adsorption characteristics of novel materials for heat transformation applications. *Applied Thermal Engineering*, **30**(13), pp.1692-1702.

Hirota, Y., Nakano, Y., Watanabe, K., Uchida, Y., Miyamoto, M., Egashira, Y. & Nishiyama, N. (2012). Effect of Crystal Size on Acetone Conversion over SAPO-34 Crystals. *Catalysis Letters*, **142**(4), pp.464-468.

Holt, Robert A., Gillian M. Stephens, & J. Gareth Morris. (1984). *Production of solvents by Clostridium acetobutylicum cultures maintained at neutral pH.* Applied and environmental microbiology **48**(6), pp.1166-1170.

Huang, H., Ramaswamy, S. & Liu, Y. (2014). Separation and purification of biobutanol during bioconversion of biomass. *Separation and Purification Technology*, **132**, pp.513-540.

Huang, X., Lin, Y., Zhang, J. & Chen, X. (2006). Ligand-Directed Strategy for Zeolite-Type Metal–Organic Frameworks: Zinc(II) Imidazolates with Unusual Zeolitic Topologies. *Angewandte Chemie*, **118**(10), pp.1587-1589.

Jang, Y., Malaviya, A., Cho, C., Lee, J. & Lee, S. (2012). Butanol production from renewable biomass by clostridia. *Bioresource Technology*, **123**, pp.653-663.

Jones, D.T. &Woods, D.R. (1986). Acetone-butanol fermentation revisited. *Microbiol. Rev.* **50**, pp.484–524.

Kim, P., Nam, H., Park, C., Wang, N., Chang, Y. and Mun, S. (2015a). Simulated moving bed separation of agarose-hydrolyzate components for biofuel production from marine biomass. *Journal of Chromatography A*, **1406**, pp.231-243.

Kim, M., Cho, I., Park, J., Choi, S. & Lee, I. (2015b). Adsorption of CO2 and CO on H-zeolites with different framework topologies and chemical compositions and a correlation to probing protonic sites using NH3 adsorption. *Journal of Porous Materials*, **23**(2), pp.291-299.

Krishna, R. & van Baten, J. (2008). Segregation effects in adsorption of CO2-containing mixtures and their consequences for separation selectivities in cage-type zeolites. *Separation and Purification Technology*, **61**(3), pp.414-423.

Krishna, R. & van Baten, J. (2010). Hydrogen Bonding Effects in Adsorption of Water−Alcohol Mixtures in Zeolites and the Consequences for the Characteristics of the Maxwell−Stefan Diffusivities. *Langmuir*, **26**(13), pp.10854-10867.

Krishna, R. and van Baten, J. (2011). Entropy-based separation of linear chain molecules by exploiting differences in the saturation capacities in cage-type zeolites. *Separation and Purification Technology*, **76**(3), pp.325-330.

Kujawska, A., Kujawski, J., Bryjak, M. and Kujawski, W. (2015). ABE fermentation products recovery methods—A review. *Renewable and Sustainable Energy Reviews*, **48**, pp.648-661.

Kumar, M. & Gayen, K. (2011). Developments in biobutanol production: New insights. *Applied Energy*, **88**(6), pp.1999-2012.

Küsgens, P., Rose, M., Senkovska, I., Fröde, H., Henschel, A., Siegle, S. & Kaskel, S. (2009). Characterization of metal-organic frameworks by water adsorption. *Microporous and Mesoporous Materials*, **120**(3), pp.325-330.

Lefevere, J., Mullens, S., Meynen, V. & Noyen, J. (2014). Structured catalysts for methanol-to-olefins conversion: a review. *Chemical Papers*, **68**(9), pp.1143-1153.

Li, Y., Wee, L., Martens, J. & Vankelecom, I. (2014). ZIF-71 as a potential filler to prepare pervaporation membranes for bio-alcohol recovery. *J. Mater. Chem. A*, **2**(26), pp.10034-10040.

Lin, X., Wu, J., Fan, J., Qian, W., Zhou, X., Qian, C., Jin, X., Wang, L., Bai, J. & Ying, H. (2012a). Adsorption of butanol from aqueous solution onto a new type of macroporous adsorption resin: Studies of adsorption isotherms and kinetics simulation. *J. Chem. Technol. Biotechnol.*, **87**(7), pp.924-931.

Lin, X., Wu, J., Jin, X., Fan, J., Li, R., Wen, Q., Qian, W., Liu, D., Chen, X., Chen, Y., Xie, J., Bai, J. & Ying, H. (2012b). Selective separation of biobutanol from acetone-butanol-ethanol fermentation broth by means of sorption methodology based on a novel macroporous resin. *Biotechnol Progress*, **28**(4), pp.962-972.

Lin, X., Li, R., Wen, Q., Wu, J., Fan, J., Jin, X., Qian, W., Liu, D., Chen, X., Chen, Y., Xie, J., Bai, J. & Ying, H. (2013). Experimental and modeling studies on the sorption breakthrough behaviors of butanol from aqueous solution in a fixed-bed of KA-I resin. *Biotechnology and Bioprocess Engineering*, **18**(2), pp.223-233.

Liu, D., Chen, Y., Ding, F., Zhao, T., Wu, J., Guo, T., Ren, H., Li, B., Niu, H., Cao, Z., Lin, X., Xie, J., He, X. & Ying, H. (2014). Biobutanol production in a Clostridium acetobutylicum biofilm reactor integrated with simultaneous product recovery by adsorption. *Biotechnol Biofuels*, **7**(1), p.5.

Lugg, G. (1968). Diffusion coefficients of some organic and other vapors in air. *Analytical Chemistry*, **40**(7), pp.1072-1077.

Maddox, I. and Murray, A. (1983). Production of n-butanol by fermentation of wood hydrolysate. *Biotechnology Letters*, **5**(3), pp.175-178.

Madihah, M., Ariff, A., Sahaid, K., Suraini, A. & Karim, M. (2001). Direct fermentation of gelatinized sago starch to acetone–butanol–ethanol by Clostridium acetobutylicum. *World Journal of Microbiology and Biotechnology*, **17**(6), pp.567-576.

Marchal, R., Blanchet, D. & Vandecasteele, J. (1985). Industrial optimization of acetone-butanol fermentation: a study of the utilization of Jerusalem artichokes. *Appl Microbiol Biotechnol*, **23**(2), pp.92-98.

Moggach, S., Bennett, T. & Cheetham, A. (2009). The Effect of Pressure on ZIF-8: Increasing Pore Size with Pressure and the Formation of a High-Pressure Phase at 1.47 GPa. *Angewandte Chemie International Edition*, **48**(38), pp.7087-7089.

Monot, F., Engasser, J. & Petitdemange, H. (1984). Influence of pH and undissociated butyric acid on the production of acetone and butanol in batch cultures of Clostridium acetobutylicum. *Appl Microbiol Biotechnol*, **19**(6), pp.422-426.

Mutschlechner, O., H. Swoboda, & J. R. Gapes. (2000). Continuous two-stage ABE-fermentation using *Clostridium beijerinckii* NRRL B 592 operating with a growth rate in the first stage vessel close to its maximal value. *Journal of molecular microbiology and biotechnology,* **2**(1), pp.101-105.

Nakamura, C. and Whited, G. (2003). Metabolic engineering for the microbial production of 1,3-propanediol. *Current Opinion in Biotechnology*, **14**(5), pp.454-459.

Nielsen, L., Larsson, M., Holst, O. & Mattiasson, B. (1988). Adsorbents for extractive bioconversion applied to the acetone-butanol fermentation. *Appl Microbiol Biotechnol*, **28**(4-5), pp.335-339.

Oudshoorn, A., van der Wielen, L. & Straathof, A. (2009). Adsorption equilibria of bio-based butanol solutions using zeolite. *Biochemical Engineering Journal*, **48**(1), pp.99-103.

Olson, D. H., Baerlocher, Ch., McCusker, L. B. (2007). *Atlas of Zeolite Framework Types.* Elsevier, Amsterdam, Nederland, 398 pp.

Park, K., Ni, Z., Cote, A., Choi, J., Huang, R., Uribe-Romo, F., Chae, H., O'Keeffe, M. & Yaghi, O. (2006). Exceptional chemical and thermal stability of zeolitic imidazolate frameworks. *Proceedings of the National Academy of Sciences*, **103**(27), pp.10186-10191.

Poling, B.E., Prausnitz, J.M. & O'Connell, J.P. (2001) *The properties of gases and liquids*. 5th edn. Boston: McGraw-Hill Professional.

Qureshi, N., Hughes, S., Maddox, I. & Cotta, M. (2005). Energy-efficient recovery of butanol from model solutions and fermentation broth by adsorption. *Bioprocess Biosyst Eng*, **27**(4), pp.215-222.

Qureshi, N. & Blaschek, H. (2000a). Economics of Butanol Fermentation using Hyper-Butanol Producing Clostridium Beijerinckii BA101. *Food and Bioproducts Processing*, **78**(3), pp.139-144.

Qureshi, N., Schripsema, J., Lienhardt, J. & Blaschek, H. (2000b). Contiuous solvent production by *Clostridium bejierinckii* BA101 immobilized by adsorption onto brick. *World Journal of Microbiology and Biotechnology*, **16**(4), pp.377-382.

Qureshi, N. & Blaschek, H. (2001a). ABE production from corn: a recent economic evaluation. *Journal of Industrial Microbiology and Biotechnology*, **27**(5), pp.292-297.

Qureshi, N., Lolas, A. & Blaschek, H. (2001b). Soy molasses as fermentation substrate for production of butanol using *Clostridium beijerinckii* BA101. *Journal of Industrial Microbiology and Biotechnology*, **26**(5), pp.290-295.

Qureshi, N., Saha, B., Hector, R., Hughes, S. & Cotta, M. (2008). Butanol production from wheat straw by simultaneous saccharification and fermentation using Clostridium beijerinckii: Part I—Batch fermentation. *Biomass and Bioenergy*, **32**(2), pp.168-175.

Palomino, M., Corma, A., Rey, F. & Valencia, S. (2010). New Insights on CO 2 −Methane Separation Using LTA Zeolites with Different Si/Al Ratios and a First Comparison with MOFs. *Langmuir*, **26**(3), pp.1910-1917.

Ranjan, A. & Moholkar, V. (2011). Biobutanol: science, engineering, and economics. *International Journal of Energy Research*, **36**(3), pp.277-323.

Roos, J., McLaughlin, J. & Papoutsakis, E. (1985). The effect of pH on nitrogen supply, cell lysis, and solvent production in fermentations of Clostridium acetobutylicum. *Biotechnol. Bioeng.*, **27**(5), pp.681-694.

Remy, T., Cousin Saint Remi, J., Singh, R., Webley, P., Baron, G. & Denayer, J. (2011). Adsorption and Separation of C1−C8 Alcohols on SAPO-34. *J. Phys. Chem. C*, **115**(16), pp.8117-8125.

Ruthven, D. (1984). *Principles of adsorption and adsorption processes*. John Wiley & Sons, New York, New York, USA. pp.453

Saravanan, V., Waijers, D., Ziari, M. & Noordermeer, M. (2009). Recovery of 1-butanol from aqueous solutions using zeolite ZSM-5 with a high Si/Al ratio; suitability of a column process for industrial applications. *Biochemical Engineering Journal*, **49**(1), pp.33-39.

Seidel-Morgenstern, A., Keßler, L. & Kaspereit, M. (2008). New Developments in Simulated Moving Bed Chromatography. *Chemical Engineering & Technology*, **31**(6), pp.826-837.

Silva, V., Pereira, C. and Rodrigues, A. (2010). PermSMBR-A new hybrid technology: Application on green solvent and biofuel production. *AIChE Journal*, **57**(7), pp.1840-1851.

Tan, H., Wu, Y. & Li, T. (2012). Pervaporation of n- butanol aqueous solution through ZSM-5-PEBA composite membranes. *Journal of Applied Polymer Science*, **129**(1), pp.105-112.

Tashiro, Y., Takeda, K., Kobayashi, G. and Sonomoto, K. (2005). High production of acetone–butanol–ethanol with high cell density culture by cell-recycling and bleeding. *Journal of Biotechnology*, **120**(2), pp.197-206.

Tashiro, Y., & K. Sonomoto. (2010). Advances in butanol production by clostridia. *Current Research, Technology and Education Topics in Applied Microbiology and Microbial Biotechnology*, pp.1383-1394.

Tashiro, Y., Yoshida, T., Noguchi, T. & Sonomoto, K. (2013). Recent advances and future prospects for increased butanol production by acetone-butanol-ethanol fermentation. *Eng. Life Sci.*, **13**(5), pp.432-445.

Thang, V., Kanda, K. & Kobayashi, G. (2010). Production of Acetone–Butanol–Ethanol (ABE) in Direct Fermentation of Cassava by Clostridium saccharoperbutylacetonicum N1-4. *Appl Biochem Biotechnol*, **161**(1-8), pp.157-170.

Tracy, B., Jones, S., Fast, A., Indurthi, D. & Papoutsakis, E. (2012). Clostridia: the importance of their exceptional substrate and metabolite diversity for biofuel and biorefinery applications. *Current Opinion in Biotechnology*, **23**(3), pp.364-381.

Tsoularis, A. & Wallace, J. (2002). Analysis of logistic growth models. *Mathematical Biosciences*, **179**(1), pp.21-55.

Trzpit, M., Rigolet, S., Paillaud, J., Marichal, C., Soulard, M. & Patarin, J. (2008). Pure Silica Chabazite Molecular Spring: A Structural Study on Water Intrusion−Extrusion Processes. *The Journal of Physical Chemistry B*, **112**(24), pp.7257-7266.

United Nations (2016). *United Nations sustainable development agenda*. http://www.un.org/sustainabledevelopment/development-agenda. Accessed on May 3, 2016.

Vane, L. (2008). Separation technologies for the recovery and dehydration of alcohols from fermentation broths. *Biofuels, Bioprod. Bioref.*, **2**(6), pp.553-588.

Van der Perre, S., Van Assche, T., Bozbiyik, B., Lannoeye, J., De Vos, D., Baron, G. & Denayer, J. (2014). Adsorptive Characterization of the ZIF-68 Metal-Organic Framework: A Complex Structure with Amphiphilic Properties. *Langmuir*, **30**(28), pp.8416-8424.

Van der Perre, S., Bozbiyik, B., Lannoeye, J., De Vos, D., Baron, G. & Denayer, J. (2015). Experimental Study of Adsorptive Interactions of Polar and Nonpolar Adsorbates in the Zeolitic Imidazolate Framework ZIF-68 via Pulse Gas Chromatography. *J. Phys. Chem. C*, **119**(4), pp.1832-1839.

Wu, J., Liu, Q., Xiong, Y., Zhu, A. & Chen, Y. (2009). Molecular Simulation of Water/Alcohol Mixtures' Adsorption and Diffusion in Zeolite 4A Membranes. *The Journal of Physical Chemistry B*, **113**(13), pp.4267-4274.

Wu, J., Zhuang, W., Ying, H., Jiao, P., Li, R., Wen, Q., Wang, L., Zhou, J. & Yang, P. (2015). Acetone-butanol-ethanol competitive sorption simulation from single, binary, and ternary systems in a fixed-bed of KA-I resin. *Biotechnol Progress*, **31**(1), pp.124-134.

Xue, C., Zhao, J., Chen, L., Bai, F., Yang, S. and Sun, J. (2014). Integrated butanol recovery for an advanced biofuel: current state and prospects. *Appl Microbiol Biotechnol*, **98**(8), pp.3463-3474.

Yang, X., Tsai, G. & Tsao, G. (1994). Enhancement of in situ adsorption on the acetone-butanol fermentation by Clostridium acetobutylicum. *Separations Technology*, **4**(2), pp.81-92.

Zhang, K., Lively, R., Zhang, C., Chance, R., Koros, W., Sholl, D. and Nair, S. (2013a). Exploring the Framework Hydrophobicity and Flexibility of ZIF-8: From Biofuel Recovery to Hydrocarbon Separations. *J. Phys. Chem. Lett.*, **4**(21), pp.3618-3622.

Zhang, K., Lively, R., Dose, M., Brown, A., Zhang, C., Chung, J., Nair, S., Koros, W. and Chance, R. (2013b). Alcohol and water adsorption in zeolitic imidazolate frameworks. *Chemical Communications*, **49**(31), pp.3245-3247.

Zhang, K., Zhang, L. and Jiang, J. (2013c). Adsorption of C 1 –C 4 Alcohols in Zeolitic Imidazolate Framework-8: Effects of Force Fields, Atomic Charges, and Framework Flexibility. *J. Phys. Chem. C*, **117**(48), pp.25628-25635.

Appendix

Appendix 1 – Calibration curves of mass flow controllers (MFC)

Helium

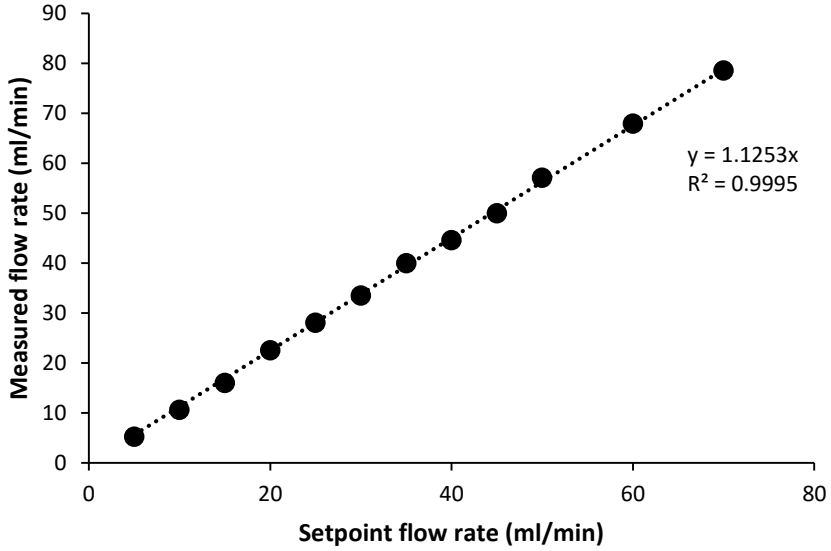

Figure A1.1: Calibration curve of MFC 1 using He

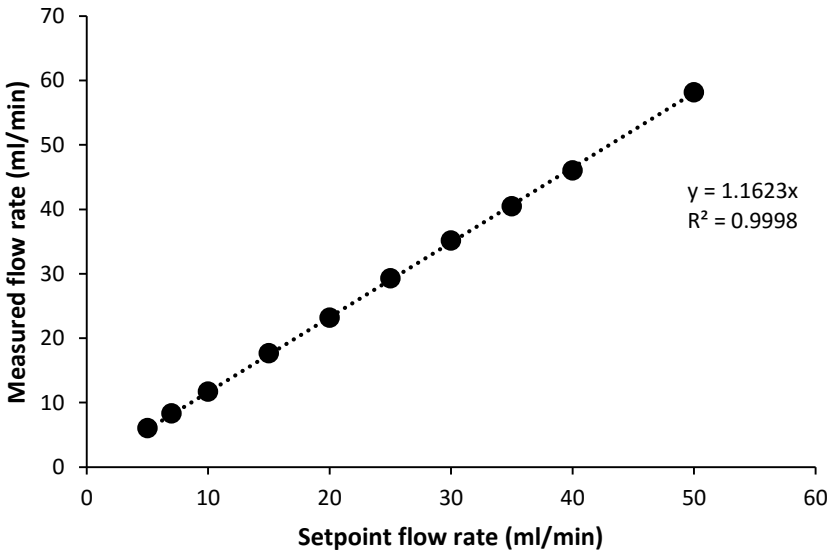

Figure A1.2: Calibration curve of MFC 2 using He

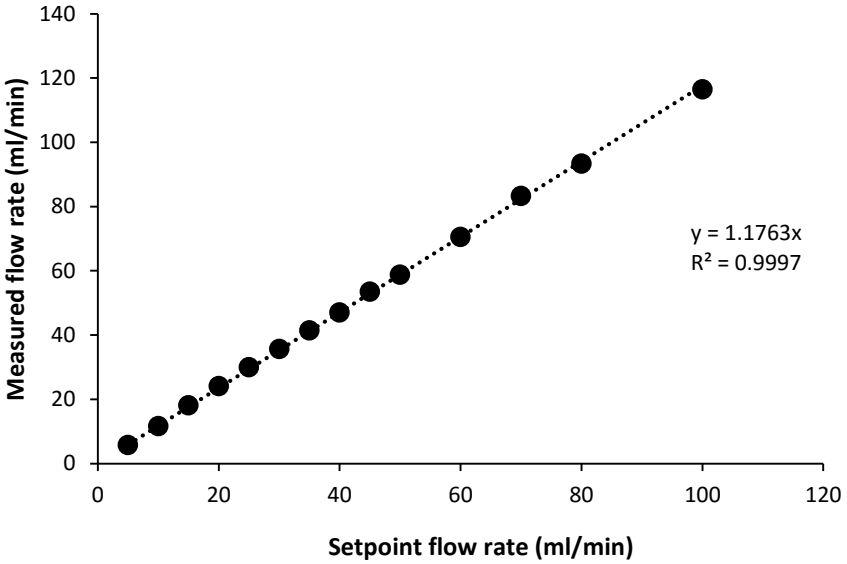

Figure A1.3: Calibration curve of MFC 3 using He

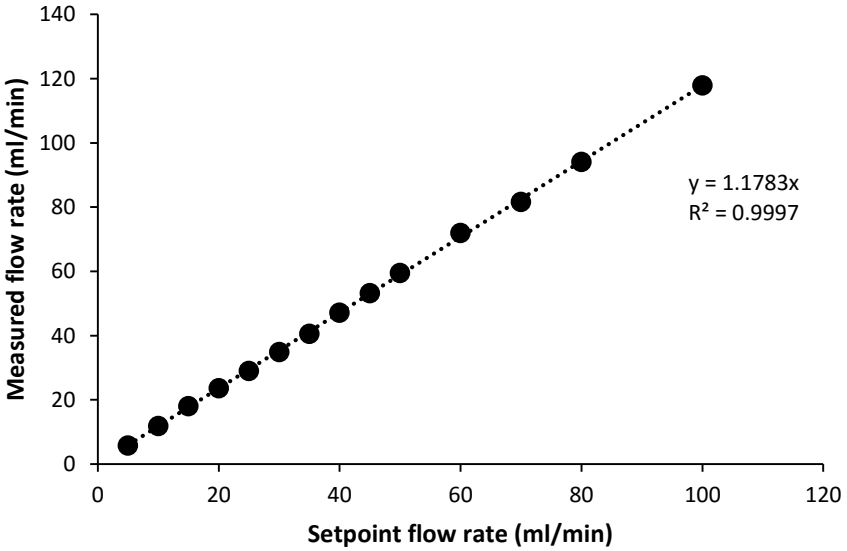

Figure A1.4: Calibration curve of MFC 4 using He

CO_2

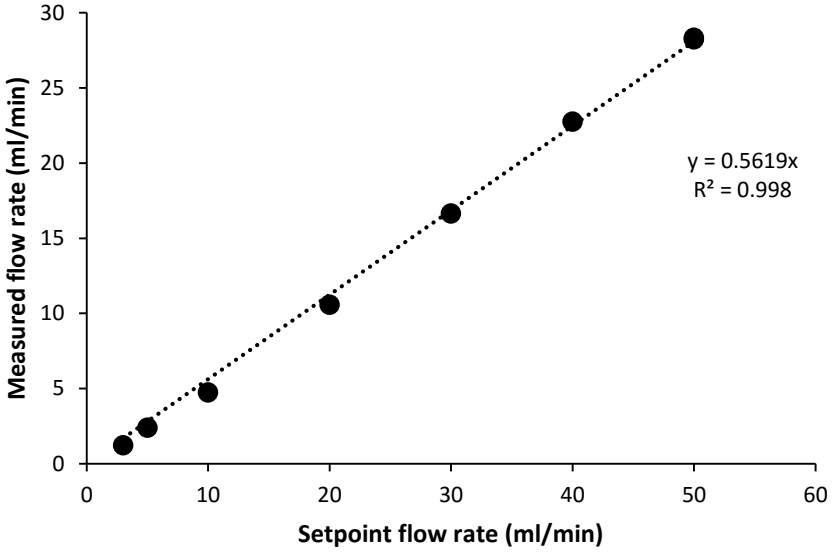

Figure A1.5: Calibration curve of MFC 1 using CO_2

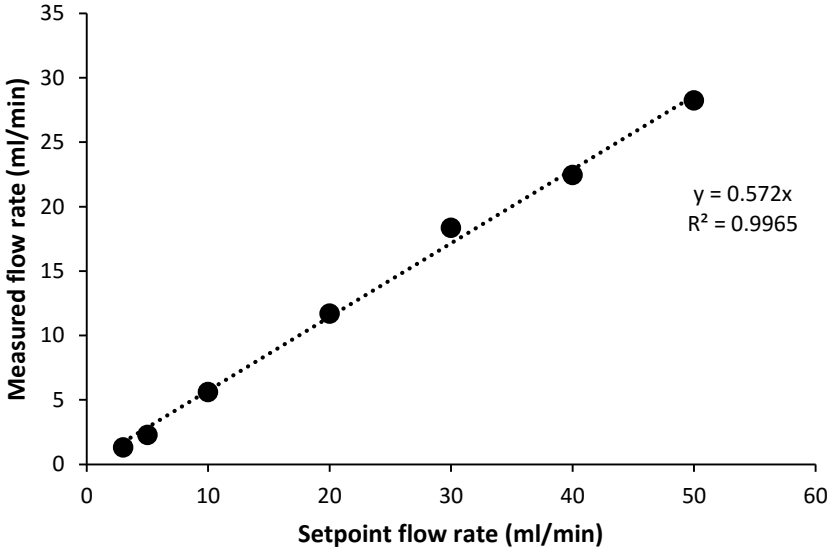

Figure A1.6: Calibration of MFC 3 using CO_2

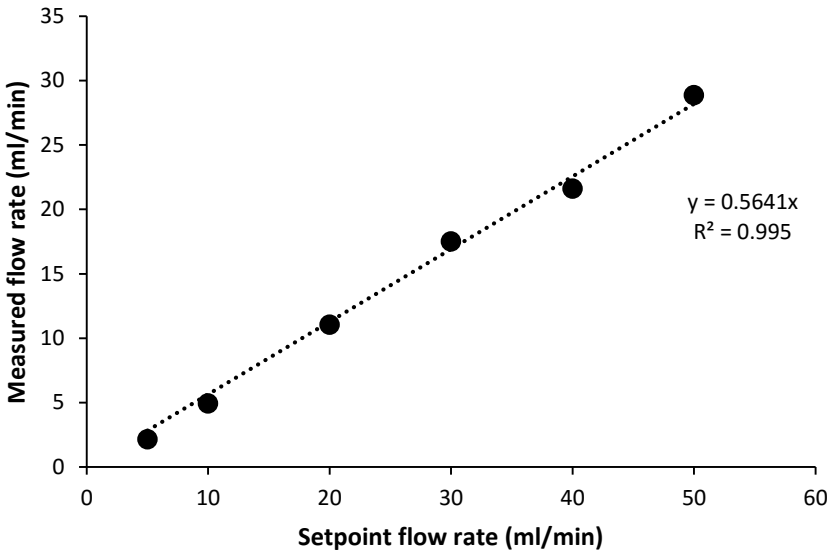

Figure A1.7: Calibration curve of MFC 4 using CO_2

Appendix 2 – Matlab® code for breakthrough modelling on Si-CHA

```
function ABE_doorbraak

close all
clear all

global R Nx N_comp ...
 L_column D_column Temp mbed eps ...
 dx x ...
 qsat_acet K_acet qsat_but K_but qsat_eth K_eth qsat_wat K_wat  ...
 h_acet h_but h_eth h_wat Dm_acet Dm_eth Dm_but Dm_wat ...
 v Flow ...
 P_in_wat P_in_acet P_in_but P_in_eth ...
 CHA_density ...
 P_tot


R = 8.314; %J/K mol
Nx = 30.0;
N_comp = 4.0;

%---------------------Systeem parameters Si CHA---------------------%

L_column = 3.65E-02; %m berekende lengte aan de hand van bulkdensiteit zie
excel
D_column = 0.2159E-02; %m
R_column = D_column/2.0; %m
Temp = 273+40; %K

mbed = 0.049E-03; % kg
CHA_density = 1.45E03; %kg/m3
volume_column = 3.14 * R_column^2.0 * L_column;
bulk_density = mbed / volume_column;

eps = 0.6;

dx = L_column/Nx;               %stap dx in ruimte
x = 0:dx:L_column;


%---------------------Adsorptie parameters --------------------%
%Single component langmuir fitting: zie fitting alle isothermen

qsat_acet = 0.2638; %mol/kg
% K_acet = 5.9607; % Pa^-1
K_acet = 5.9607E-02; % Pa^-1 % aangepast voor goede doorbraak aceton

qsat_but = 3.791; %mol/kg
K_but = 0.000237; % Pa^-1

qsat_eth = 3.4885; %mol/kg
K_eth = 0.0006; % Pa^-1

qsat_wat = 31.67; %mol/kg
K_wat = 2.4E-05; % Pa^-1



%---------------------Massaoverdracht-------------------------%
```

```
h_acet = 0.005E-04;
Dm_acet = 1.090E-05; %m2/s

h_but = 0.0005E-03;
Dm_but = 8.40E-05; %m2/s

h_eth = 0.004; %1/s
Dm_eth = 2.51E-05; %m2/s

h_wat = 1.5;
Dm_wat = 4.350E-05;


%---------------------- Doorbraak adsorptie -------------------------%
%--------------------------------------------------------------------%
%--------------------------------------------------------------------%

% Flow = 15.9 * 10^(-6) / 60; % m3/s
Flow = 15.9 * 10^(-6) / 60; % m3/s

P_tot = 1.930E05; %Pa


P_in_acet = 0.00192051E05; %Pa
P_in_but = 0.00298675E05; %Pa
P_in_eth = 0.00049862E05; %Pa
P_in_wat = 0.021863915 * P_tot; %Pa

x_in_acet = P_in_acet/P_tot
x_in_but = P_in_but/P_tot

% P_in_acet = 0.0;
% P_in_but = 0.0;
% P_in_eth = 0.02E05;
% P_in_wat = 0.0; %Pa


v = Flow/(3.14 * (R_column)^2.0) % lege buissnelheid m/s


%----------------------Beginvoorwaarden ----------------------------%

Conc_0 = zeros(2*N_comp*(Nx+1),1); %vector bvw conc en ads onder elkaar


%----------------------Oplossen tijdsdifferentiaalvgl --------------%

t_start_doorbraak = 0.0;
t_end_doorbraak = 6000.0;
% t_end_doorbraak = 30000.0;
t_stap = 10.0;
tspan = [t_start_doorbraak : t_stap : t_end_doorbraak];

tic
[T,Y] = ode15s (@rigid, tspan, Conc_0);
toc

%-----------------Resultaten-----------------------------------------%

for i = 1:Nx+1
    P_acet(:,i) = Y(:,i);
```

```
    q_acet(:,i) = Y(:,Nx + 1 +i);
    P_but(:,i)  = Y(:,2*Nx+2+i);
    q_but(:,i) = Y(:,3*Nx+3+i);
    P_eth(:,i) = Y(:,4*Nx+4+i);
    q_eth(:,i) = Y(:,5*Nx+5+i);
    P_wat(:,i) = Y(:,6*Nx+6+i);
    q_wat(:,i) = Y(:,7*Nx+7+i);
end

N_dT = length(T);

x_acet = P_acet/P_tot;
x_but = P_but/P_tot;
x_eth = P_eth/P_tot;
x_wat = P_wat/P_tot;


T(N_dT)/N_dT;


doorbraaktijd_acet = 0.0;
doorbraaktijd_but = 0.0;
doorbraaktijd_eth = 0.0;
doorbraaktijd_wat = 0.0;

x0_acet = P_in_acet/P_tot;
x0_but = P_in_but/P_tot;
x0_eth = P_in_eth / P_tot;
x0_wat = P_in_wat/P_tot;


for i = 1:N_dT
    doorbraaktijd_acet = doorbraaktijd_acet + (x0_acet -
x_acet(i,Nx+1))/x0_acet  * t_stap;
    doorbraaktijd_but = doorbraaktijd_but + (x0_but - x_but(i,Nx+1))/x0_but
* t_stap;
    doorbraaktijd_eth = doorbraaktijd_eth + (x0_eth - x_eth(i,Nx+1))/x0_eth
* t_stap;
    doorbraaktijd_wat = doorbraaktijd_wat + (x0_wat - x_wat(i,Nx+1))/x0_wat
* t_stap;
end

doorbraaktijd_acet = doorbraaktijd_acet / 60.0
doorbraaktijd_but = doorbraaktijd_but / 60.0
doorbraaktijd_eth = doorbraaktijd_eth / 60.0
doorbraaktijd_wat = doorbraaktijd_wat / 60.0

%-------------------------Figuren---------------------------------%

Tijd = T/60.0;

xlswrite('Si_CHA_adsorptie.xlsx',Tijd,1)
xlswrite('Si_CHA_adsorptie.xlsx',x_acet(:,Nx+1),2)
xlswrite('Si_CHA_adsorptie.xlsx',x_but(:,Nx+1),3)
xlswrite('Si_CHA_adsorptie.xlsx',x_eth(:,Nx+1),4)
xlswrite('Si_CHA_adsorptie.xlsx',x_wat(:,Nx+1),5)


% %%%%%%%%%%%%%%%%%%%%%%%%% Desorptie %%%%%%%%%%%%%%%%%%%%%%%%%%%%%%%%
%%%%%%%%%%%%%%%%%%%%%%%%%%%%%%%%%%%%%%%%%%%%%%%%%%%%%%%%%%%%%%%%%%%%%
```

```
Flow = 11.4 * 10^(-6) / 60; % m3/s

P_in_acet = 0.0; %Pa
P_in_but = 0.0; %Pa
P_in_eth = 0.0; %Pa
P_in_wat = 0.0; %Pa


P_tot = 2.760E05; %Pa

v = Flow/(3.14 * (R_column)^2.0) % lege buissnelheid m/s

%--------------------------Beginvoorwaarden desorptie -------------%
% Kolom is gevuld
for i=1:Nx+1
    Conc_0(i) = P_acet(N_dT,i);
    Conc_0(Nx+1+i) = q_acet(N_dT, i);
    Conc_0(2*Nx+2+i) = P_but(N_dT,i);
    Conc_0(3*Nx+3+i) = q_but(N_dT,i);
    Conc_0(4*Nx+4+i) = P_eth(N_dT,i);
    Conc_0(5*Nx+5+i) = q_eth(N_dT,i);
    Conc_0(6*Nx+6+i) = P_wat(N_dT,i);
    Conc_0(7*Nx+7+i) = q_wat(N_dT,i);
end

%---------------------Oplossen tijdsdiff vgl ----------------------%

t_start_doorbraak = 0.0;
t_end_doorbraak = 60000;
t_stap = 100.0;
tspan = [t_start_doorbraak : t_stap : t_end_doorbraak];

tic
[T,Y] = ode15s (@rigid, tspan, Conc_0);
toc

%----------------------Resultaten ---------------------------------%

[m,n] = size(Y)
lengte = length(T)
for i=1:Nx+1
    P_acet_des(:,i) = Y(:,i);
    q_acet_des(:,i) = Y(:,Nx+1+i);
    P_but_des(:,i) = Y(:,2*Nx+2+i);
    q_but_des(:,i) = Y(:,3*Nx+3+i);
    P_eth_des(:,i) = Y(:,4*Nx+4+i);
    q_eth_des(:,i) = Y(:,5*Nx+5+i);
    P_wat_des(:,i) = Y(:,6*Nx+6+i);
    q_wat_des(:,i) = Y(:,7*Nx+7+i);
end

%-----------------Figuren-----------------------------------------%

Tijd = T/60.0;

x_acet_des = P_acet_des/P_tot;
x_but_des = P_but_des/P_tot;
x_eth_des = P_eth_des/P_tot;
x_wat_des = P_wat_des/P_tot;
```

```
figure
hold on
title('Doorbraak')
plot(Tijd,P_acet_des(:,Nx+1))
plot(Tijd,P_but_des(:,Nx+1))
plot(Tijd,P_eth_des(:,Nx+1))
yyaxis right
plot(Tijd,P_wat_des(:,Nx+1))
legend('aceton', 'butanol', 'ethanol', 'water')
% legend('aceton', 'butanol', 'ethanol')
xlabel ('tijd (min)')
ylabel ('druk (Pa)')

%--------------------------differential equations-------------------%
function dy = rigid(t,y)

global R Nx N_comp ...
 L_column D_column Temp mbed eps ...
 dx x ...
 qsat_acet K_acet qsat_but K_but qsat_eth K_eth qsat_wat K_wat  ...
 h_acet h_but h_eth h_wat Dm_acet Dm_eth Dm_but Dm_wat ...
 v Flow ...
 P_in_wat P_in_acet P_in_but P_in_eth ...
 CHA_density ...
 P_tot

dy = zeros(2*N_comp*Nx+2*N_comp,1);


for i = 1:Nx+1
    P_acet(i) = y(i);
    q_acet(i) = y(Nx+1+i);
    P_but(i) = y(2*Nx+2+i);
    q_but(i) = y(3*Nx+3+i);
    P_eth(i) = y(4*Nx+4+i);
    q_eth(i) = y(5*Nx+5+i);
    P_wat(i) = y(6*Nx+6+i);
    q_wat(i) = y(7*Nx+7+i);
end

for i = 1:Nx+1
    noemer(i) = (K_but * P_but(i) + K_eth * P_eth(i) + K_wat  * P_wat(i) +
1);

    q_eq_acet(i) = K_acet * qsat_acet * P_acet(i) / noemer(i);
    q_eq_but(i) = K_but * qsat_but * P_but(i) / noemer(i);
    q_eq_eth(i) = K_eth * qsat_eth * P_eth(i) / noemer(i);
    q_eq_wat(i) = K_wat * qsat_wat * P_wat(i) / noemer(i);

    Rq_acet(i) = h_acet * (q_eq_acet(i) - q_acet(i));
    Rq_but(i) = h_but * (q_eq_but(i) - q_but(i));
    Rq_eth(i) = h_eth * (q_eq_eth(i) - q_eth(i));
    Rq_wat(i) = h_wat * (q_eq_wat(i) - q_wat(i));

    R_acet(i) = (1-eps)/eps * (R*Temp) * CHA_density * Rq_acet(i);
    R_but(i) = (1-eps)/eps * (R*Temp) * CHA_density * Rq_but(i);
    R_eth(i) = (1-eps)/eps * (R*Temp) * CHA_density * Rq_eth(i);
    R_wat(i) = (1-eps)/eps * (R*Temp) * CHA_density * Rq_wat(i);

end
```

```
%----------------------implementatie discretisatie ----------------%

% % % % % % Aceton

for i=1:Nx
    if i==1
        u_i_1=P_acet(1)-dx*v/Dm_acet*(P_acet(1)-P_in_acet);  % LBC
        %u_i_1 = C_inlet neumann randvoorwaarde: massabalans op het eerste
punt;
        dy(1) = Dm_acet/(dx*dx)*(P_acet(i+1)-2*P_acet(i)+u_i_1)-
v/eps/dx*(P_acet(i)-u_i_1) - R_acet(i);
    else
        dy(i) = Dm_acet/(dx*dx)*(P_acet(i+1)-2*P_acet(i)+P_acet(i-1))-
v/eps/dx*(P_acet(i)-P_acet(i-1))-R_acet(i);
    end
end
                                        % RBC  ---> U(x+2) = U(x+1)
dy(Nx+1) = Dm_acet/(dx*dx)*(P_acet(Nx+1)-2*P_acet(Nx+1)+P_acet(Nx))-
v/eps/dx*(P_acet(Nx+1)-P_acet(Nx))-R_acet(Nx+1);

% ---- mass balance amount adsorbed ---- %
for i=1:Nx+1
    dy((Nx+1)+i) = Rq_acet(i);
end

% % % % % % % Butanol

for i=1:Nx
    if i==1
        u_i_1=P_but(1)-dx*v/Dm_but*(P_but(1)-P_in_but);  % LBC
        %u_i_1 = C_inlet neumann randvoorwaarde: massabalans op het eerste
punt;
        dy(1 + 2* Nx + 2) = Dm_but/(dx*dx)*(P_but(i+1)-2*P_but(i)+u_i_1)-
v/eps/dx*(P_but(i)-u_i_1) - R_but(i);
    else
        dy(i + 2* Nx + 2) = Dm_but/(dx*dx)*(P_but(i+1)-2*P_but(i)+P_but(i-
1))-v/eps/dx*(P_but(i)-P_but(i-1))-R_but(i);
    end
end
                                        % RBC  ---> U(x+2) = U(x+1)
dy(3*Nx+3) = Dm_but/(dx*dx)*(P_but(Nx+1)-2*P_but(Nx+1)+P_but(Nx))-
v/eps/dx*(P_but(Nx+1)-P_but(Nx))-R_but(Nx+1);

% ---- mass balance amount adsorbed ---- %
for i=1:Nx+1
    dy((3*Nx+3)+i) = Rq_but(i);
end

% % % % % % % Ethanol

for i=1:Nx
    if i==1
        u_i_1=P_eth(1)-dx*v/Dm_eth*(P_eth(1)-P_in_eth);  % LBC
        %u_i_1 = C_inlet neumann randvoorwaarde: massabalans op het eerste
punt;
        dy(4*Nx + 4 + 1) = Dm_eth/(dx*dx)*(P_eth(i+1)-2*P_eth(i)+u_i_1)-
v/eps/dx*(P_eth(i)-u_i_1) - R_eth(i);
    else
        dy(4*Nx + 4 + i) = Dm_eth/(dx*dx)*(P_eth(i+1)-2*P_eth(i)+P_eth(i-
1))-v/eps/dx*(P_eth(i)-P_eth(i-1))-R_eth(i);
    end
```

```
end
                                        % RBC  ---> U(x+2) = U(x+1)
dy(5*Nx+5) = Dm_eth/(dx*dx)*(P_eth(Nx+1)-2*P_eth(Nx+1)+P_eth(Nx))-
v/eps/dx*(P_eth(Nx+1)-P_eth(Nx))-R_eth(Nx+1);

% ---- mass balance amount adsorbed ---- %
for i=1:Nx+1
    dy((5*Nx+5)+i) = Rq_eth(i);
end


% % % % % % % % % % Water

for i=1:Nx
    if i==1
        u_i_1=P_wat(1)-dx*v/Dm_wat*(P_wat(1)-P_in_wat);  % LBC
        %u_i_1 = C_inlet neumann randvoorwaarde: massabalans op het eerste
punt;
        dy(6*Nx + 6 + 1) = Dm_wat/(dx*dx)*(P_wat(i+1)-2*P_wat(i)+u_i_1)-
v/eps/dx*(P_wat(i)-u_i_1) - R_wat(i);
    else
        dy(6*Nx + 6 + i) = Dm_wat/(dx*dx)*(P_wat(i+1)-2*P_wat(i)+P_wat(i-
1))-v/eps/dx*(P_wat(i)-P_wat(i-1))-R_wat(i);
    end
end
                                        % RBC  ---> U(x+2) = U(x+1)
dy(7*Nx+7) = Dm_wat/(dx*dx)*(P_wat(Nx+1)-2*P_wat(Nx+1)+P_wat(Nx))-
v/eps/dx*(P_wat(Nx+1)-P_wat(Nx))-R_wat(Nx+1);

% ---- mass balance amount adsorbed ---- %
for i=1:Nx+1
    dy((7*Nx+7)+i) = Rq_wat(i);
end
```

Appendix 3 – Matlab® code for multicolumn adsorption

```
function ABE_doorbraak

close all
clear all

global R Nx N_comp ...
 L_column D_column Temp mbed eps ...
 dx x ...
 qsat_acet K_acet qsat_but K_but qsat_eth K_eth qsat_wat K_wat  ...
 h_acet h_but h_eth h_wat Dm_acet Dm_eth Dm_but Dm_wat ...
 v Flow ...
 P_in_wat P_in_acet P_in_but P_in_eth ...
 crystal_density ...
 P_tot ...
 dynamic tijd_eerste_kolom index ...
 P_acet_eerste_kolom P_but_eerste_kolom P_eth_eerste_kolom
P_wat_eerste_kolom


R = 8.314; %J/K mol
Nx = 30.0;
N_comp = 4.0;
dynamic = 0;
index = 1;

%----------------------Systeem parameters SAPO-34----------------------%

% L_column = 10E-02; %m
L_column = 36E-02; %m
D_column = 0.2159E-02; %m
R_column = D_column/2.0; %m
Temp = 273+40; %K

mbed = 0.23E-03; % kg
crystal_density = 1.506E03; %kg/m3
volume_column = 3.14 * R_column^2.0 * L_column;
bulk_density = mbed / volume_column;

eps = 0.67;

dx = L_column/Nx;               %stap dx in ruimte
x = 0:dx:L_column;



%----------------------Adsorptie parameters -------------------%
%Single component langmuir fitting: zie fitting alle isothermen

qsat_acet = 0.6832; %mol/kg %Acetone proxy = Si CHA data
% K_acet = 5.9607E-02; % Pa^-1
K_acet = 5.9607E-04;

qsat_but = 0.0001; %mol/kg %BuOH adsorbeert niet
K_but = 0.00001; % Pa^-1

qsat_eth = 4.1; %mol/kg
K_eth = 7.48E-03; %Pa^-1
```

```
qsat_wat = 13.4; %mol/kg
K_wat = 1.95E-03; % Pa^-1


%---------------------Massaoverdracht-------------------------%

h_acet = 0.0009; %1/s %expres laag
Dm_acet = 1.090E-05; %m2/s

h_but = 0.000005; %1/s %expres laag
Dm_but = 8.40E-05; %m2/s

% h_eth = 0.1; %1/s
h_eth = 0.0002;
Dm_eth = 1.10E-05; %m2/s

h_wat =  0.005; %1/s
Dm_wat = 2.40E-05; %m2/s

%---------------------- Doorbraak adsorptie ------------------------------%
%-------------------------------------------------------------------------
%-------------------------------------------------------------------------

% Flow = 15.9 * 10^(-6) / 60; % m3/s
Flow = 15.53 * 10^(-6) / 60; % m3/s

P_tot = 2.760E05; %Pa


P_in_acet = 0.001939207E05; %Pa
P_in_but = 0.00301362E05; %Pa
P_in_eth = 0.00050214E05; %Pa
P_in_wat = 0.04209472E05; %Pa

v = Flow/(3.14 * (R_column)^2.0); % lege buissnelheid m/s;


%----------------------Beginvoorwaarden --------------------------------%

Conc_0 = zeros(2*N_comp*(Nx+1),1); %vector bvw conc en ads onder elkaar


%---------------------Oplossen tijdsdifferentiaalvgl ----------------%

t_start_doorbraak = 0.0;
% t_end_doorbraak = 6000.0;
t_end_doorbraak = 30000.0;
t_stap = 1.0;
tspan = [t_start_doorbraak : t_stap : t_end_doorbraak];

tic
[T,Y] = ode15s (@rigid, tspan, Conc_0);
toc

%-----------------Resultaten-----------------------------------------%

for i = 1:Nx+1
    P_acet_eerste_kolom(:,i) = Y(:,i);
    q_acet_eerste_kolom(:,i) = Y(:,Nx + 1 +i);
    P_but_eerste_kolom(:,i)  = Y(:,2*Nx+2+i);
    q_but_eerste_kolom(:,i) = Y(:,3*Nx+3+i);
```

```
    P_eth_eerste_kolom(:,i) = Y(:,4*Nx+4+i);
    q_eth_eerste_kolom(:,i) = Y(:,5*Nx+5+i);
    P_wat_eerste_kolom(:,i) = Y(:,6*Nx+6+i);
    q_wat_eerste_kolom(:,i) = Y(:,7*Nx+7+i);
end

tijd_eerste_kolom = T;

x_acet = P_acet_eerste_kolom/P_tot;
x_but = P_but_eerste_kolom/P_tot;
x_eth = P_eth_eerste_kolom/P_tot;
x_wat = P_wat_eerste_kolom/P_tot;

ads_acetone = 0.0;
ads_butanol = 0.0;
ads_ethanol = 0.0;
ads_water = 0.0;

% berekening geadsorbeerde hoeveelheden in mol!
% 15601 = tijdstip 200 min
for i = 1:Nx
    acet_gem = (q_acet_eerste_kolom(15601,i) +
q_acet_eerste_kolom(15601,i+1))/2;
    but_gem = (q_but_eerste_kolom(15601,i) +
q_but_eerste_kolom(15601,i+1))/2;
    eth_gem = (q_eth_eerste_kolom(15601,i) +
q_eth_eerste_kolom(15601,i+1))/2;
    wat_gem = (q_wat_eerste_kolom(15601,i) +
q_wat_eerste_kolom(15601,i+1))/2;
    ads_acetone = ads_acetone + crystal_density * 3.14 * R_column^2 * dx *
(1-eps) * acet_gem;
    ads_butanol = ads_butanol + crystal_density * 3.14 * R_column^2 * dx *
(1-eps) * but_gem;
    ads_ethanol = ads_ethanol + crystal_density * 3.14 * R_column^2 * dx *
(1-eps) * eth_gem;
    ads_water = ads_water + crystal_density * 3.14 * R_column^2 * dx * (1-
eps) * wat_gem;
end

%omzetting naar gewicht g met MW in g/mol
ads_acetone = ads_acetone * 58.08;
ads_butanol = ads_butanol * 74.12;
ads_ethanol = ads_ethanol * 46.07;
ads_water = ads_water * 18;

% naar workspace exporteren
assignin('base','ads_acetone_SAPO',ads_acetone);
assignin('base','ads_butanol_SAPO',ads_butanol);
assignin('base','ads_ethanol_SAPO',ads_ethanol);
assignin('base','ads_water_SAPO',ads_water);

% zuiverheid butanol
purity_ethanol = ads_ethanol / (ads_acetone + ads_butanol + ads_ethanol +
ads_water);

assignin('base','purity_ethanol',purity_ethanol)
xlswrite('SAPO_voor_Si_LTA.xlsx',purity_ethanol,'Summary','U18')

%--------------------------Figuren---------------------------------%

Tijd = T/60.0;
```

```
% xlswrite('SAPO_voor_Si_LTA.xlsx',Tijd,1)
% xlswrite('SAPO_voor_Si_LTA.xlsx',P_acet_eerste_kolom(:,Nx+1),2)
% xlswrite('SAPO_voor_Si_LTA.xlsx',P_but_eerste_kolom(:,Nx+1),3)
% xlswrite('SAPO_voor_Si_LTA.xlsx',P_eth_eerste_kolom(:,Nx+1),4)
% xlswrite('SAPO_voor_Si_LTA.xlsx',P_wat_eerste_kolom(:,Nx+1),5)


%---------------------- Doorbraak op Si LTA  ----------------------------%
%------------------------------------------------------------------------%
%------------------------------------------------------------------------%

%----------------------- Systeem parameters Si LTA ----------------------%
L_column = 10E-02; %m
D_column = 0.2159E-02; %m
R_column = D_column/2.0; %m
Temp = 273+40; %K

mbed = 0.108E-03; % kg
crystal_density = 1.29E03; %kg/m3
volume_column = 3.14 * R_column^2.0 * L_column;
bulk_density = mbed / volume_column;

eps = 0.45;

dx = L_column/Nx;               %stap dx in ruimte
x = 0:dx:L_column;

%---------------------Adsorptie parameters -------------------%
%Single component langmuir fitting: zie fitting alle isothermen

qsat_acet = 1.2474; %mol/kg
K_acet = 0.0003; % Pa^-1

qsat_but = 2.0498; %mol/kg
K_but = 0.0529; % Pa^-1

qsat_eth = 0.8591; %mol/kg %fitting uit alle isothermen met punten tot 500
Pa en dan aanpassen K tot doorbraak goed
K_eth = 0.04; % Pa^-1

qsat_wat = 0.9841; %mol/kg
K_wat = 0.0005395; % Pa^-1


%---------------------Massaoverdracht-------------------------%

% h_acet = 0.01; %1/s
h_acet = 0.005;
Dm_acet = 1.090E-05; %m2/s

h_but = 0.003; %1/s
Dm_but = 8.40E-05; %m2/s

h_eth = 0.5; %1/s
Dm_eth = 1.10E-05; %m2/s

h_wat =  0.18; %1/s
Dm_wat = 2.40E-05; %m2/s

%----------------------------BVW--------------------------%
```

```
Conc_0 = zeros(2*N_comp*(Nx+1),1); %vector bvw conc en ads onder elkaar

%---------------------Oplossen tijdsdifferentiaalvgl ----------------%

t_start_doorbraak = 0.0;
t_eind_doorbraak = 30000.0;
t_stap = 1.0;
dynamic = 1;
tspan = [t_start_doorbraak : t_stap : t_eind_doorbraak];

tic
[T,Y] = ode15s (@rigid, tspan, Conc_0);
toc

%-----------------Resultaten-----------------------------------------%

for i = 1:Nx+1
    P_acet_tweede_kolom(:,i) = Y(:,i);
    q_acet_tweede_kolom(:,i) = Y(:,Nx + 1 +i);
    P_but_tweede_kolom(:,i)  = Y(:,2*Nx+2+i);
    q_but_tweede_kolom(:,i) = Y(:,3*Nx+3+i);
    P_eth_tweede_kolom(:,i) = Y(:,4*Nx+4+i);
    q_eth_tweede_kolom(:,i) = Y(:,5*Nx+5+i);
    P_wat_tweede_kolom(:,i) = Y(:,6*Nx+6+i);
    q_wat_tweede_kolom(:,i) = Y(:,7*Nx+7+i);
end

N_dT = length(T);

x_acet = P_acet_tweede_kolom/P_tot;
x_but = P_but_tweede_kolom/P_tot;
x_eth = P_eth_tweede_kolom/P_tot;
x_wat = P_wat_tweede_kolom/P_tot;


T(N_dT)/N_dT;

x0_acet = P_in_acet/P_tot;
x0_but = P_in_but/P_tot;
x0_eth = P_in_eth / P_tot;
x0_wat = P_in_wat/P_tot;

ads_acetone = 0.0;
ads_butanol = 0.0;
ads_ethanol = 0.0;
ads_water = 0.0;

% berekening geadsorbeerde hoeveelheden in mol!
% 15601 = tijdstip 200 min
for i = 1:Nx
    acet_gem = (q_acet_tweede_kolom(15601,i) +
q_acet_tweede_kolom(15601,i+1))/2;
    but_gem = (q_but_tweede_kolom(15601,i) +
q_but_tweede_kolom(15601,i+1))/2;
    eth_gem = (q_eth_tweede_kolom(15601,i) +
q_eth_tweede_kolom(15601,i+1))/2;
    wat_gem = (q_wat_tweede_kolom(15601,i) +
q_wat_tweede_kolom(15601,i+1))/2;
    ads_acetone = ads_acetone + crystal_density * 3.14 * R_column^2 * dx *
(1-eps) * acet_gem;
```

```
    ads_butanol = ads_butanol + crystal_density * 3.14 * R_column^2 * dx *
(1-eps) * but_gem;
    ads_ethanol = ads_ethanol + crystal_density * 3.14 * R_column^2 * dx *
(1-eps) * eth_gem;
    ads_water = ads_water + crystal_density * 3.14 * R_column^2 * dx * (1-
eps) * wat_gem;
end

%omzetting naar gewicht g met MW in g/mol
ads_acetone = ads_acetone * 58.08;
ads_butanol = ads_butanol * 74.12;
ads_ethanol = ads_ethanol * 46.07;
ads_water = ads_water * 18;

% naar workspace exporteren
assignin('base','ads_acetone_LTA',ads_acetone);
assignin('base','ads_butanol_LTA',ads_butanol);
assignin('base','ads_ethanol_LTA',ads_ethanol);
assignin('base','ads_water_LTA',ads_water);

% zuiverheid butanol
purity_butanol = ads_butanol / (ads_acetone + ads_butanol + ads_ethanol +
ads_water);

assignin('base','purity_butanol',purity_butanol)
xlswrite('SAPO_voor_Si_LTA.xlsx',purity_butanol,'Summary','U15')




% --------------------------Figuren---------------------------------

Tijd = T/60.0;

xlswrite('SAPO_voor_Si_LTA.xlsx',Tijd,6)
xlswrite('SAPO_voor_Si_LTA.xlsx',P_acet_tweede_kolom(:,Nx+1),7)
xlswrite('SAPO_voor_Si_LTA.xlsx',P_but_tweede_kolom(:,Nx+1),8)
xlswrite('SAPO_voor_Si_LTA.xlsx',P_eth_tweede_kolom(:,Nx+1),9)
xlswrite('SAPO_voor_Si_LTA.xlsx',P_wat_tweede_kolom(:,Nx+1),10)

%-------------------------differential equations----------------------%
function dy = rigid(t,y)

global R Nx N_comp ...
 L_column D_column Temp mbed eps ...
 dx x ...
 qsat_acet K_acet qsat_but K_but qsat_eth K_eth qsat_wat K_wat  ...
 h_acet h_but h_eth h_wat Dm_acet Dm_eth Dm_but Dm_wat ...
 v Flow ...
 P_in_wat P_in_acet P_in_but P_in_eth ...
 crystal_density ...
 P_tot ...
 dynamic tijd_eerste_kolom index ...
 P_acet_eerste_kolom P_but_eerste_kolom P_eth_eerste_kolom
P_wat_eerste_kolom


dy = zeros(2*N_comp*Nx+2*N_comp,1);

if dynamic == 1
    if t > tijd_eerste_kolom(length(tijd_eerste_kolom))
```

```
        P_in_acet = P_in_acet;
        P_in_but = P_in_but;
        P_in_eth = P_in_eth;
        P_in_wat = P_in_wat;
    else
    end

    if t < tijd_eerste_kolom(index+1)
        P_in_acet = P_acet_eerste_kolom(index,Nx+1);
        P_in_but = P_but_eerste_kolom(index,Nx+1);
        P_in_eth = P_eth_eerste_kolom(index,Nx+1);
        P_in_wat = P_wat_eerste_kolom(index,Nx+1);
    elseif t < tijd_eerste_kolom(length(tijd_eerste_kolom))
        while t > tijd_eerste_kolom(index+1)
            index = index + 1;
        end
        P_in_acet = P_acet_eerste_kolom(index,Nx+1);
        P_in_but = P_but_eerste_kolom(index,Nx+1);
        P_in_eth = P_eth_eerste_kolom(index,Nx+1);
        P_in_wat = P_wat_eerste_kolom(index,Nx+1);
    else
    end
end

for i = 1:Nx+1
    P_acet(i) = y(i);
    q_acet(i) = y(Nx+1+i);
    P_but(i) = y(2*Nx+2+i);
    q_but(i) = y(3*Nx+3+i);
    P_eth(i) = y(4*Nx+4+i);
    q_eth(i) = y(5*Nx+5+i);
    P_wat(i) = y(6*Nx+6+i);
    q_wat(i) = y(7*Nx+7+i);
end

for i = 1:Nx+1
    noemer(i) = (K_but * P_but(i) + K_eth * P_eth(i) + K_wat  * P_wat(i) +
1);

    q_eq_acet(i) = K_acet * qsat_acet * P_acet(i) / noemer(i);
    q_eq_but(i) = K_but * qsat_but * P_but(i) / noemer(i);
    q_eq_eth(i) = K_eth * qsat_eth * P_eth(i) / noemer(i);
    q_eq_wat(i) = K_wat * qsat_wat * P_wat(i) / noemer(i);

    Rq_acet(i) = h_acet * (q_eq_acet(i) - q_acet(i));
    Rq_but(i) = h_but * (q_eq_but(i) - q_but(i));
    Rq_eth(i) = h_eth * (q_eq_eth(i) - q_eth(i));
    Rq_wat(i) = h_wat * (q_eq_wat(i) - q_wat(i));

    R_acet(i) = (1-eps)/eps * (R*Temp) * crystal_density * Rq_acet(i);
    R_but(i) = (1-eps)/eps * (R*Temp) * crystal_density * Rq_but(i);
    R_eth(i) = (1-eps)/eps * (R*Temp) * crystal_density * Rq_eth(i);
    R_wat(i) = (1-eps)/eps * (R*Temp) * crystal_density * Rq_wat(i);

end

%----------------------implementatie discretisatie ------------------%

% % % % % % Aceton

for i=1:Nx
```

```
    if i==1
        u_i_1=P_acet(1)-dx*v/Dm_acet*(P_acet(1)-P_in_acet);  % LBC
        %u_i_1 = C_inlet neumann randvoorwaarde: massabalans op het eerste
punt;
        dy(1) = Dm_acet/(dx*dx)*(P_acet(i+1)-2*P_acet(i)+u_i_1)-
v/eps/dx*(P_acet(i)-u_i_1) - R_acet(i);
    else
        dy(i) = Dm_acet/(dx*dx)*(P_acet(i+1)-2*P_acet(i)+P_acet(i-1))-
v/eps/dx*(P_acet(i)-P_acet(i-1))-R_acet(i);
    end
end
                                        % RBC  ---> U(x+2) = U(x+1)
dy(Nx+1) = Dm_acet/(dx*dx)*(P_acet(Nx+1)-2*P_acet(Nx+1)+P_acet(Nx))-
v/eps/dx*(P_acet(Nx+1)-P_acet(Nx))-R_acet(Nx+1);

% ---- mass balance amount adsorbed ---- %
for i=1:Nx+1
    dy((Nx+1)+i) = Rq_acet(i);
end

% % % % % % % Butanol

for i=1:Nx
    if i==1
        u_i_1=P_but(1)-dx*v/Dm_but*(P_but(1)-P_in_but);  % LBC
        %u_i_1 = C_inlet neumann randvoorwaarde: massabalans op het eerste
punt;
        dy(1 + 2* Nx + 2) = Dm_but/(dx*dx)*(P_but(i+1)-2*P_but(i)+u_i_1)-
v/eps/dx*(P_but(i)-u_i_1) - R_but(i);
    else
        dy(i + 2* Nx + 2) = Dm_but/(dx*dx)*(P_but(i+1)-2*P_but(i)+P_but(i-
1))-v/eps/dx*(P_but(i)-P_but(i-1))-R_but(i);
    end
end
                                        % RBC  ---> U(x+2) = U(x+1)
dy(3*Nx+3) = Dm_but/(dx*dx)*(P_but(Nx+1)-2*P_but(Nx+1)+P_but(Nx))-
v/eps/dx*(P_but(Nx+1)-P_but(Nx))-R_but(Nx+1);

% ---- mass balance amount adsorbed ---- %
for i=1:Nx+1
    dy((3*Nx+3)+i) = Rq_but(i);
end

% % % % % % % Ethanol

for i=1:Nx
    if i==1
        u_i_1=P_eth(1)-dx*v/Dm_eth*(P_eth(1)-P_in_eth);  % LBC
        %u_i_1 = C_inlet neumann randvoorwaarde: massabalans op het eerste
punt;
        dy(4*Nx + 4 + 1) = Dm_eth/(dx*dx)*(P_eth(i+1)-2*P_eth(i)+u_i_1)-
v/eps/dx*(P_eth(i)-u_i_1) - R_eth(i);
    else
        dy(4*Nx + 4 + i) = Dm_eth/(dx*dx)*(P_eth(i+1)-2*P_eth(i)+P_eth(i-
1))-v/eps/dx*(P_eth(i)-P_eth(i-1))-R_eth(i);
    end
end
                                        % RBC  ---> U(x+2) = U(x+1)
dy(5*Nx+5) = Dm_eth/(dx*dx)*(P_eth(Nx+1)-2*P_eth(Nx+1)+P_eth(Nx))-
v/eps/dx*(P_eth(Nx+1)-P_eth(Nx))-R_eth(Nx+1);
```

```
% ---- mass balance amount adsorbed ---- %
for i=1:Nx+1
    dy((5*Nx+5)+i) = Rq_eth(i);
end


% % % % % % % % % % Water

for i=1:Nx
    if i==1
        u_i_1=P_wat(1)-dx*v/Dm_wat*(P_wat(1)-P_in_wat);  % LBC
        %u_i_1 = C_inlet neumann randvoorwaarde: massabalans op het eerste
punt;
        dy(6*Nx + 6 + 1) = Dm_wat/(dx*dx)*(P_wat(i+1)-2*P_wat(i)+u_i_1)-
v/eps/dx*(P_wat(i)-u_i_1) - R_wat(i);
    else
        dy(6*Nx + 6 + i) = Dm_wat/(dx*dx)*(P_wat(i+1)-2*P_wat(i)+P_wat(i-
1))-v/eps/dx*(P_wat(i)-P_wat(i-1))-R_wat(i);
    end
end
                                        % RBC  ---> U(x+2) = U(x+1)
dy(7*Nx+7) = Dm_wat/(dx*dx)*(P_wat(Nx+1)-2*P_wat(Nx+1)+P_wat(Nx))-
v/eps/dx*(P_wat(Nx+1)-P_wat(Nx))-R_wat(Nx+1);

% ---- mass balance amount adsorbed ---- %
for i=1:Nx+1
    dy((7*Nx+7)+i) = Rq_wat(i);
end
```

Appendix 4 – Isotherms

Si CHA isotherms under N_2

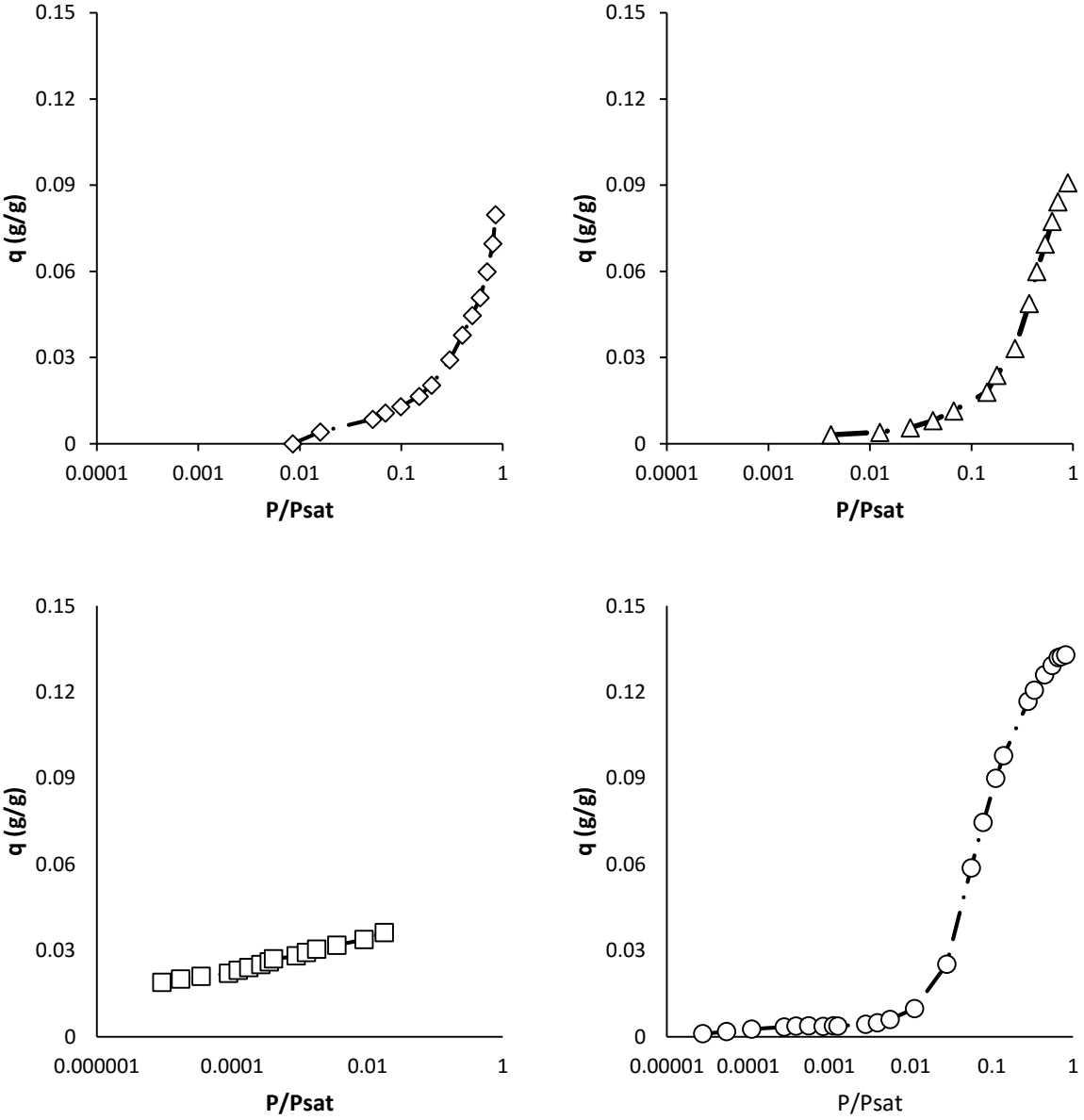

Figure A4.1: Adsorption isotherms of water (◇), butanol (△), acetone (❑) and ethanol (○) on Si CHA using N_2 as carrier gas (Gelin, 2015).

CO_2 isotherm on Si LTA

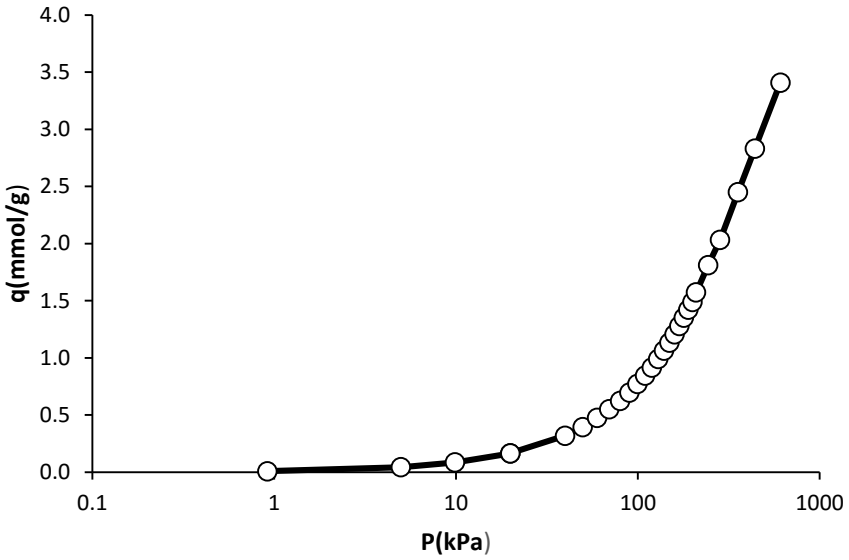

Figure A4.2: CO_2 adsorption isotherm of Si LA at 40 °C. High pressure isotherm points were not at compete equilibrium.

Appendix 5 – Single column breakthrough profiles

Empty column breakthrough – data oscillations

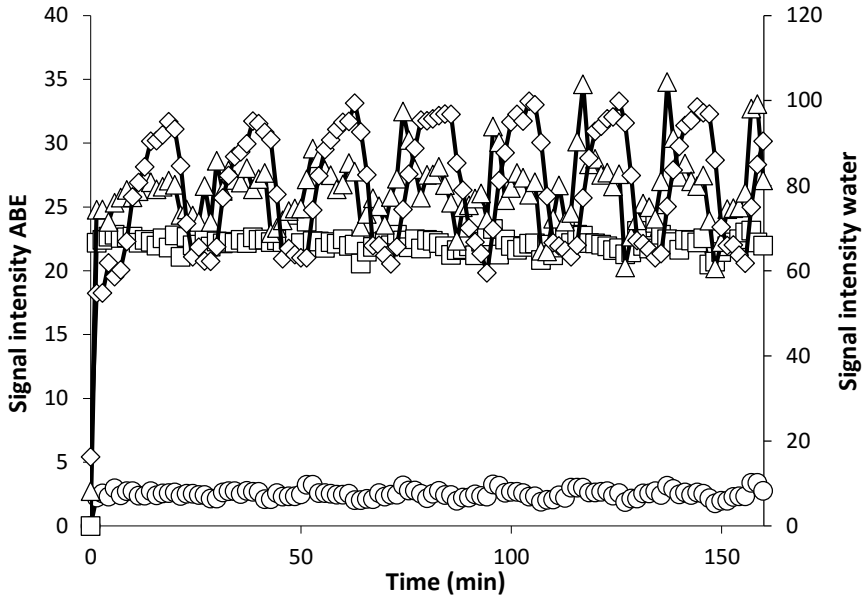

Figure A5.1: Empty column breakthrough profile showing oscillatory behavior of data. TCD detector signal intensities of acetone (❑), butanol (△), ethanol (○) and water (◇) are plotted as function of time.

Desorption profile of Si-LTA using CO_2 as carrier gas

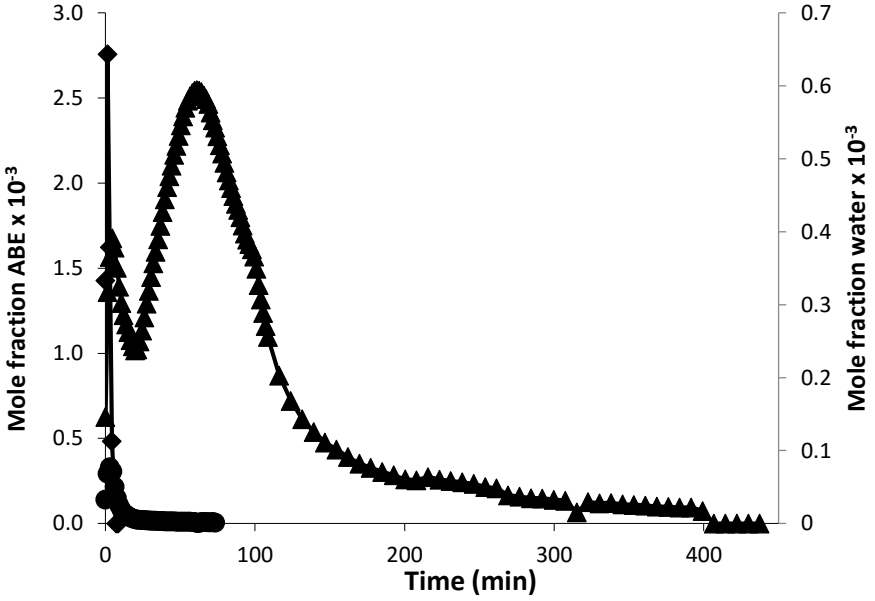

Figure A5.2: Desorption profile of the Si-LTA column using CO_2 as carrier gas during adsorption and desorption. Butanol (▲), ethanol (●) and water (◆) profiles are shown.

Adsorption profile of ZIF-8 using CO_2 as carrier gas

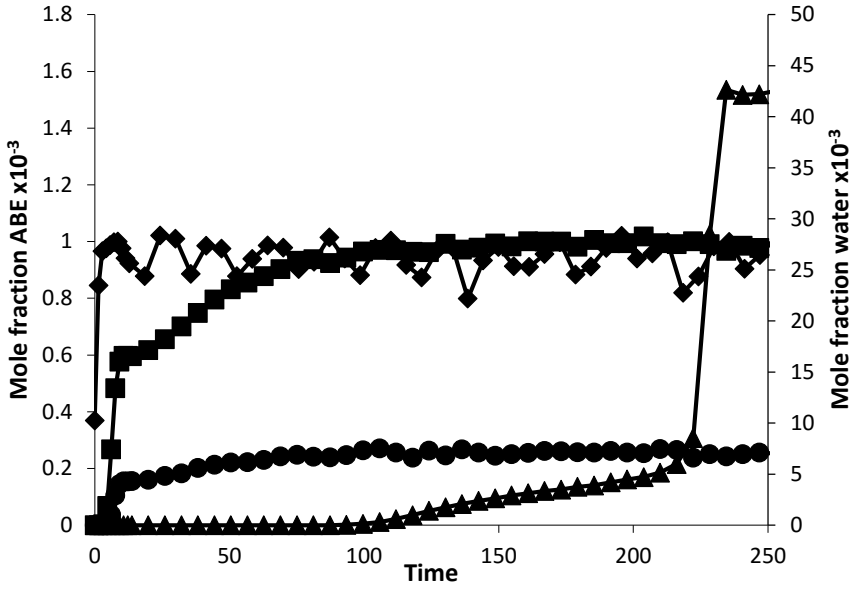

Figure A5.3: Adsorption breakthrough profile at 40 °C on the ZIF-8 column using CO_2 as carrier gas. Acetone (■), butanol (▲), ethanol (●) and water (◆) profiles are shown. Vapor phase partial pressures at the column inlet were 50 Pa for ethanol, 305 Pa for butanol, 196 Pa for acetone and 4185Pa for water.

Isothermal desorption profile of ZIF-8

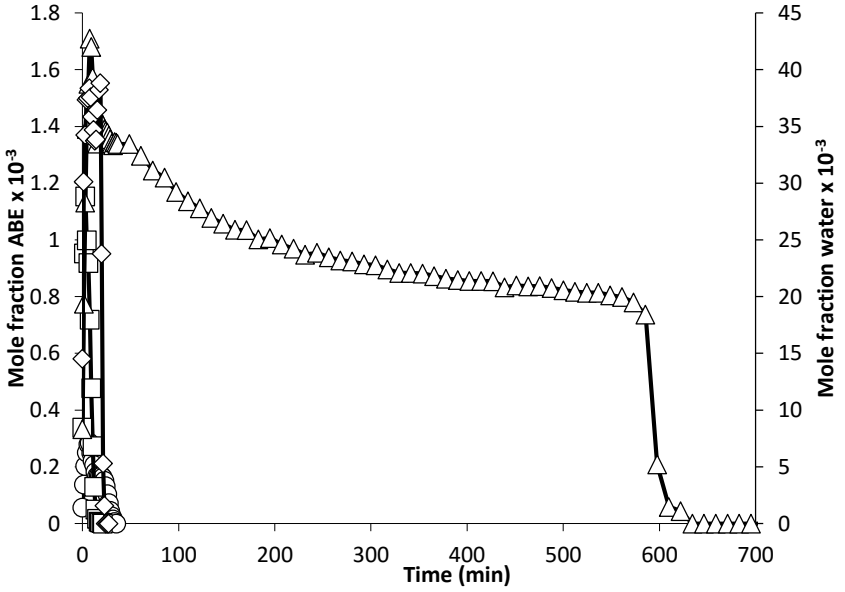

Figure A5.4: Desorption profile of ZIF-8 at 40 °C using He as carrier gas. Acetone (□), butanol (△), ethanol (○) and water (◇) desorption profiles are shown.

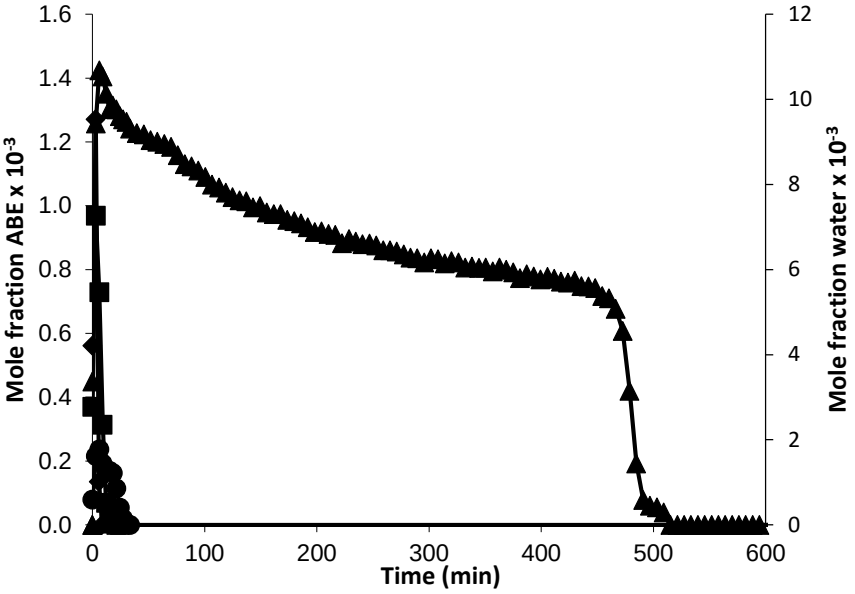

Figure A5.5: Isothermal desorption profile using CO_2 as carrier gas during adsorption and desorption. Acetone (■), butanol (▲), ethanol (●) and water (◆) profiles are shown.

Appendix 6 – Chromatograms of catalytic products

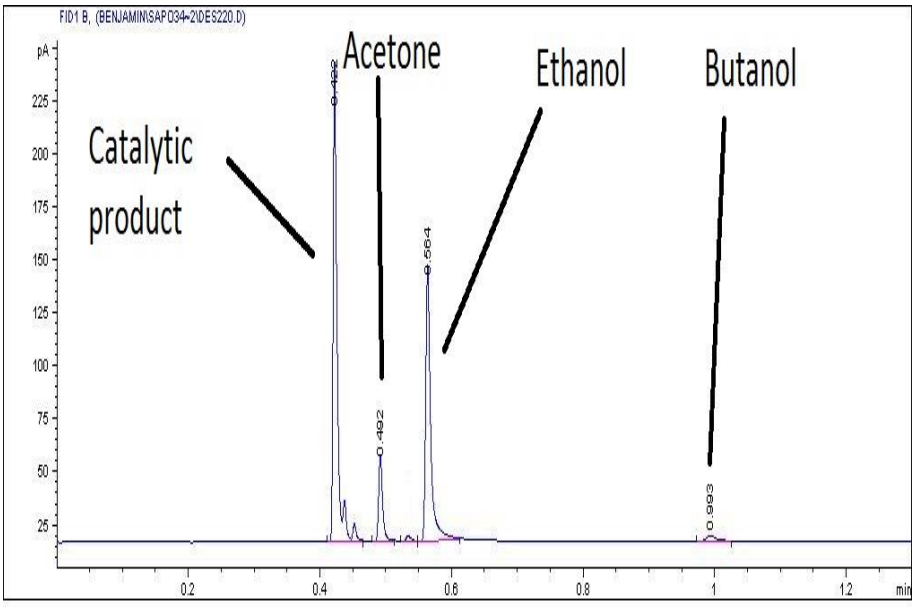

Figure A6.1: Chromatogram measured during desorption of the SAPO-34 column, showing the catalytic product formed at higher temperature.

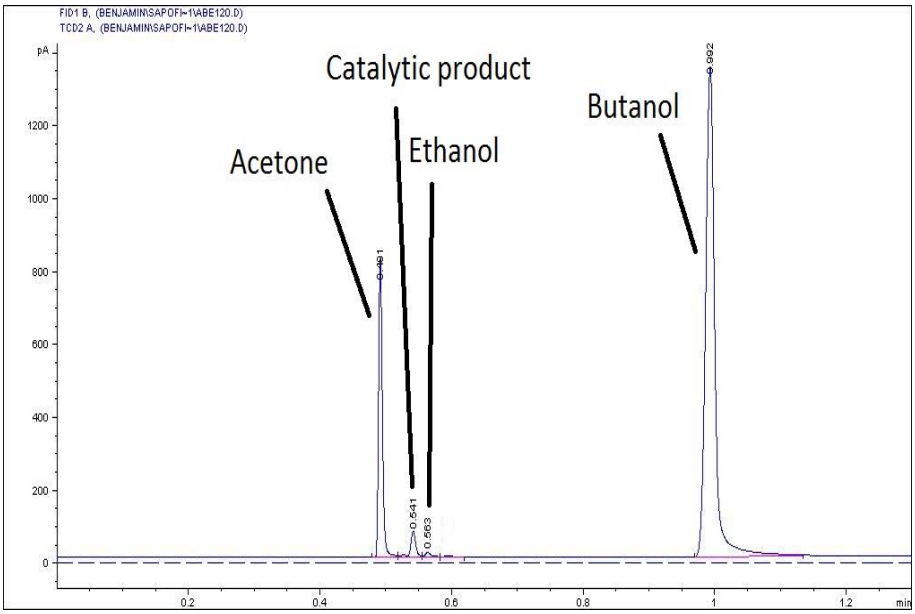

Figure A6.2: Chromatogram showing the catalytic product formed during ABE adsorption using CO_2 as carrier gas.

Appendix 7 – Multicolumn breakthrough profiles

Si LTA

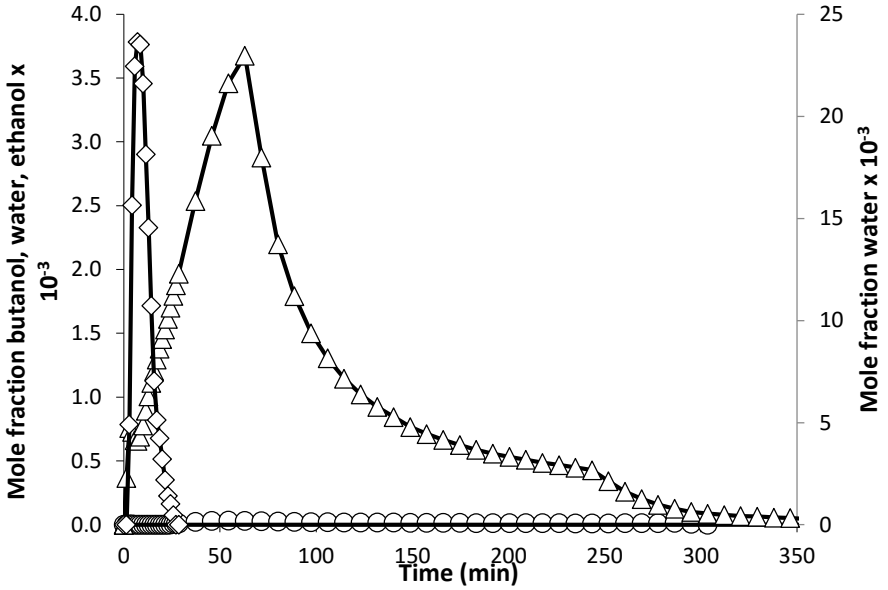

Figure A7.1: Desorption profile of the Si-LTA column in combination with the Si-CHA column for the whole duration of the desorption using He as carrier gas. After a certain amount of time, ethanol starts desorbing from the Si-CHA column, as is illustrated with a close-up in figure A7.2.

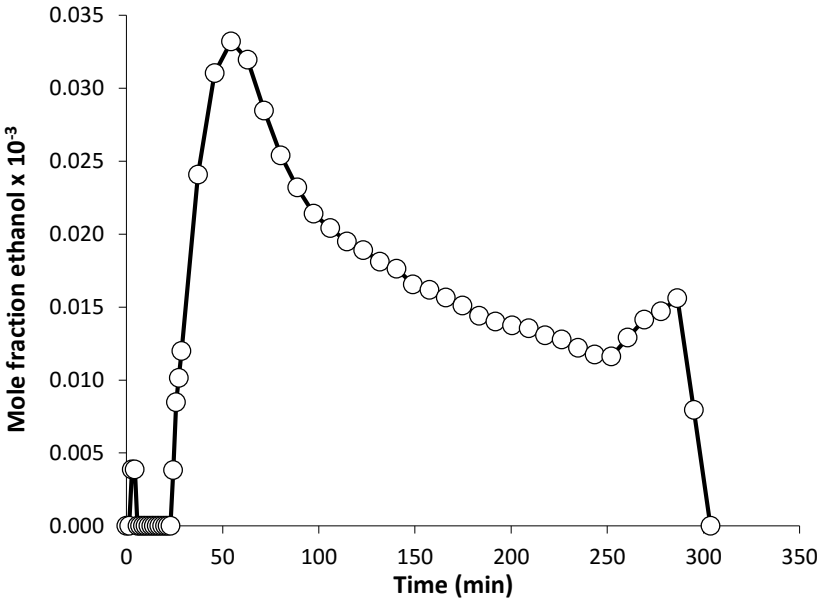

Figure A7.2: Close up of the ethanol desorption profile of figue A7.1.

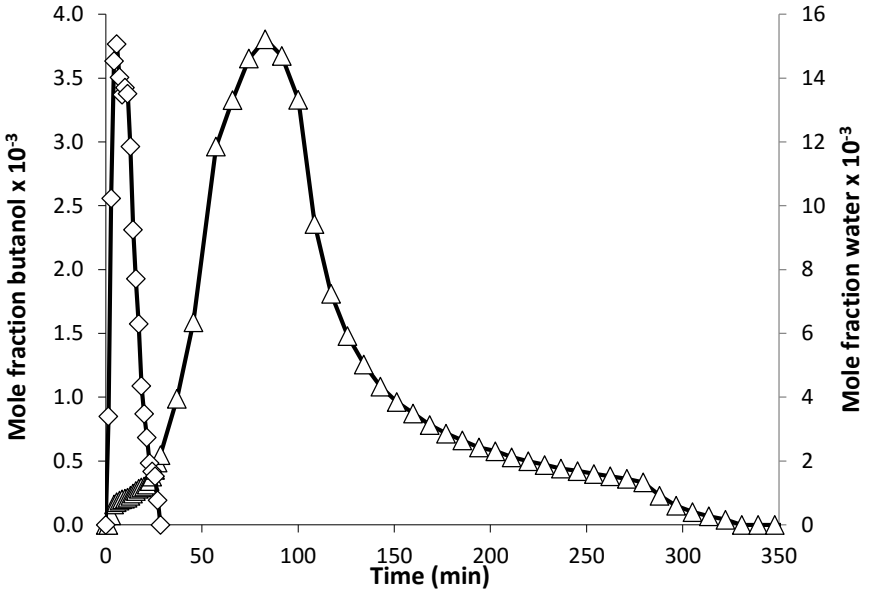

Figure A7.1: Desorption profile of the combination of the Si-LTA column with the Si-CHA column (50 min). Water (◇) and butanol (△) desorption profiles are shown, since only a trace amount of acetone and ethanol was observed. He was used as carrier gas.

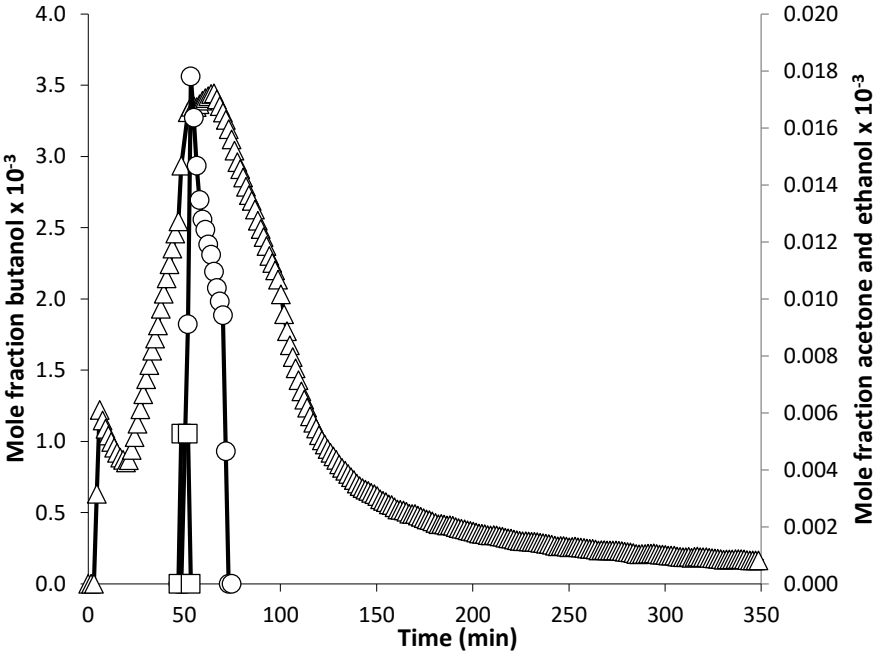

Figure A7.2: Desorption profile of the Si-LTA column in combinations with the SAPO-34 column (50 min) using He as carrier gas. Butanol (△), acetone (□) and ethanol profiles (O) are shown. No desorption of water was observed.

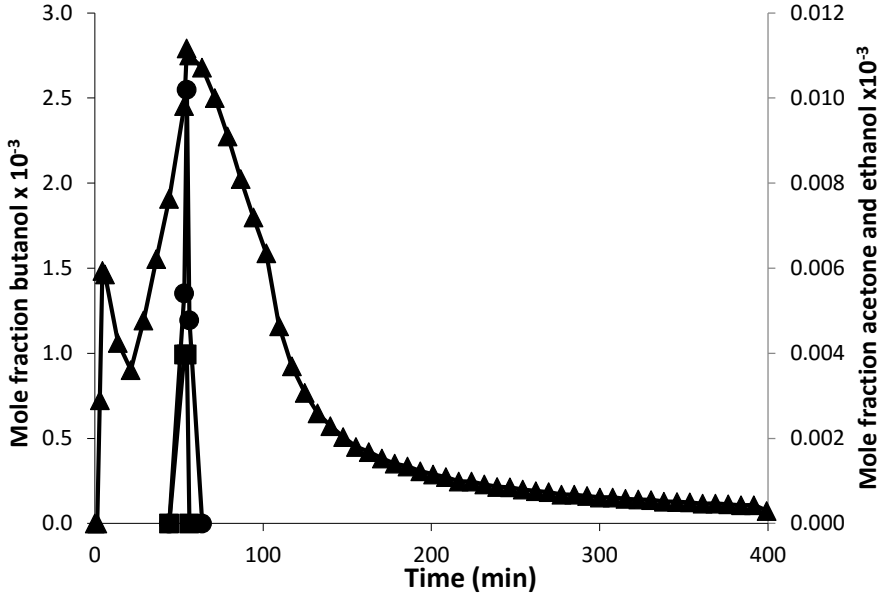

Figure A7.3: Desorption profile of the Si-LTA column in combination with SAPO34 using CO_2 as carrier gas. Butanol (▲), acetone (■) and ethanol (●) profiles are shown. No water breakthrough was observed.

ZIF-8

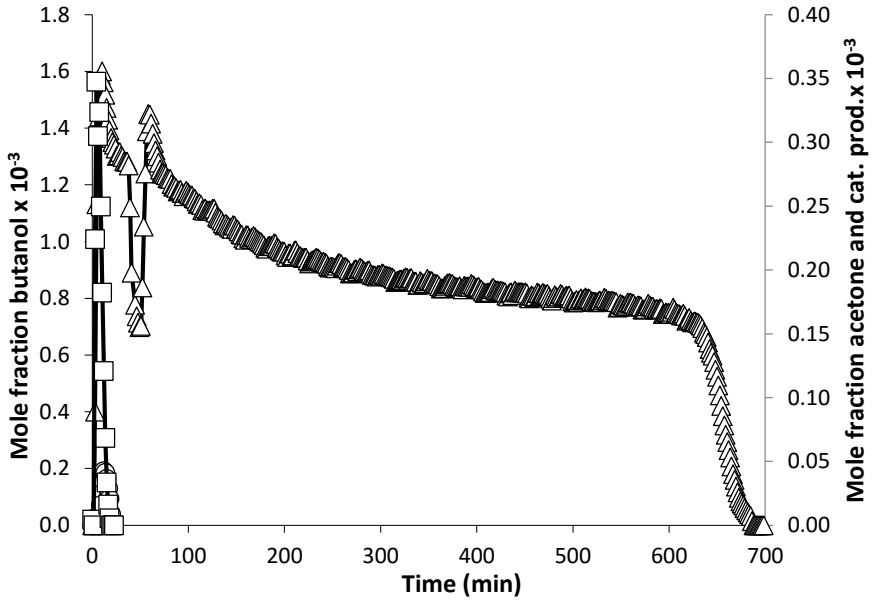

Figure A7.4: Isothermal desorption profile of ZIF-8 in combination with SAPO-34 (40 min). Butanol (△), acetone (❑) and catalytic product profiles (○) are shown. No desorption of water was observed. He was used as carrier gas0

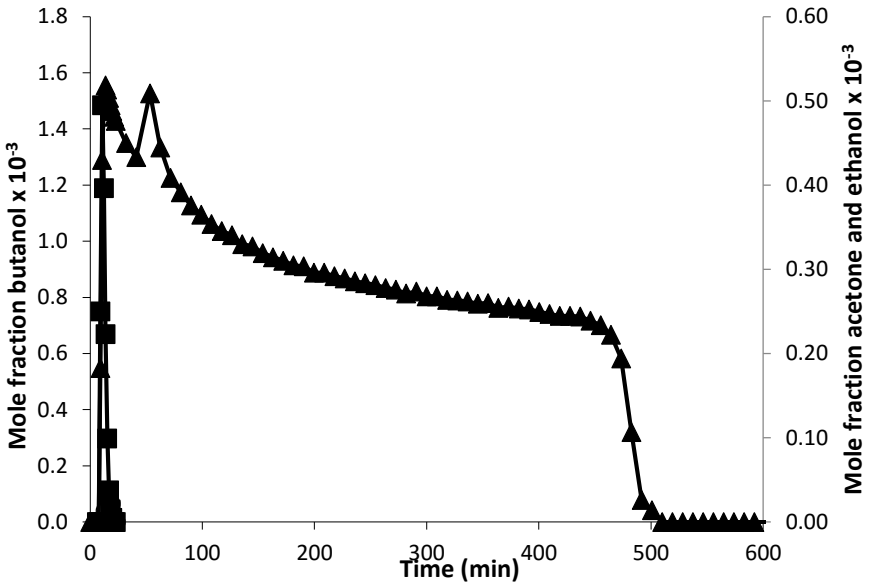

Figure A7.5: Isothermal desorption profile of ZIF-8 in combination with SAPO-34 (40 min). Butanol (▲), acetone (■) and catalytic product (●) profiles are shown. No desorption of water was observed. CO_2 was used as carrier gas.

Appendix 8 – Fitted isotherm models

Si-LTA

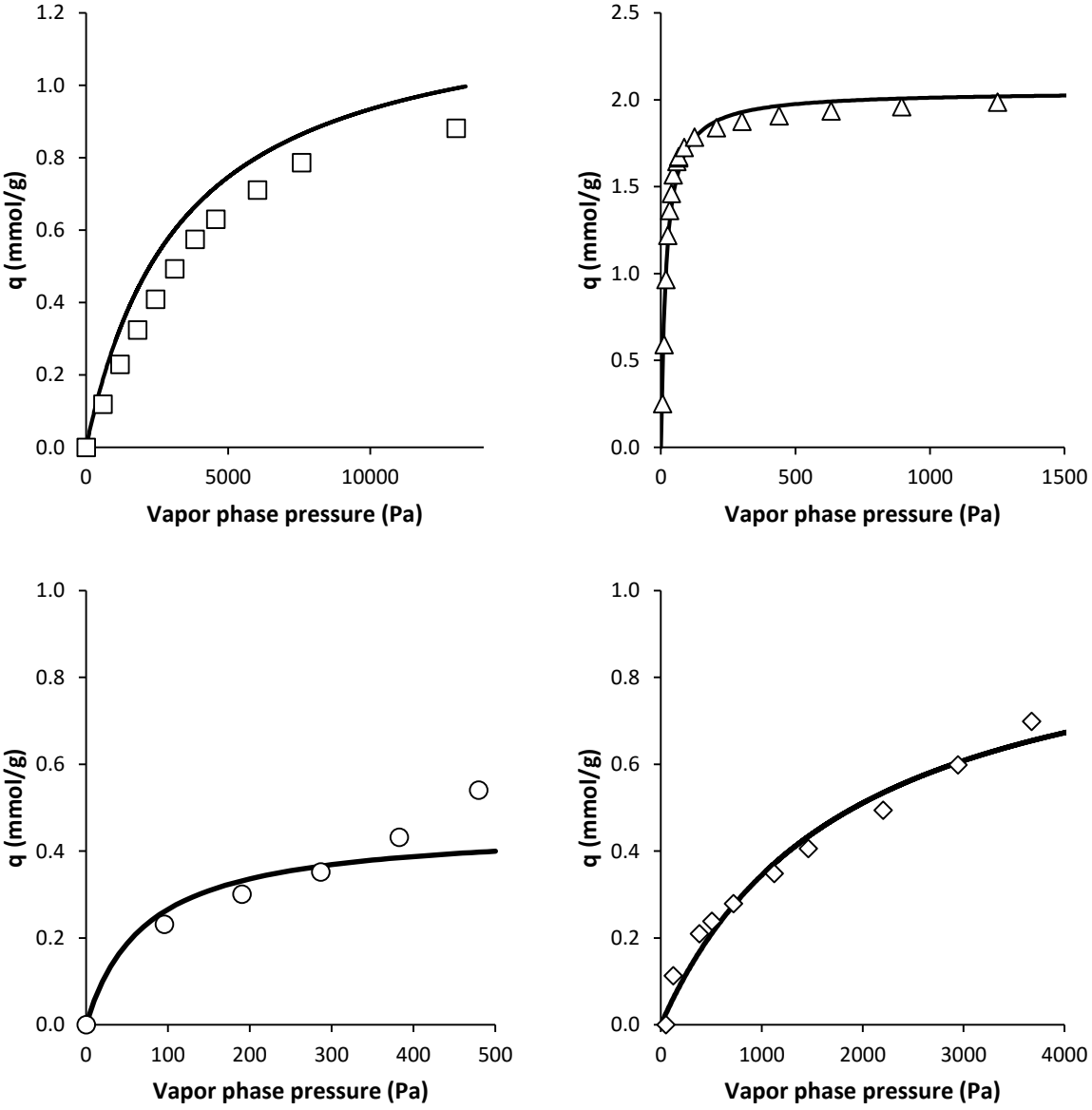

Figure A8.1: Comparison between fitted and experimental isotherm data on Si-LTA, acetone (❑), butanol (△), ethanol (○) and water (◇) data is shown. N_2 isotherm data was used for model fitting.

ZIF-8

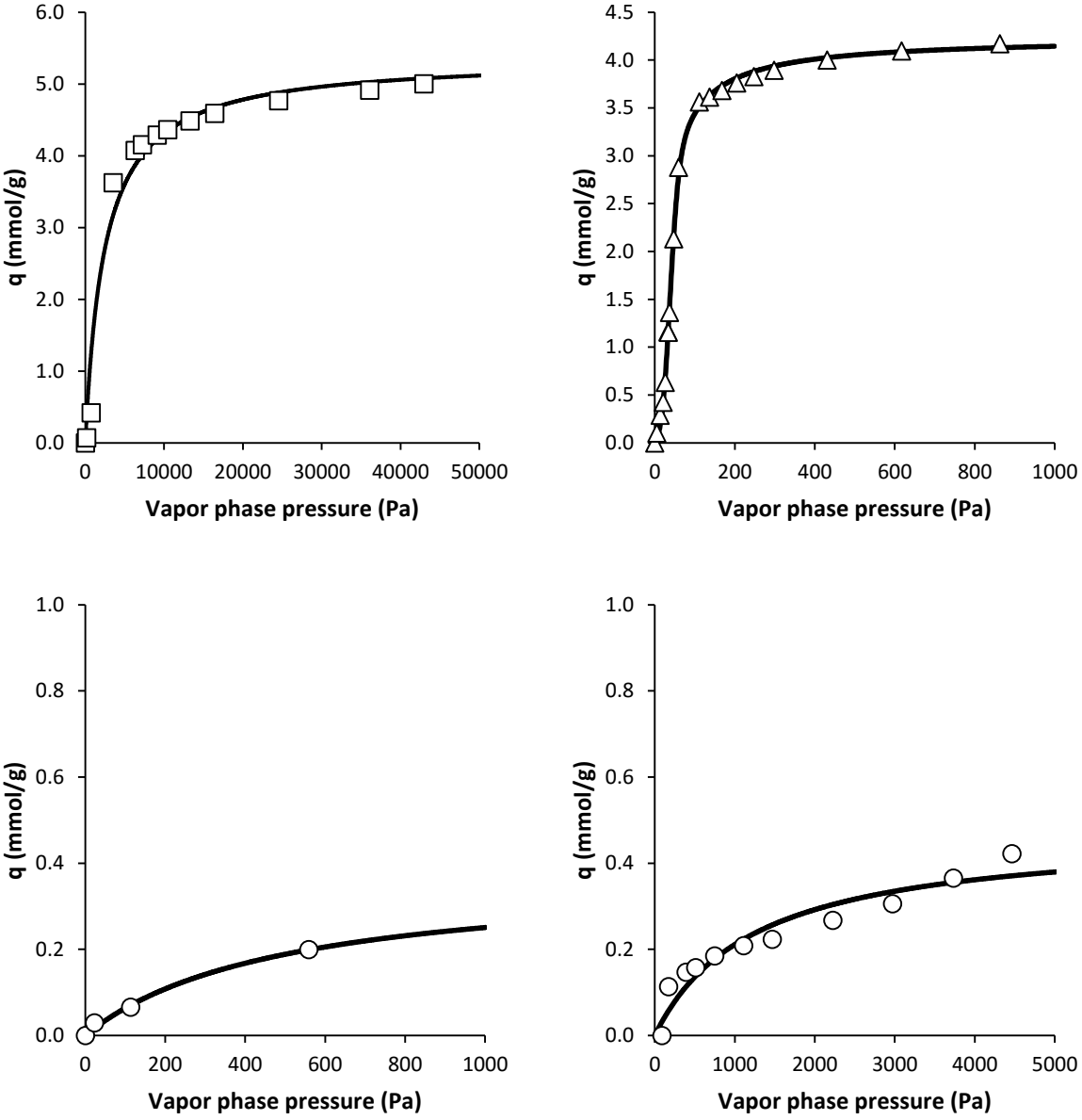

Figure A8.2: Comparison between fitted and experimental isotherm data on ZIF-8, acetone (❑), butanol (△), ethanol (○) and water (◇) data is shown. N_2 isotherm data was used for model fitting.

Si-CHA

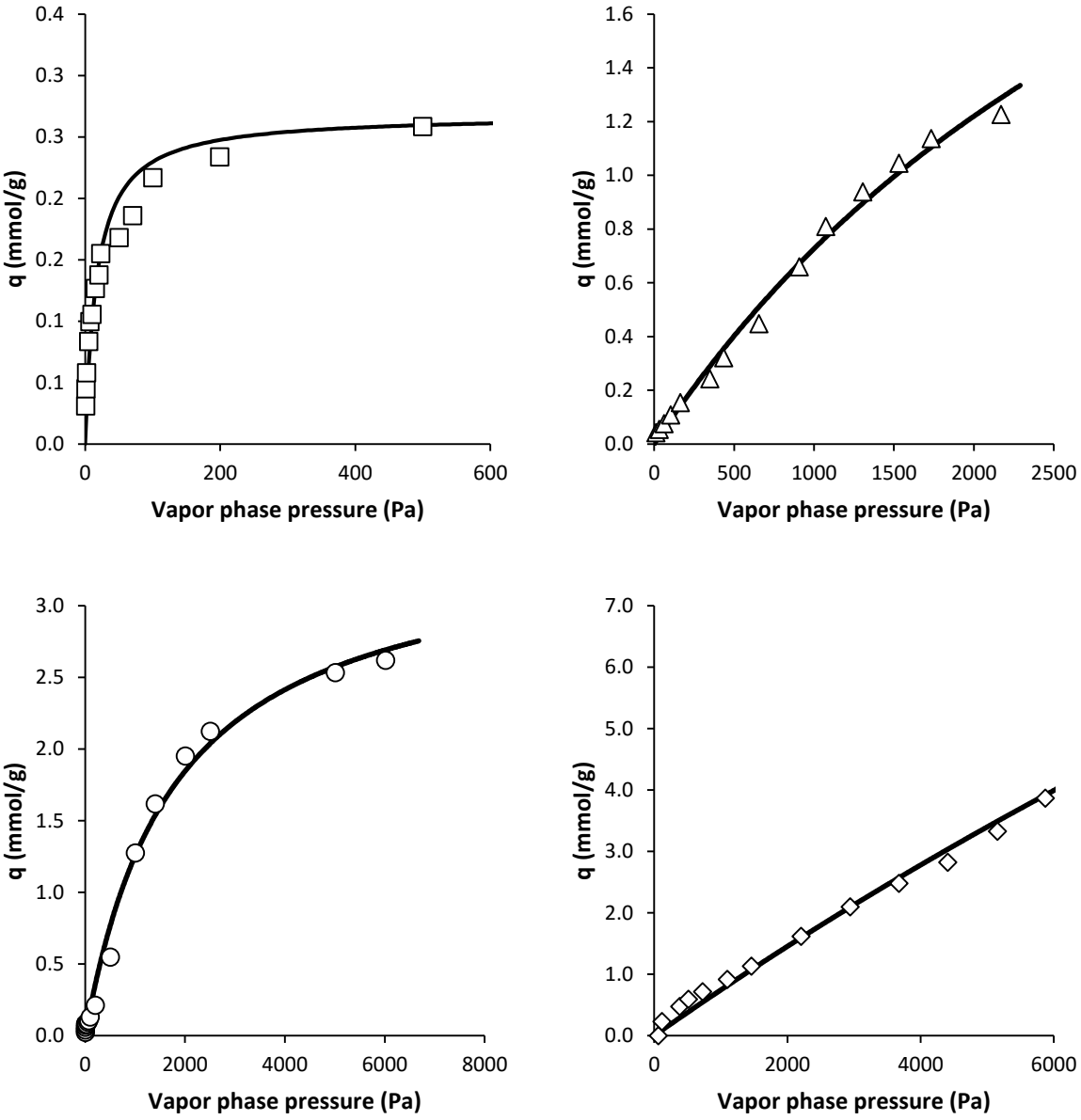

Figure A8.3: Comparison between fitted and experimental isotherm data on Si-CHA, acetone (❑), butanol (△), ethanol (○) and water (◇) data is shown. N_2 isotherm data was used for model fitting.

SAPO-34

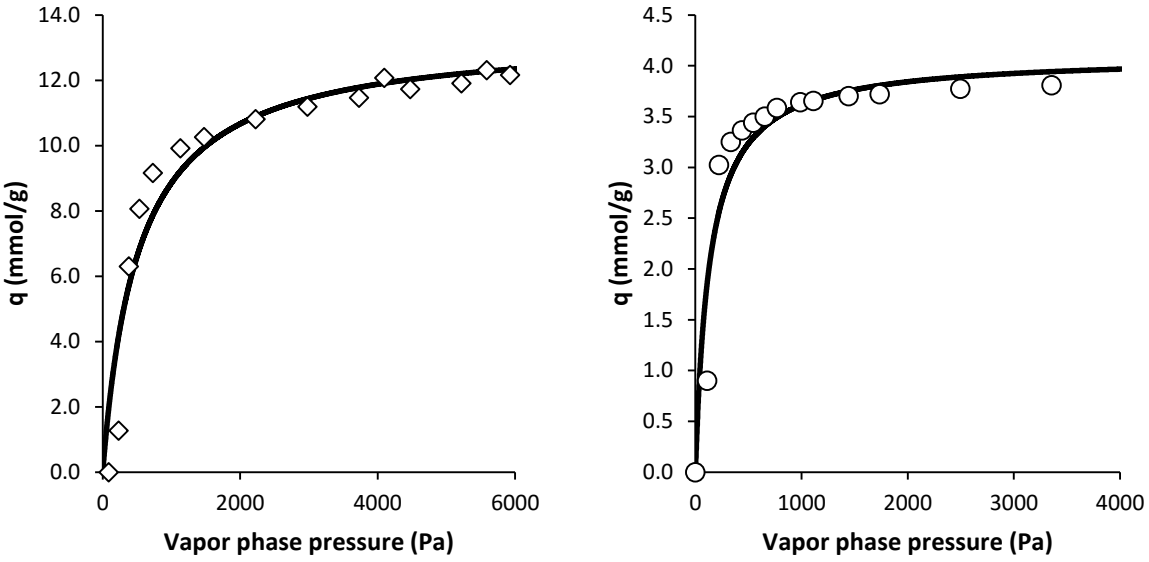

Figure A8.4: Comparison between fitted and experimental isotherm data on Si-CHA: ethanol (○) and water (◇) data is shown. N_2 isotherm data was used for model fitting.

Appendix 9 – Simulation results

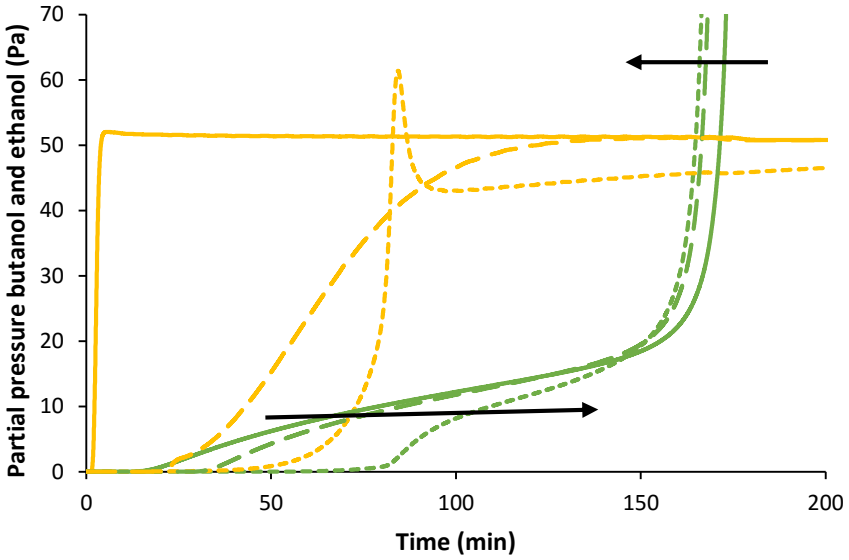

Figure A9.1: Close up of the simulated breakthrough profile on the ZIF-8 column in combination with a SAPO-34 column (short dotted lines) and a Si-CHA column (long dotted lines). The native breakthrough profile was also added (uninterrupted lines). The only components shown are butanol (green) and ethanol (yellow). The shift of the butanol breakthrough profile is marked by the two arrows.

Appendix 10 – Isotherm classification

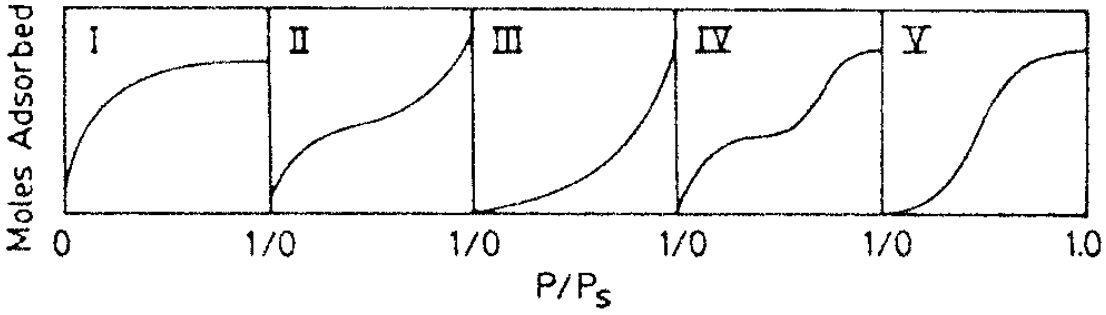

Figure A10.1: Classification of adsorption isotherms (Ruthven, 1984).